



PB94-203635

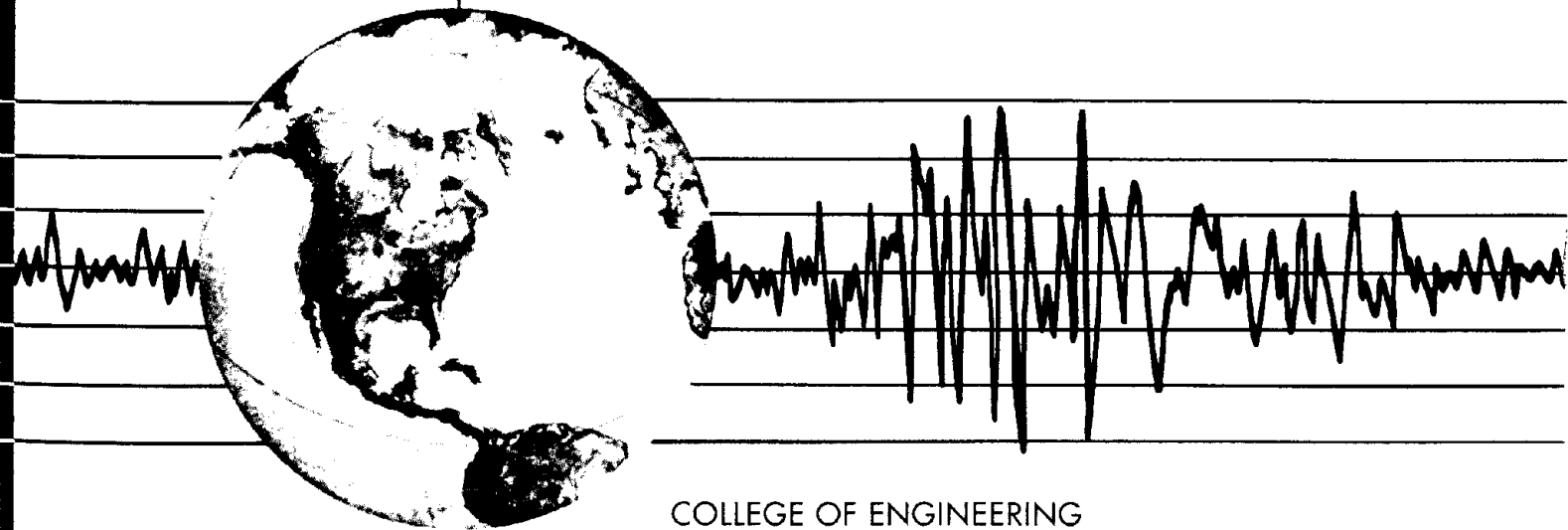
REPORT NO.
UCB/EERC-94/08
JUNE 1994

EARTHQUAKE ENGINEERING RESEARCH CENTER

**PRELIMINARY REPORT ON THE
PRINCIPAL GEOTECHNICAL ASPECTS
OF THE JANUARY 17, 1994
NORTHRIDGE EARTHQUAKE**

edited by

JONATHAN P. STEWART
JONATHAN D. BRAY
RAYMOND B. SEED
NICHOLAS SITAR



COLLEGE OF ENGINEERING

UNIVERSITY OF CALIFORNIA AT BERKELEY

REPRODUCED BY
U.S. DEPARTMENT OF COMMERCE
NATIONAL TECHNICAL
INFORMATION SERVICE
SPRINGFIELD, VA 22161

For sale by the National Technical Information Service, U.S. Department of Commerce, Springfield, Virginia 22161

See back of report for up to date listing of EERC reports.

DISCLAIMER

Any opinions, findings, and conclusions or recommendations expressed in this publication are those of the authors and do not necessarily reflect the views of the Sponsors or the Earthquake Engineering Research Center, University of California at Berkeley.

PRELIMINARY REPORT ON
THE PRINCIPAL GEOTECHNICAL ASPECTS OF
THE JANUARY 17, 1994 NORTHRIDGE EARTHQUAKE

edited by

Jonathan P. Stewart, Jonathan D. Bray, Raymond B. Seed, and Nicholas Sitar

with other contributions from:

Scott A. Ashford
Anthony J. Augello
Susan W. Chang
Chih-Cheng Chin
Margaret A. Ennis
William B. Gookin
Leslie F. Harder, Jr.
Terence L. Jenkins
Alan L. Kropp
Carlos A. Lazarte
David J. McMahon

Michael T. McRae
Scott M. Merry
Diane Murbach
Ellen M. Rathje
Gretchen A. Rau
Michael F. Riemer
Barbara A. Romanowicz
Alisa F. Stewart
Kenichi Soga
Patricia A. Thomas
Jorge G. Zornberg

Report No. UCB/EERC-94/08

Earthquake Engineering Research Center
College of Engineering
University of California at Berkeley

June 1994

PREFACE

This report has been prepared to document the available geotechnical data which emerged following the Northridge Earthquake of January 17, 1994. It contains preliminary information from a wide variety of sources including researchers, consulting engineers, public officials and many others. Detailed investigations involving further field, analytical and laboratory work have been initiated for several of the particularly interesting and important aspects of this earthquake at numerous academic and non-academic institutions. Therefore, more definitive conclusions regarding the earthquake and its effects will continue to emerge in subsequent literature.

Data currently available suggest that the Northridge Earthquake was the most costly natural disaster in United States history. The widespread damages resulting from the earthquake included: (1) structural failures in residential, commercial, industrial, and transportation facilities, (2) thousands of breaks in water, gas, sewer, and other buried pipelines, (3) distressed geotechnical structures including dams and landfills, (4) numerous landslides in mountainous areas surrounding the epicentral region, (5) disruption of pavements from ground failure, and (6) damage to non-structural elements and contents of structures. In all, approximately 61 deaths, 18,500 injuries, and \$13 to 15 billion in damages are directly attributed to this earthquake.

Much of the damage was a result of the unfortuitous location of the fault rupture directly beneath a heavily developed and populated portion of Los Angeles. Large inertial forces associated with the very strong ground motions in the near-field simply overwhelmed many inadequately designed structures. However, high concentrations of damage also occurred in several geographically well-defined areas relatively distant from the zone of energy release. These concentrations of damage in portions of Sherman Oaks, Canoga Park, Hollywood, Santa Monica, and central Los Angeles appear to have been influenced by geologic factors such as soil amplification or basin effects. In other areas, such as the City of San Fernando, Granada Hills, and Santa Clarita, ground failure may have influenced structural damage patterns. The principal geotechnical features of this earthquake include the following:

- Unusually high levels of peak ground acceleration were recorded at a few instrument stations near the fault rupture source zone. Significant concentrations of damage occurred in the epicentral area and in several geographically well-defined regions more distant from the fault rupture zone. These damage concentrations suggest that local site conditions (subsurface stratigraphy and materials as well as topographic effects), directionality effects, and deep structural basins may have significantly affected the characteristics and distribution of strong ground motions.
- Widespread ground failure, much of which appears to have been due to soil liquefaction, occurred during the earthquake and caused significant damage to pipelines and pavements in the San Fernando Valley, Simi Valley, the Santa Clara River area, coastal areas, and the central Los Angeles area.

- Landslides and rockfalls in several mountainous areas closed many roads and damaged numerous homes.
- Several geotechnical structures either failed or performed poorly, including a failed tailings dam.
- A large number of geotechnical structures such as dams, hillside structural fills, retaining walls, and municipal solid waste landfills were strongly shaken. These structures generally performed well, and represent an excellent source of case histories from which valuable insights regarding the seismic performances of these types of structures can be gained.

Historically, technological advances in earthquake engineering have rapidly accelerated following major seismic events. As with many previous significant earthquakes, there are a number of important lessons to be gleaned from the Northridge event. It is our responsibility in the profession to learn as much as possible from major earthquakes so as to further advance both the state-of-knowledge and the state-of-practice. It is primarily through such advances, and the subsequent implementation of the lessons learned by practicing engineers, that public safety can be improved for the inevitable earthquakes still to come.

Jonathan P. Stewart
Jonathan D. Bray
Raymond B. Seed
Nicholas Sitar
June 22, 1994

ACKNOWLEDGEMENTS

This report was made possible by the volunteer efforts of many people from the University of California at Berkeley and numerous other organizations. It was only through the co-operative spirit of these individuals from across the State of California that the information contained herein could be compiled.

Support for initial investigative efforts as well as the printing and distribution of this document have been provided by Awards Nos. CMS-9414375 and BCS-9157083 from the U.S. National Science Foundation, the David and Lucile Packard Foundation, and the Earthquake Engineering Research Center (EERC), and this support is gratefully acknowledged.

Very special thanks are extended to the members of the geotechnical reconnaissance team from U.C. Berkeley, whose surveys of the affected areas immediately following the earthquake provided much of the data presented herein. This group was comprised of graduate students and faculty from the Geotechnical Group at Berkeley and included Dr. Scott Ashford, Anthony Augello, Dr. Jonathan Bray, Susan Chang, Chih-Cheng Chin, Margaret Ennis, William Gookin, Carlos Lazarte, Dr. Mike McRae, Scott Merry, Gretchen Rau, Dr. Michael Riemer, Dr. Raymond Seed, Dr. Nicholas Sitar, Jonathan Stewart, Dr. Kenichi Soga, Patricia Thomas, and Jorge Zornberg. Invaluable contributions to this report were also provided by Dr. Leslie F. Harder, Jr. of the California Department of Water Resources, Dr. Barbara Romanowicz of the University of California at Berkeley, Alan Kropp and David McMahon of Alan Kropp and Associates, Diane Murbach and Dr. Thomas Rockwell of San Diego State University, Dr. Ross Boulanger and Dr. I.M. Idriss of the University of California at Davis, Ralph Ricketson of the California Department of Transportation, and Dr. John Tinsley of the U.S. Geological Survey. In addition, the data provided by Mark Williams and Kevin Miller of the Governor's Office of Emergency Services, Alex Newton of the Federal Emergency Management Agency, and Neil Blais of EQE International is gratefully acknowledged.

The authors of Chapter Two would particularly like thank Dr. Douglas Dreger, Suzanna Loper, and Michael Pasyanos of the U.C. Berkeley Seismographic Station, Dr. Patrick Williams of the Lawrence Berkeley Laboratory, and Grant Marshall and Ross Stein of the U.S. Geological Survey.

The authors of Chapter Three wish to thank the following for their invaluable assistance and helpful comments: Dr. Douglas Dreger of the U.C. Berkeley Seismographic Station, Robert Darragh of the California Strong Motion Instrumentation Program, Dr. John Tinsley and Ronald Porcella of the U.S. Geological Survey, Dr. Faiz Makdisi and Dr. C.Y. Chang of Geomatrix Consultants, Richard O'Reilly of the Los Angeles Times, Bill Rome of the City of Santa Monica, Kevin Miller of OES/FEMA, Paul Michalski and Glenn Hirano of the City of Los Angeles, Walter J. Silva of Pacific Engineering and Analysis, Thomas Schantz and Dr. Clifford Roblee of the California Department of Transportation, and William Gookin and Patricia Thomas of U.C. Berkeley.

The authors of Chapter Four gratefully acknowledge the information contributed by Linda Nasitka and Scott Munson of the City of Los Angeles Department of Water and Power, Jerry Wedding of the City of San Fernando, Charles Samo of the Office of the State Fire Marshall, Gan Mukhopadhyay of Leighton and Associates, William Peci of the Los Angeles Metropolitan Water District, George Burke of the City of Simi Valley, Chet Anderson and Kyle Snay of the Southern California Water Company, Mark Delisle and Michael Reichle of the California Division of Mines and Geology, David Schwartz of the U.S. Geological Survey, James Harter of the Newhall Land and Farming Company, Scott Lindvall of Lindvall Richter Benuska Associates, Jean DiAngelouf of the Newhall County Water District, William Manetta of the Santa Clarita Water Company, Peter Ngoon of the Valencia Water Company, William Buol of the City of Santa Monica, Kenneth Westphal of the Los Angeles County Water Works, Desi Alvarez of the City of Redondo Beach, Dr. Geoff Martin and Dr. Jean Bardet of the University of Southern California, Richard Woodcopp and Doug Thiessen of the Port of Los Angeles, Robert Hayden of Hayward Baker, Inc., Howard Fischkes and Curt Zabriski of the City of Beverly Hills, Bernard Quiroga of the California America Water Company, and Jim Roberts and Jim Gates of the California Department of Transportation.

The authors of Chapter Five would like to thank Tim McCrink of the California Division of Mines and Geology, Mark McCowsky of the City of Los Angeles Department of Water and Power, Rob Hancock of the City of Los Angeles, Steven Lipshie and Ray Salehpour of the County of Los Angeles Department of Public Works.

Information for the wide variety of topics covered in Chapter Six was provided by numerous organizations across the State of California. For the section on dams, the authors extend very special thanks to Duane Buchholz, Mitchell Sakado, Craig Davis, and Roger Roux of City of Los Angeles, Department of Water and Power. The authors would also like to thank Robert Kroll of the Los Angeles County Department of Public Works, Tim McCrink of the California Division of Mines and Geology, Rick Mendoza of United Water Conservation District, Rich Sanchez of the California Division of Safety of Dams, and Jim Patrick of the California Department of Water Resources. Information pertaining to the failure of the Tapo Canyon Tailings Dam was generously provided by Phil Gillibrand of the P.W. Gillibrand Company, Thomas Robertson, Donald Jensen of the Jensen Design Group, Mason Redding and Doug Patay of Pacific Materials Lab, Jim Fischer of Ventura County, Dr. Lloyd Cluff of the Pacific Gas and Electric Company, Dr. Yoshi Moriwaki of Woodward-Clyde Consultants, and the United States Air Force. Data for the section on hillside fills was provided by numerous consultants and public agencies including the Governor's Office of Emergency Services, California Division of Mines and Geology, Los Angeles County Department of Building and Safety, County of Ventura Public Works Agency, Thomas Blake, Frank Denison, Fred Gebhardt, Robert Hollingsworth, James Krohn, Mark Mackowski, Clay Masters, Mark Swiateck, and Steven Watry. The authors of the section on earth retaining structures are grateful to Gary Garofalo, Office of Geotechnical Engineering, and to Kirsten Stahl, District 7 of the State of California Department of Transportation for their support in gathering the information presented in this section of the report. The authors of the section on solid waste landfills would like to thank Pete Mundy of CDM Federal Programs, Robert Anderson, John Clinkenbeard and Darryl Petker of the California Integrated Waste Management Board, Dr. Ed Kavazanjan of Geosyntec Consultants, and Charles Dowdell of

the Los Angeles County Sanitation Districts, all of whom visited several of the sites mentioned in this article and generously provided their field reconnaissance data. In addition, the authors are grateful to Dean Affeldt of the PRA Group, Doug Corcoran of Waste Management, and Dean Wise of Browning-Ferris Industries, all of whom provided access to their sites in the days immediately following the earthquake. Also, special thanks are extended to Rod Nelson of the California Regional Water Quality Control Board and Neven Matasovic of Geosyntec Consultants. The authors of the various sections would also like to extend special thanks to William Gookin of U.C. Berkeley for his help in drafting several figures for the chapter.

The professional editorial services of Carol Cameron at EERC enabled the report to be printed and distributed in a timely manner. The editors would like to thank Susan Chang and William Gookin of U.C. Berkeley for their tireless efforts in helping to produce and finalize this report. Finally, the editors and authors would like to extend their sincerest gratitude to Alisa Stewart of Morrison-Knudson for her expertise and many long hours in preparing the maps comprising 37 key figures of this report.

Page Intentionally Left Blank

TABLE OF CONTENTS

Preface	i
Acknowledgements	iii
Chapter One: Introduction	1
Chapter Two: Seismology	7
2.1 General Seismology	7
2.2 Measured Tectonic Displacements	13
Chapter Three: Ground Motions and Local Site Effects	19
3.1 Introduction	19
3.2 Regional Geology and Implications for Ground Motions	19
3.3 Observed Ground Motions from the Northridge Earthquake	20
3.3.1 Strong Motion Station Locations	20
3.3.2 Maximum Horizontal Acceleration and Acceleration-Time Histories	21
3.3.3 Attenuation Relationships for MHA vs. Distance (free-field strong- motion stations)	33
3.3.4 Maximum Horizontal Acceleration vs. Maximum Vertical Acceleration ...	36
3.3.5 Calculated Response Spectra from Recorded Motions	39
3.3.6 Spectral Acceleration at One-Second Period	45
3.3.7 Comparison of Observed Free-Field Motions and Recordings from the Base of Structures	45
3.3.8 Comparison of MHA with the 1971 San Fernando Earthquake	45
3.4 Damage Patterns and the Effects of Local Site Conditions	49
3.4.1 Effects of Local Site Conditions	49
3.4.2 Computed Response Spectra at Strong Motion Stations Near Areas of Damage Concentration	63
3.4.3 Other Contributions to Localized Damage	67
3.5 Preliminary Analyses for the Sylmar-County Hospital Parking Lot Site	67
3.6 Summary	69

Chapter Four: Ground Failure	71
4.1 Introduction	71
4.2 San Fernando Valley Area	71
4.2.1 Introduction	71
4.2.2 Geologic and Groundwater Conditions	71
4.2.3 General Damage Distributions	72
4.2.4 Granada Hills Area	75
4.2.5 Northridge-Reseda-Canoga Park Area	82
4.2.6 Sherman Oaks Area	85
4.2.7 City of San Fernando	87
4.2.8 Van Norman Complex and Vicinity	87
4.2.9 Hansen Dam Area	97
4.3 Simi Valley	97
4.4 Santa Clara River Area	106
4.4.1 Introduction	106
4.4.2 Potrero Canyon	106
4.4.3 Santa Clarita	115
4.4.4 River Bank Areas Between Santa Clarita and Fillmore	123
4.5 Coastal Areas	123
4.5.1 Introduction	123
4.5.2 Santa Monica and Marina del Rey	125
4.5.3 Redondo Beach	129
4.5.4 Port of Los Angeles	135
4.6 Central Los Angeles Area	135
4.7 Miscellaneous Topics	141
4.7.1 Ground Failure Effects on Deep Foundations	141
4.7.2 Liquefaction of Evaporite Bearing Deposits	143
4.8 Summary	144
Chapter Five: Landslides	147
5.1 Introduction	147
5.2 Marine Terrace Deposits: Santa Monica and the Pacific Palisades	147

5.3 San Gabriel Mountains	151
5.4 Santa Susana Mountains, Big Mountain, and Simi Hills	152
5.5 Urban Los Angeles	156
Chapter Six: Performance of Geotechnical Structures	157
6.1 Introduction	157
6.2 Performance of Dams	157
6.2.1 General	157
6.2.2 Pacoima Dam	159
6.2.3 Lower San Fernando Dam	164
6.2.4 Upper San Fernando Dam	166
6.2.5 Los Angeles Reservoir Dam	170
6.2.6 Castaic Dam	175
6.2.7 Santa Felicia Dam	175
6.2.8 Encino Dam	176
6.2.9 Stone Canyon and Upper Stone Canyon Dam	176
6.2.10 Upper Franklin and Lower Franklin No. 2 Dams	178
6.2.11 Miscellaneous Embankment Dam Performance	179
6.2.12 Summary	179
6.3 Failure of Tapo Canyon Tailings Dam	179
6.3.1 General	179
6.3.2 Construction History	181
6.3.3 Description of Flow Slide	182
6.4 Hillside Structural Fills	190
6.5 Earth Retaining Structures	195
6.6 Solid Waste Landfills	199
6.6.1 Introduction	199
6.6.2 Operating Industries Inc. Landfill	202
6.6.3 Chiquita Canyon Landfill	210
6.6.4 Sunshine Canyon Landfill	218
6.6.5 Lopez Canyon Landfill	218
6.6.6 Other MSW Landfills	221
6.6.7 Summary	225

Chapter Seven: Summary and Conclusions 227

 7.1 General 227

 7.2 Ground Motions 227

 7.3 Ground Failure 228

 7.4 Landslides 229

 7.5 Geotechnical Structures 229

 7.6 Conclusions 230

References 231

Chapter One: Introduction

Although overall damage evaluations are not yet complete, the Northridge Earthquake of January 17, 1994 appears to have been the single most costly natural disaster in U.S. history. The main shock of the earthquake, which was centered near Northridge, occurred at 4:30 a.m. local time, and was assessed by the U.C. Berkeley seismographic station to have a moment magnitude of $M_w=6.7$. Damages resulting from the earthquake were widespread and included six sections of collapsed highway structures, thousands of damaged or destroyed residential and commercial structures, widespread disruption of utilities and other lifeline facilities in the epicentral region, a number of soil embankment failures, and numerous landslides.

The earthquake resulted in 61 deaths, many of these from the collapse of residential structures in the Northridge/Granada Hills area. The economic toll was also high, with the current damage estimates approaching roughly \$13 to 15 billion. Perhaps the most vivid examples of damage from this earthquake are the collapsed freeway structures, the catastrophic collapse of an apartment structure near the California State University at Northridge campus, the collapse of a multi-story parking structure at the California State University at Northridge, the partial collapse of portions of the Northridge Fashion Center, and the partial collapse of the Kaiser Permanente office building in Northridge. However, the effects of the earthquake were truly widespread and extend far beyond these few examples. Estimates by the Governor's Office of Emergency Services (OES) indicate that over 14,000 structures in 28 cities were damaged by the earthquake, and that approximately 2,900 of these were sufficiently damaged as to be unsafe for entry. In addition, over 414,000 families were temporarily displaced from their homes and applied for housing aid. Table 1.1 presents a summary of preliminary data regarding the approximate distribution of damages to structures in the jurisdictions most affected by the earthquake.

The general geologic conditions of the affected area are shown in Figure 1.1, while Figure 1.2 presents a satellite view showing the region's general morphology. As can be seen from these figures, the affected area consists of wide mountainous regions separated by broad alluvial basins. Bedrock in the mountainous areas is heavily faulted and folded, and is primarily derived from sedimentary, marine, or volcanic sources. Basins have been filled in over Upper Pleistocene and Holocene time by alluvial sediments, which may reach great depths in some areas. Basin areas strongly impacted by the Northridge Earthquake included the San Fernando Valley, the Los Angeles Basin, and Simi Valley.

This report presents a preliminary overview of the principal geotechnical aspects of this earthquake including (1) the characteristics of the ground motions and consequent damage patterns, (2) the occurrences of ground failure and landslides, and (3) the performance of geotechnical structures including dams, structural fills, earth retaining structures, and solid waste landfills. A general overview of some of the principal locations of landslides and ground failure (e.g. liquefaction and dynamic ground compaction) is presented in Figure 1.3. Also notable from a geotechnical standpoint was the influence of local site conditions on the severity of structural damages. Although much of the damage was in the highly developed epicentral area where intense shaking levels would be expected, "site effects" appear to have contributed to additional significant concentrations of damage in communities outside of the San Fernando Valley such as Hollywood, Central Los Angeles, and Santa Monica.

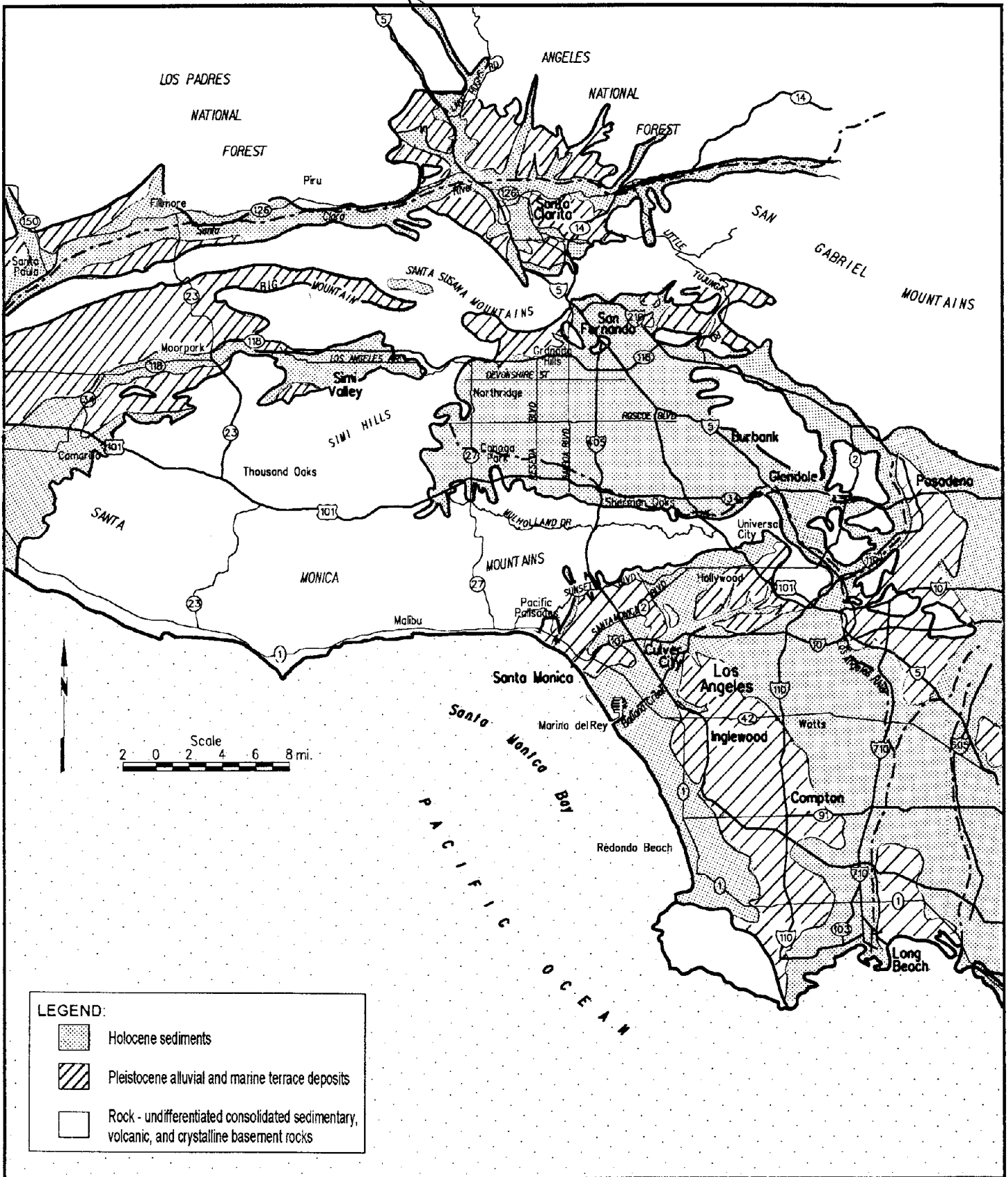


Fig. 1.1: Generalized geologic conditions in the Los Angeles Area
 (Source: Los Angeles County, 1990; California Division of Mines and Geology, 1969)

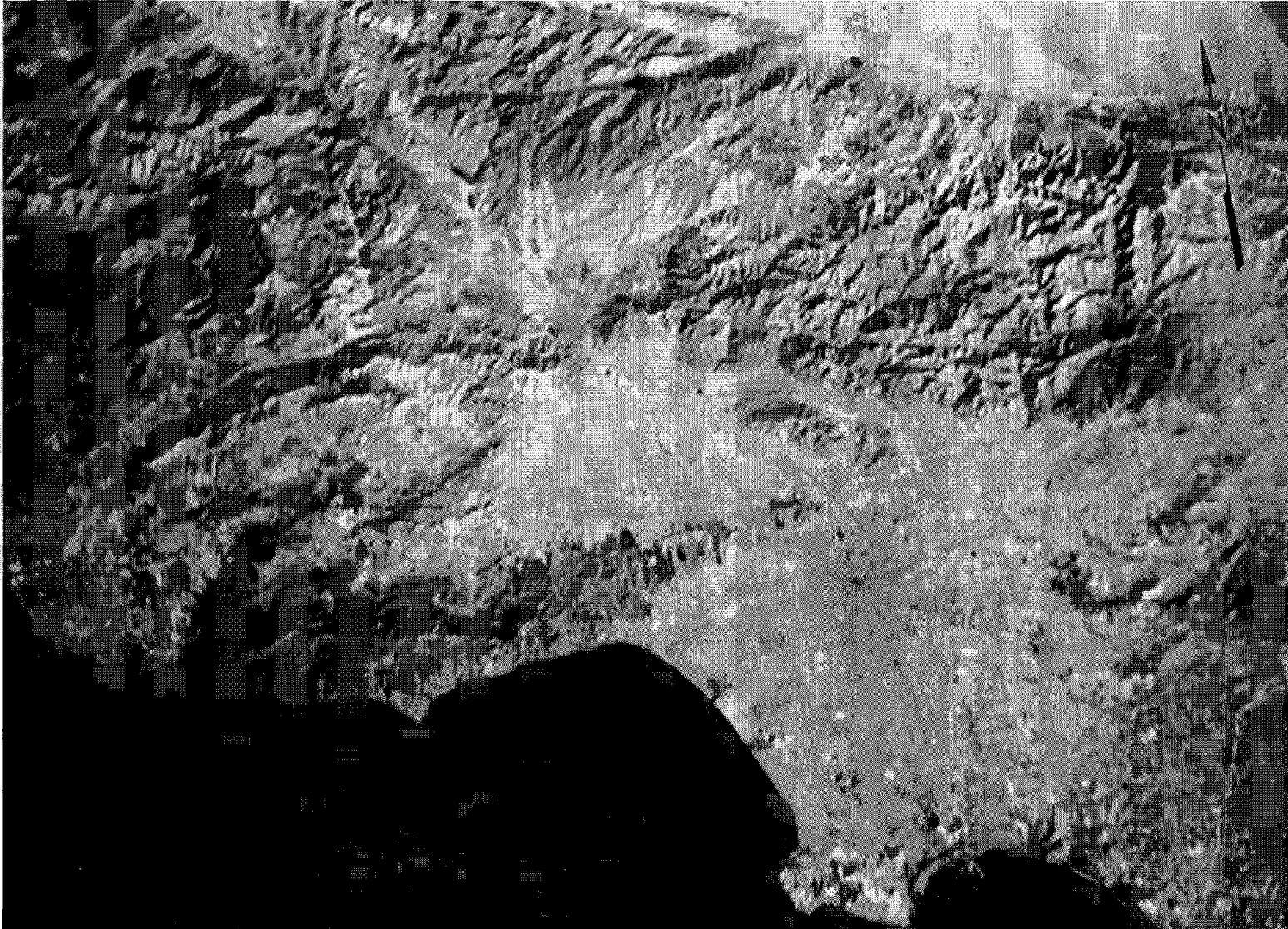


Fig. 1.2: Satellite view of the Los Angeles Area (photo courtesy of Dr. John Tinsley, U.S. Geological Survey)

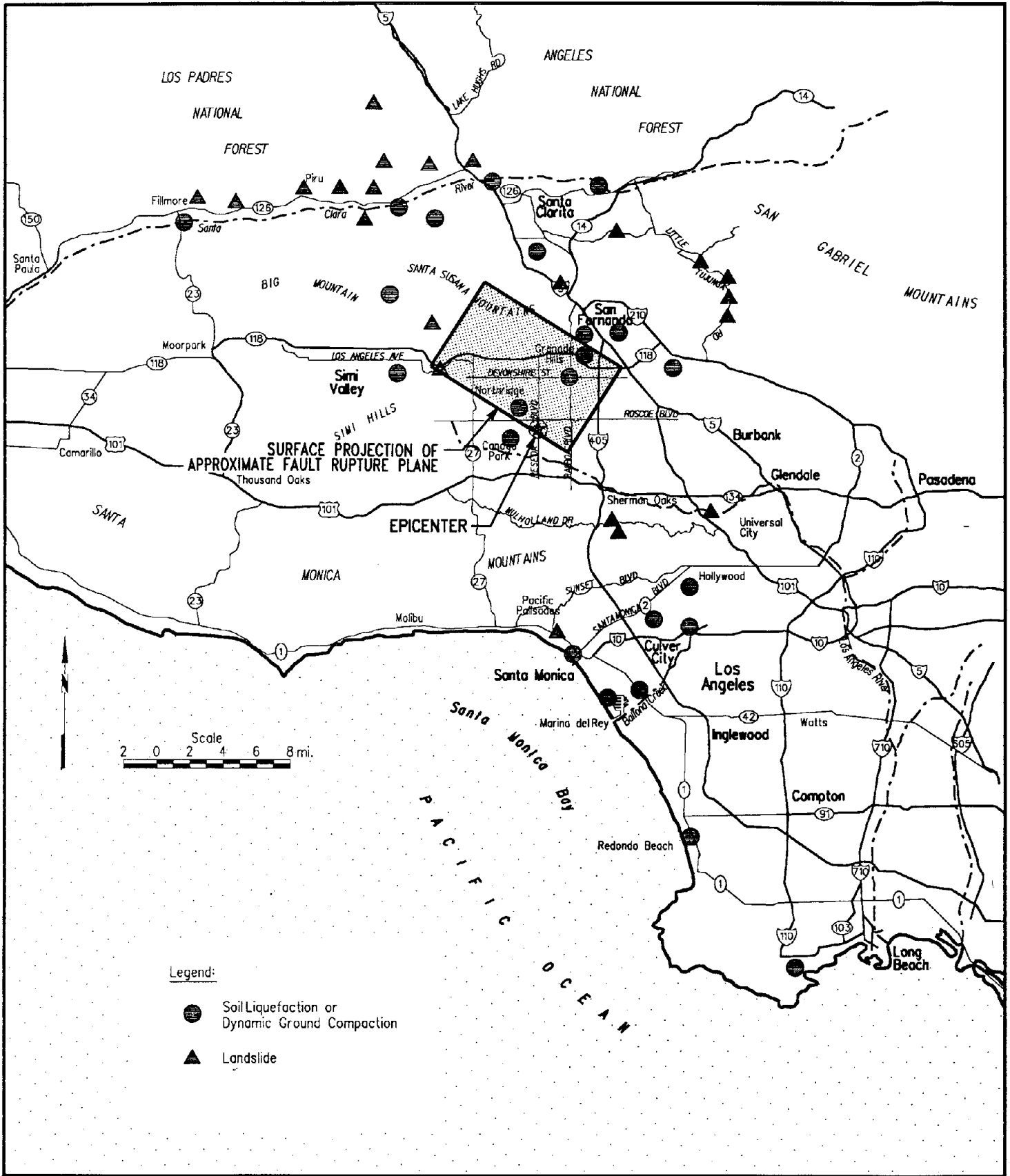


Fig. 1.3: Principal locations of ground failure and landslides induced by the Northridge Earthquake

Table 1.1: Damage statistics from the Northridge Earthquake (OES, as of 3/31/94)

Jurisdiction	Damaged Buildings	Severely Damaged Buildings	Damaged Commercial or Industrial Buildings
Agoura Hills	1	1	0
Alhambra	13	5	1
Anaheim	2	1	0
Beverly Hills	0	0	17
Commerce	1	1	N/A
Burbank	133	36	N/A
Calabasas	319	4	N/A
Culver City	42	15	15
Fillmore	501	200	29
Glendale	50	37	16
Hidden Hills	50	1	0
Los Angeles City	10,899	2058	1550
Los Angeles County	152	49	40
Manhattan Beach	259	5	N/A
Moorpark	27	3	3
Pasadena	28	11	8
San Fernando	293	147	40
Santa Clarita	350	124	83
Santa Monica	423	107	111
Santa Paula	22	0	N/A
Simi Valley	526	60	223
South Gate	3	2	2
Thousand Oaks	186	57	4
Ventura County	71	22	7
Vernon	3	2	3
West Hollywood	13	4	1
Westlake Village	0	0	1
Whittier	7	1	5
Total	14,374	2953	2159

This report first provides an overview of the seismological aspects of the Northridge Earthquake in Chapter Two, including a discussion of the source mechanism and measured tectonic displacements resulting from the fault rupture. Chapter Three provides an overview of both strong ground motions and the effects of local site conditions on these ground motions, with emphasis on the possible influence of both soil amplification and deep basin effects. Chapter Four describes the principal occurrences of ground failure resulting from the earthquake. For the purpose of this report, the term "ground failure" refers to permanent ground deformations caused primarily by liquefaction and ground compaction. Landsliding and other types of slope movements are treated separately in Chapter Five. Chapter Six presents an overview of the performance of various geotechnical structures including dams, hillside structural fills, earth retaining structures, and solid waste landfills.

Lastly, a summary of the geotechnical features of the Northridge Earthquake is presented in Chapter Seven. Many of the types of damage observed from this earthquake came as little surprise to the engineering community, whereas others were not well documented previously. Great strides have been made in recent years in both state-of-the-art and state-of-practice procedures for recognition and mitigation of seismic geotechnical hazards such as site effects and soil liquefaction. It is hoped that findings from this and previous earthquakes will continue to stimulate research to improve public safety in future earthquakes.

Chapter Two: Seismology

by Barbara Romanowicz, Patricia Thomas, and Jonathan D. Bray

2.1 General Seismology

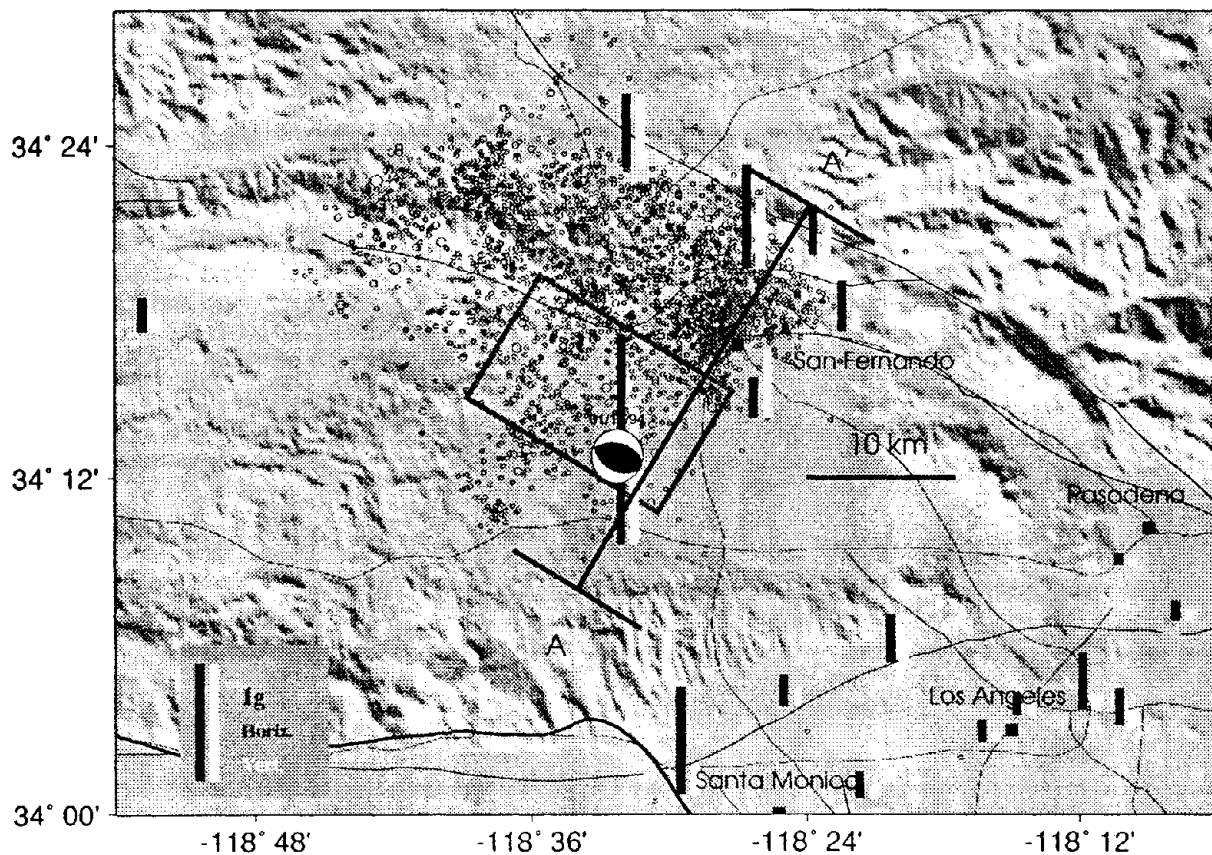
The Northridge Earthquake of January 17, 1994 occurred at 4:30 am (PST) under the north-western end of the San Fernando Valley, Los Angeles. The epicenter location determined by the U.S. Geological Survey is 34.213 N and 118.537 W, with a focal depth of 18.4 km. A moment magnitude of $M_w=6.7$ was estimated by the U.C. Berkeley Seismographic Station from the modelling of broadband records for the main shock from the TERRAscope network and the Berkeley Digital Seismic Network (BDSN). This is in good agreement with the local magnitude $M_L=6.7$ as determined by Caltech.

The Northridge Earthquake took place in a complex, transitional region of predominant south dipping reverse faults to the west (Yeats, 1994) and north dipping structures to the east (Heaton, 1982; Hauksson and Jones, 1989). It occurred on a south dipping fault, adjacent to the north dipping structures involved in the 1971 San Fernando Earthquake ($M_w=6.6$). The aftershock distribution clearly defines this structure at depths greater than 5 to 10 km (Figure 2.1). At shallower depths, the pattern is more complex and the rupture did not extend all the way to the surface. The aftershocks define a wedge-shaped volume with no clear planar structures (Hauksson et al., 1994), and the rupture did not make it to the surface. It remains unclear whether this earthquake occurred on an eastward extension of the Oak Ridge Fault (Yeats, 1994; Williams et al., 1994, Figure 2.2), a previously unknown "blind thrust" which is truncated at depth by the north dipping Sierra Madre fault system (Hauksson et al., 1994) or a "blind" back thrust of the Elysian Park system (Davis and Namson, 1994).

The main shock mechanism is well constrained, with both planes striking approximately 10° north of west and dipping approximately 45° (Figure 2.3). Results of the empirical Green's function deconvolution analysis at U.C. Berkeley reveal a source duration of approximately 6 seconds (Figure 2.4), with evidence for directivity towards the north, indicating that the event ruptured primarily updip. The thrust mechanism of this earthquake and the direction of rupture propagation may be partly responsible for the unusually strong shaking experienced in some areas (Figure 2.1).

There is nothing unusual about the time sequence of aftershocks for the Northridge Earthquake (Figure 2.5). The sequence had 6 aftershocks of magnitude greater than 5, the largest of which was $M_w=6.0$, and had a similar mechanism to the main shock. A number of these events occurred in the western half of the aftershock zone at relatively shallow depths and may have contributed to the observed geodetic displacement field, which is underpredicted at sites in the Ventura basin when models obtained using only surrounding sites are considered (Hudnut et al., 1994). Preliminary moment tensor solutions were obtained at the U.C. Berkeley Seismographic Station using two regional methodologies, namely time domain inversion of three-component waveforms (Dreger and Helmberger, 1993) and inversion of regional surface wave amplitude and phase spectra (Romanowicz et al., 1993) in nearly real time. Data from both the BDSN and TERRAscope were used in the

A) Northridge Earthquake of January 17, 1994
 Mainshock mechanism, aftershock distribution (01/17-01/31)
 and peak vertical and horizontal accelerations



B)

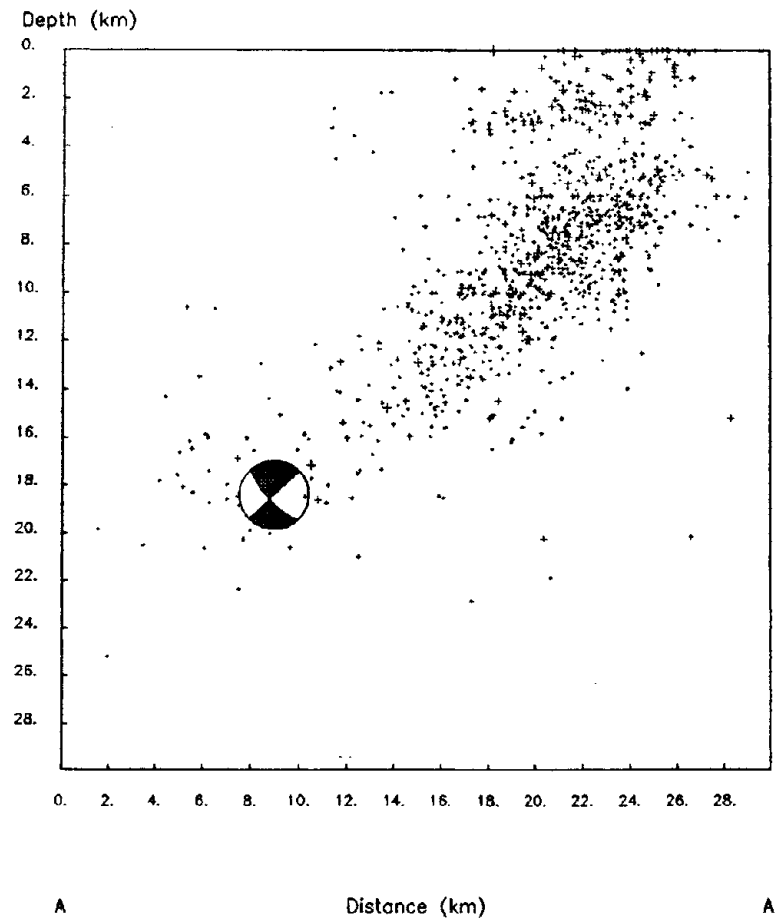


Fig. 2.1: A) Map view of Northridge sequence epicentral locations and peak accelerations for the main shock (Source: CIT catalog and CDMG). B) Depth cross along AA' in A)

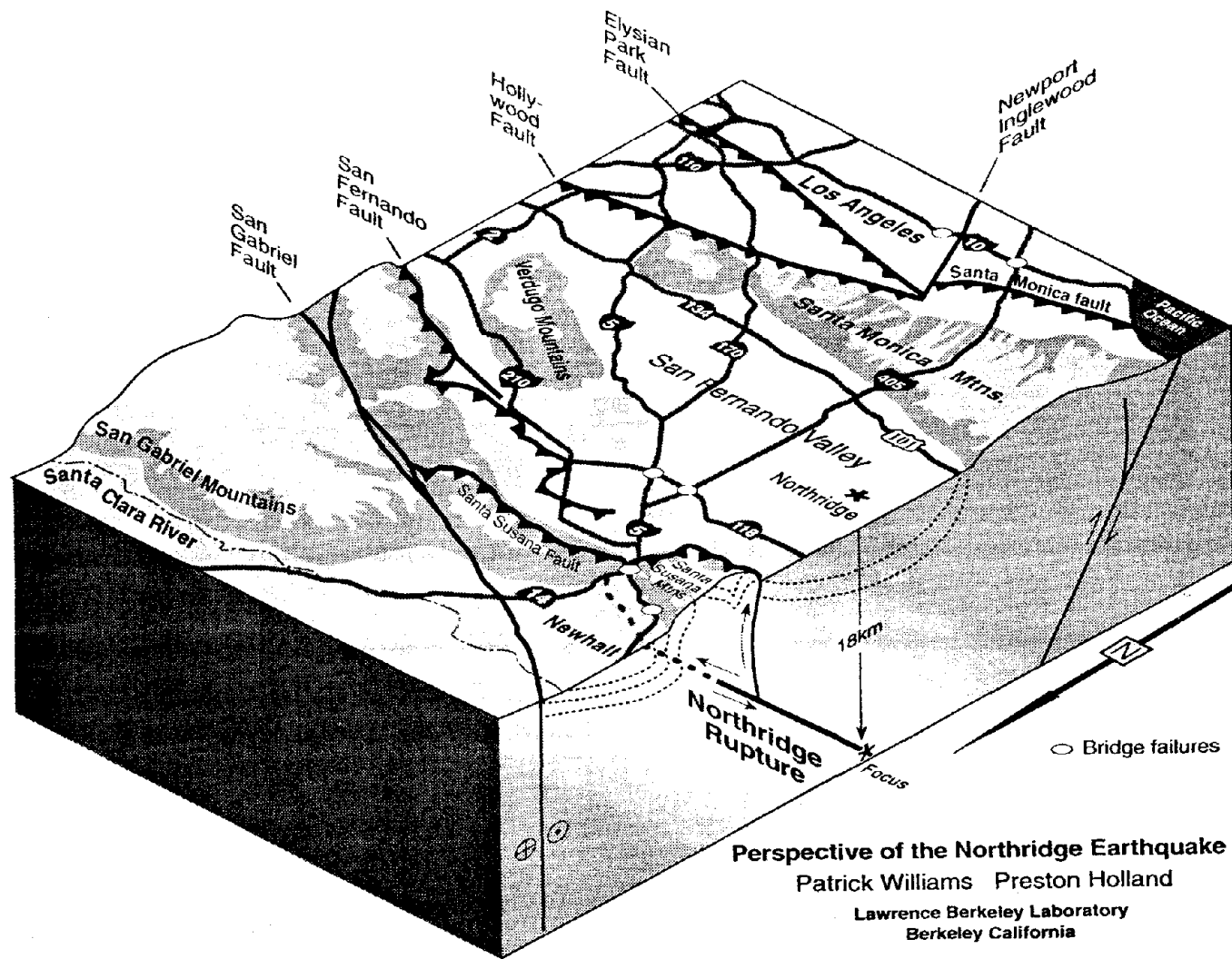


Fig. 2.2: Geologic model of the Northridge Earthquake. View is to the southeast. As compiled from the analysis of regional and local seismic data by U.C. Berkeley, USGS, and Caltech. The rupture began about 18 km below the surface, and propagated up to a depth of about 5 km. The fault plane dipped 40 to 45 degrees to the south, and projects to the northern margin of the Santa Susana Mountains. Sedimentary rocks are closely folded in the rupture area, reflecting north-verging compressional shortening of the Santa Susana Mountains. Some of the extensional fractures observed in these mountains were likely produced by the "bending-movement" growth of these folds.

January 17, 1994 Northridge Mainshock (Mw6.7)

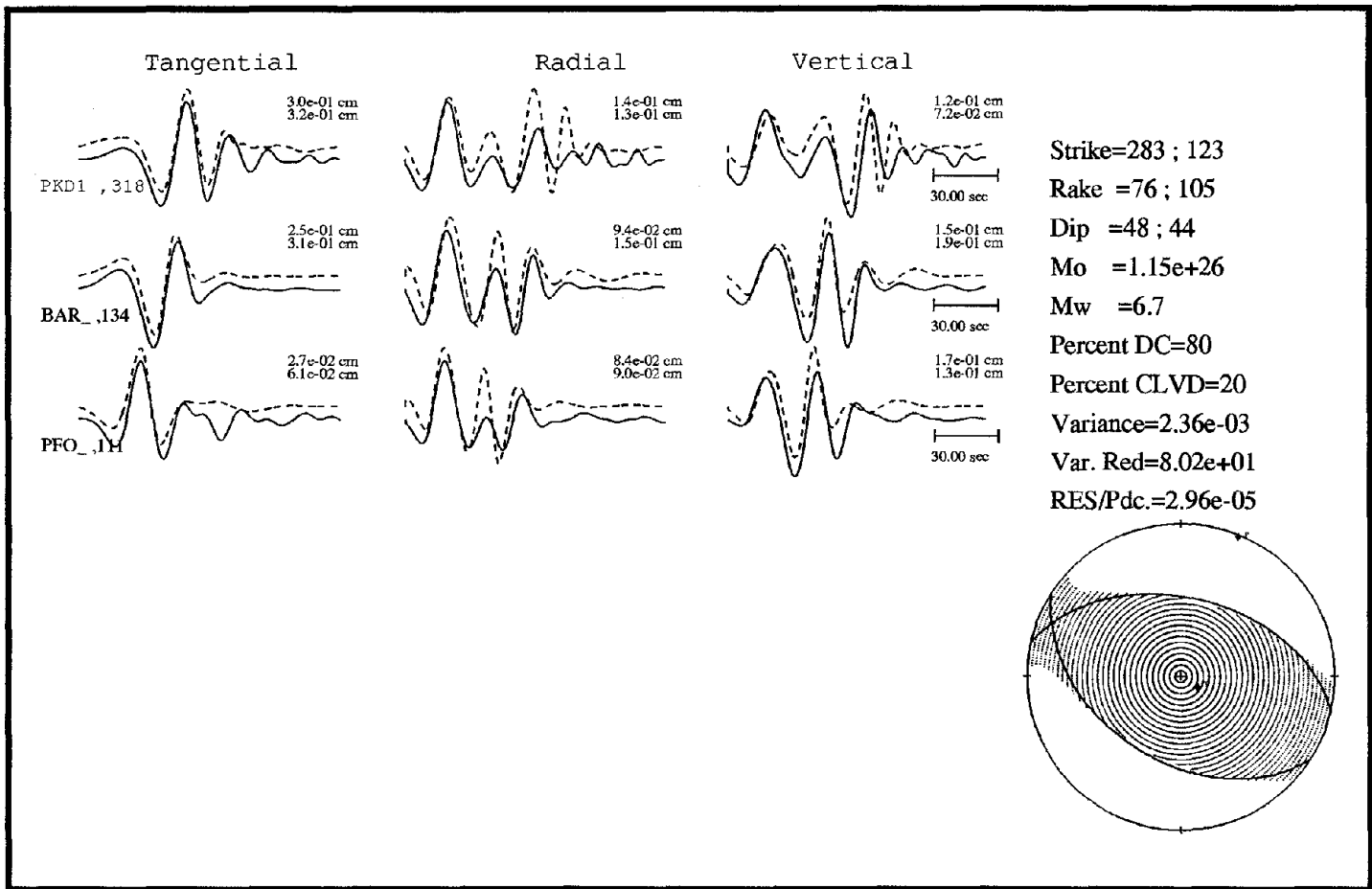


Fig. 2.3: Example of output from the time domain moment tensor inversion code. The data (solid) and synthetics (dashed) are bandpassed filtered between 0.01 and 0.05 Hz. The strike, rake, and dip for both possible nodal planes, the seismic moment (M_0), and moment magnitude (M_w) are given. (Contribution: D. Dreger)

Source Time Functions for the 9401171231 Northridge, Ca. Earthquake Estimated from Empirical Green's Function Deconvolution

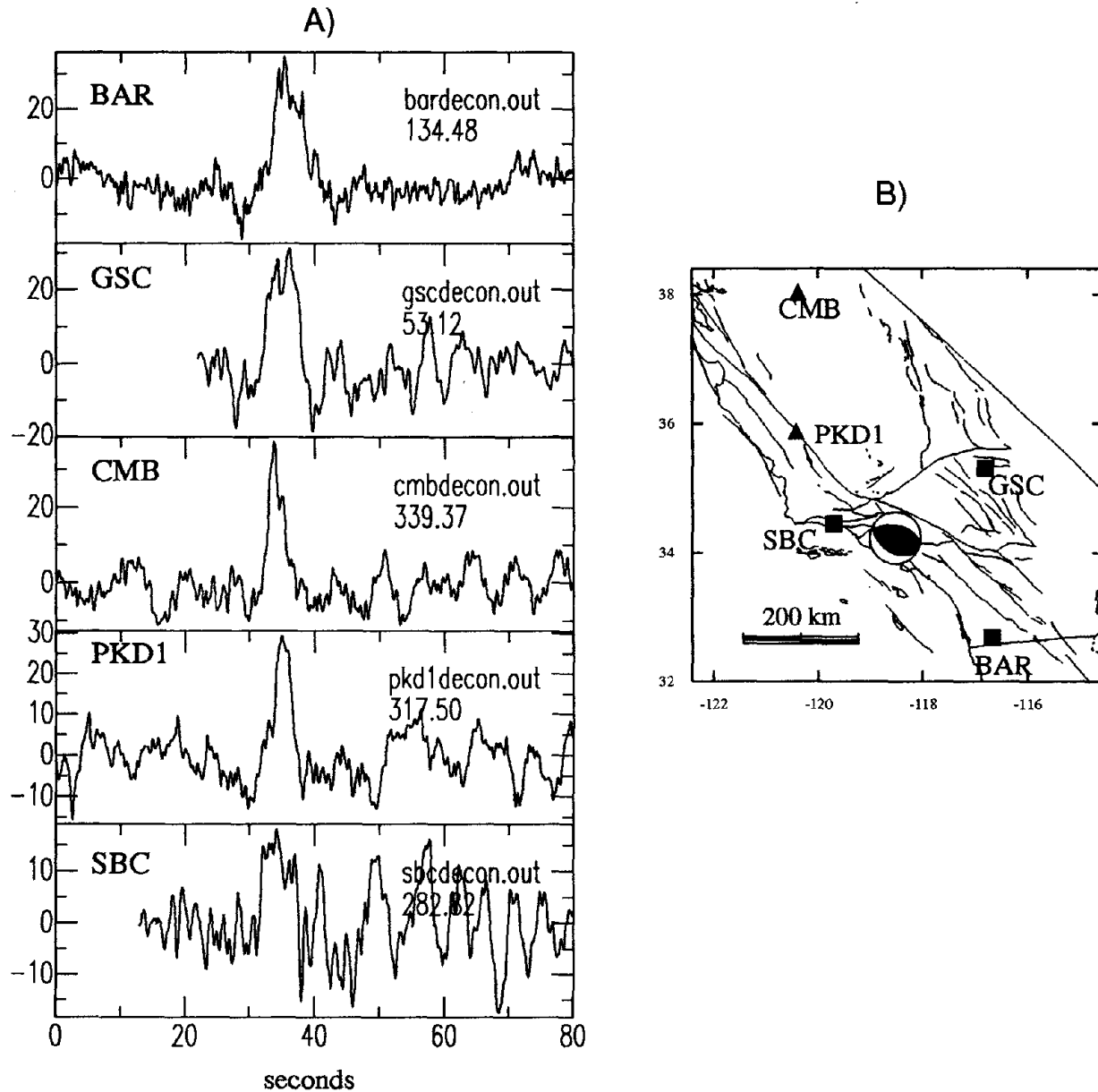


Fig. 2.4:

A) Source time function obtained by deconvolving the motions of a nearby collocated aftershock with a focal mechanism similar to that of the main shock. The deconvolution was performed in the spectral domain and the empirical Green's function spectra was corrected with 1% water level to minimize instability introduced during the deconvolution process. Stations BAR, GSC, and SBC reveal 6 second source durations. The duration at PKD1 is shorter (5.7 sec.) indicating a component of northward directivity during the earthquake rupture. Assuming a circular fault, a duration of 6 seconds gives a fault radius of 8.2 km. Considering the seismic moment obtained from inversion of complete waveforms (1.2×10^{26} dyne-cm) and a rigidity of 3.6×10^{11} dyne/cm², the average slip on the fault plane is estimated to be approximately 1.6 meters. A lower bound on slip is 66 cm based on the area of the after shock zone. B) Locations of stations used in the analysis. (Source: D. Dreger)

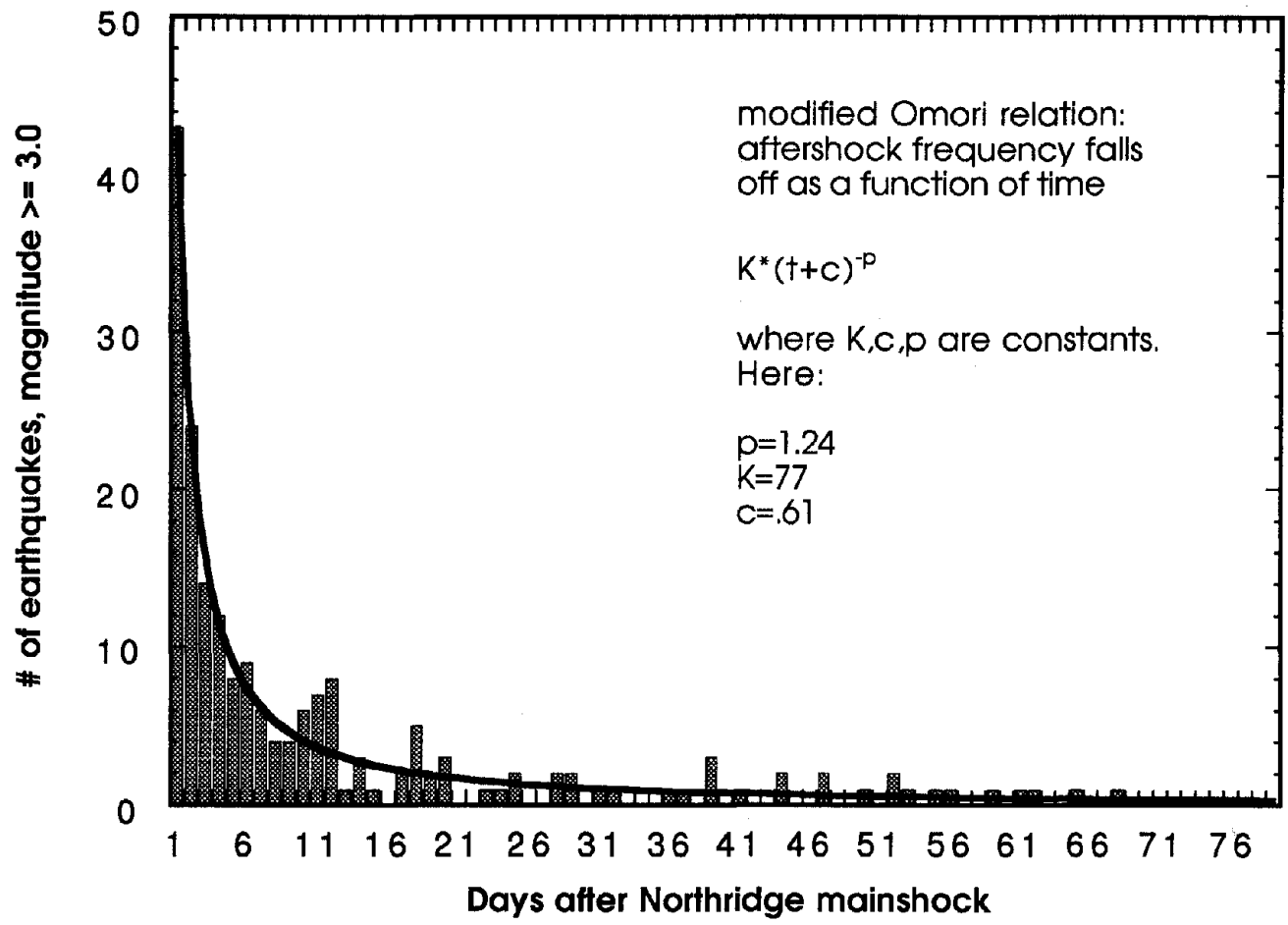


Fig. 2.5: Aftershock rate for January 17, 1994 Northridge Earthquake, from CIT catalog (mag > 3.0)

analysis. Figure 2.6 shows solutions for events ranging in size from $M_w=4.5$ to $M_w=6.7$. These events have principally west-southwest striking reverse mechanisms, however there are significant rotations of fault strike in the western half of the sequence, and there are several large strike-slip events. The most notable of the strike-slip events occurred on January 29, 1994 at shallow depth and caused the collapse of a previously damaged parking structure on the California State University Northridge campus. This event also produced 4 cm of southward displacement at the Oat Mountain GPS site (Donnellan et al., 1994). Oat Mountain was observed to move up and to the northwest prior to the occurrence of the January 29 aftershock. Further to the west, the GPS models fail to explain the westward motions, which could be due in part to large aftershocks contributing to the observed displacement field. The seismic moment and orientation of the largest aftershock (01/17/94 12:31; $M_w=6.0$) provide an additional 2 cm to the predicted displacements, but they still fall short of explaining the observed motions in the Ventura basin (A. Donnellan, 1994).

The Northridge Earthquake is the latest, and so far the largest, in a series of significant earthquakes that have occurred since 1987 in this part of the Transverse Ranges. The largest of these were the 1987 Whittier Narrows Earthquake ($M_w=6.0$) and the 1991 Sierra Madre Earthquake ($M_w=5.6$). All of these earthquakes occurred to the east of the Northridge epicenter and had similar thrust mechanisms. In contrast to the Northridge event, however, they occurred on north-dipping planes, as did the San Fernando (Sylmar) Earthquake of February 9, 1971 ($M_w=6.6$). The latter occurred at a depth of 13 km (Heaton and Helmberger, 1979; Langston, 1978; Hanks, 1974) on a previously unmapped fault, and surface rupture was found in a zone directly to the east of the surface projection of the Northridge fault plane.

All of these earthquakes are expressions of the north-south compressive deformation occurring across the Transverse Ranges of southern California. This deformation results from the convergence across the "big bend" of the San Andreas fault system between Gorman and Cajon Pass.

2.2 Measured Tectonic Displacements

Current technology enables precise measurements of the earth's surface relative, to an absolute datum, to be made with the use of satellites. The global positioning system (GPS), originally developed for military use, has been applied to study the deformation of the earth's crust. Along most of the California coast, the Pacific Plate is moving north approximately one centimeter per year relative to the North American Plate. This movement essentially occurs continuously, causing strain to build up over time on plate contacts (faults) due to inter-plate friction. When the accumulated strain is suddenly released in the form of an earthquake, pronounced localized displacements of the plates occur in the vicinity of the ruptured fault segment. In 1991, through a cooperative effort between state and federal agencies, the global positioning system was used to tie 260 GPS measurements together to develop the California High Precision Geodetic Network (HPGD). The minimum accuracy for these points was 1 part per million. This is a 3-dimensional network, which can provide constraints for smaller surveys. It allows scientists to improve their understanding of plate tectonics, and engineers to study the effects of seismically-induced permanent ground

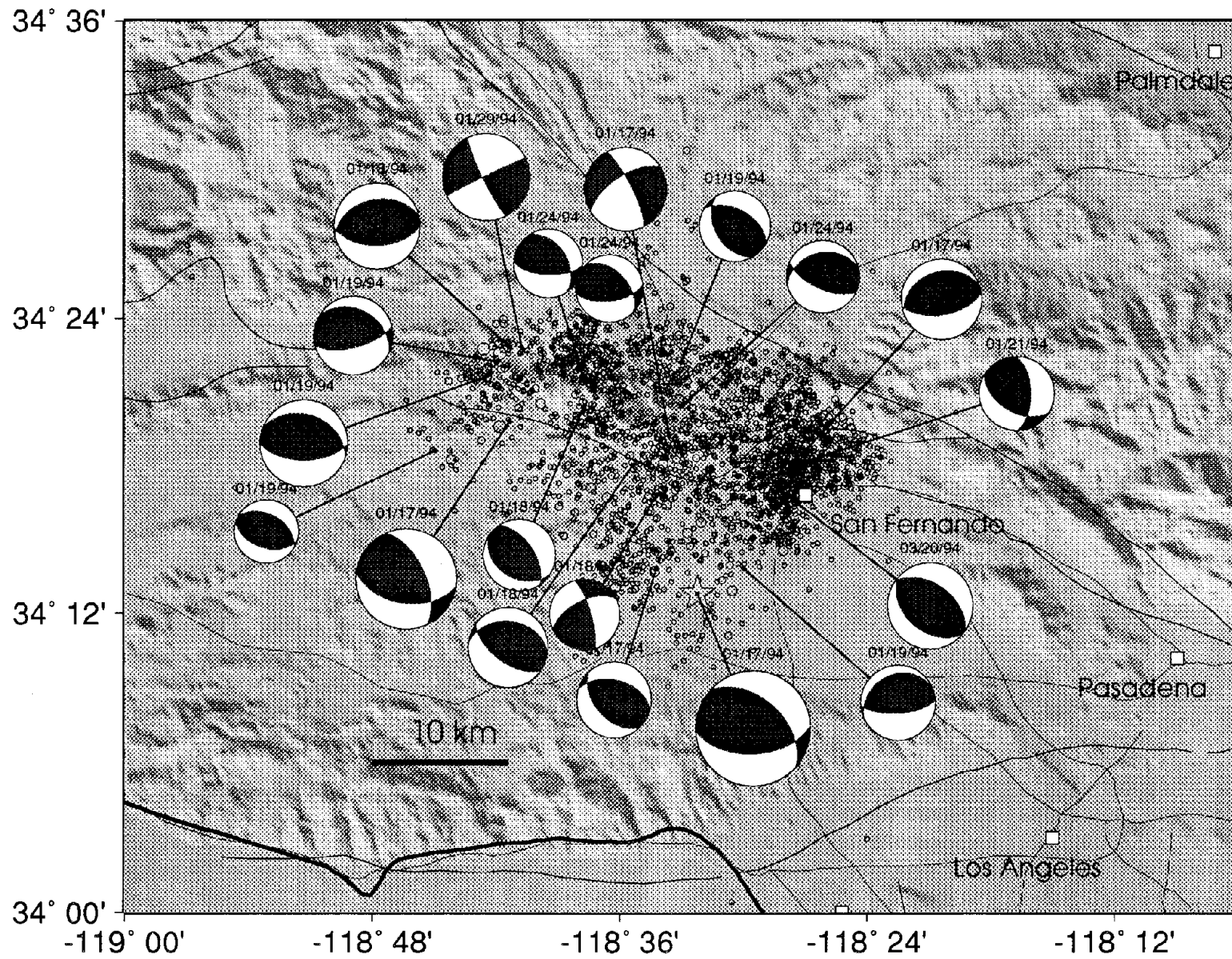


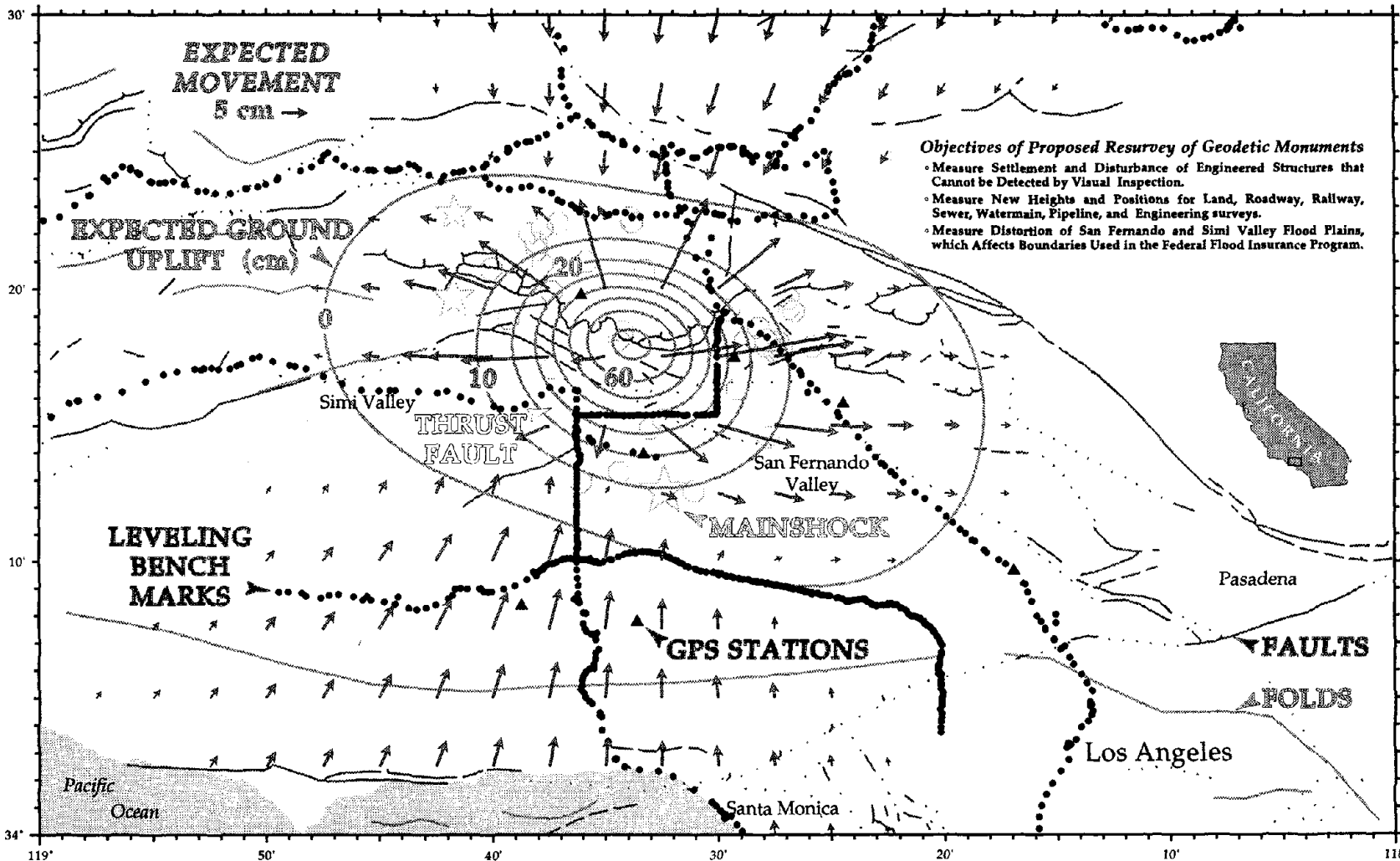
Fig. 2.6: Moment tensor solutions obtained from regional surface waves spectra for events ranging from M_W 4.5 to M_W 6.7. (Contribution: M. Pasyanos)

displacements on structures.

During the first days following the Northridge event, the U.S. Geological Survey (USGS) obtained GPS data from 12 locations throughout the Los Angeles area. This data was used in an elastic half-space model of the earth's crust to predict the ground displacements resulting directly from the fault rupture throughout the Los Angeles basin. Contours of the expected vertical ground movements and vectors of expected horizontal displacements are shown in Figure 2.7, prepared by Grant Marshall and Ross Stein of the USGS. The USGS has obtained funding from the Federal Emergency Management Agency and the California State Office of Emergency Services to re-level roadway corridors and other monuments. This will enable the measurement of ground movements in areas near damaged structures. The ground movement data will also record the general distortion of the San Fernando and Simi Valley flood plains, which affects boundaries used in the Federal Flood Insurance program (Grant Marshall, 1994).

The California Department of Transportation, in cooperation with the National Geodetic Survey, has also analyzed GPS data to obtain preliminary estimates of the tectonically-induced displacements which occurred during and shortly following the Northridge event. An unordered survey for investigative purposes only was performed at the end of February to delineate the boundaries of the area where deformation occurred (Jay Satalich, 1994). Ninety GPS stations were used, including fifteen locations in the California HPGN. Station coordinates acquired during 1992 were then updated to reflect what they would have been at the time of the new survey had the earthquake not occurred. The corrections were performed using the Horizontal Time Dependent Positioning Program (HTDP-CA-91), a program developed by Dr. Richard Snay at the National Geodetic Survey, which models secular crustal motion. The difference between the updated 1992 coordinates and the new coordinates measured after the Northridge Earthquake gives displacements due solely to the earthquake and aftershocks which occurred during the following month. Approximate horizontal and vertical displacements are shown on Figures 2.8 and 2.9.

It should be noted that the measured displacements are consistent with the rupture sequence mechanism discussed in Section 2.1. In particular, the displacement vectors indicate a convergence of the earth's crust at the approximate location of the epicentral region. Moreover, site-specific ground deformation patterns are being analyzed to evaluate the effects of ground movements on the seismic performance of long structures, such as bridges. The California Department of Transportation recently completed a survey at the site of the collapsed Highway 14 - Interstate Highway 5 interchange, which was performed in part to investigate the possibility that differential movements of the bridge supports and/or abutments may have contributed to the damages. However, the results of this survey are not yet available.



SOURCES:
 United States Geological Survey
 California Institute of Technology
 University of California Riverside
 City and County of Los Angeles
 Federal Emergency Management Agency
 Southern California Earthquake Center
 National Geodetic Survey
 Caltrans

The most damaging earthquake in U.S. history struck the northern flank of the Los Angeles basin on January 17. The Northridge earthquake occurred on an inclined thrust fault rooted under the San Fernando Valley. The earthquake raised the mountains by an average 40 cm (>1 foot). This is the fifth in a series of magnitude > 5 earthquakes to strike the northern Los Angeles basin since 1987. All of these earthquakes have been related to a broad system of thrust faults that accommodate compression and produce uplift of the ranges, and subsidence of the Los Angeles basin.

Prepared by Grant A. Marshall
 with assistance by Ross S. Stein
 gmarshall@isd.mnl.wr.usgs.gov
 rstein@isd.mnl.wr.usgs.gov

17 February 1994

Fig. 2.7: Predicted contours of tectonic ground displacements induced by the Northridge Earthquake (figure and data courtesy of Grant Marshall and Ross Stein, U.S. Geological Survey)

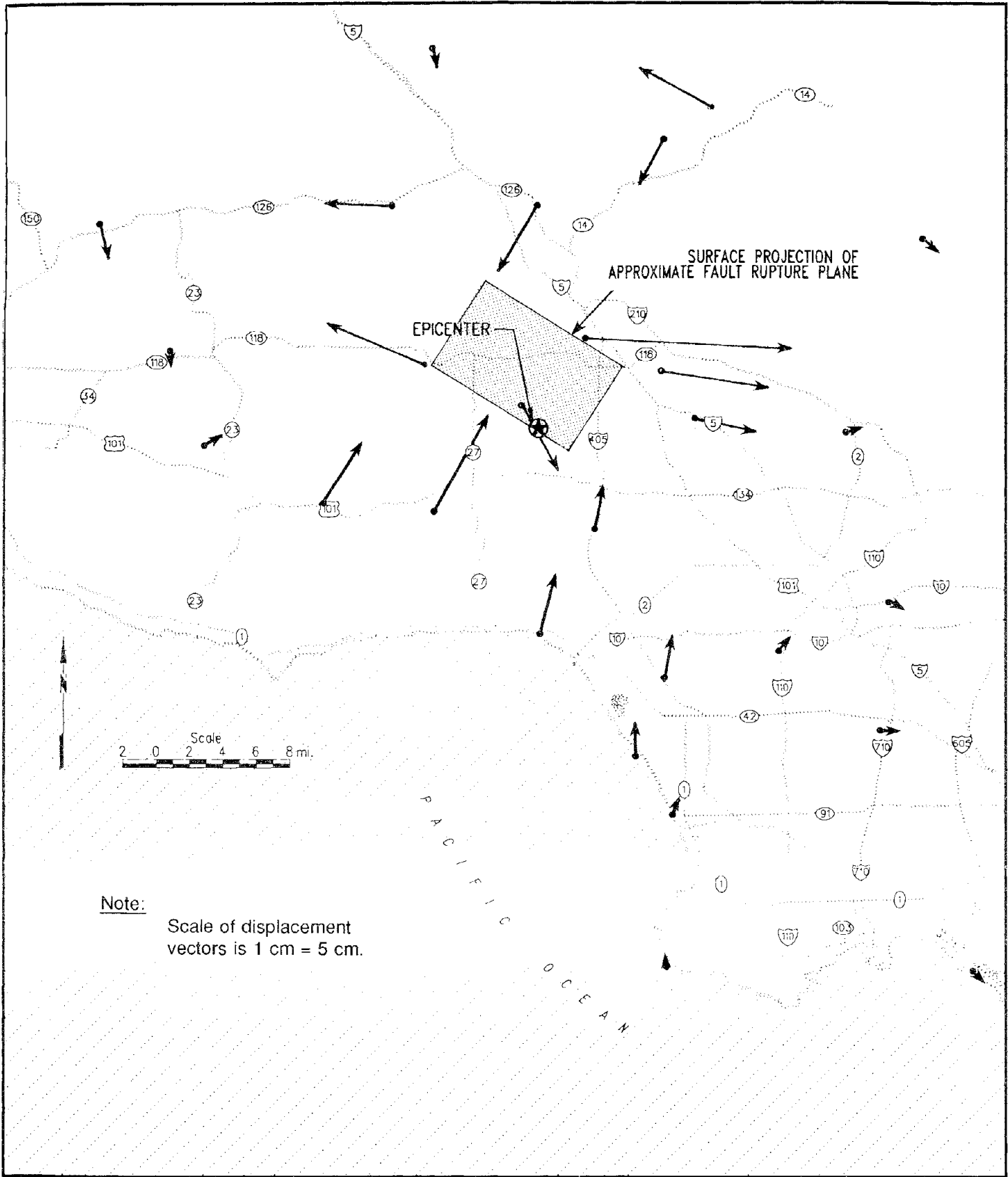


Figure 2.8: Approximate horizontal ground displacements (data courtesy of California Department of Transportation)

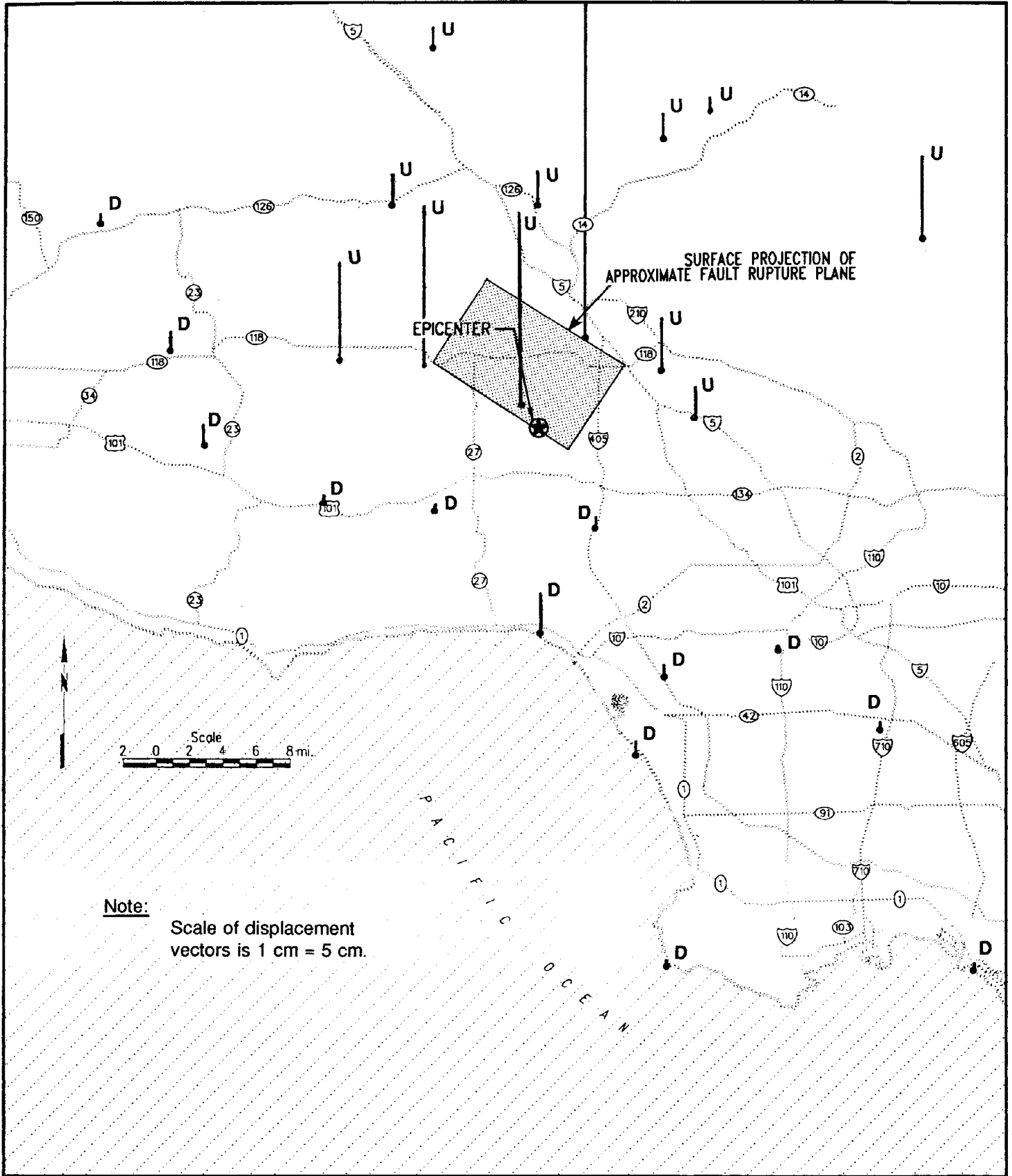


Figure 2.9: Approximate vertical ground displacements (data courtesy of California Department of Transportation)

Chapter Three: Ground Motions and Local Site Effects

by Susan W. Chang, Jonathan D. Bray, and Raymond B. Seed

3.1 Introduction

Ground motions from the 1994 Northridge Earthquake generated a large number of strong motion recordings from stations throughout the Los Angeles area. The dense array of strong motion stations captured much of the regional variations in ground motions, and the resulting data provides an excellent opportunity to evaluate the effects of local site conditions, as well as basin geometry, on ground response. In this chapter, ground motions recorded at numerous strong ground motion stations are evaluated and compared to existing attenuation relationships to assess whether the intensity and other characteristics of the recorded motions could have been predicted. The effects of geologic site conditions on the recorded motions are also discussed, followed by a comparison between calculated response spectra from strong motion recordings and current 1991 Uniform Building Code (UBC) design spectra. A brief discussion of ground motions recorded during the 1971 San Fernando Earthquake, which affected much of the same geographic area, is included for comparison.

As in many previous earthquakes (e.g. 1985 Mexico City, 1989 Loma Prieta), the damage patterns from the Northridge Earthquake indicate that geotechnical factors, including both "site effects" and basin response, contributed significantly to the nature and severity of ground shaking. The influence of these effects from the Northridge event is illustrated by a comparison between the geographic distribution of heavily damaged structures and (a) contours of recorded ground accelerations and (b) mapped surficial geology. Other factors that may have led to localized concentrations of damage are also discussed, and the results of preliminary seismic site response analyses for a near-field alluvial site are presented.

3.2 Regional Geology and Implications for Ground Motions

An overview of the general geology of the area is presented in Figure 1.1, shown previously in Chapter One. A brief discussion of the regional geology of the affected areas follows.

The Los Angeles Basin area is a structurally complex, folded and faulted region about 80 km (50 miles) long and 32 km (20 miles) wide. The crystalline basement complex rock forming the Los Angeles Basin is exposed in the Palos Verdes Hills and the Santa Monica Mountains, and the basin is filled in by as much as 9 km (30,000 feet) of sedimentary and middle Miocene volcanic rocks formed since the late Cretaceous time. The northwest trending basin is bounded by the Santa Monica Mountains and the Elysian, Repetto, and Puente Hills to the north and by the Palos Verdes Hills and the Pacific Ocean to the south. The thickness of Quaternary (Pleistocene and Holocene) deposits blanketing the area is at least 1 km (4000 feet) at some locations according to Yerkes et. al. (1965). The Holocene deposits include fine to very coarse grained stream channel, alluvial fan, flood plain, and dune deposits. The surficial Pleistocene deposits range from fine to very coarse grained alluvium

and marine terrace deposits.

The San Fernando Valley, located north of the Los Angeles Basin, is an east-west trending, fairly flat plain approximately 30 km (19 miles) long and 16 km (10 miles) wide. It is bounded on the north by the Santa Susana and the San Gabriel Mountains, on the east by the Verdugo Hills, on the south by the Santa Monica Mountains, and on the west by the Simi Hills. The valley is a faulted series of folds, and the rocks of the basement complex are overlain by as much as 4.5 km (15,000 feet) of Cenozoic and Mesozoic rocks. The maximum depth of the Quaternary alluvial valley deposits is unknown but probably extends to depths of about 1/2 km (1500 feet) according to the State Water Rights Board (1962). The surficial alluvial materials are generally Holocene stream channel, alluvial fan, flood plain, and dune deposits, with coarser materials predominating in the eastern portions of the valley.

Surficial shear wave velocities of the Quaternary alluvial materials throughout the Los Angeles area generally range from about 120 m/s (400 ft/s) to 300 m/s (1000 ft/s) at the surface and increase with depth. Upper Pleistocene and Holocene deposits of gravel, sand, silt, and clay vary considerably across the basin, but most of the soil sites in this region may be classified as either UBC site types S1 or S2. Thus, the 1991 UBC suggests that the effects of local soil conditions would not be expected to be overly important in the Los Angeles area, as most of the sites would have UBC site coefficients of 1.0 or 1.2.

A clear picture of the variation of the depth to bedrock throughout the Los Angeles area is not available at this time, although approximate depth to basement rock contours (Yerkes, 1965) and contours of the base of upper Pliocene rock (Conrey, 1967) have been compiled. It is known that basin effects and other topographic features may complicate the observed seismic response of sites within this region. Additional work is required to develop more precise and reliable estimates of the depth to bedrock at individual strong motion stations and to identify sites that may be significantly affected by underlying three-dimensional bedrock geometries.

For the purposes of obtaining an overview of seismic site response characteristics, the major geologic units of the Los Angeles and San Fernando areas can be categorized as (1) bedrock sites, (2) stiff shallow soil sites, and (3) deep alluvial sites; however, this report will only generally differentiate between rock and soil sites since the depth of sediments at many of the strong ground motion stations is not yet known.

3.3 Observed Ground Motions from the Northridge Earthquake

3.3.1 Strong Motion Station Locations

Several agencies, including the California Division of Mines and Geology Strong Motion Instrumentation Program (CSMIP), the U.S. Geological Survey (USGS), and the University of Southern California (USC) each maintain relatively extensive strong motion instrumentation networks in the affected region. Smaller groups of stations are maintained by Caltech, Southern California Edison, the Los Angeles Department of Water and Power (LADWP), the California Department of Water Resources (CDWR), and other agencies.

Figure 3.1 shows the locations of strong motion stations belonging to CSMIP, USGS, USC, and selected stations from LADWP and CDWR located in the region of interest. The surface projection of the approximate fault rupture plane is also shown in Figure 3.1. The fault rupture plane used in this report is the uniform slip model defined by the U.C. Berkeley Seismographic Station (Dreger, 1994). The plane has a strike of 122 degrees and dips to the south at 44 degrees. The along-strike width is 16 km and the down dip width is 14 km; the depth to the top of the plane is about 10 km.

In Figure 3.2, these stations are identified as rock or soil sites, and in Figure 3.3, they are identified as being either "free-field" stations or stations at the bases of structures. It should be noted that the geologic site conditions for the USGS stations were determined by plotting the station coordinates on geologic maps; the site conditions for the remaining stations were designated by the owner/agency. The determination of whether a station could be considered as a free-field station was based on descriptive data and personal correspondence with the various agencies and consulting firms involved.

Strong motion stations recorded maximum horizontal accelerations (MHA) of greater than 0.01g at distances of up to approximately 250 km from the fault rupture plane. The free-field instrument on rock closest to the fault rupture plane (excluding the USC stations, for which only preliminary data has been released to date) was located at the west abutment of the Los Angeles Reservoir (LADWP), approximately 10 km from the primary fault plane, where a MHA of 0.43g was recorded. The largest free-field acceleration recorded on rock (aside from the Pacoima Dam left abutment record) was 0.49g recorded at the Los Angeles 7-story University Hospital grounds (CSMIP station), 36 km southeast of the epicenter and 34 km from the primary fault plane. The free-field instrument on soil closest to the fault rupture plane was located at the Jensen Filtration Plant generator building grounds (USGS station) at a distance of about 12 km northeast of the epicenter and 10 km from the primary fault plane; a MHA of 0.98g was recorded at this site. The largest ground acceleration recorded was a peak horizontal acceleration of 1.82g, recorded at the Tarzana-Cedar Hill Nursery (CSMIP station). Tarzana is a free-field station situated on a small hill of thin alluvium over rock at a distance of approximately 17 km from the fault rupture surface.

3.3.2 Maximum Horizontal Acceleration and Acceleration-Time Histories

Contours of maximum horizontal ground acceleration are presented in Figure 3.4 along with the location of the surface projection of the approximate fault rupture plane. All strong motion stations for which ground response data were available, including stations outside of the region shown in Figure 3.1, were used to develop these contours, except for the stations at Tarzana-Cedar Hill Nursery and the Pacoima Dam left abutment. The MHA's of 1.82g and 1.58g measured at the Tarzana and Pacoima Dam left abutment sites, respectively, were removed to lessen the distortion of the contours due to possible topographic effects at these sites. The acceleration contours were developed using the MHA values measured on both rock and soil sites and should thus be interpreted with caution; however, it appears that the contour lines are more closely spaced north of the fault rupture plane, indicating some northward directivity effects. Close contours in the Santa Monica area are due to the MHA of 0.90g measured at the Santa Monica City Hall grounds; however, it should be noted that

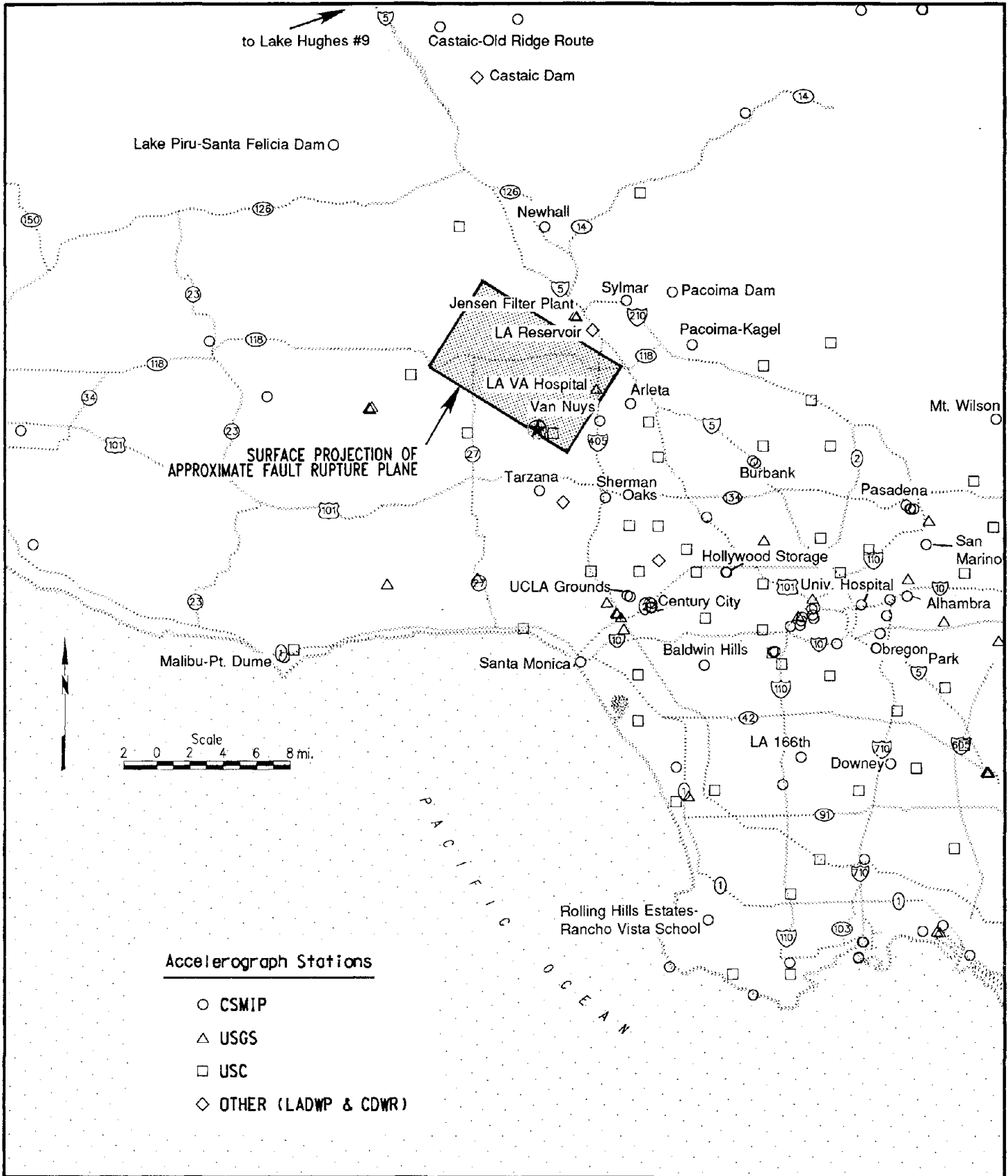


Fig. 3.1: Approximate locations of selected strong motion stations

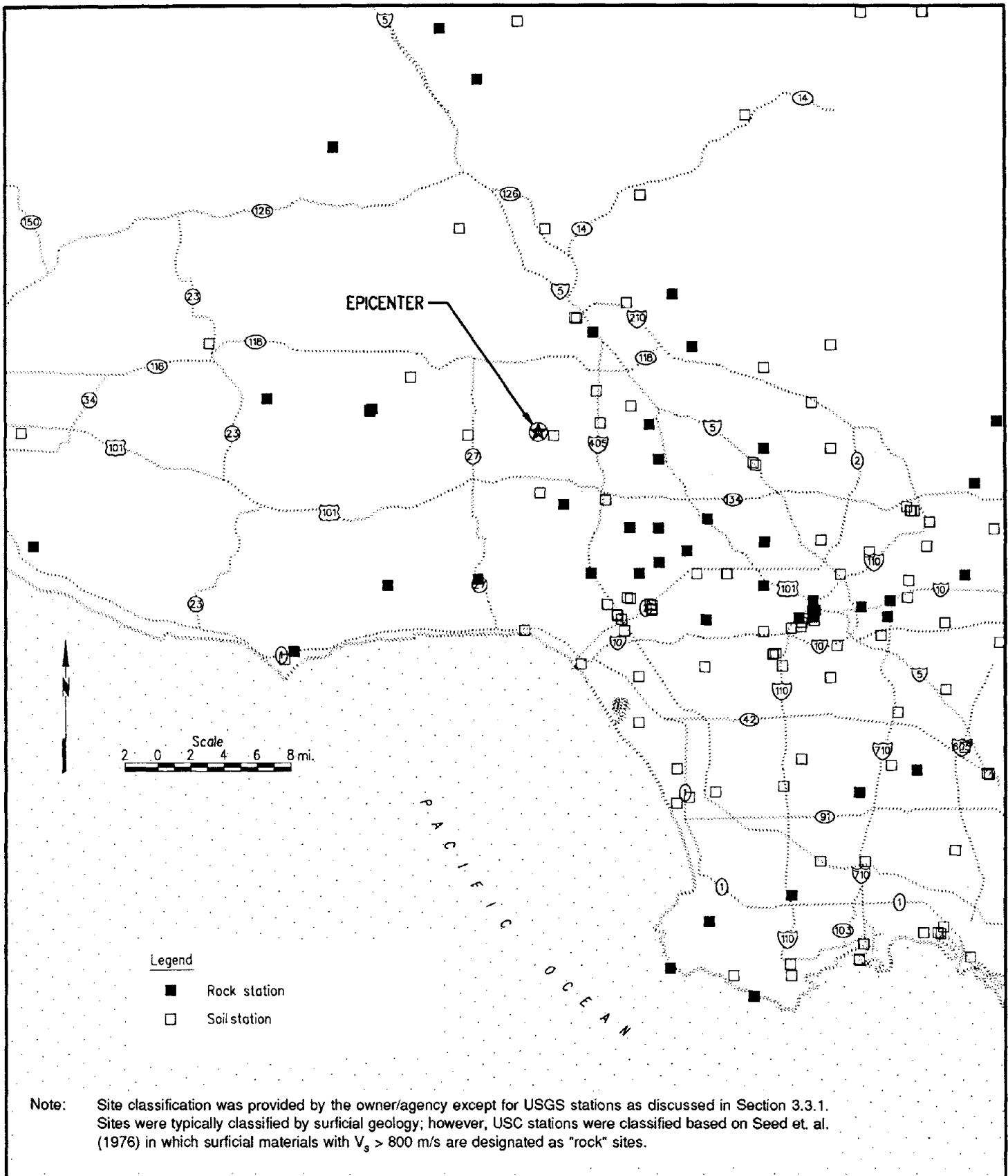


Fig. 3.2: Strong motion station sites classified according to surficial geologic conditions

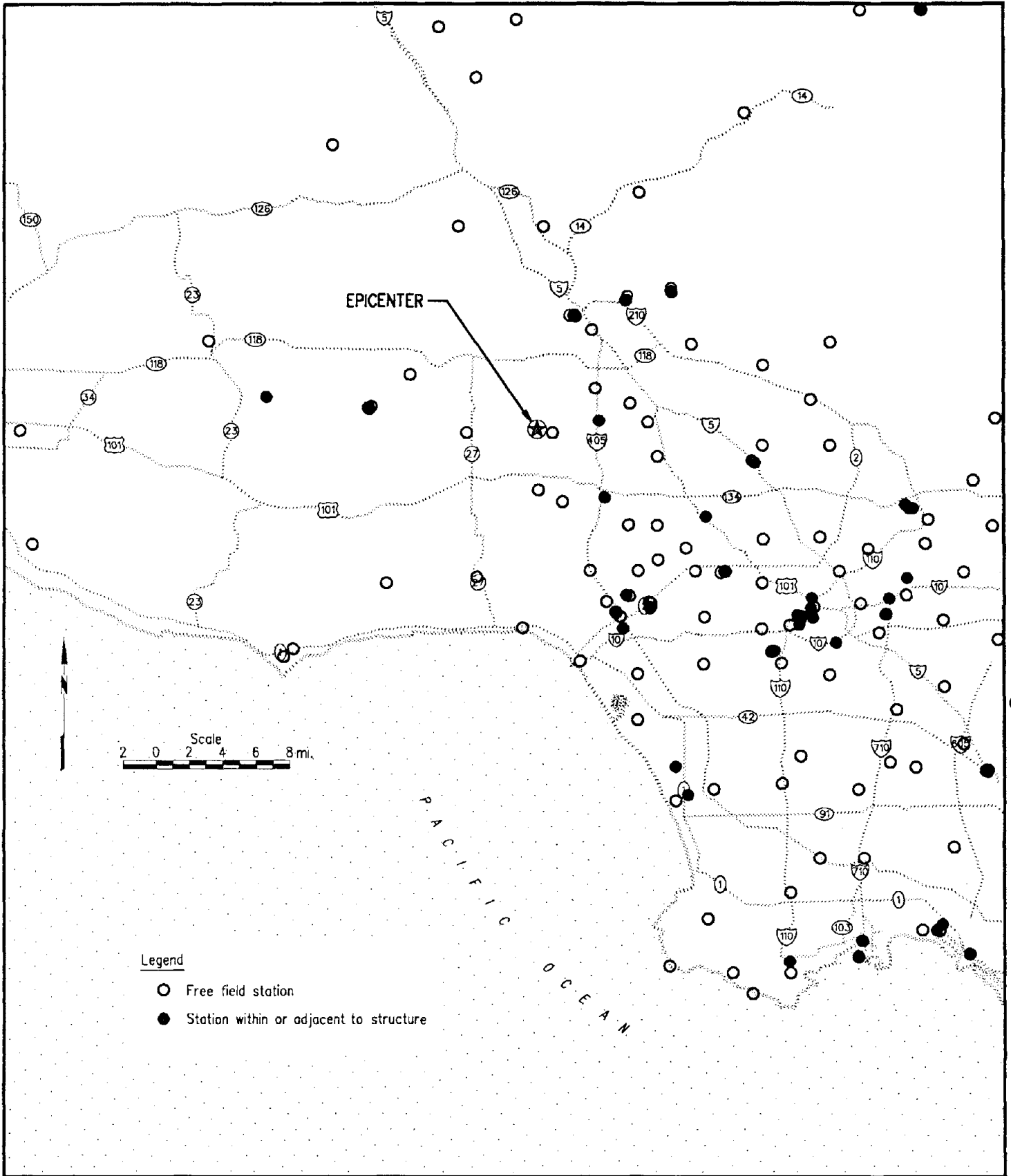


Fig. 3.3: Strong motion station sites identified as free-field or at the base of a structure

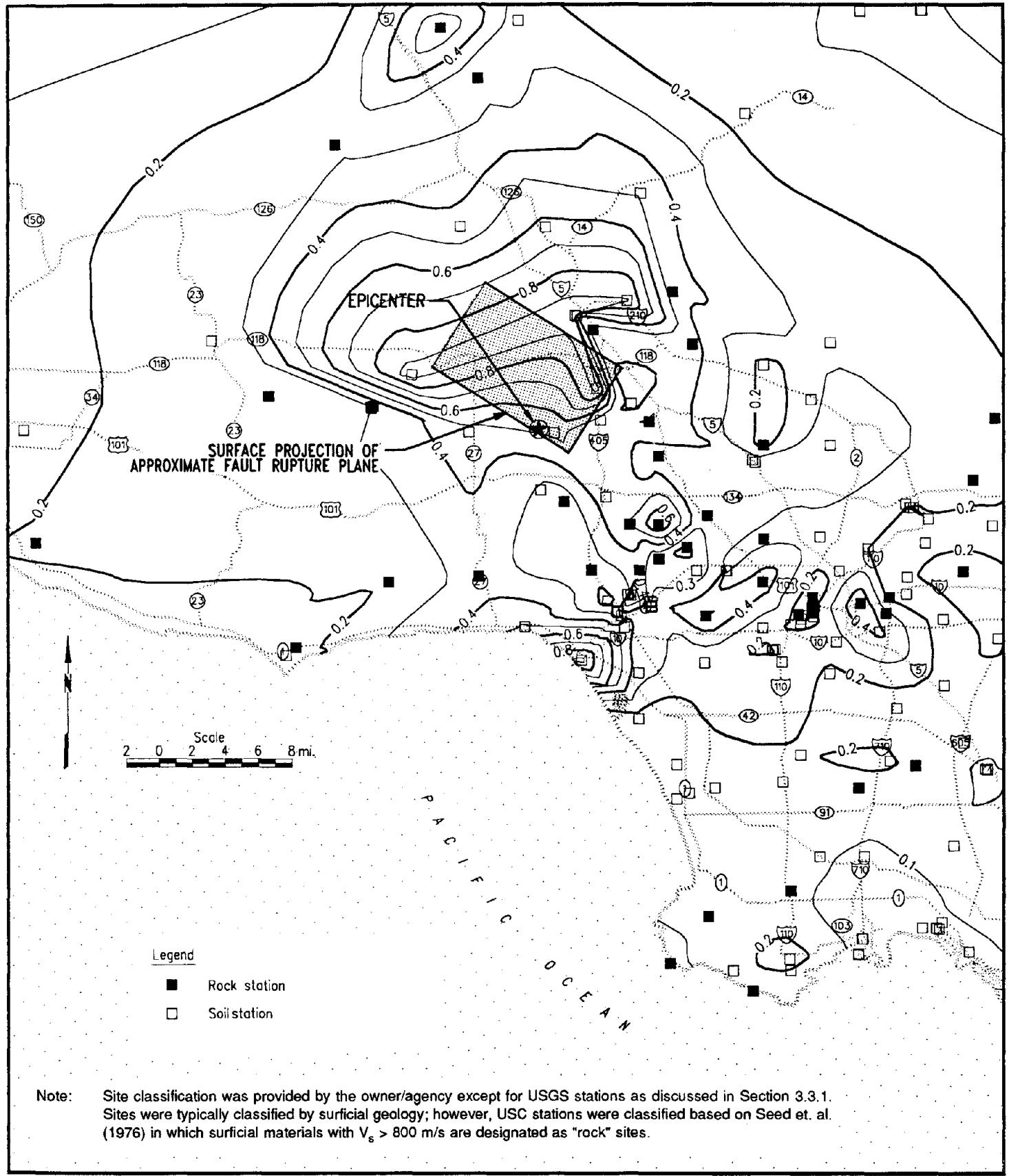


Fig. 3.4: Contours of maximum horizontal acceleration based on recordings at rock and soil sites

the secondary (orthogonal) horizontal peak ground acceleration component at the site was only 0.41g. Figure 3.5 shows MHA contours based only on those motions recorded at rock sites. The strong motion stations on rock used to develop the contours are also shown. It should be noted that the classification of the strong motion instrument locations as "rock" or "soil" sites was provided by the owner/agency, with the exception of USGS stations, as discussed in Section 3.3.1. Contours of MHA recorded at soil sites are plotted in Figure 3.6, along with the locations of strong motion stations on soil.

As of June 1994, digitized and instrument-corrected accelerograms were available from CSMIP for twenty-eight free-field sites (including one dam abutment) and for three multi-story building sites. From the catalog of available time histories, recorded motions for three free-field rock sites close to the fault rupture plane are shown in Figure 3.7, and these indicate that the duration of strong shaking ranged from about 5 to 15 seconds at these sites, where the strong shaking is defined as accelerations greater than or equal to 0.05g.

Acceleration time histories for three near-field alluvial sites are shown in Figure 3.8; an increase in predominant period is apparent in the recorded motions from the Sylmar-County Hospital Parking Lot and the Newhall-Los Angeles County Fire Station sites, located 16 km and 20 km north of the epicenter, respectively. Both sites are approximately 12 km from the fault rupture plane, and the time histories indicate that the duration of strong shaking ranged from about 12 to 15 seconds. Of the digitized records available from CSMIP, particularly significant peak ground velocities of about 129 cm/s and 95 cm/s were recorded at the Sylmar-County Hospital Parking Lot and the Newhall-LA County Fire Station site, respectively. No structural damage was reported at the six-story Sylmar (Olive View) hospital building, which experienced a peak ground velocity of 112 cm/s.

Figure 3.9 shows illustrative acceleration time histories for free-field alluvial sites at intermediate distances. The duration of strong shaking ranges from about 13 to 16 seconds. The most notable of this group are the motions recorded at the Santa Monica City Hall grounds, located approximately 23 km south of the epicenter and 28 km from the fault rupture plane. For the 90 and 360 degree components at this site, maximum horizontal accelerations (MHA) of 0.90g and 0.41g were recorded, respectively.

As noted previously, the largest amplitude free-field records were obtained at the Tarzana-Cedar Hill Nursery, approximately 5 km south of the epicenter and about 17 km from the primary fault plane. The Tarzana site consists of approximately 6 to 10 meters of soil/highly weathered shale over siltstone/shale. Downhole shear wave velocity measurements by the USGS at the site indicate a shear wave velocity of about 300 m/s in the upper 6 meters, increasing to about 400 m/s to the bottom of the borehole at 30 m. Peak horizontal and vertical accelerations of 1.82g and 1.18g, respectively were recorded, and the records are remarkable in that repeated accelerations of more than 1g were recorded over a period of up to 8 seconds. Figure 3.10(a) is a copy of the record reproduced from CSMIP Report OSMS 94-07. It should be noted that the Tarzana station recorded much higher accelerations than stations with similar distances during the 1994 Northridge Earthquake, as well as during the 1987 Whittier Narrows and 1991 Sierra Madre earthquakes. Several portable seismographs were deployed by CSMIP in the Tarzana area in the days following the earthquake, and

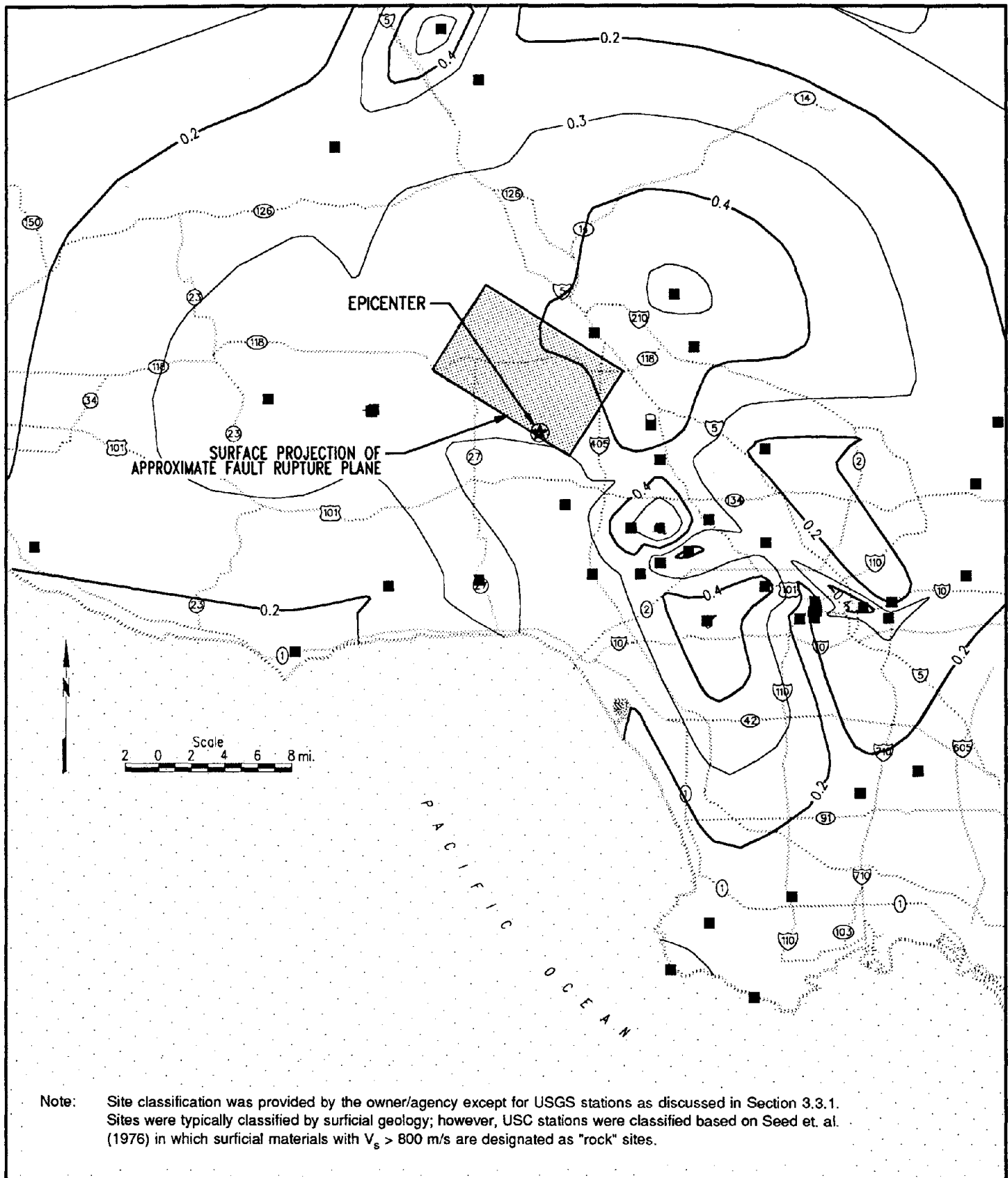


Fig. 3.5: Contours of maximum horizontal acceleration based on recordings at rock sites

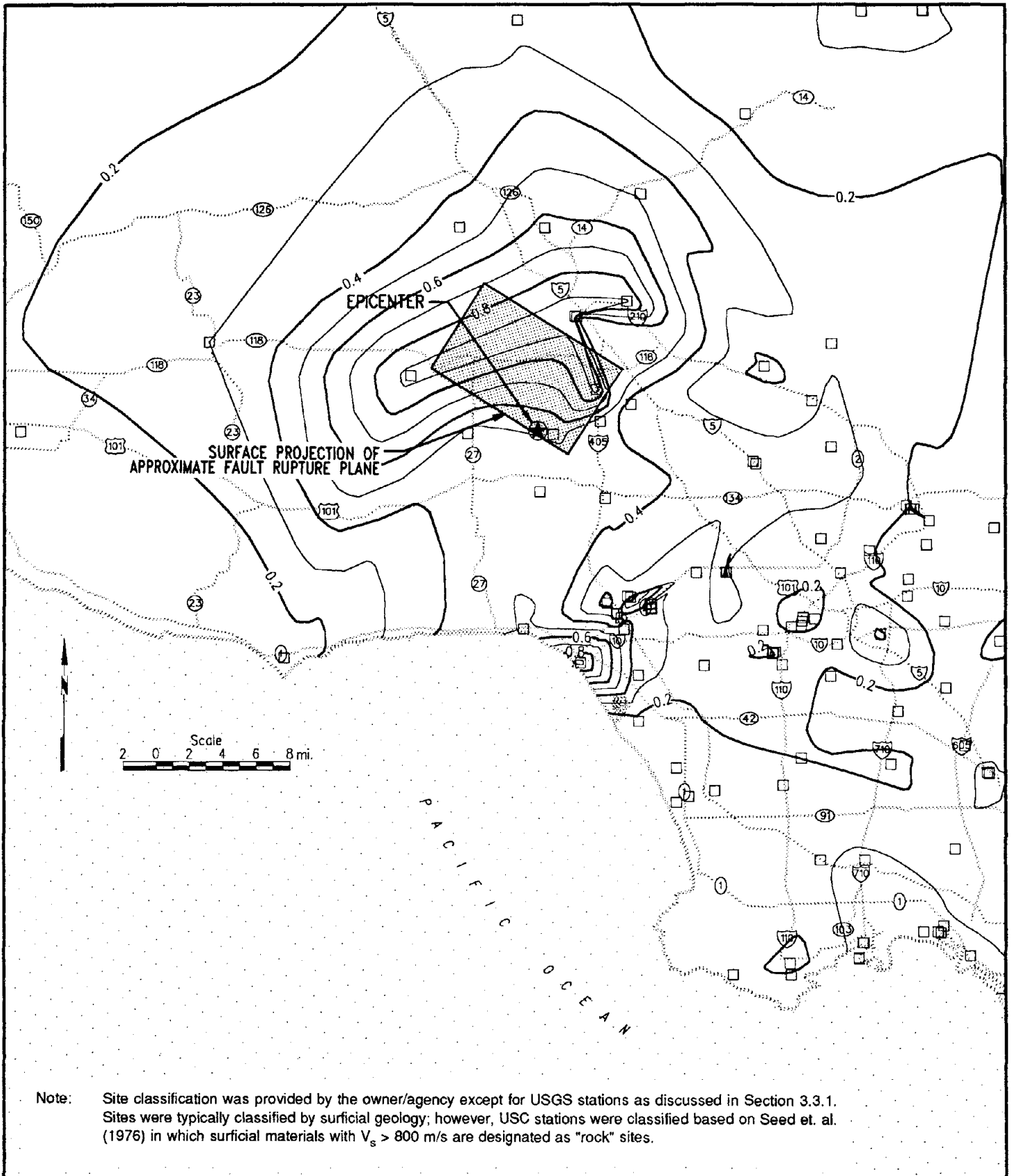


Fig. 3.6: Contours of maximum horizontal acceleration based on recordings at soil sites

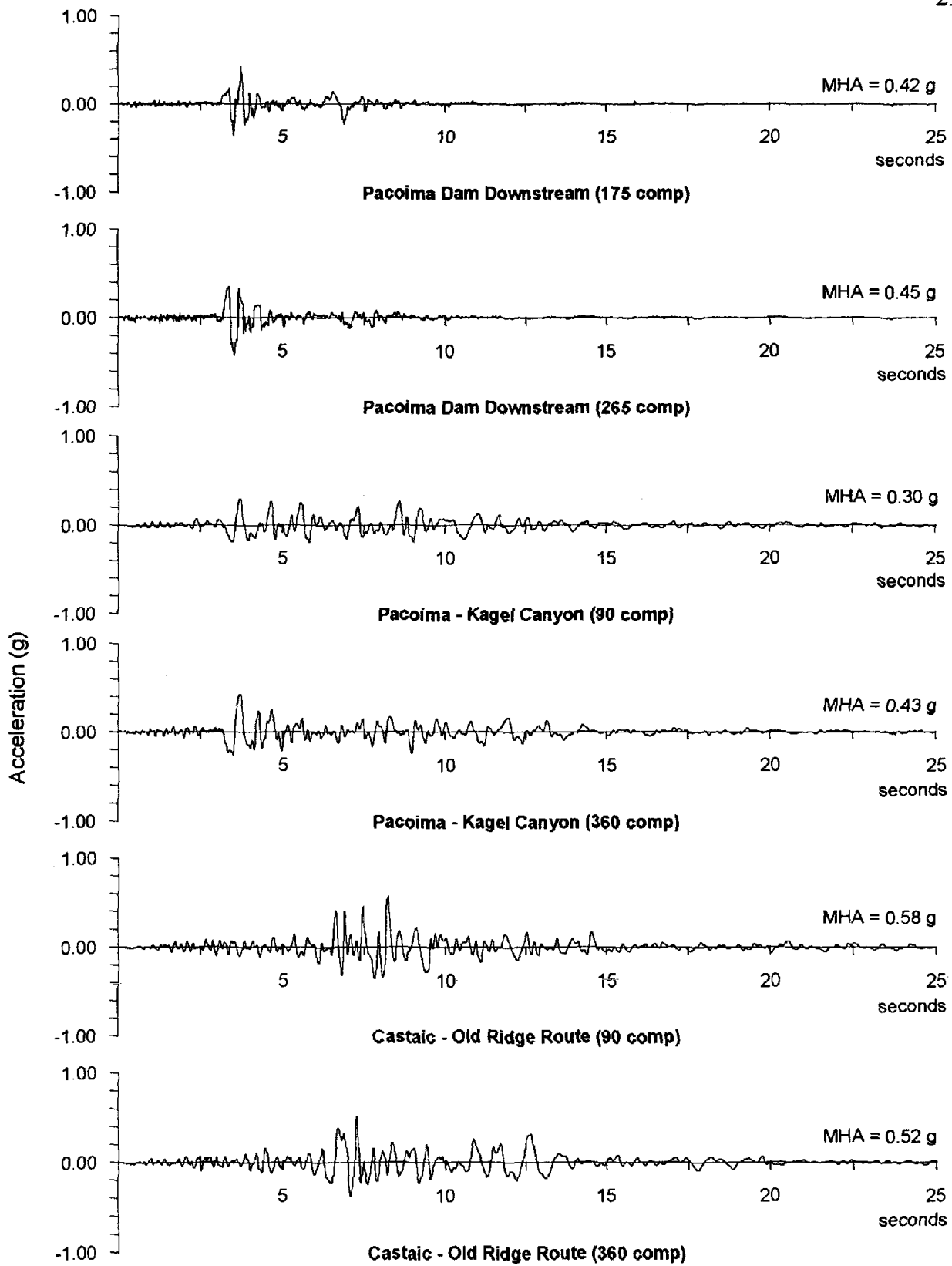


Fig. 3.7: Acceleration time histories recorded at three rock sites (instrument corrected data from CSMIP, 1994)

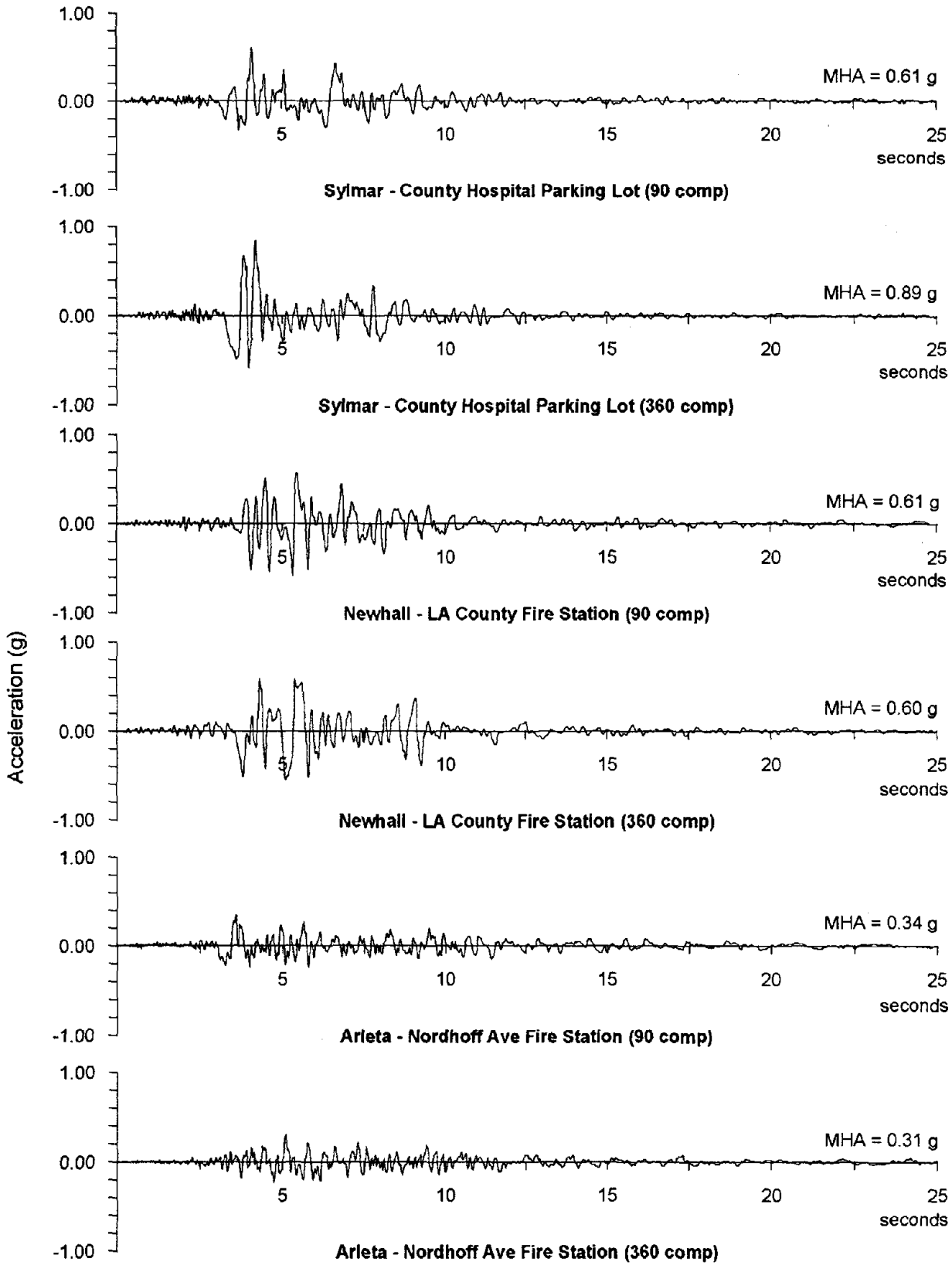


Fig. 3.8: Acceleration time histories recorded at three near-field soil sites (instrument corrected data from CSMIP, 1994)

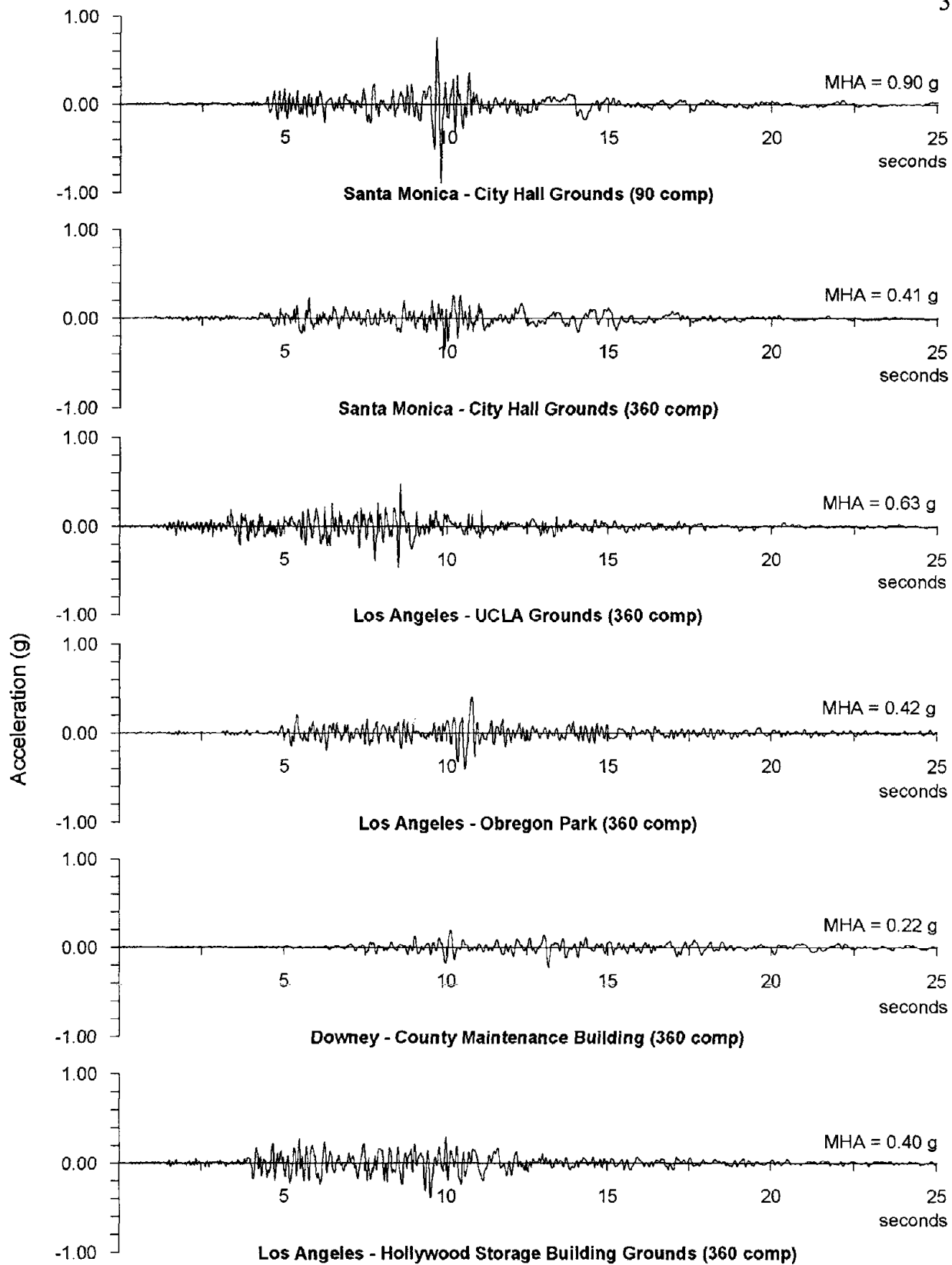


Fig. 3.9: Acceleration time histories recorded at selected soil sites at intermediate distances (instrument corrected data from CSMIP, 1994)

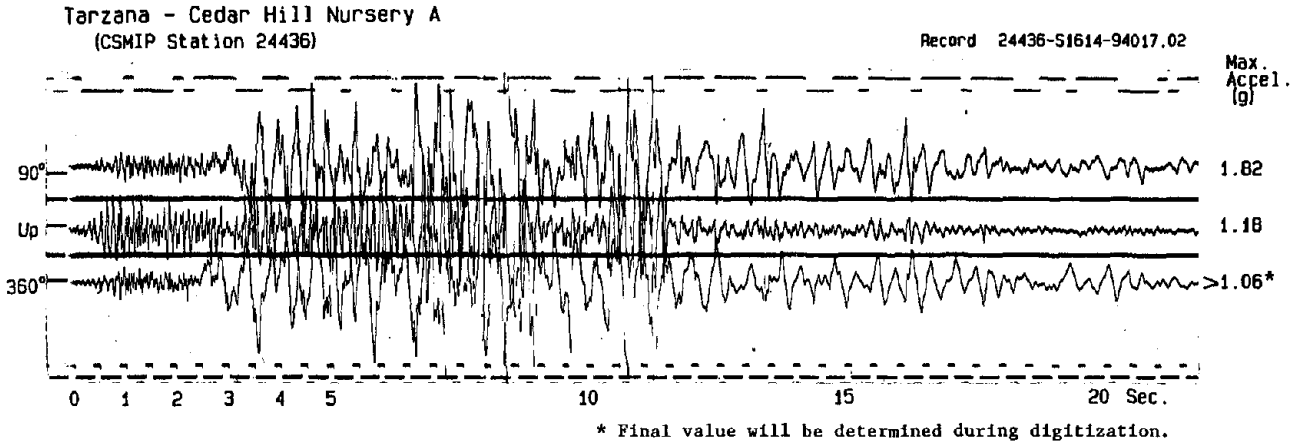


Fig. 3.10(a): Acceleration time histories recorded at the Tarzana - Cedar Hill Nursery (reproduced from CSMIP Report OSMS 94-07)

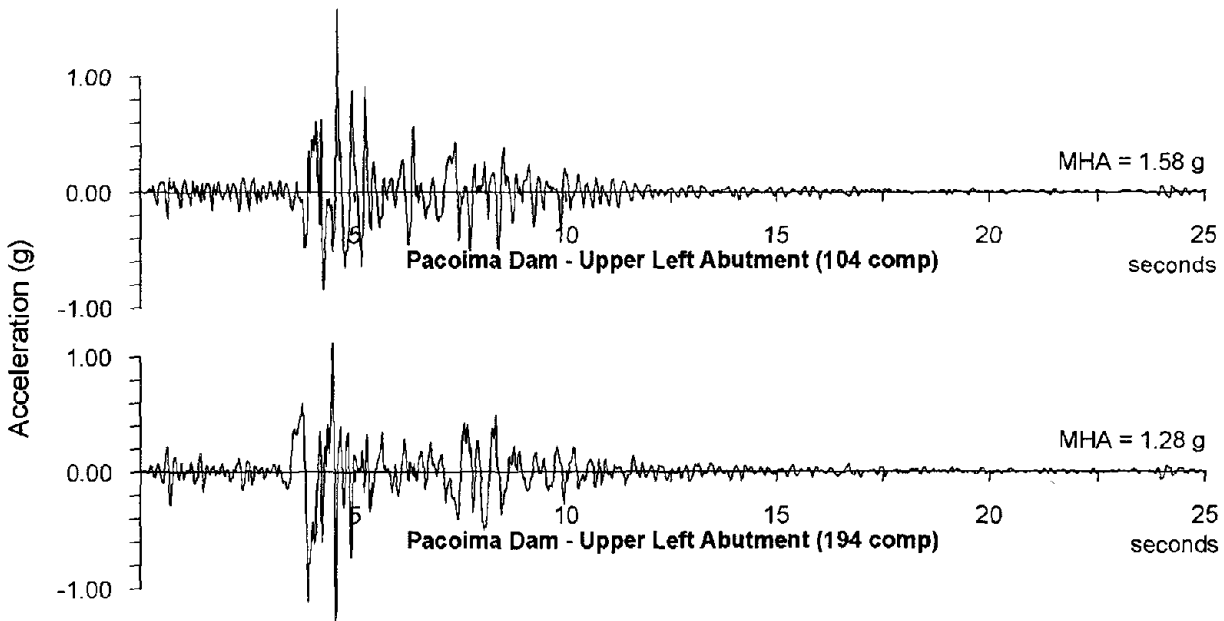


Fig. 3.10(b): Acceleration time histories recorded at the left abutment of Pacoima Dam (instrumented corrected data from CSMIP, 1994)

although the data is still being analyzed, it appears that the high accelerations may be localized since the permanent instrument is located on a small hill. Homes and businesses in the area do not appear to have experienced unusually high levels of damage.

Figure 3.10(b) shows the acceleration time histories recorded at the Pacoima Dam left abutment, located approximately 19 km northeast of the epicenter and 13 km from the fault rupture plane. The 365 foot high arch dam is located in a steep narrow canyon so that topographic amplification, as well as weakening of the highly jointed rock abutment, most likely contributed to the unusually high MHA of 1.58g recorded at the site. During the 1971 San Fernando Earthquake, this instrument recorded a MHA of 1.25g.

3.3.3 Attenuation Relationships for MHA vs. Distance (free-field strong motion stations)

In this section, all free-field strong motion stations for which ground response data were available were used except as noted. Stations located outside of the regions shown in Figure 3.1 were also included in the analyses.

a. Free-Field Rock Sites

Figures 3.11(a) through 3.11(d) present plots of MHA recorded at free-field rock sites as a function of distance from the fault rupture surface, along with the attenuation relationships for rock/stiff soil sites for a moment magnitude (M_w) 6.7 thrust fault event as proposed by Joyner and Boore (1988), Idriss (1991), Sadigh et.al. (1993), and Abrahamson and Silva (1993), respectively. It should be emphasized that distance is defined by Joyner and Boore (1988) as the closest distance from the strong motion station site to the vertical projection of the fault rupture plane to the ground surface, whereas for the remaining three attenuation relationships considered, distance is defined as the distance from the site to the nearest point on the actual (apparent) fault rupture surface. In this report, the fault rupture surface used in the calculations for distance was the uniform slip model defined by the U.C. Berkeley Seismographic Station (Dreger, 1994). The surface projection of this plane is shown as the shaded area in Figure 3.1.

In Figure 3.11(a), the larger of the two recorded components of ground motions recorded at free-field rock sites during the Northridge Earthquake generally plot above the mean attenuation relationship for rock proposed by Joyner and Boore (1988). It should be noted that MHA values from strong motion stations located on dam abutments were not included in this figure since they were also deleted by Joyner and Boore in the development of their attenuation relationship. Data from the USC stations (for which only one maximum horizontal component of acceleration at each site was available) were included in Figure 3.11(a); however, they were not included in Figures 3.11(b) through 3.11(d) since the arithmetic or geometric mean of the two maximum horizontal acceleration components recorded at each site was required.

In Figure 3.11(b), it can be seen that the data from free-field rock sites generally conform well to the Idriss (1991) attenuation relationship for rock, with approximately 60% of the data points plotting at or above the mean and 40% of the points falling below the mean. The

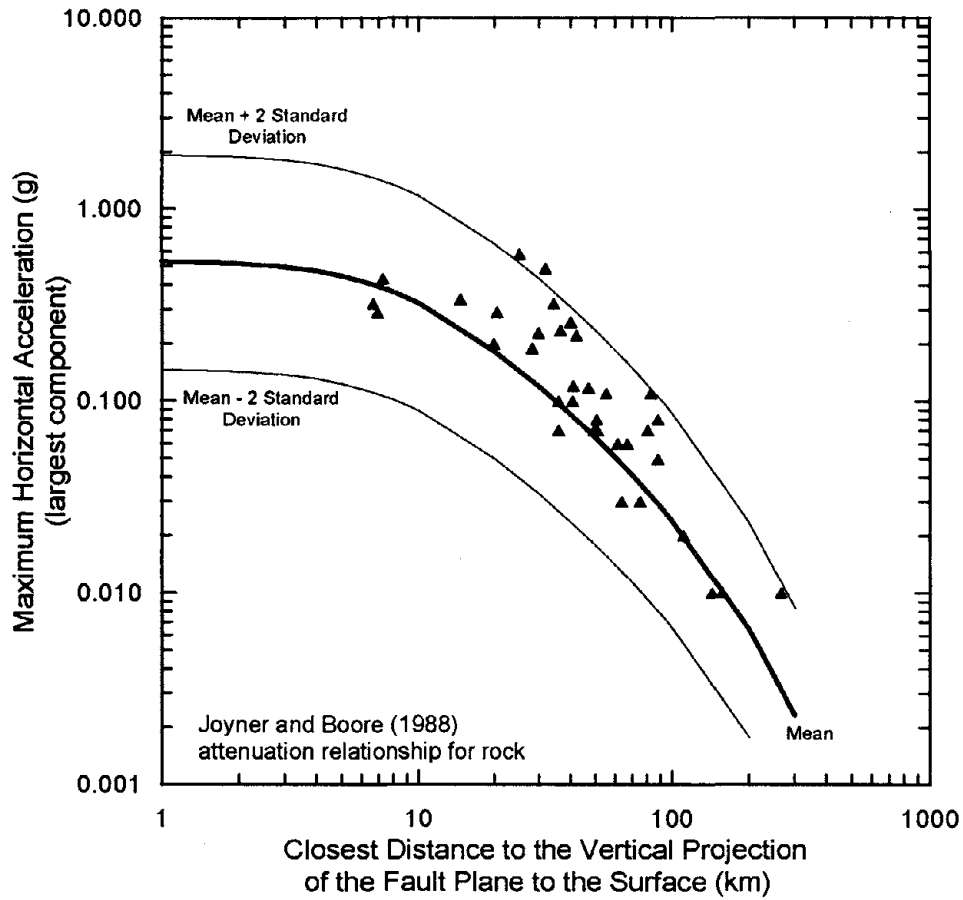


Fig. 3.11(a): Recorded maximum horizontal ground surface accelerations at free-field rock sites and the attenuation relationship proposed by Joyner and Boore (1988) for rock sites

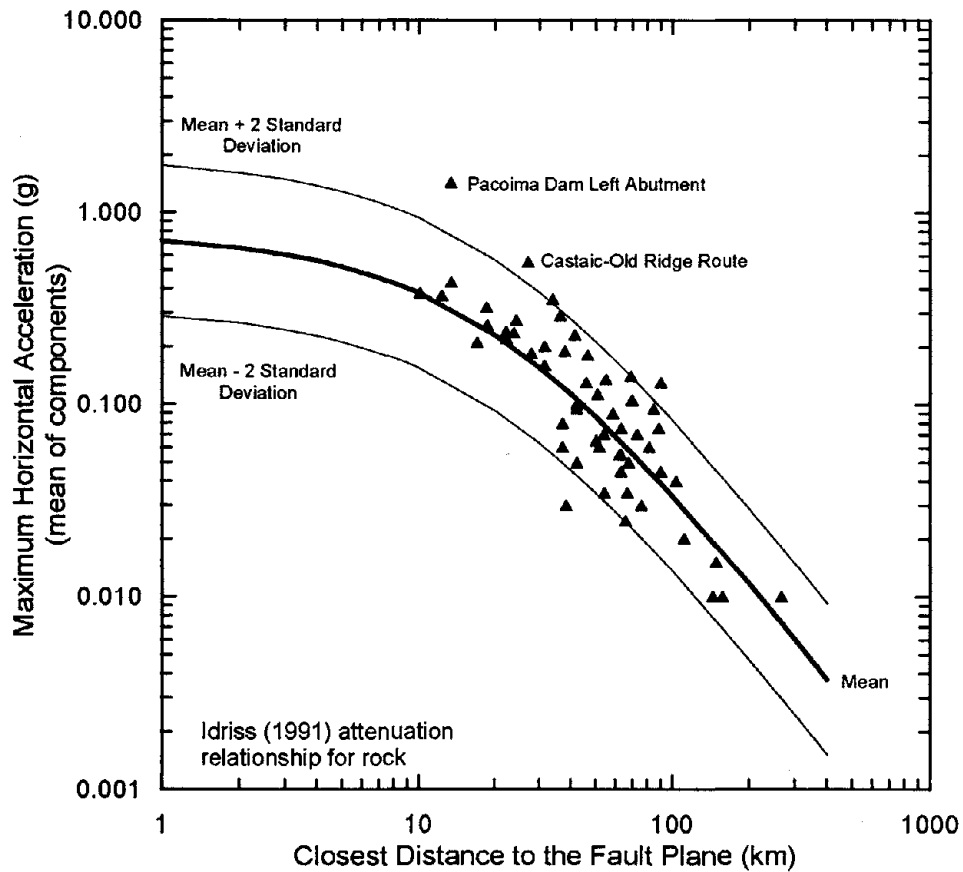


Fig. 3.11(b): Recorded mean maximum horizontal ground surface accelerations at free-field rock sites and the attenuation relationship proposed by Idriss (1991) for rock sites

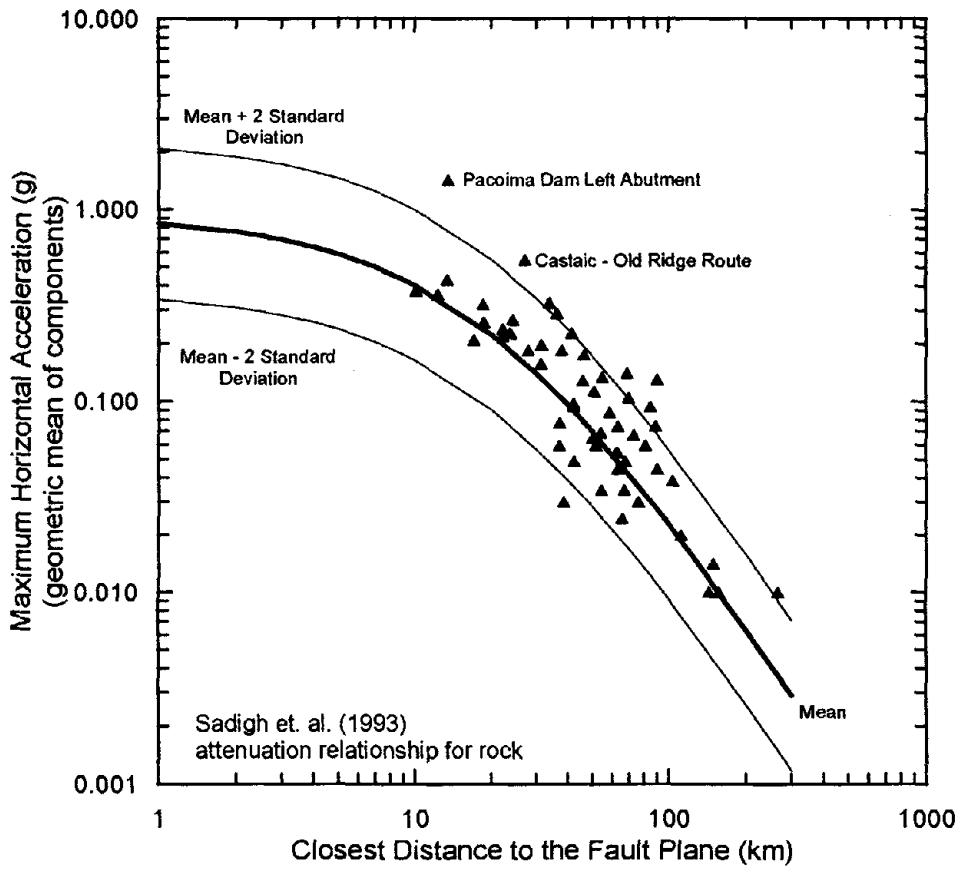


Fig. 3.11(c): Recorded mean maximum horizontal ground surface accelerations at free-field rock sites and the attenuation relationship proposed by Sadigh et. al. (1993) for rock sites

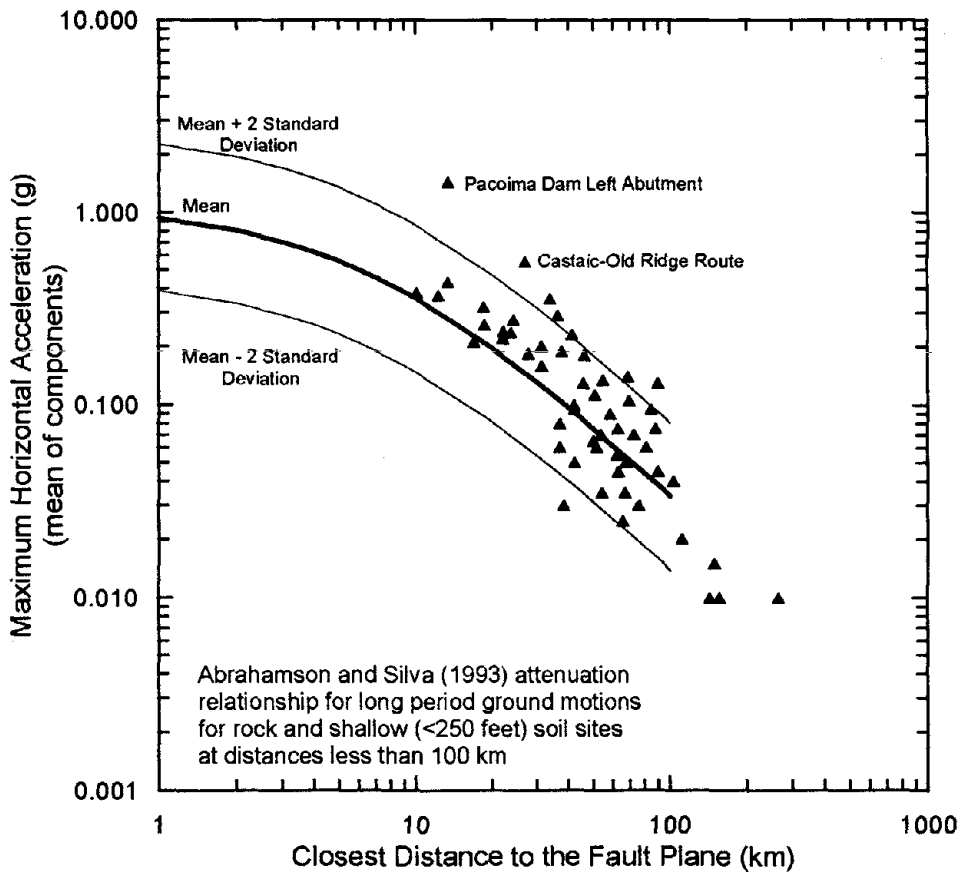


Fig. 3.11(d): Recorded mean maximum horizontal ground surface accelerations at free-field rock sites and the attenuation relationship proposed by Abrahamson and Silva (1993) for rock and shallow soil sites.

recorded accelerations at rock sites are generally enveloped within the mean \pm two standard deviation curves with notable exceptions at the Pacoima Dam left abutment and Castaic-Old Ridge Route. As discussed previously, the Pacoima Dam left abutment station recorded unusually high accelerations during the Northridge and the 1971 San Fernando Earthquakes, perhaps as a result of topographic amplification and shattering of the rock at the abutment. The high accelerations at Castaic-Old Ridge Route may in part be explained by topographic effects as well as the high degree of weathering of the rock; shear wave velocity measurements from seismic refraction surveys made at the site by Duke et. al. (1971) indicate that the shear wave velocity of the surficial materials ranges from about 200 m/s (640 ft/s) to 375 m/s (1230 ft/s) to a depth of 15 m (50 ft) to 21 m (70 ft) before encountering hard rock with shear wave velocities of about 1460 m/s (4790 ft/s). Downhole shear wave velocity measurements made at the site by the USGS (1984) resulted in measured shear wave velocities of about 360 m/s (1180 ft/s) in the top 10 m (33 ft) and about 900 m/s (2950 ft/s) to a depth of 28 m (92 ft).

In Figure 3.11(c), the MHA recorded at free-field rock sites is presented against the relationship for rock proposed by Sadigh et. al. (1993), also known as the Geomatrix (1991) relationship. Approximately 75% of the data points plot at or above the mean with the remainder falling below. In both Figures 3.11(b) and 3.11(c), the attenuation relationships appear to work well for distances greater than about 30 km. The MHA recorded at free-field rock sites is also presented in Figure 3.11(d) along with the Abrahamson and Silva (1993) attenuation relationship for long period ground motions for rock and shallow (<250 feet) soil sites.

b. Free-Field Soil Sites

In Figure 3.12(a), the recorded MHA at both free-field rock and soil sites are plotted against the attenuation relationship for rock proposed by Idriss (1991). The amplification of the maximum horizontal acceleration recorded at soil sites appears to be more pronounced at greater distances from the fault rupture plane (i.e. at approximately 100 km). Most of the data points from soil sites plot above the mean relationship for rock, and a significant number are more than two standard deviations greater than the mean. The data for "soil" sites only is replotted in Figure 3.12(b). A nonlinear regression analysis was used to develop the "best-fit" curve drawn through the MHA data recorded at the free-field soil sites. The "best-fit" free-field soil curve generally plots approximately one standard deviation above the mean Idriss (1991) attenuation relationship for rock, indicating the importance of local site conditions on the intensity of ground shaking.

3.3.4 Maximum Horizontal Acceleration vs. Maximum Vertical Acceleration

Figure 3.13 presents a plot of maximum horizontal accelerations recorded at all free-field stations vs. the maximum vertical accelerations recorded at these stations. In general, maximum vertical accelerations were typically less than or equal to approximately two-thirds of the maximum horizontal accelerations, though higher levels of vertical motion were notable at CSMIP stations Arleta-Nordhoff Avenue Fire Station and Newhall-Los Angeles County Fire Station and at USC stations numbers 9 and 53.

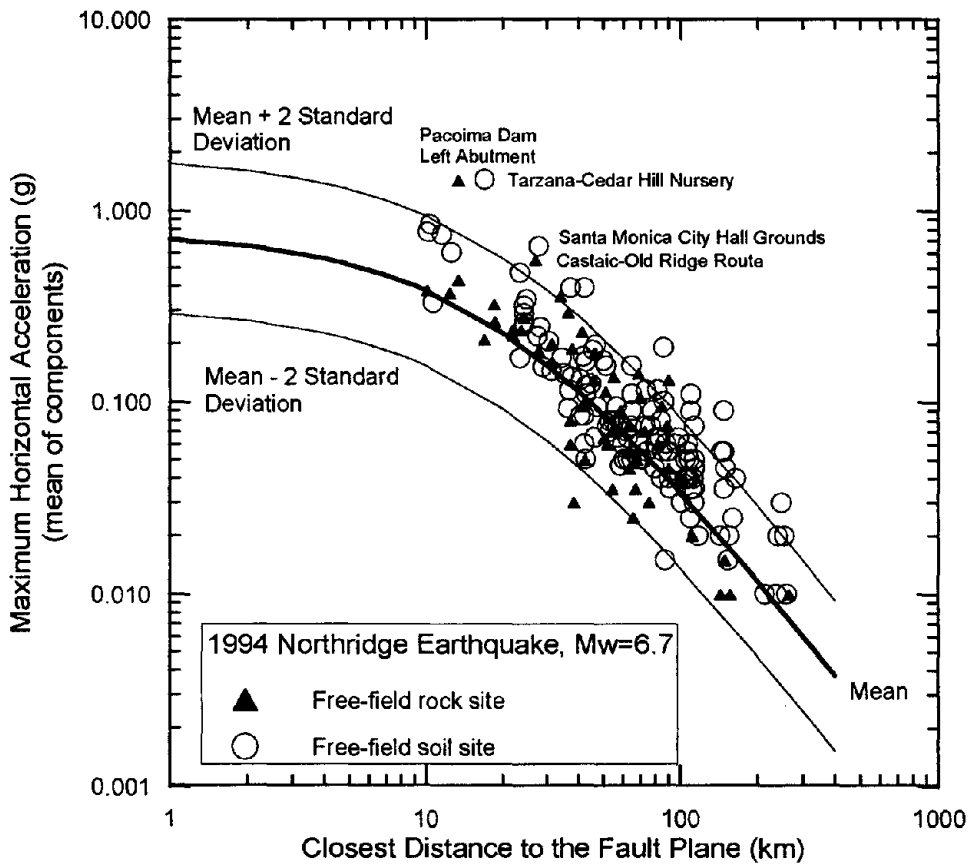


Fig. 3.12(a): Recorded mean maximum horizontal ground surface accelerations at free-field rock and soil sites and the attenuation relationship for rock proposed by Idriss (1991)

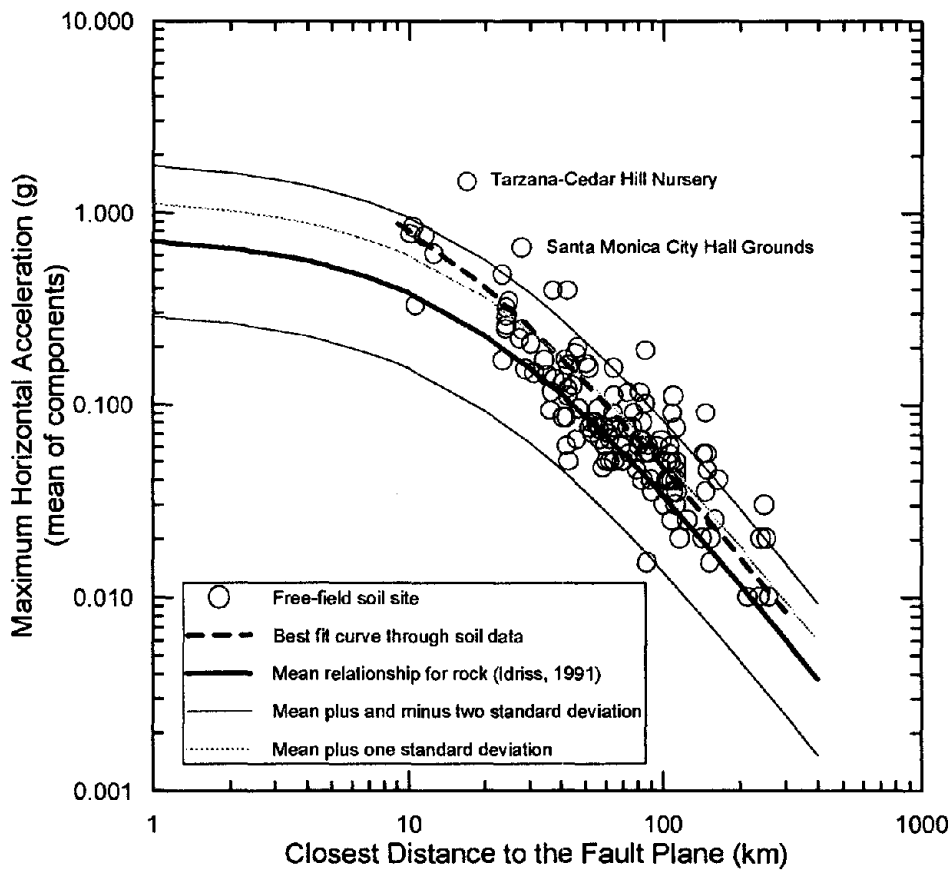


Fig. 3.12(b): Recorded mean maximum horizontal ground surface accelerations at free-field soil sites compared to the attenuation relationship for rock proposed by Idriss (1991)

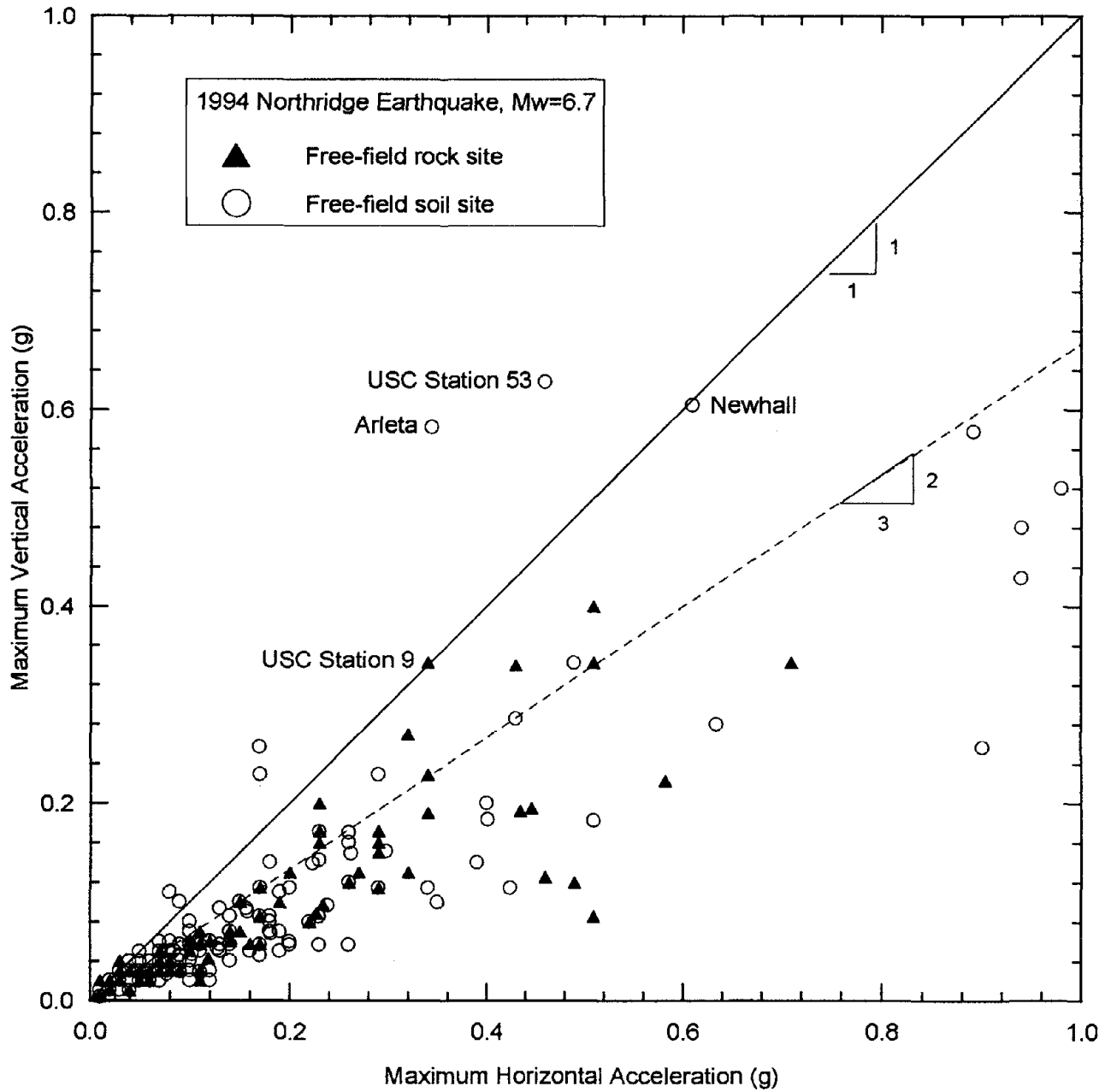


Fig. 3.13: Comparison of maximum vertical acceleration to maximum horizontal acceleration recorded at free-field sites

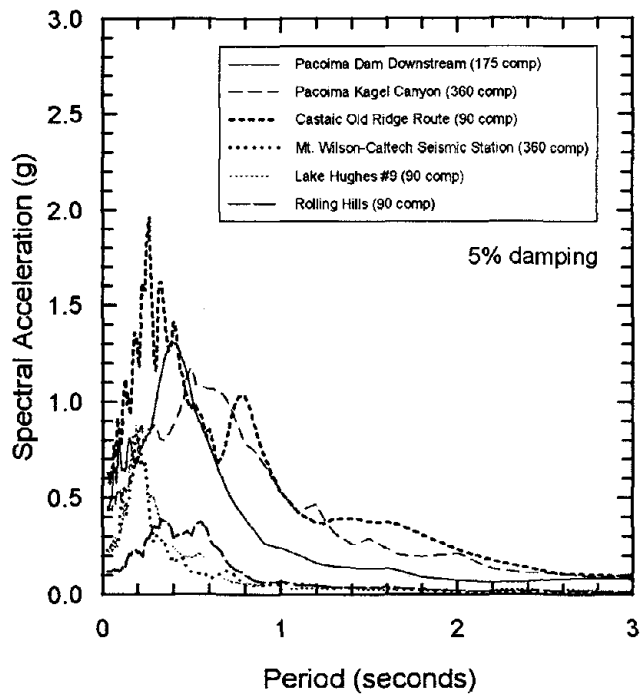
3.3.5 Calculated Response Spectra from Recorded Motions

Computed acceleration response spectra for the "stronger" component of ground motions recorded at selected free-field rock sites and near-field soil sites are shown in Figures 3.14(a) and 3.14(b). The "weaker" component is also shown for the Newhall-LA County Fire Station in Figure 3.14(b). Figure 3.14(c) illustrates the substantial difference in characteristics of the two components of motion recorded at the Santa Monica City Hall grounds, a free-field alluvial site. In Figure 3.14(d), representative acceleration response spectra for free-field alluvial sites at intermediate distances are presented. Figures 3.15(a) through 3.15(d) are corresponding figures showing computed spectral velocity for most of the sites mentioned in Figure 3.14.

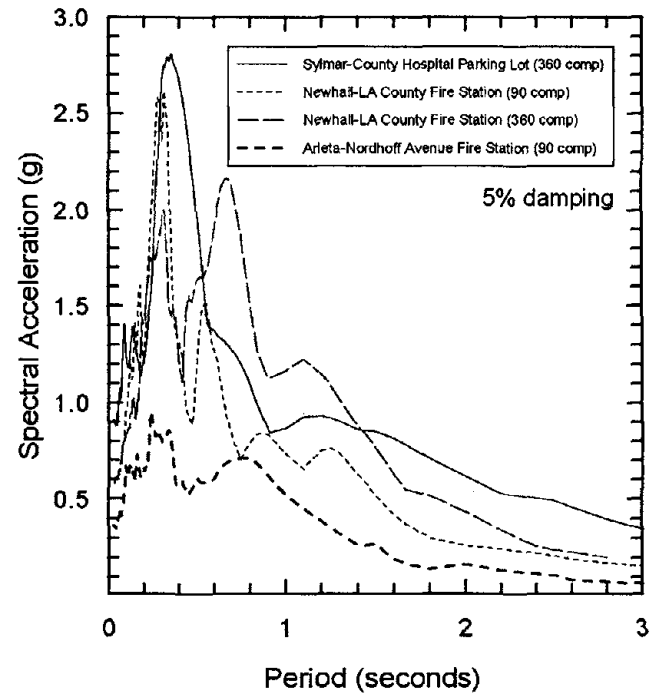
Acceleration response spectra computed for both components of strong motions recorded at six currently available CSMIP free-field rock sites are shown in Figure 3.16(a), along with the 1991 UBC design spectrum for Soil Type 1 (rock and stiff soils) at the maximum UBC MHA level of 0.4g. The free-field "rock" sites included in this figure are Pacoima Dam Downstream, Pacoima-Kagel Canyon, Castaic-Old Ridge Route, Mt. Wilson-Caltech Seismic Station, Rolling Hills, and Lake Hughes #9. Several of the computed spectra from the closer station recordings shown in this figure exceed the current maximum UBC design response spectrum. Figure 3.16(b) shows the spectral acceleration for the same sites normalized by the MHA at each site, along with the 1991 UBC normalized design spectrum for Soil Type 1. The average of the computed normalized spectral acceleration, shown as the dark dotted line in the figure, conforms to the normalized design spectrum quite well and never exceeds this UBC design spectrum; however, several of the individual normalized spectra are larger than the design spectrum.

Figure 3.17(a) shows the response spectra computed for both components of strong motions recorded at three free-field, near-field alluvial sites: Arleta, Sylmar-County Hospital Parking Lot, and Newhall-LA County Fire Station. For comparison, the 1991 UBC design spectrum for Soil Type 2 (deep cohesionless soils and stiff clay) at the maximum UBC MHA level of 0.4g is also presented. The UBC design spectrum is significantly exceeded in the near-field at both short and long periods. In Figure 3.17(b), the spectral accelerations for the three near-field sites are normalized by the MHA at each site. The normalized UBC design spectrum for Soil Type 2 is presented, as well as the average of the computed normalized spectral accelerations. Again, the average of the normalized spectra is enveloped well by the code's normalized design spectrum. This would suggest that the shape of the normalized response spectrum used in the 1991 UBC may be adequately representative, but that the "anchoring" value of MHA by which these normalized spectra are scaled for design purposes in the UBC may be too low in the near-field.

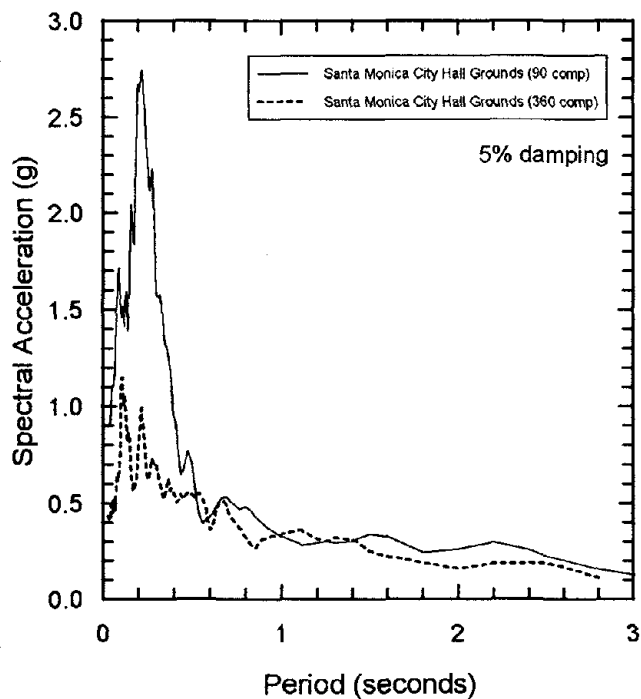
Figure 3.18(a) shows the acceleration response spectra computed for both components of horizontal strong motions recorded at the remaining available CSMIP free-field soil sites, excluding those with MHA less than 0.1g. Comparison with the 1991 UBC design spectrum for Soil Type 2 at the maximum MHA of 0.4g shows that even at intermediate distances, the UBC design spectrum can be exceeded. Figure 3.18(b) shows the data for the same sites with the spectral acceleration normalized by the MHA at each site. Again, the average of the



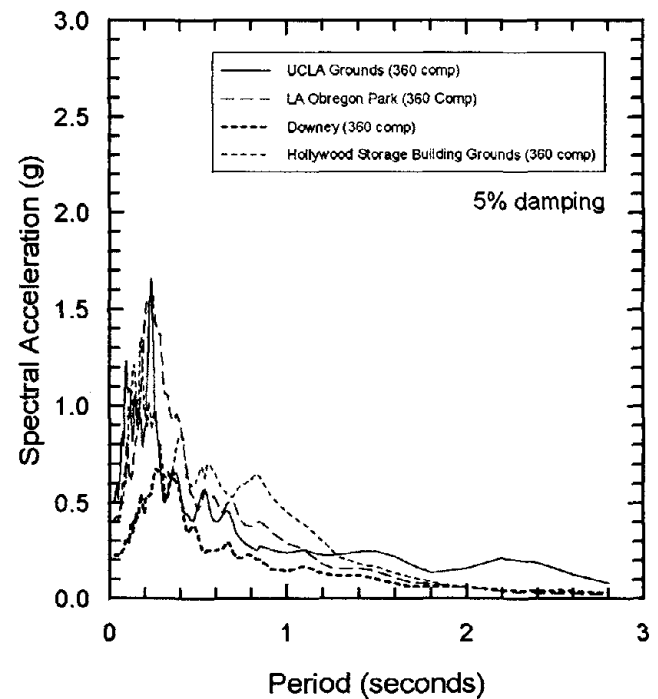
(a)



(b)



(c)



(d)

Fig. 3.14: Computed acceleration response spectra for selected free-field stations
 (a) on rock
 (b) on soil in the near-field
 (c) in Santa Monica
 (d) on soil at intermediate distances

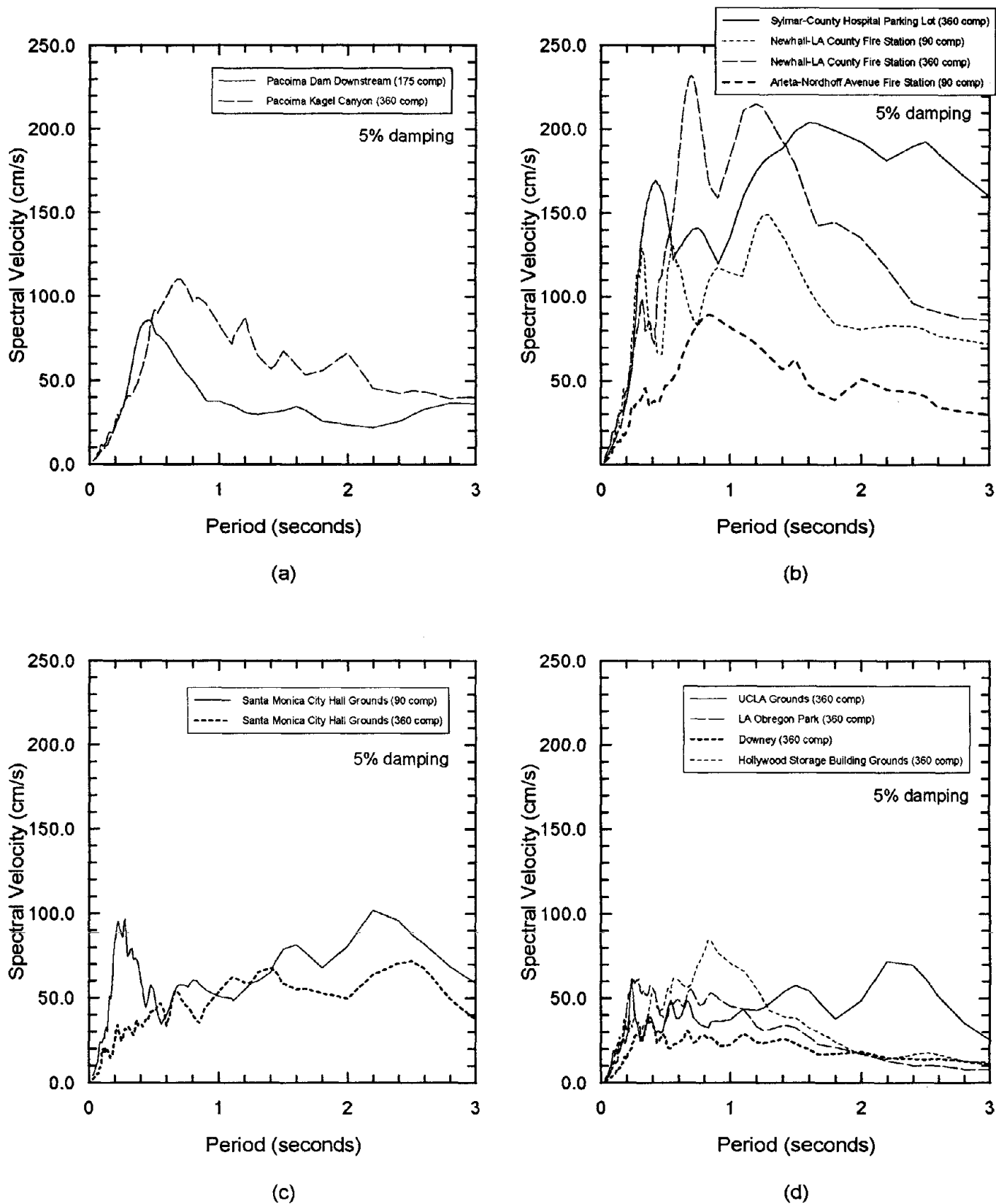


Fig. 3.15: Computed velocity response spectra for selected free-field stations
 (a) on rock
 (b) on soil in the near-field
 (c) in Santa Monica
 (d) on soil at intermediate distances

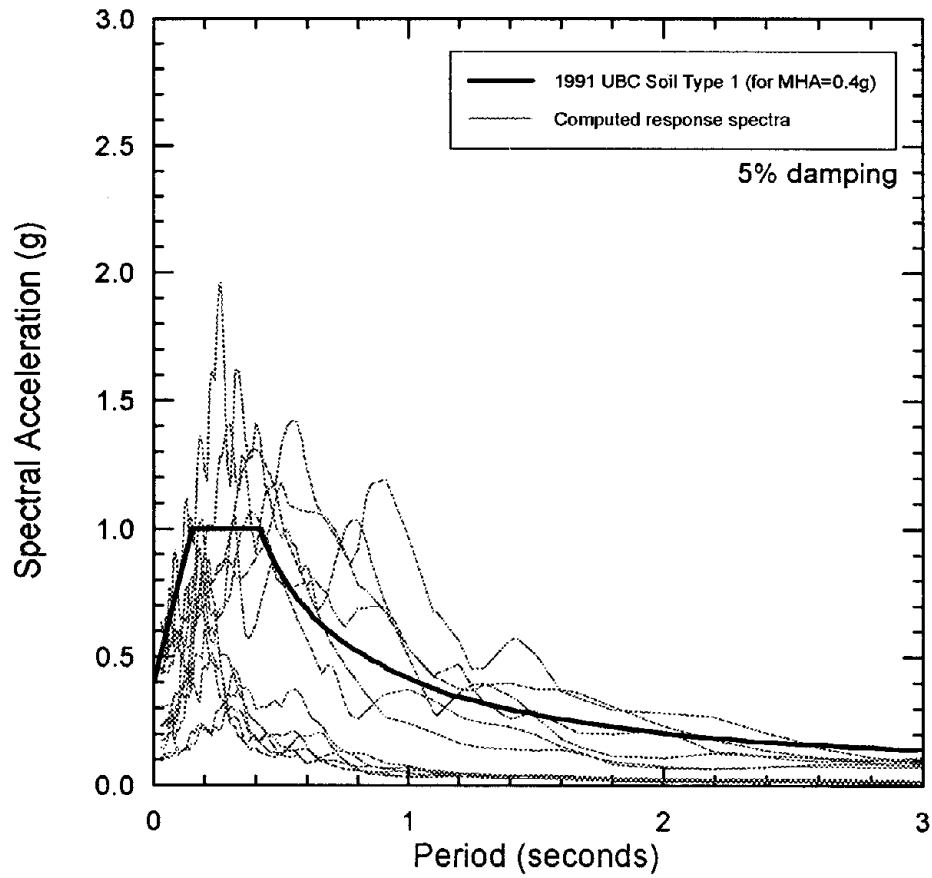


Fig. 3.16(a): Computed spectral acceleration from six CSMIP rock sites compared to the 1991 UBC design spectrum for Soil Type 1 for MHA = 0.4g

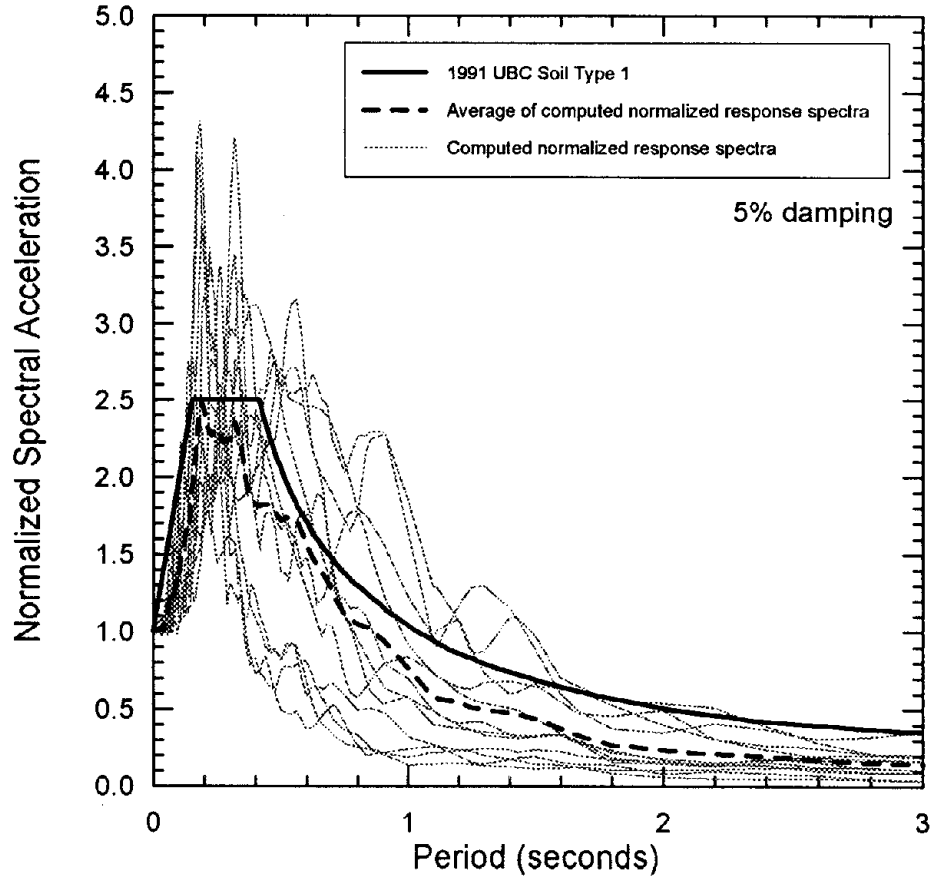


Fig. 3.16(b): Computed normalized spectral acceleration from six CSMIP rock sites compared to the 1991 UBC normalized design spectrum for Soil Type 1

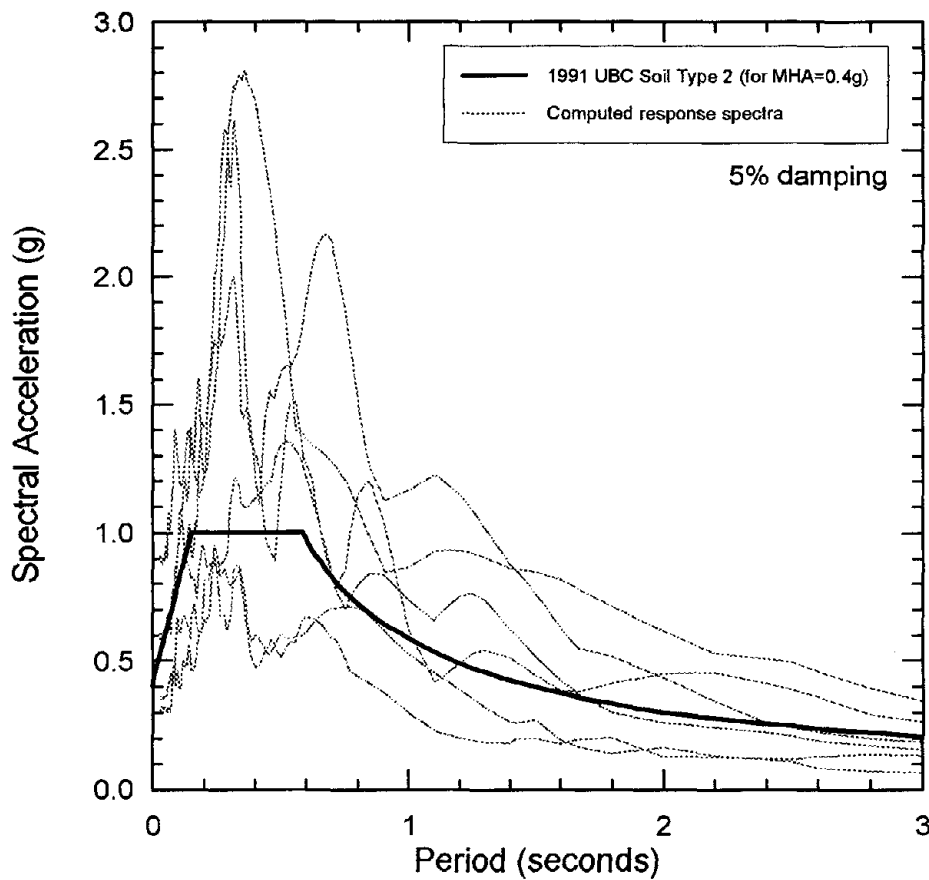


Fig. 3.17(a): Computed spectral acceleration from three near-field CSMIP soil sites compared to the 1991 UBC design spectrum for Soil Type 2 for MHA = 0.4g

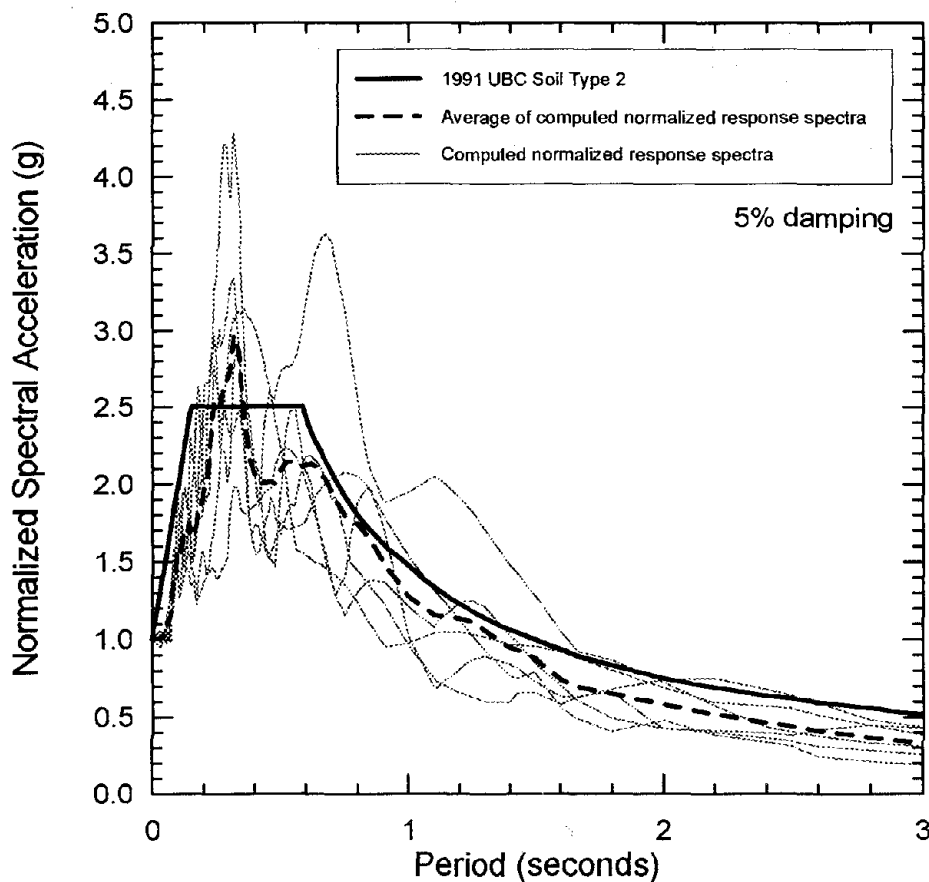


Fig. 3.17(b): Computed normalized spectral acceleration from three near-field CSMIP soil sites compared to the 1991 UBC normalized design spectrum for Soil Type 2

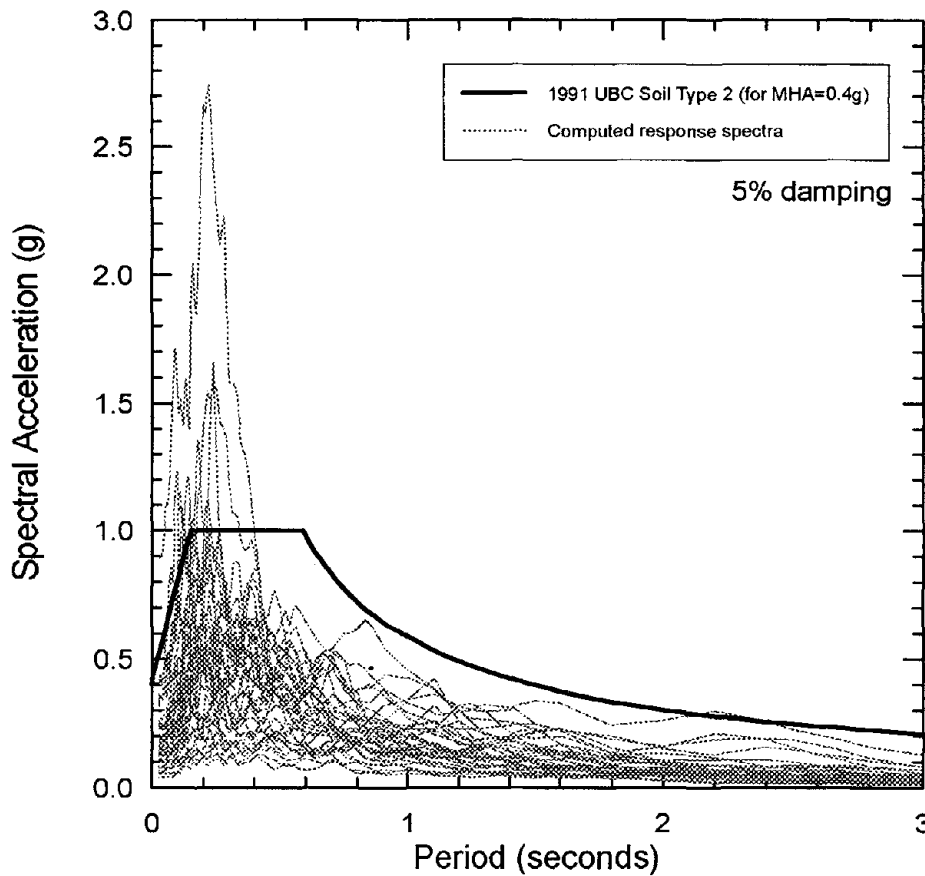


Fig. 3.18(a): Computed spectral acceleration from the available motions recorded at CSMIP soil sites (excluding near-field stations) compared to the 1991 UBC design spectrum for Soil Type 2 for MHA = 0.4g

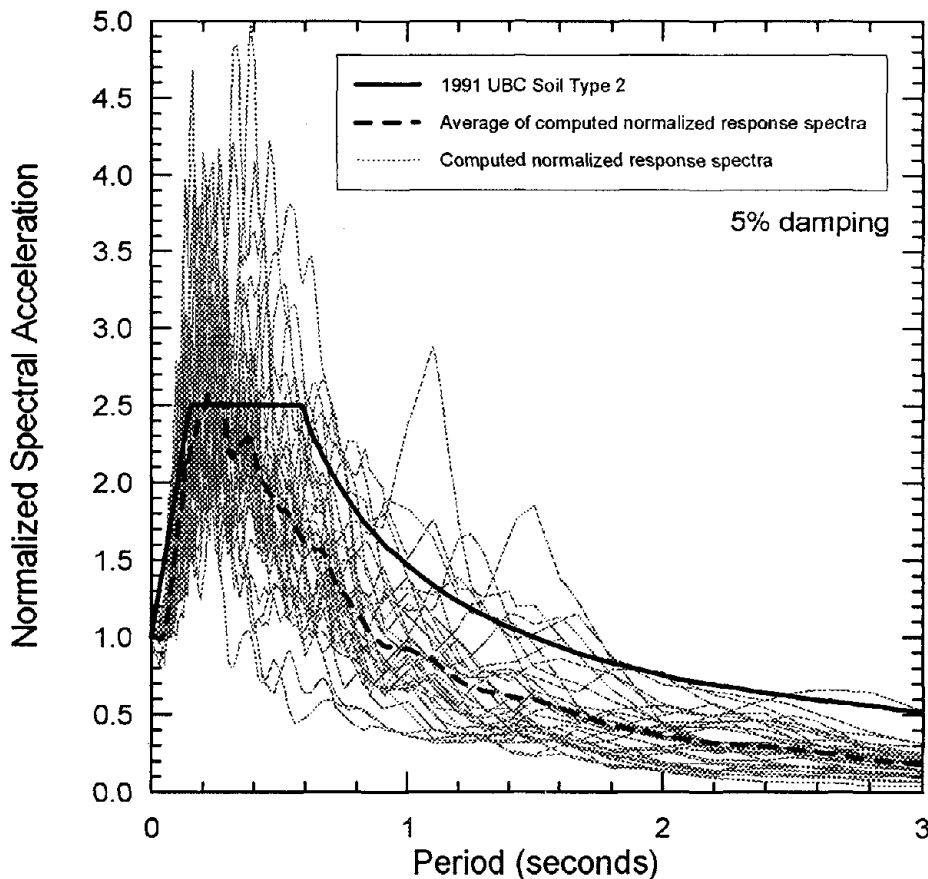


Fig. 3.18(b): Computed normalized spectral acceleration from the available motions recorded at CSMIP soil sites (excluding near-field stations) compared to the 1991 UBC normalized design spectrum for Soil Type 2

normalized spectra is enveloped by the UBC normalized design spectrum for Soil Type 2.

3.3.6 Spectral Acceleration at One-Second Period

The spectral acceleration at a period of one second calculated from the accelerograms recorded at the free-field soil and rock sites currently available from CSMIP (excluding the record from the Pacoima Dam left abutment) are shown in Figure 3.19 along with the spectral acceleration vs. distance relationship for rock proposed by Idriss (1991). The spectral ordinates from two rock sites, Castaic-Old Ridge Route and Lake Hughes #9, fall outside of the mean \pm two standard deviation curves. This Idriss (1991) relationship is not intended to be applicable to soil sites, and it can be seen that nearly all of the one-second period spectral accelerations for soil sites are above the mean, and many well above it, illustrating well the influence of site conditions.

3.3.7 Comparison of Observed Free-Field Motions and Recordings from the Base of Structures

Figure 3.20 shows "best-fit" curves from nonlinear regression analyses drawn for mean MHA vs. distance for motions recorded at free-field soil sites and for instruments located at the base of multi-story structures on soil. In general, the data show that the MHA at the base of a building on soil is slightly lower than the MHA recorded at a free-field soil site at distances of up to about 40 km. At larger distances, the difference becomes negligible. The number of instrumented structures on rock was too small to develop conclusions based on comparisons with recordings obtained at free-field rock sites.

Acceleration response spectra were computed for multiple components of motion recorded at the ground floors of three CSMIP building sites: Van Nuys 7-story Hotel, Sylmar 6-story County Hospital, and Burbank 6-story Commercial Building. The distance from each of these buildings to the fault rupture surface is approximately 11 km, 11.5 km and 19 km, respectively. The computed response spectra are shown in Figure 3.21(a) along with the 1991 UBC design spectrum for Soil Type 2 at MHA=0.4g. Again, many of the computed spectra for individual instruments exceed the design spectrum. A corresponding figure for normalized spectra is presented in Figure 3.21(b) along with the normalized UBC design spectrum for Soil Type 2. The average of the computed normalized response spectra is greater than the code spectrum in the 0.15 to 0.4 second period range, but the normalized code spectrum represents the Northridge data well overall.

3.3.8 Comparison of MHA with the 1971 San Fernando Earthquake

Comparison of the ground motions from the Northridge Earthquake and the 1971 San Fernando Earthquake is interesting in that both earthquakes were of moment magnitude 6.6 to 6.7, occurred on thrust faults (although the fault planes were dipping in opposite directions), and affected much of the same area. Figure 3.22 is a plot of mean MHA recorded at free-field rock and soil sites during the 1971 event, along with the attenuation relationship for rock proposed by Idriss (1991). The data points from the 1971 earthquake generally fall below the mean, while the data from the Northridge Earthquake (Figure

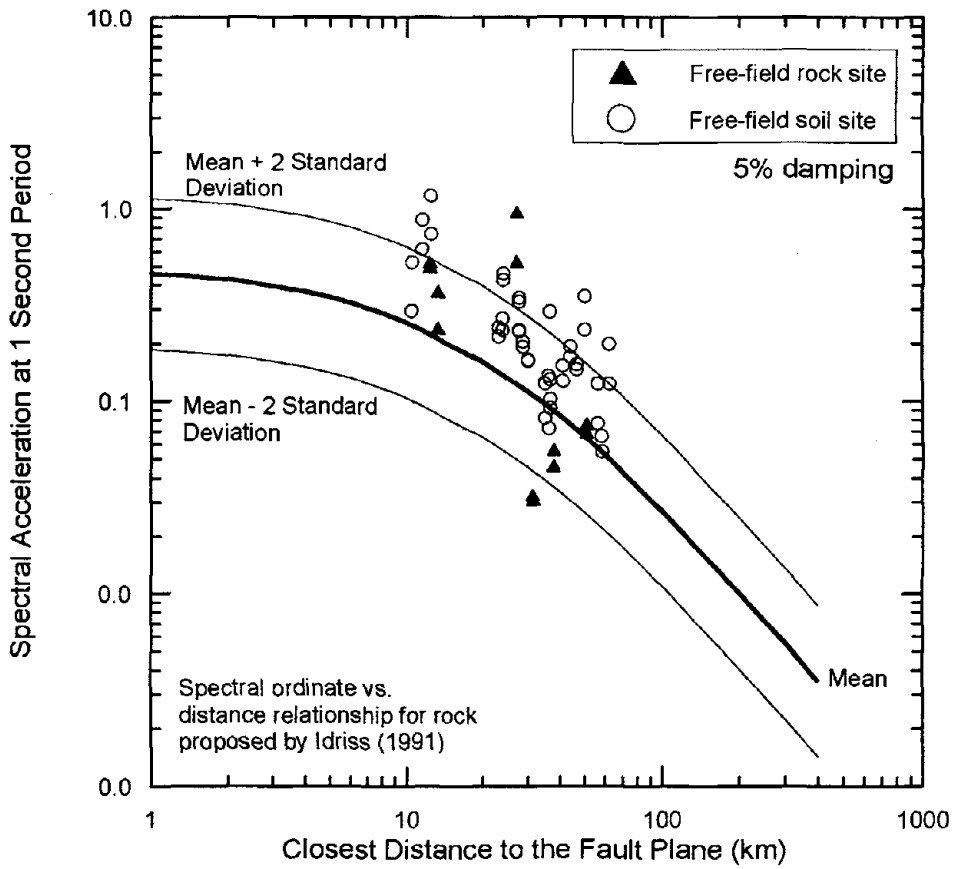


Fig. 3.19: Spectral acceleration at one second period calculated from motions recorded on rock and soil sites along with the spectral ordinate vs. distance relationship for rock proposed by Idriss (1991)

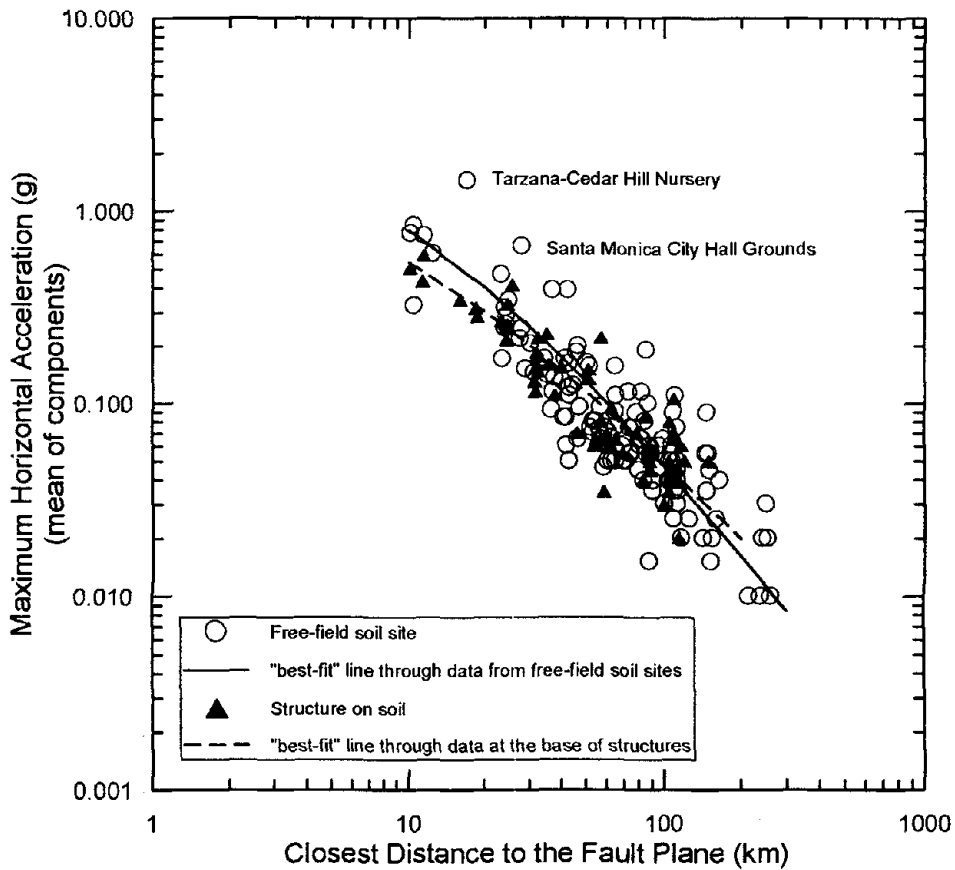


Fig. 3.20: Mean maximum horizontal ground surface accelerations recorded at free-field stations on soil vs. accelerations recorded at the base of structures on soil

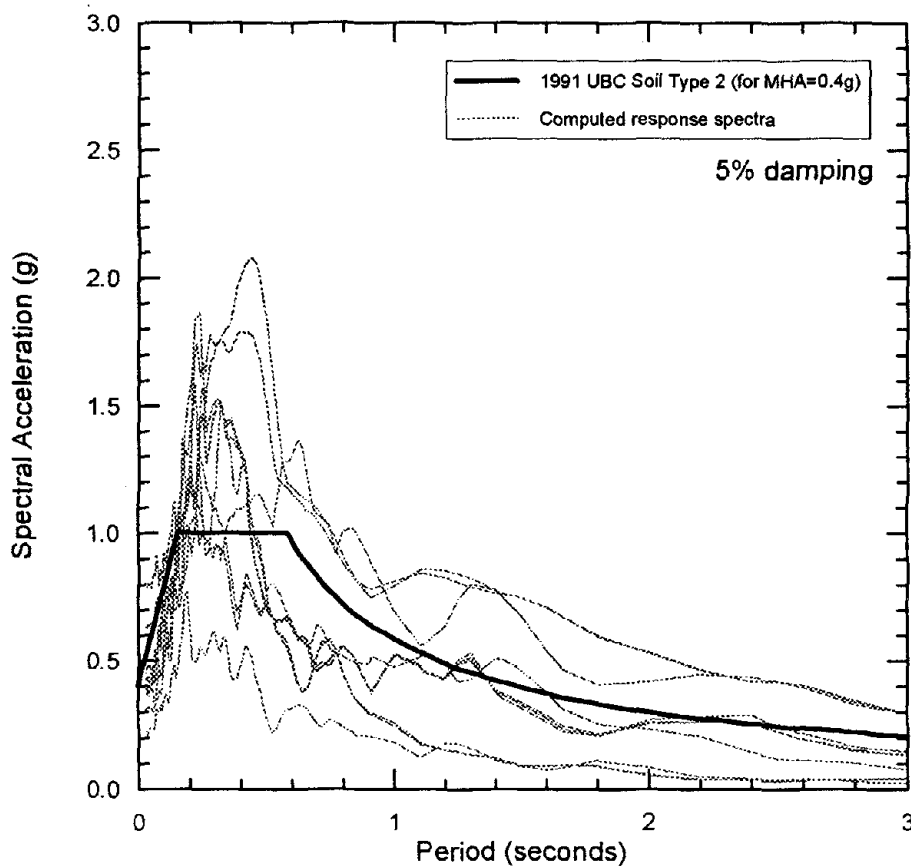


Fig. 3.21(a): Computed spectral acceleration from ground motions recorded at the base of three multi-story buildings on soil compared to the 1991 UBC design spectrum for Soil Type 2 for MHA = 0.4g

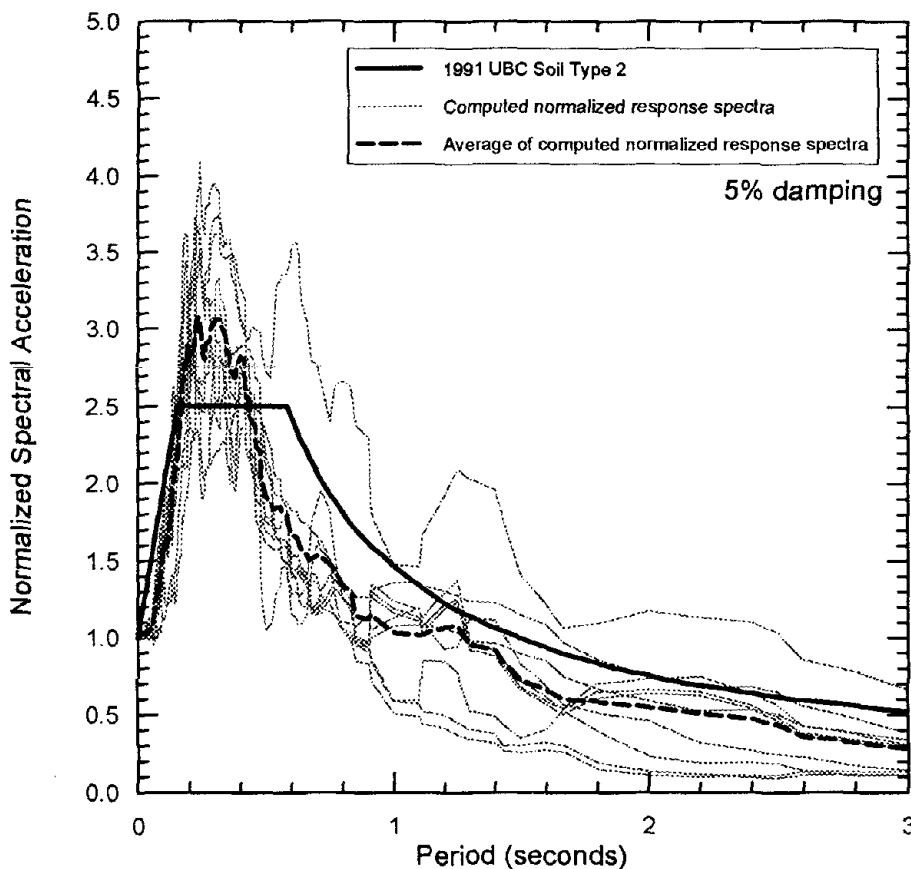


Fig. 3.21(b): Computed normalized spectral acceleration from ground motions recorded at the base of three multi-story buildings on soil compared to the 1991 UBC normalized design spectrum for Soil Type 2

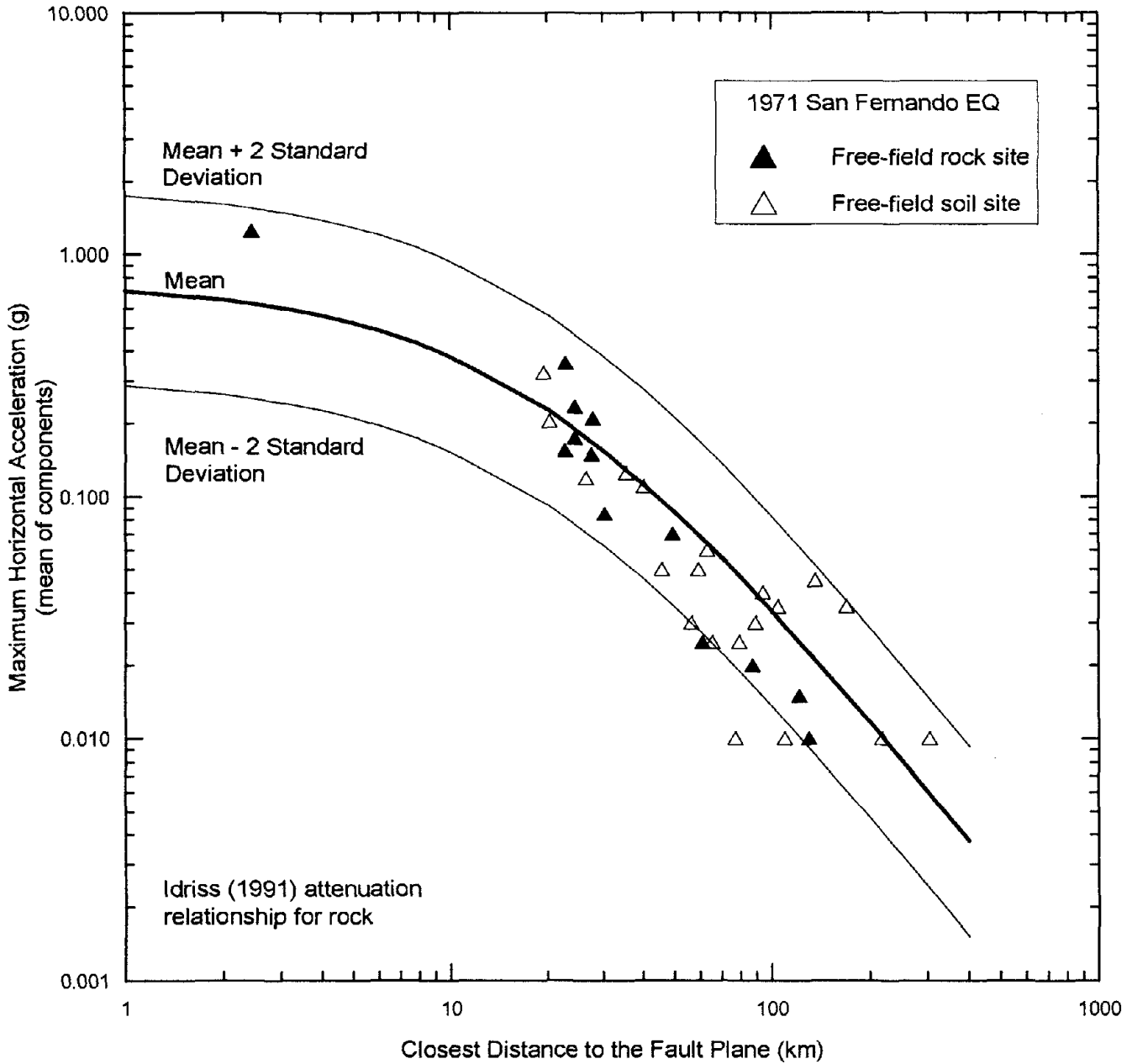


Fig. 3.22: Recorded maximum horizontal ground surface accelerations at free-field rock and soil sites during the 1971 San Fernando Earthquake and the attenuation relationship for rock proposed by Idriss (1991)

3.11(b)) are well represented by the Idriss attenuation relationship. It should be noted that in developing Figure 3.22, the hinged fault plane model described in Heaton (1982) was used to calculate closest distance to the fault plane for the 1971 San Fernando Earthquake.

3.4 Damage Patterns and the Effects of Local Site Conditions

3.4.1 Effects of Local Site Conditions

A plot of red-tagged (unsafe) structures in the earthquake area as of April 1994 is shown in Figure 3.23. According to the Governor's Office of Emergency Services (OES), approximately 2900 structures had been red-tagged and 11,000 had been issued yellow tags (limited entry) as of April 1994. As expected, there is a concentration of damage in the Northridge epicentral region; however, several significant concentrations of structural damage also occurred in a number of areas away from the epicentral region including: (a) Sherman Oaks, near Highway 101 just east of Highway 405, (b) at Hollywood, north of Santa Monica Boulevard between Interstate 5 and La Brea Avenue, (c) along an arc in central Los Angeles just to the northeast of Culver City, (d) in the Newhall area east of Interstate 5 in the Santa Clarita Valley, and (e) in Santa Monica, north of Colorado Avenue. Smaller pockets of damage were also found as far west as Fillmore, north to the Santa Clarita area, east to Pasadena and south to the Port of Los Angeles. By combining the map of damage patterns from Figure 3.23 with the generalized geologic map from Figure 1.1, it appears that many of the areas of concentrated structural damage are underlain by deep Holocene deposits and pronounced alluvial basins, as shown in Figure 3.24.

Similarly compelling evidence of the importance of local site conditions is apparent when the damage patterns from Figure 3.23 are compared to areas of "potentially liquefiable deposits," as identified by the Los Angeles County (1990) Safety Element of the General Plan. This is not meant to imply that liquefaction resulted in the observed damage concentration; these deposits are simply zones which are likely to contain softer or more recent soil deposits and relatively shallow groundwater. It is also possible that some partial pore pressure generation within potentially liquefiable deposits could have led to softening of soil at these sites, altering the soil's dynamic properties in such a way as to influence site amplification effects and thereby contribute to the observed structural damage by affecting the characteristics of the ground motions. As shown in Figure 3.25, there is a very strong correlation between these areas and the areas in which structural damage was concentrated, particularly outside of the epicentral region.

The plot of damage patterns is again shown in Figure 3.26 along with the maximum horizontal acceleration contours previously presented in Figure 3.4. Some correlation between MHA and localized damage is also evident.

a. Epicentral Area

A closer look at damage patterns in the epicentral San Fernando Valley area is presented in Figure 3.27. Surficial fine to coarse grained Holocene deposits, shown as shaded areas, essentially blanket the valley floor. Although damage appears to be widespread throughout



Fig. 3.24: Damage patterns from the 1994 Northridge Earthquake and generalized geologic conditions in the Los Angeles Area (Sources: Governor's Office of Emergency Services, 1994; Los Angeles County, 1990; California Division of Mines and Geology, 1969)

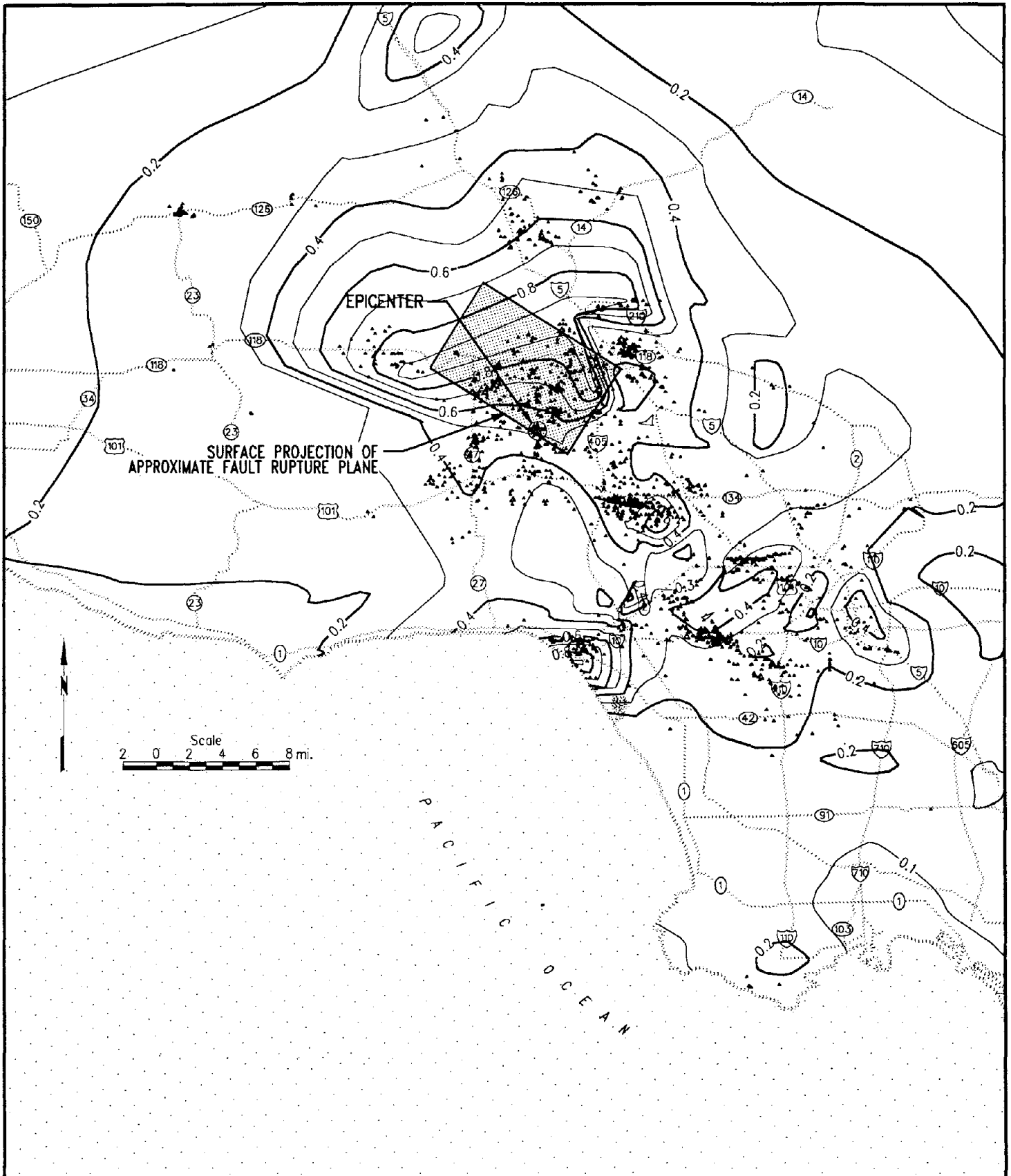
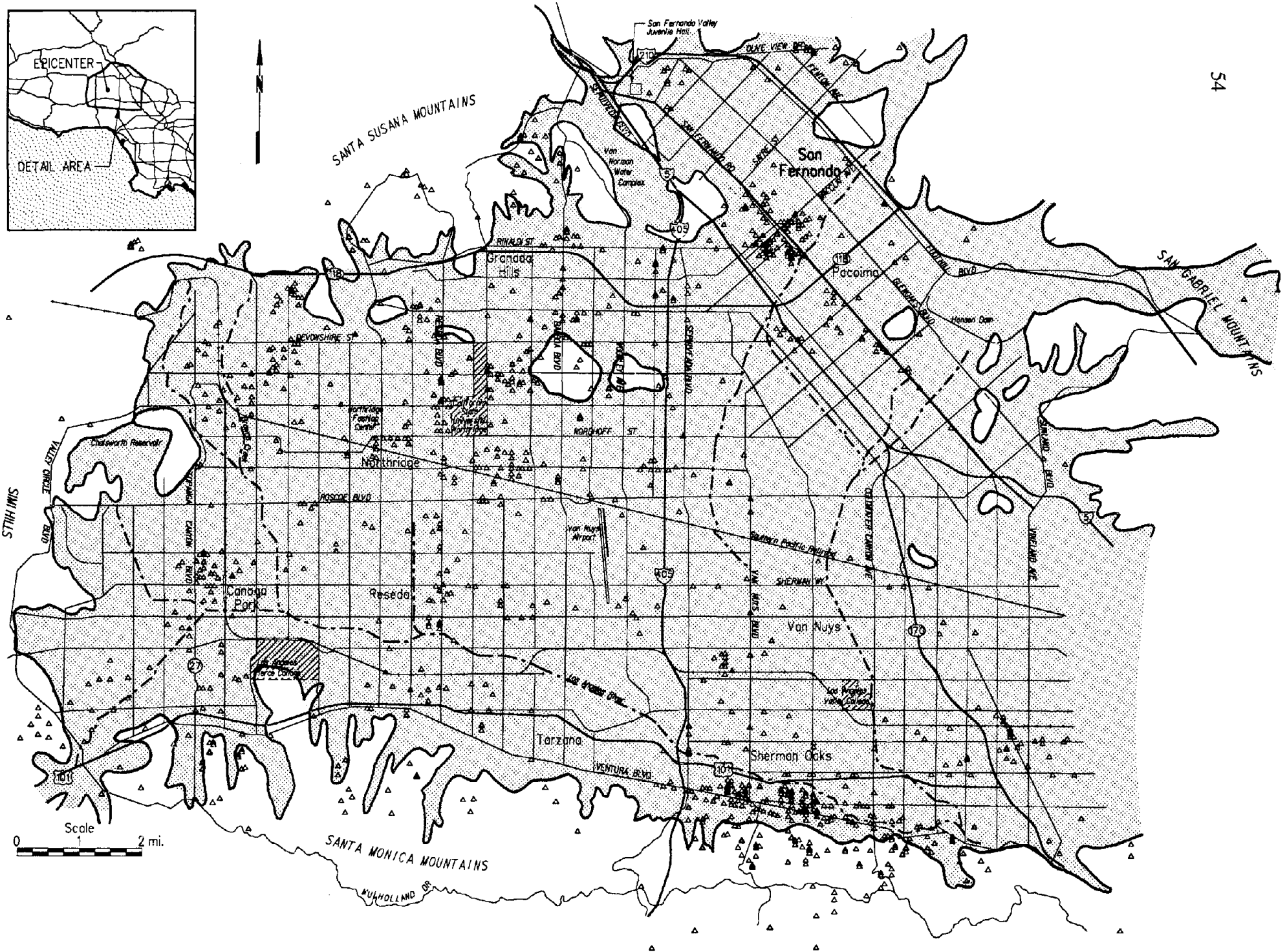


Fig. 3.26: Damage patterns from the Northridge Earthquake and contours of maximum horizontal acceleration based on recordings at rock and soil sites

Fig. 3.27: Map of San Fernando Valley showing locations of red-tagged structures and Holocene sediments



the valley, pockets of damage are evident which may be related to changes in site response characteristics resulting from partial pore pressure generation within potentially liquefiable deposits or to ground failure, as discussed in Section 4.2.

A cursory survey of damage concentration in the epicentral region by members of the U.C. Berkeley Geotechnical Group reconnaissance team indicated that damaged structures in the epicentral area included residential and commercial buildings of all types of construction, typically from one to three stories in height. Collapse of several modern multi-story concrete parking structures and damage to shopping malls was also observed. Structures with soft bottom stories and unreinforced masonry (URM) buildings were particularly vulnerable. Partial collapse of the first floor of a three-story wood-frame apartment complex in Northridge, shown in Figure 3.28(a), resulted in the deaths of 16 people. Residential homes generally suffered from collapsed chimneys and failure of masonry walls, as well as diagonal shear cracking in stucco walls. Dramatic failures also occurred at the Kaiser Permanente Office Building on Balboa Boulevard in Granada Hills and at a 5-story building at Sherman Way and Lindley Avenue in Reseda, shown in Figures 3.28(b) and 3.28(c), respectively.

b. Sherman Oaks

Damage concentration in the Sherman Oaks area is shown in the lower right corner of Figure 3.27, near the base of the Santa Monica Mountains and along the banks of the Los Angeles River. In Figure 3.25, it can be seen that the same area of damage concentration closely corresponds with a narrower band of potentially liquefiable Holocene deposits in the Sherman Oaks area (also see Figure 4.6 in Chapter 4). A 13-story building on Ventura Boulevard in Sherman Oaks recorded a maximum horizontal ground acceleration of 0.46g at the basement level. The Van-Nuys 7-story Hotel, discussed previously in Section 3.3.7, is located a few miles to the north and experienced an MHA of 0.45g at the ground floor.

As in the epicentral area, two- to four-story apartment buildings with soft stories were extensively damaged. Figure 3.29(a) shows the partial collapse of a two-story apartment building located at Hazeltine Avenue and Milbank Street. A yellow-tagged four-story apartment building of fairly recent construction is shown in Figure 3.29(b). This structure is located on Fulton Avenue near the banks of the Los Angeles River. Residential homes in the area are typically one story in height and generally suffered from chimney collapses and diagonal shear cracking in walls, although more serious structural damage was also observed. Cracking in shear walls was observed in a 13-story reinforced concrete building in the downtown area, as shown in Figure 3.29(c), and a 12-story hotel in the vicinity was red-tagged as shown in Figure 3.29(d).

c. Hollywood

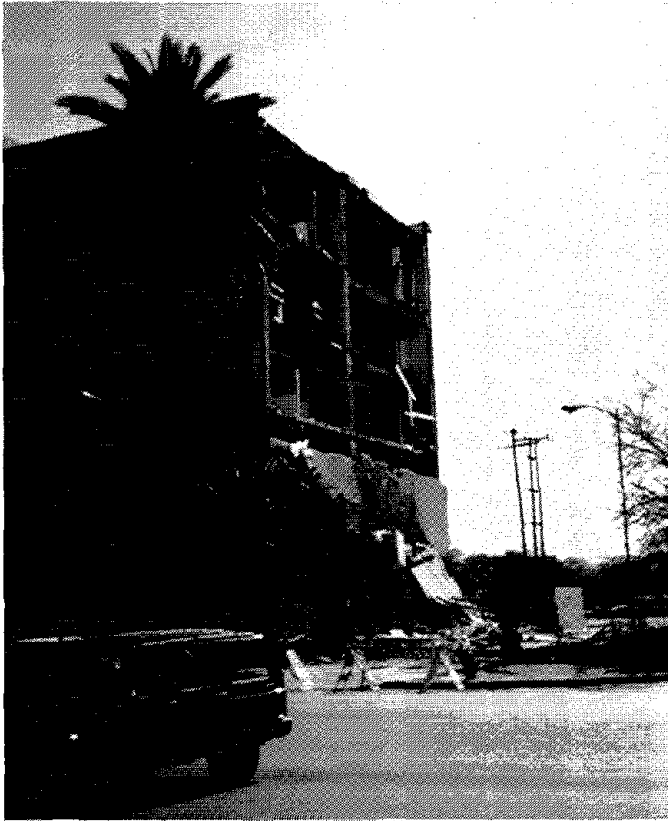
Concentrations of unsafe buildings in the Hollywood area are presented in Figure 3.30. Again, the fine shaded areas represent surficial fine to coarse Holocene deposits and appear to correlate well with the location of red-tagged structures. Zones of potentially liquefiable deposits are also essentially delineated by these shaded areas. At the Hollywood Storage Building grounds, located west of 1100 Highland Avenue just south of Santa Monica



(a)



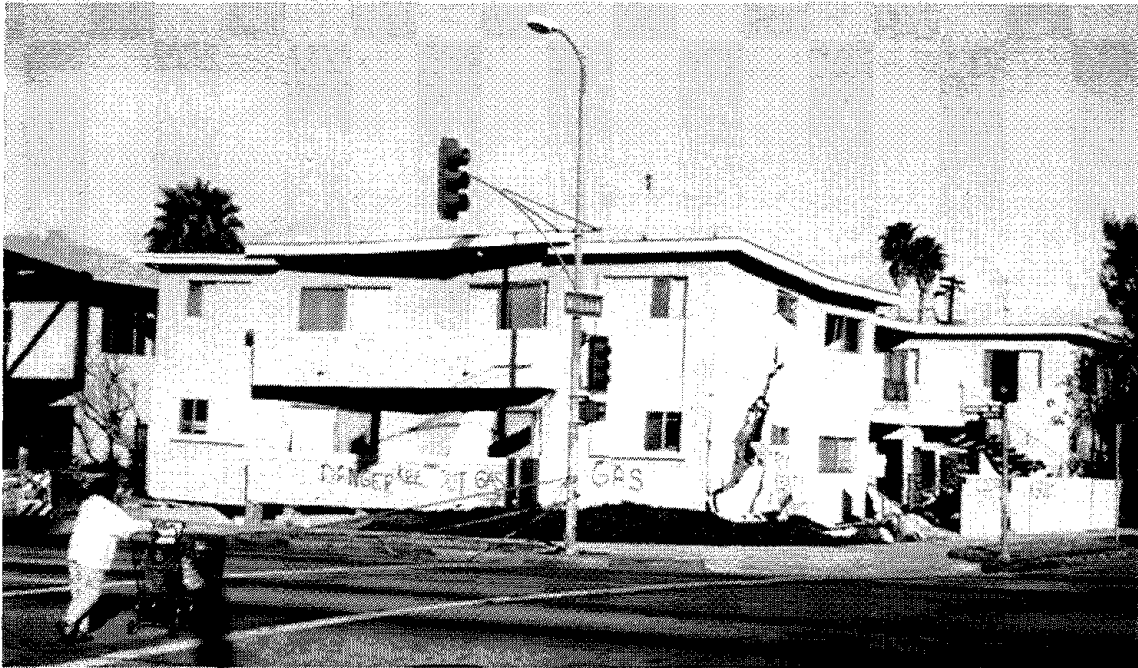
(b)



(c)

Fig. 3.28: Damaged structures in the Northridge epicentral area

- (a) Soft story collapse of a three-story wood frame apartment building in Northridge
- (b) Partially collapsed 5-story Kaiser Permanente office building in Granada Hills
- (c) Heavily damaged 5-story building at Sherman Way and Lindley Ave. in Reseda



(a): Heavily damaged apartment building with soft story at Hazeltine Avenue and Milbank Street



(b): Yellow-tagged 4-story apartment building on Fulton Way, near the banks of the Los Angeles River

Fig. 3.29: Damaged structures in the Sherman Oaks area



(c): Cracking in shear wall of a 13-story reinforced concrete structure on Ventura Boulevard



(d): Red-tagged 12-story hotel on Ventura Boulevard

Fig. 3.29: Damaged structures in the Sherman Oaks area

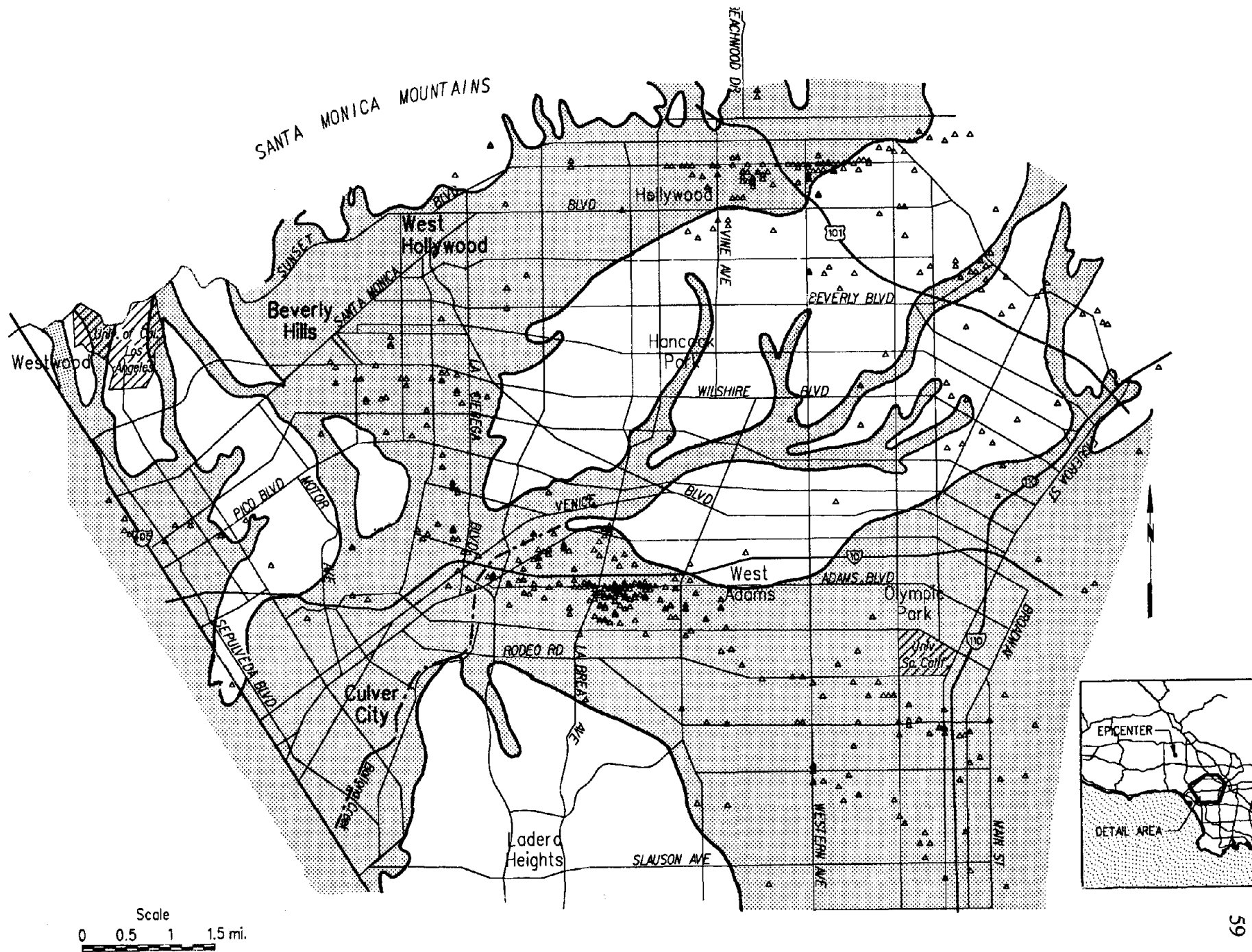


Fig. 3.30: Map of the Central Los Angeles region showing locations of red-tagged structures and Holocene sediments

Boulevard between Vine and La Brea Avenues, an MHA of 0.40g was recorded.

In the Hollywood area, shear cracking and chimney damage to single-story residences, as well as damage to soft story apartments and buildings of up to 12 stories in height, were observed. Typical damage to a URM building is shown in Figure 3.31.

d. Central Los Angeles

A map showing the locations of unsafe structures in the central Los Angeles area is also presented in Figure 3.30. The locations of zones of surficial Holocene deposits correlate well with the damage patterns. Of the USGS and CSMIP stations, the closest station to the damage concentration in central Los Angeles is located just to the south in Baldwin Hills; however, this instrument is situated on thin fill or alluvium over rock. The LA Century City North site, which recorded an MHA of 0.26g, appears to be the next closest station on alluvium.

An example of damage in the central Los Angeles area with possible contributions from site effects is the collapse of the Interstate 10 overcrossing structure (Bridge No. 53-1609) at Venice and La Cienega Boulevards, shown in Figure 3.32, and just to the east at the Interstate 10 overcrossing (Bridge No. 53-1580) at Fairfax and Washington. The site of both bridges is part of the drainage area for Ballona Creek and is a recovered swamp area. The two bridges are also located in the shaded areas shown in Figure 4.92, which show zones of saturated Holocene deposits. Based on boring logs and personal communication with the California Department of Transportation (Caltrans), soils with low blow counts are found within the shaded zones along Interstate 10 shown in Figure 4.92; outside of this zone, the soils become denser. It should be noted that other highway bridges in this zone of relatively loose soils did not collapse.

Structures in the central Los Angeles area typically appeared to be small residences, one- to three-story warehouses and commercial buildings, and low-rise apartments. Again, damage to URM buildings and apartments with soft stories was observed. Much of the damage appeared to be to residential structures; cracks in walls, collapsed chimneys, and shifting off of foundations was observed. A typical damaged home is shown in Figure 3.33.

e. Santa Clarita area

As shown in Figure 3.34, damage in the Newhall area, located in the City of Santa Clarita (north of San Fernando Valley) was generally confined to Quaternary deposits covering the valley floors. The maximum horizontal acceleration as well as the maximum vertical acceleration recorded at the Newhall-LA County Fire Station was approximately 0.6g. Severe damage to steel moment frame structures of medium height in Santa Clarita was reported by Hall (1994).

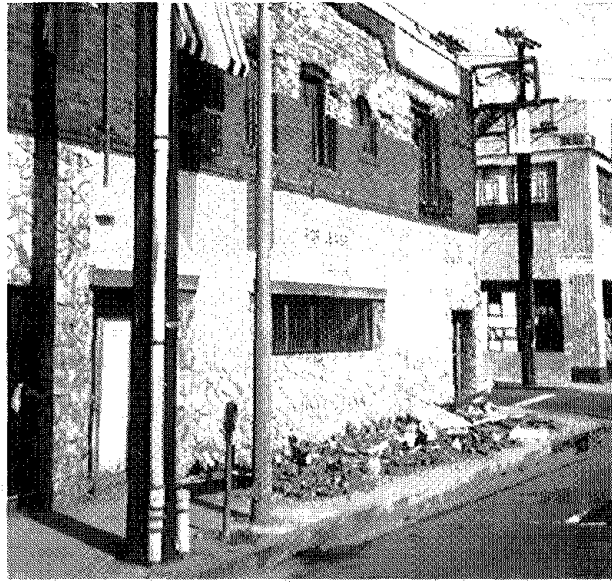


Fig. 3.31: Damage to an URM building in Hollywood



Fig. 3.32: Collapse of the I-10 overcrossing structure at Venice and La Cienega Boulevards.



Fig. 3.33: Typical damage to a two-story residence in Central Los Angeles

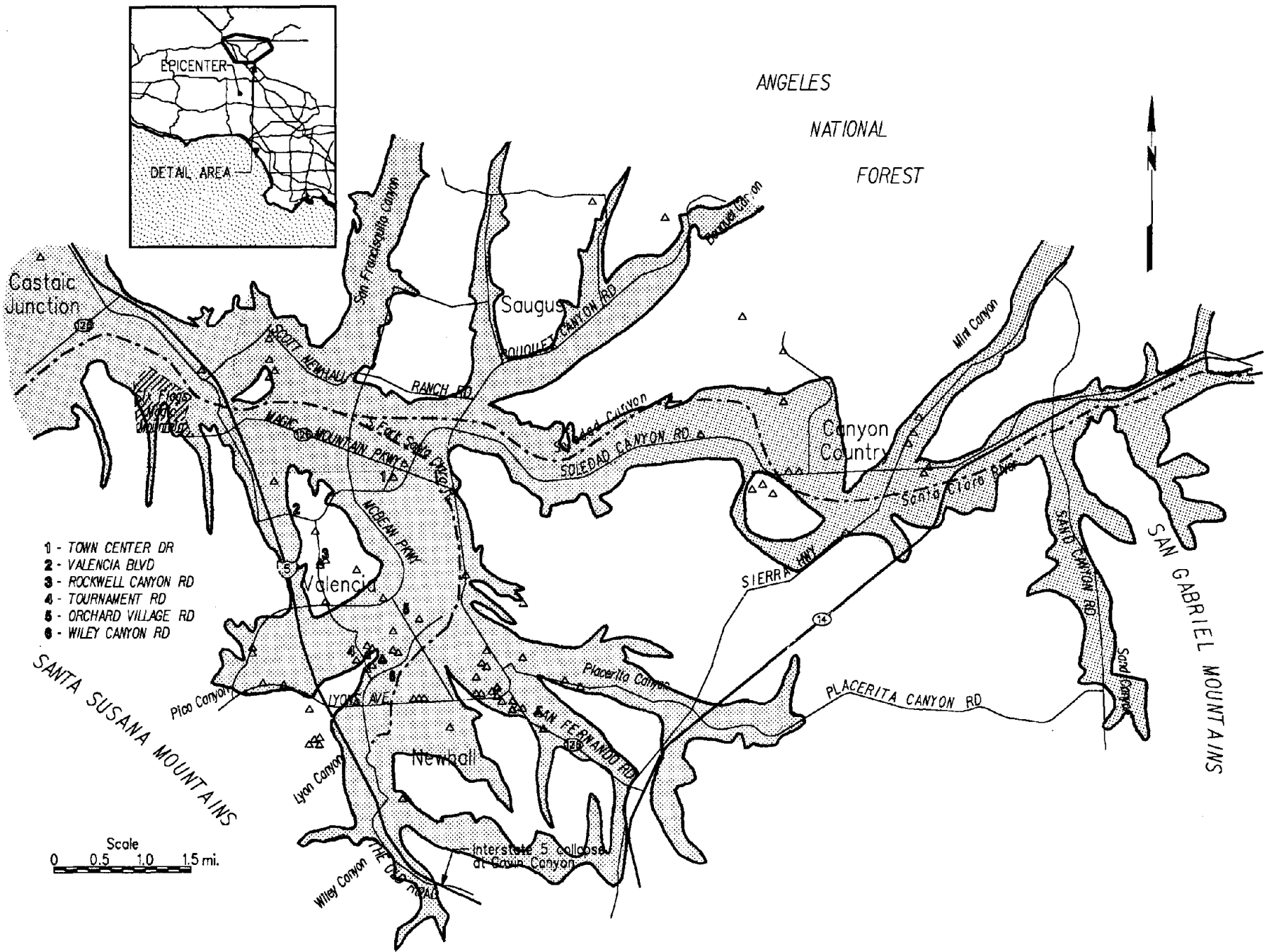


Fig. 3.34: Map of the Santa Clarita Valley showing locations of red-tagged structures and Quaternary sediments

f. Santa Monica area

As shown in Figure 3.35, the cluster of red-tagged structures in the Santa Monica area is concentrated in an area of surficial fine to coarse grained Pleistocene alluvium north of Colorado Boulevard, not in the area of surficial Holocene deposits as was the case for the areas described previously. According to the City of Santa Monica, the buildings south of Colorado Avenue experienced minimal damage due to the earthquake, although the area has over 50 unreinforced masonry buildings as well as many structures constructed before the 1920's. In all, approximately 129 buildings were red-tagged and 358 buildings were yellow tagged as of April 1994. Although further study is warranted, the damage concentration in the Santa Monica area may be a possible case history for significant site amplification by deep, older stiff soils.

In addition, topographic features that may represent active traces of the north dipping Santa Monica fault (Leighton and Associates, et. al. 1992) appear to run through the northern one-third to one-half of the area in which earthquake damage was concentrated; however, it should be noted that no sympathetic movement appears to have occurred on these fault traces during the Northridge earthquake.

The Santa Monica-City Hall grounds strong motion station, located at 1685 Main Street north of Pico Boulevard, recorded MHA's of 0.90g and 0.41g for the 90 degree and 360 degree components, respectively. Boring logs to a maximum depth of about 10.5 m (35 feet), drilled for the construction of the City Hall addition and an office building located across the street at 1700 Main Street, indicate that the surficial deposits at the site include up to 4.5 meters (15 feet) of stiff silty clay and sandy silt with occasional gravel over dense gravelly, silty sand. Although the depth to bedrock in the area is not precisely known, the Quaternary alluvium at the VA Hospital site, located approximately 4-1/2 km (2-3/4 miles) northeast of the Santa Monica City Hall, is believed to be about 120 m (400 feet) thick (James E. Slosson & Associates, 1972).

Damage to low-rise apartment buildings with soft stories was again observed. A typical building is shown in Figure 3.36(a). Cracks in the shear walls of a 6-story commercial building are shown in Figure 3.36(b). An example of typical damage to a URM building is presented in Figure 3.36(c). At least 34 URM buildings were red-tagged and 51 URM buildings were yellow tagged in the City of Santa Monica. Red tags were also issued to five health care facilities in Santa Monica. North of Santa Monica in Pacific Palisades, extensive damage was observed along Chataqua Boulevard. The area is underlain by Holocene deposits, and an example of typical damage is shown in Figure 3.36(d).

3.4.2 Computed Response Spectra at Strong Motion Stations Near Areas of Damage Concentration

Figure 3.37 shows computed response spectra for recordings from CSMIP stations located near areas of significant damage concentration. Comparison between the computed recorded response spectra and the 1991 UBC Soil Type 2 design spectrum for MHA=0.4g shows that the code spectrum is exceeded at several of the strong motion station locations,

SANTA MONICA MOUNTAINS

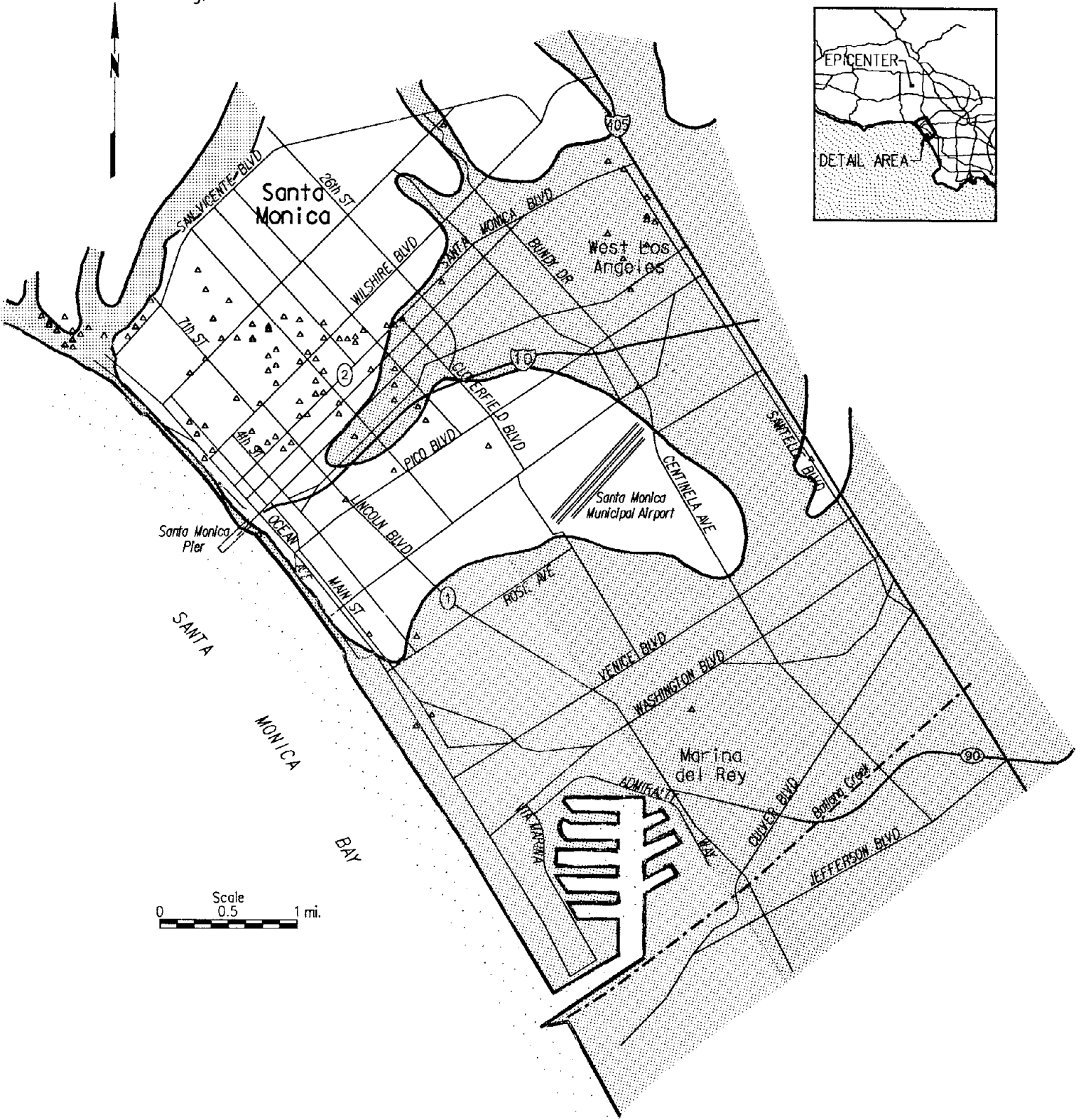
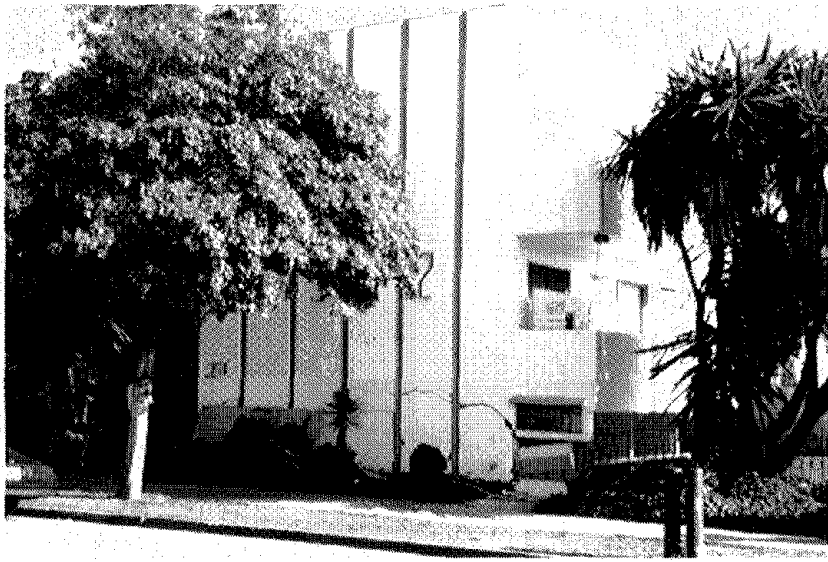


Fig. 3.35: Map of the Santa Monica - Marina del Rey area showing locations of red-tagged structures and Holocene sediments



(a) Typical damage to a soft story apartment building



(b) Cracks in the shear walls of a 6-story commercial building



(c) Heavily damaged URM building



(d) Typical damage along Chataqua Boulevard

Fig. 3.36: Damage in the Santa Monica Area

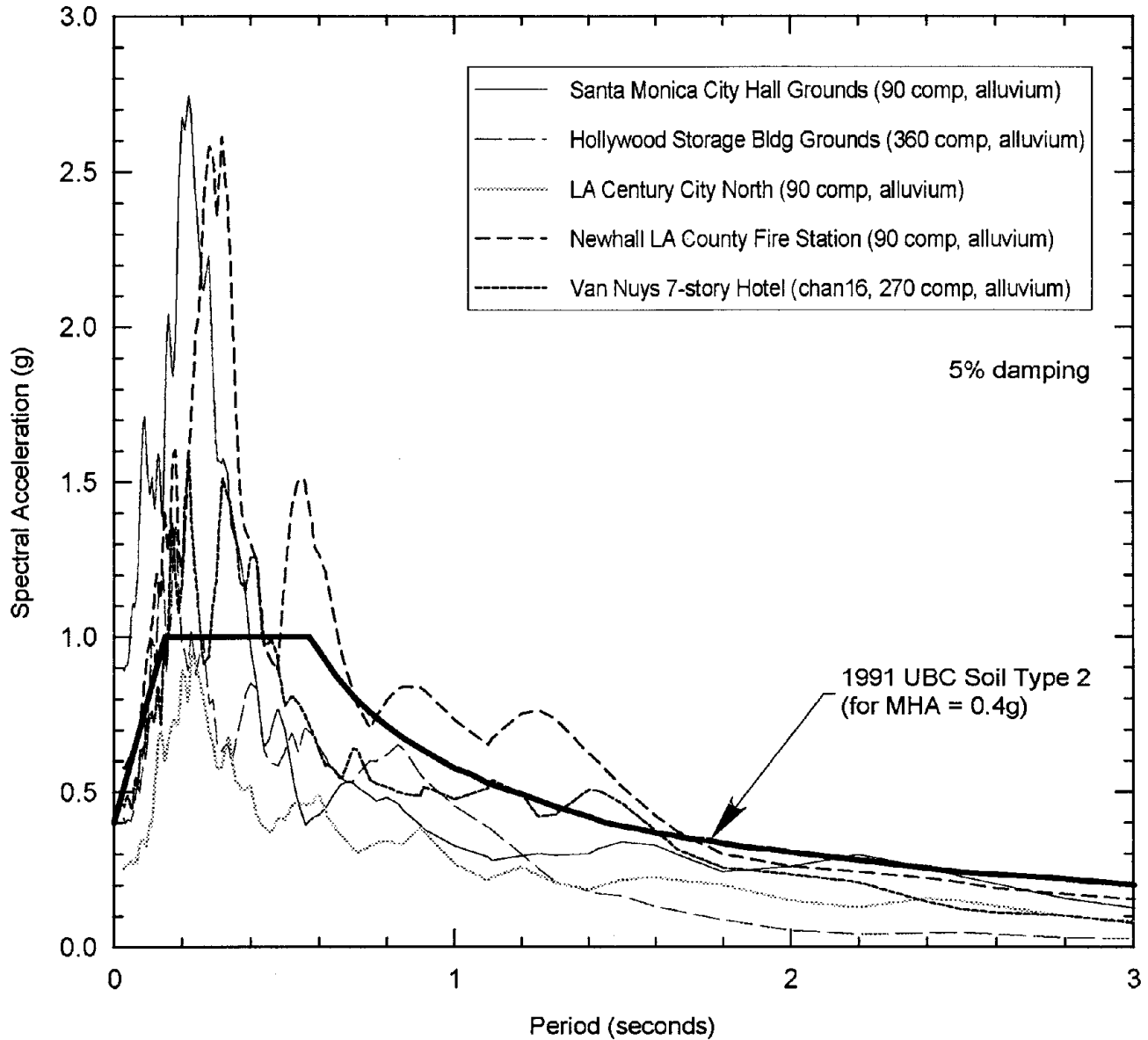


Fig. 3.37: Comparison of computed response spectra for strong motions recorded near areas of damage concentration along with the UBC Soil Type 2 design spectrum for MHA = 0.4g

and that the code spectrum was significantly exceeded at relatively short periods of approximately 0.1 to 0.5 seconds at several stations.

3.4.3 Other Contributions to Localized Damage

In addition to the apparent effects of subsurface soil conditions and topographic effects, further study is required to determine the effects on ground motions and damage patterns caused by variations in the earthquake source and wave propagation path. Focusing of energy due to basin and edge effects may have contributed significantly to concentrations of structural damage. Many of the areas with localized damage are generally concentrated near the edges of soil-filled basins, such as adjacent to the Santa Monica Mountains or other topographic relief. Basin model studies of the Los Angeles area, such as Saikia et. al. (1994), have proposed explanations for these types of variations in recorded ground motions due to irregular basin structure and local site geology.

It should be noted that concentrations of damage are also affected by the building type and quality of construction. As in previous earthquakes, URM buildings and structures with soft lower stories generally fared poorly during the Northridge event.

3.5 Preliminary Analyses for the Sylmar-County Hospital Parking Lot Site

The influence of local soil conditions on ground shaking characteristics can be seen from a preliminary analysis of the Sylmar-County Hospital Parking Lot site. The free-field strong ground motion instrument, located in the hospital parking lot, recorded a MHA of about 0.89g during the Northridge event. The original Olive View Hospital was heavily damaged at this site during the 1971 San Fernando Earthquake. SHAKE91 (Idriss and Sun, 1992), a one-dimensional equivalent linear analysis program, was used to calculate the seismic response of the site.

According to Duke et. al. (1971), the site is underlain by approximately 91 m (300 feet) of alluvium, and a generalized profile is shown in Figure 3.38(a). The shear wave velocity profile of the site was modified after Duke et.al. (1971), and the nearby Pacoima Dam Downstream (175 comp) record was used as the input. The modulus degradation curves for sands proposed by Iwasaki (1988) were used along with the approximate lower bound damping curves for sand proposed by Seed and Idriss (1970).

The response spectra of the motions recorded at the site, the input rock motion, and the computed response are shown in Figure 3.38(b). At short periods, the response of the site is captured fairly well by the analyses; the analyses correctly predicted the approximate doubling of the peak horizontal ground surface acceleration, and captured reasonably well the spectral acceleration peak at a period of about 0.4 seconds. The calculated response is, however, missing much of the recorded response at long periods of greater than about one second. This can probably be attributed to the lack of long period energy in the input rock motion and to the limitations imposed by one-dimensional equivalent linear analyses, which do not model long-period surface waves. Calculations using the nearby Pacoima-Kagel Canyon record as the input rock motion, which contains somewhat more energy in the longer periods, did not produce significantly more satisfactory results in the longer period range.

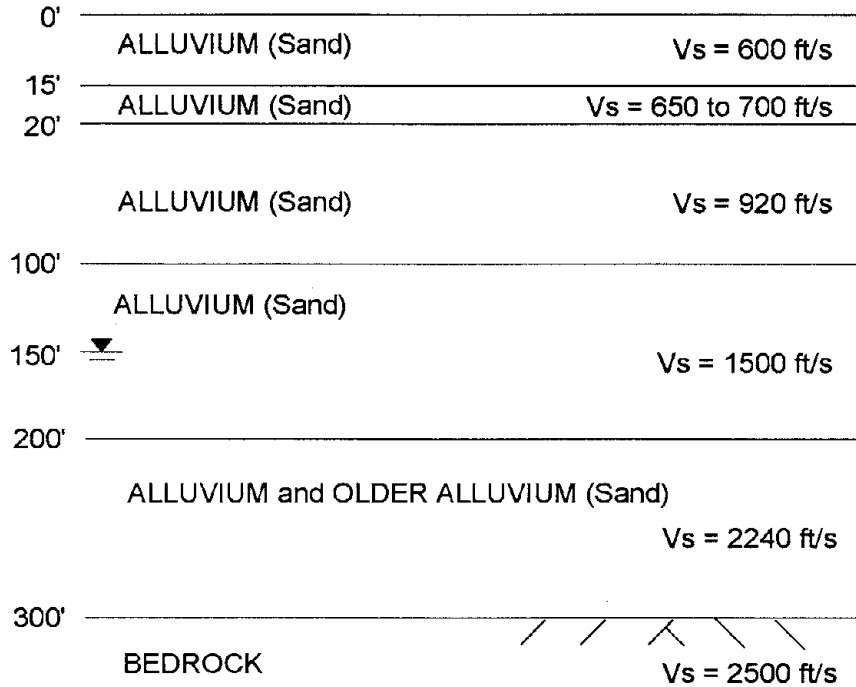


Fig. 3.38(a): Soil profile for the Sylmar - County Hospital Parking Lot Site (Olive View Hospital) modified after C.M. Duke et. al. (1971)

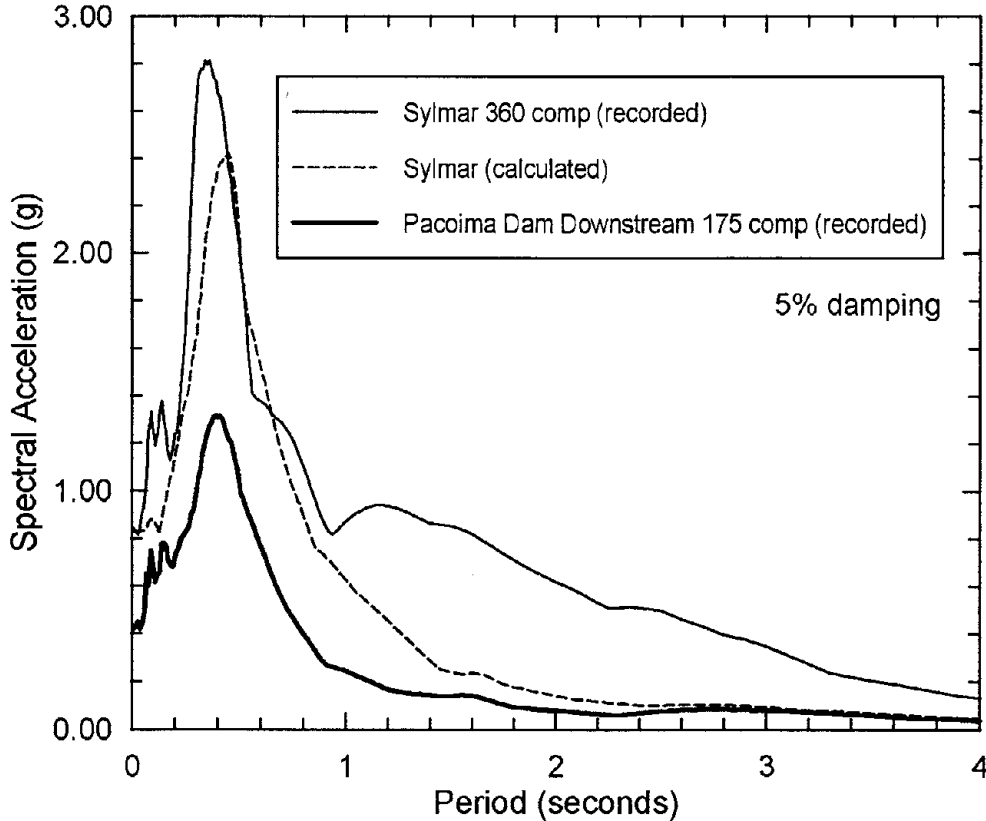


Fig. 3.38(b): Comparison of acceleration response spectra for the recorded and calculated motions at the Sylmar-County Hospital Parking Lot site. The response spectrum for the input motion (Pacoima Dam Downstream) is also shown.

3.6 Summary

The ground motions experienced in the Los Angeles area during the Northridge Earthquake were not unusual in magnitude except for in a few areas, such as Tarzana and Santa Monica. The mean MHA on rock for this $M_w=6.7$ thrust fault event appear to have been generally well-represented by the attenuation relationship for rock proposed by Idriss (1991). The mean MHA on soil tended to be about one standard deviation above the mean MHA on rock, indicating the importance of local site conditions. The ratio of maximum vertical accelerations to maximum horizontal accelerations followed generally accepted relationships. Comparison of computed acceleration response spectra (from the recorded motions available from CSMIP) with the 1991 UBC design spectra show that the code design spectra are exceeded at numerous sites when the UBC maximum horizontal acceleration "cap" or limit of $MHA \leq 0.4g$ is used; however, the shape of the UBC normalized design spectrum captured the available data well.

The importance of local site conditions on damage patterns was apparent based on the geographic distribution of heavily damaged structures in the area and correlations of zones of concentrated damage with the locations of softer, surficial Holocene deposits. The damage concentration in the City of Santa Monica may also be a case history for site amplification due to deep, older, stiffer soils. Localized pockets of damage near the edges of basins indicate that focusing of energy due to basin and edge effects may have also been a significant factor. Site response analyses performed for the Sylmar-County Hospital Parking Lot site indicate that much of the site amplification effects can be captured with one-dimensional, equivalent linear vertical wave propagation analyses, but suggest that some potentially significant long-period response may be underpredicted by this approach.

Page Intentionally Left Blank

Chapter Four: Ground Failure

by Jonathan P. Stewart, Patricia Thomas, William B. Gookin,
Raymond B. Seed, and Jonathan D. Bray

4.1 Introduction

A general overview of damage caused by ground failure during the Northridge Earthquake is presented in this chapter, with the exception of ground failure effects on geotechnical structures, which are discussed separately in Chapter 6. Ground failure by soil liquefaction and dynamic ground compaction affected sites over a large area, including sites as far as 36 miles from the epicenter, as shown previously in Figure 1.3. The region most heavily impacted by ground failure was the San Fernando Valley, where consequent damages included widespread pipe breakage, pavement disruption, and, in some cases, structural distress. Outside of the San Fernando Valley epicentral region, ground failure by soil liquefaction or partial liquefaction occurred to the west in Simi Valley, to the north at a number of locations near the Santa Clara River, and to the south in several coastal areas and possibly in central Los Angeles. Ground failure by soil liquefaction at considerable depths and/or by dynamic ground compaction (which results from soil particle re-arrangement and matrix densification under strong levels of ground shaking) appears to have strongly impacted the Granada Hills area as well as portions of several surrounding regions including Simi Valley and Santa Clarita. Damage resulting from soil liquefaction or dynamic ground compaction typically consisted of broken utility pipes, disruption of pavements, and occasional moderate distress to structures. In most cases, structural damage appears to have primarily resulted from large inertial forces associated with strong ground shaking.

4.2 San Fernando Valley Area

4.2.1 Introduction

Ground failure caused extensive damage in the San Fernando Valley communities of Northridge, Canoga Park, Granada Hills, and San Fernando. Due in no small part to their close proximity to the zone of energy release, these near-field areas generally experienced very strong levels of shaking, with peak horizontal ground accelerations on the order of 0.4g to 0.9g having been recorded at soil sites (Figure 3.4). Ground failure in surficial sandy soils resulted in sand boils, lateral spreading, settlement, pavement damage, and damage to buried utility pipes. Widespread damage to structures also occurred in the San Fernando Valley, but a majority of this damage can be attributed to large inertial forces resulting from the strong levels of ground shaking and does not appear to be the direct result of ground failure. In some areas, however, ground failure appears to have contributed to structural damage patterns.

4.2.2 Geologic and Groundwater Conditions

The San Fernando Valley overlies a deep bedrock basin filled in over Quaternary time by alluvial sediments. Some of these alluvial sediments consist of recent sandy stream channel deposits which can be sufficiently loose to exhibit contractive behavior during shear.

Hence, when saturated, these materials are potentially vulnerable to liquefaction under strong earthquake shaking. In addition to soil type, liquefaction potential is also dependant upon the depth to groundwater. Portions of the San Fernando Valley are underlain by perched aquifers which result in relatively shallow groundwater depths (less than 30 feet), whereas outside of these zones, groundwater depths often exceed 50 feet. Generally, the water table depth is highly variable across the region, a condition likely resulting from geologic and land use heterogeneity as well as groundwater pumping operations. It should be noted that the groundwater table may have been unusually low in portions of the strongly shaken region due to an unusual period of six weeks of unseasonably low precipitation which preceded the earthquake. These unseasonably low groundwater levels may have influenced the occurrences of liquefaction in some areas.

For liquefaction microzonation and planning purposes, Holocene-age geologic units comprised in part of cohesionless soils are typically classified as "liquefiable" when the depth to groundwater is less than 30 feet, and as "potentially liquefiable" at groundwater depths of 30 to 50 feet (Youd, et al., 1978, Los Angeles County, 1990). This type of mapping technique is necessarily very approximate, as individual sites within broad "liquefiable" zones may well be underlain by unliquefiable soil types. In addition, the mapped zones are not intended to encompass all liquefiable soils, but only to identify those broad regions within which the liquefaction hazard is generally highest.

Figure 4.1 shows zones classified and mapped as "liquefiable" from the Safety Element of the Los Angeles County General Plan (Los Angeles County, 1990). The delineation of these zones was based in part on groundwater data collected over the last several decades, and hence may not reflect the groundwater conditions in January 1994 precisely. However, the mapping does provide a reasonable starting point for identifying broad zones that might have shallower groundwater depths and higher liquefaction susceptibilities. Mapped "liquefiable" soil zones include broad areas in the west, southwest, and south portions of the San Fernando Valley, as well as a relatively narrow zone encompassing the Van Norman Complex, several adjacent areas in the City of San Fernando, and the Hansen Dam area. The vast majority of the remaining areas not shown as "liquefiable" in Figure 4.1 have groundwater depths in excess of 50 feet, and hence would generally be described as having a very low liquefaction susceptibility.

4.2.3 General Damage Distribution

Damages due to ground failures in communities within the San Fernando Valley such as Granada Hills, Northridge, San Fernando, and Sherman Oaks were significant and widespread. Broken water lines such as that shown in Figure 4.2 disrupted water service to some areas for weeks. Also broken were numerous gas lines, leading to devastating fires which destroyed a number of homes as shown in Figures 4.3 and 4.4. As shown in Figure 4.3, some of these fires were spread by "burning water" which resulted from ignition of leaked natural gas being carried along by the flow from broken water pipes. Most of the damage in these areas was of a less spectacular nature, however, and occurred as relatively minor, but very pervasive, damage to pavements and utility lines distressed by localized lateral compression, extension, and differential settlements.

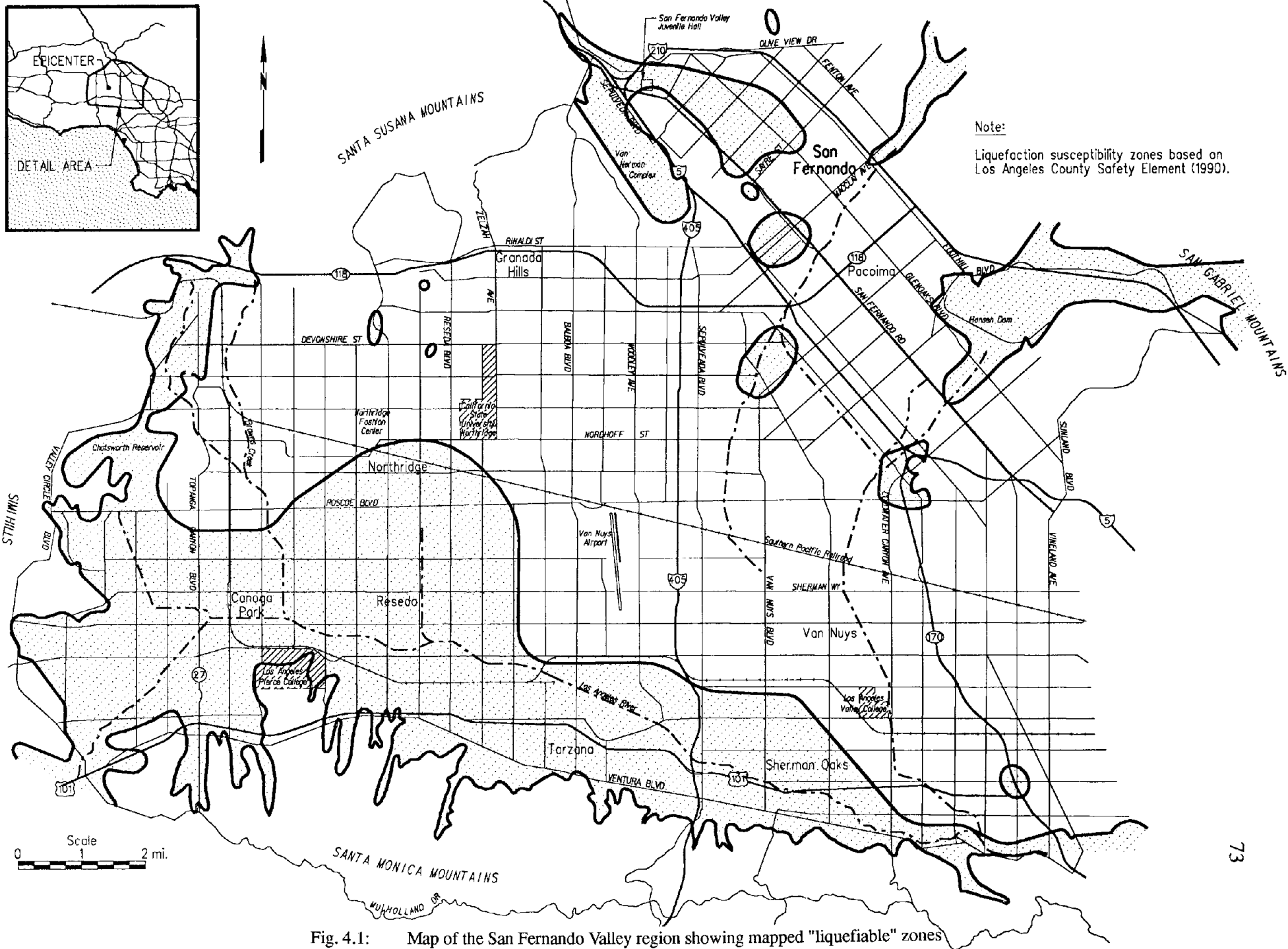


Fig. 4.1: Map of the San Fernando Valley region showing mapped "liquefiable" zones



Fig. 4.2: Geyser from broken water pipe in Sherman Oaks



Fig. 4.3: Flooding, fires, and burned homes in Granada Hills along Balboa Boulevard. Photo by Los Angeles Times.



Fig. 4.4: Homes destroyed by fires in Pacoima

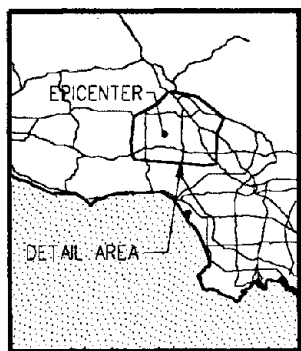
Over 1,600 breaks and leaks occurred in the water distribution system for the San Fernando Valley area, as shown in Figure 4.5, which also incorporates the outlines of the zones of highest predicted liquefaction hazard from Figure 4.1 (City of Los Angeles, 1994). Concentrated zones of distress to the water pipe network are located in the Northridge-Reseda-Canoga Park area southwest of the California State University (CSU) Northridge campus, in the Granada Hills area near Highway 118, in Sherman Oaks along Ventura Boulevard, and in the Santa Monica Mountains south of the San Fernando Valley. In addition, hundreds of breaks in water and gas lines were reported in the City of San Fernando southwest of the intersection of San Fernando Road and Maclay Avenue, although the locations of individual breaks were not available at the time this report was prepared (City of San Fernando, 1994). Also plotted in Figure 4.5 are the locations of breaks in a proprietary oil pipeline which traverses the northeast portion of the San Fernando Valley between San Fernando Road and Laurel Canyon Boulevard (California State Fire Marshall, 1994). As shown in Figure 4.5, most of the zones of concentrated pipe breakage occur within mapped "liquefiable" areas. The primary exception to this general trend is the concentration of breaks in Granada Hills near Highway 118, an area approximately bounded by the Santa Susana Mountains to the north, and by Sepulveda Boulevard, Nordhoff Street, and Zelzah Avenue to the east, south, and west, respectively.

In general, only zones with concentrated pipe breakage patterns are considered to have experienced significant ground failure. As shown in Figure 4.5, outside of the heavily affected zones discussed above, a relatively scattered and dispersed pattern of pipe distress occurred throughout the general epicentral region. This dispersed breakage pattern is unlikely to have resulted primarily from ground failure. Rather, many of these breaks and leaks likely occurred primarily in old, brittle pipes broken or cracked by ground movements directly associated with strong shaking.

Figure 4.6 shows the locations of structures deemed "unsafe" as indicated by red post-earthquake inspection tags, along with the outlines of soil zones having the highest predicted liquefaction hazard from Figure 4.1 (FEMA, 1994). Unlike the distribution of pipe breaks, a large amount of the structural damage occurred outside of mapped "liquefiable" soil zones in the Northridge-Granada Hills area, north of the CSU Northridge campus. However, it should be noted that high concentrations of structural damage also occurred in "liquefiable" zones more than 6 miles from the epicenter along the Ventura Boulevard corridor in Sherman Oaks and in the City of San Fernando southwest of San Fernando Road near Maclay Avenue.

4.2.4 Granada Hills Area

Some of the most vivid examples of ground failure to result from the Northridge Earthquake occurred just north of the epicenter in Granada Hills. This area experienced a large concentration of pipe breaks north of Highway 118 approximately between Balboa Boulevard and Woodley Avenue (see Figure 4.5), including several broken water mains and gas lines along Balboa Boulevard. Soil erosion resulting from broken water mains formed large craters in some streets, and leaking gas ignited at several locations leading to damaging fires, as shown in Figure 4.7. During repairs, some broken water and gas lines along Balboa Boulevard just north of Rinaldi Street were found to have experienced 6 to 12 inches of

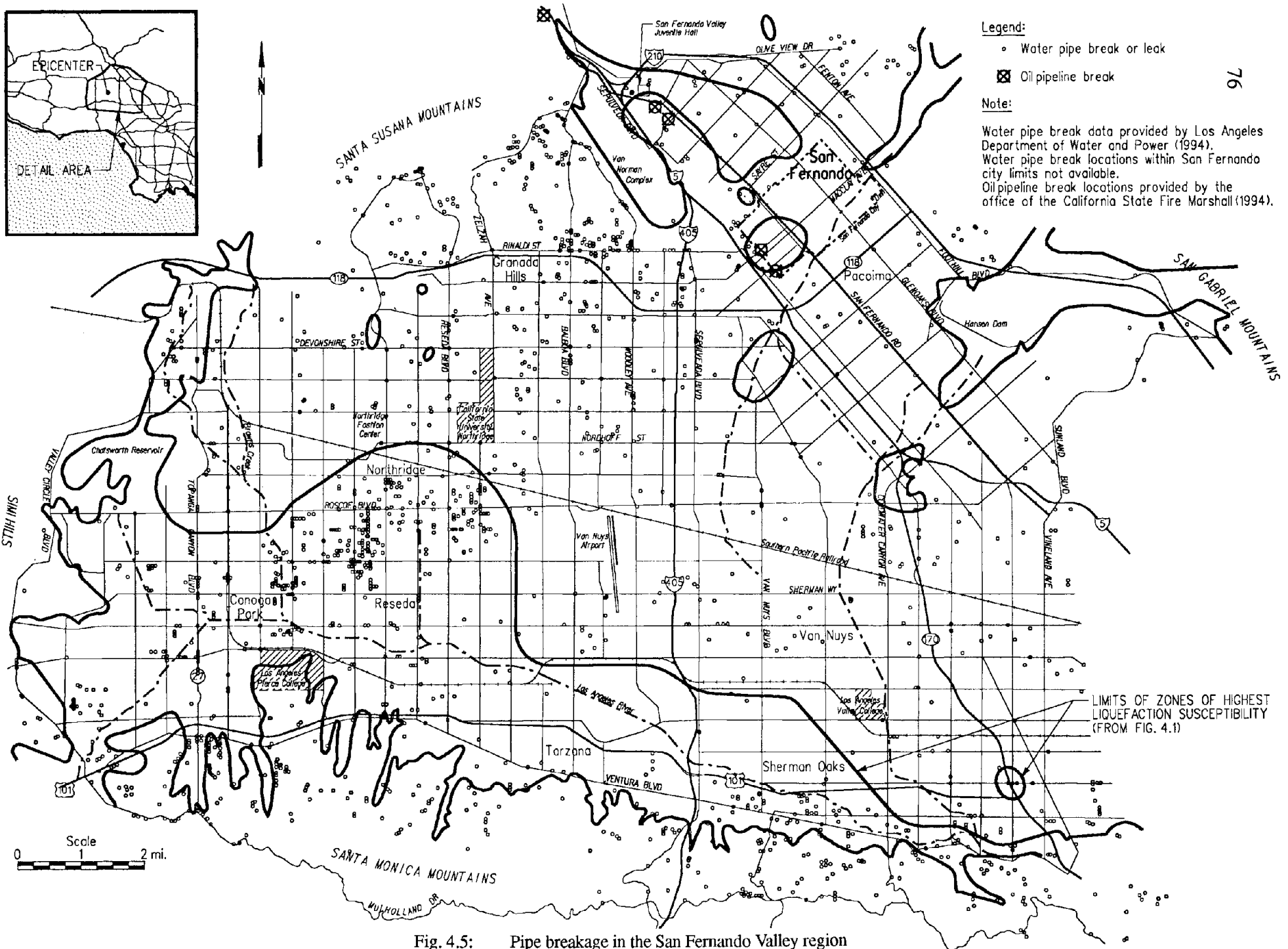


Legend:

- Water pipe break or leak
- ⊠ Oil pipeline break

Note:

Water pipe break data provided by Los Angeles Department of Water and Power (1994).
 Water pipe break locations within San Fernando city limits not available.
 Oil pipeline break locations provided by the office of the California State Fire Marshall (1994).



LIMITS OF ZONES OF HIGHEST LIQUEFACTION SUSCEPTIBILITY (FROM FIG. 4.1)

Fig. 4.5: Pipe breakage in the San Fernando Valley region

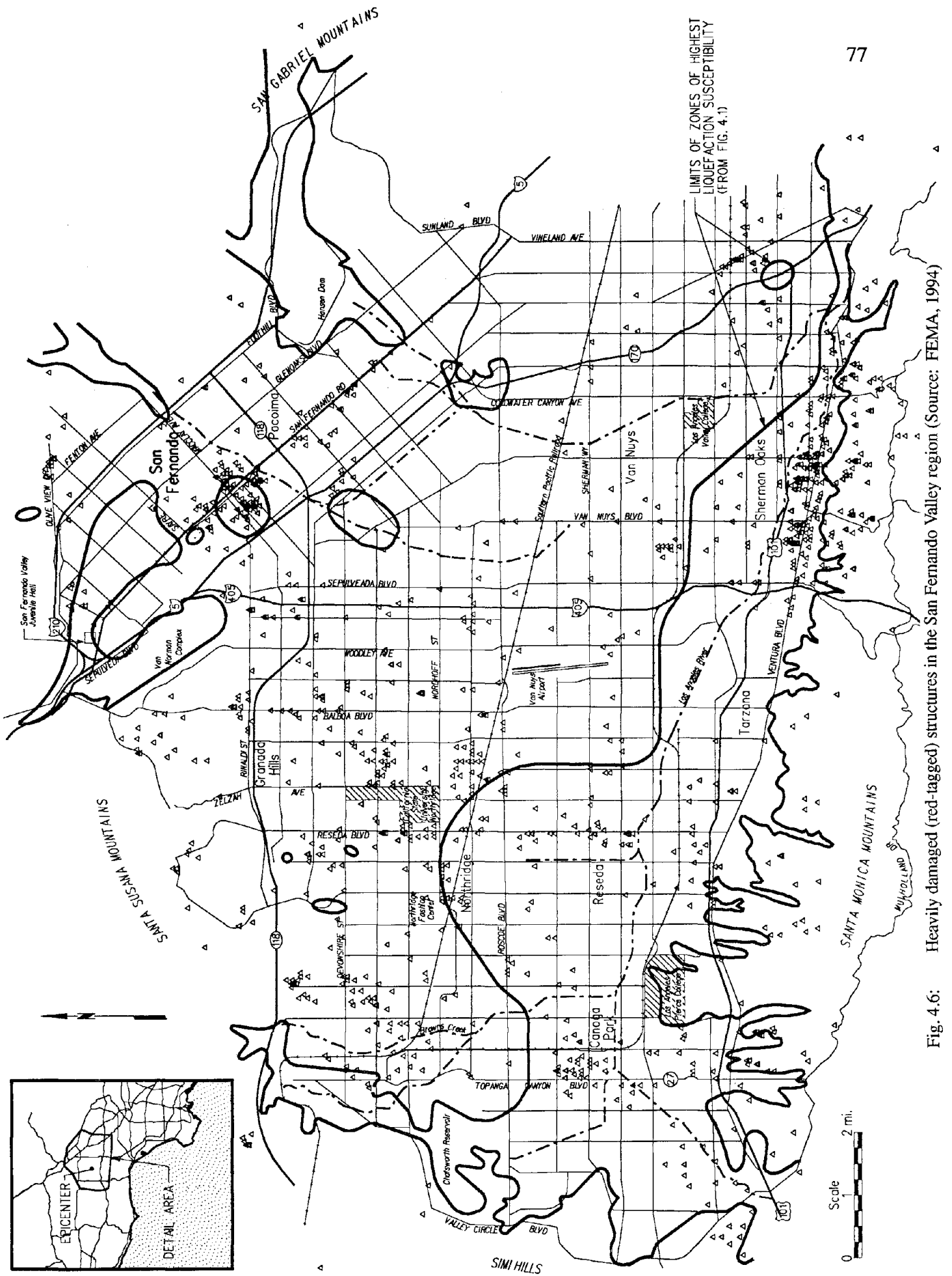


Fig. 4.6: Heavily damaged (red-tagged) structures in the San Fernando Valley region (Source: FEMA, 1994)



Fig. 4.7: Ground crater and fire resulting from pipe breakage, Balboa Boulevard, Granada Hills. Photo by Los Angeles Times.



Fig. 4.8: Water pipe broken by extensional ground movement, Balboa Boulevard, Granada Hills

separation in extension. Figure 4.8 shows a typical extensional water pipe break in this area.

In addition to pipe breakage, the area also experienced widespread ground cracking, primarily in lateral extension and settlement, although some lateral compression was also observed. Figures 4.9 to 4.11 show examples of pavement breakage in neighborhoods just north of Rinaldi Street due to localized differential settlement, lateral extension, and lateral compression, respectively. Figure 4.12 shows evidence of extensional ground movements adjacent to a house. Surficial lateral and vertical differential offsets in pavements were generally on the order of 2 to 6 inches, but in isolated instances, differential lateral extension and compression of up to one foot and more were observed. The ground cracking in these areas was not accompanied by sand boils or sand fissures, and the distress often formed a distinct linear pattern oriented in an east-west direction, generally sub-parallel to the slope contours.

Some of the largest displacements were observed above and below an apparently intact surface soil "block" along Balboa Boulevard which appears to have translated to the south. This apparent block is approximately 500 feet in length with an as-yet undetermined width, and appears to have translated laterally to the south producing an extensional fissure approximately 15 to 20 inches wide (with resulting tensile pipe breaks) at the north end, and a compressional feature (with resulting compressional pipe failures) of apparently similar magnitude at the southern end of the block.

As shown in Figures 4.5 and 4.6, the locations of unsafe, or red-tagged structures in the Granada Hills area correlates reasonably well with the locations of ground failures as indicated by pipe breaks and leaks. Some of these damaged structures were the product of fires started from ruptured gas lines, thus decreasing the robustness of the apparent correlation between structural damage and ground failure. Nonetheless, the quality of the correlation, particularly in the area north of Rinaldi Street and west of Balboa Boulevard, suggests that ground failure may have contributed to the occurrences of structural damage in the area.

The damage in Granada Hills is of particular interest because the area is not mapped as "liquefiable" due to relatively deep groundwater (Los Angeles County, 1990). Hence, ground failures in the area likely resulted from mechanisms other than near-surface soil liquefaction. Possible alternative mechanisms include the following:

- Dynamic ground compaction: volumetric compression, and resulting settlements, of relatively loose, unsaturated, sandy soils under cyclic loading from earthquake shaking.
- Deep soil liquefaction: liquefaction and associated strength loss of saturated soils at depth leading to block-like movements (both lateral spreading and compression, as well as tipping and differential settlements) of overlying unsaturated surficial soil masses.
- Induced tectonic deformations: deformations at the ground surface resulting from underlying bedrock movements associated with primary or secondary faulting.



Fig. 4.9: Pavement crack from settlement and extension on Rinaldi Street near Balboa Boulevard, Granada Hills



Fig. 4.10: Pavement crack from extensional ground movements, Granada Hills



Fig. 4.11: Pavement buckling in compression, Granada Hills



Fig. 4.12: Evidence of extensional ground movement near a house. Small masonry wall and adjacent ground separated from house.

It is not obvious at this time which of these ground failure mechanisms may have been responsible for the observed damage. In speculating on the feasibility of the various mechanisms, it should be noted that the soils in the area appear to have experienced widespread modest lateral displacements in the downslope direction. As noted previously, these movements varied from a few inches to almost two feet at a few locations. Slopes inclinations in the area generally decrease from approximately 2 - 3 percent north of Rinaldi Street to roughly 2 percent south of Rinaldi Street. Hence, the particularly high concentration of ground failure (as evidenced by pipe breakage) north of Rinaldi Street relative to areas slightly farther south may be due in part to the influence of slope inclination on the magnitudes of significant regional lateral movements. That is, the slightly steeper slopes north of Rinaldi Street may have been subject to somewhat greater lateral movements than adjacent southern areas, contributing to the greater damage intensities observed there. In addition, it should also be recalled that ground fissures in the area were often oriented sub-parallel to the slope contours, and that the depth to groundwater is greater than 50 feet throughout much of the region.

The mechanism of liquefaction at considerable depth, producing "blocky" movements of the largely intact overlying soil masses, is consistent with many of the observed ground deformation patterns. In particular, this mechanism would appear to account for the widespread lateral downslope displacements and distress patterns generally oriented sub parallel to the slope, as downslope migration of the upper soil "blocks" would tend to open up cracks and fissures aligned with the slope contours. Historically, liquefaction of soils at significant depth (i.e. > 50 feet) has not been thought to represent a significant hazard for surficial soil failure for the following reasons: (1) deeper soils tend to be relatively older and denser, and hence less prone to liquefaction, and (2) the overlying "mantle" of non-liquefied surficial soils would serve as a buffer to minimize the surficial expression of soil movements at depth. It is not yet known to what extent soils may have liquefied at depth in the Granada Hills area during the Northridge Earthquake. However, if deep soil liquefaction occurred, the resulting relatively large-scale "blocky" surficial soil movements might also have combined with localized ground deformations caused by dynamic ground compaction to produce the variety of lateral compression, extension, and vertical settlement features observed in the area.

Dynamic ground compaction is a recognized phenomena in relatively loose, sandy soils, and is likely to have caused some of the observed localized differential settlement features. In addition, some minor lateral movements may have also been induced by ground compaction due to the heterogeneity of the soils and the modest slopes in the area. However, due to the inherent non-uniformity of dynamic ground compaction, vertical and lateral ground deformations resulting from it would not be expected to occur in a clearly recognizable regional pattern, as was observed throughout much of Granada Hills. Furthermore, ground compaction would be unlikely to result in large magnitude lateral ground movements as was observed at several locations in Granada Hills.

The mechanism of induced tectonic deformation (involving folding and extension of the surface soil mantle due to underlying fault displacements), though possible, would appear to be unlikely to have produced significant surface distress in the zone along Rinaldi Street near Balboa Boulevard, where the most pronounced intensity of ground failure in Granada Hills

occurred. The soil thicknesses over rock in these areas are believed to be significant; data from the freeway collapse sites along Highway 118 at Bull Creek and the Mission-Gothic intersection (about 3000 feet south of Rinaldi Street) suggest that highly consolidated (rock-like) materials with shear wave velocities greater than or equal 2500 feet per second occur at depths on the order of 400 to 450 feet below the ground surface (California Department of Transportation, 1994). The bedrock-level tectonic movements occurring at these depths are likely to have been moderate to small, as they would be associated with secondary shears from the main fault. These moderate deformations would be unlikely to propagate through the thick alluvium and produce localized deformation patterns such as those observed near Rinaldi Street.

Further north, where the soil cover is much thinner and rock is found at the surface in some areas, the potential for surficial ground failure from tectonic movements might appear to be somewhat more likely. Figure 4.13 shows the locations of pipe breaks and leaks in the portion of Granada Hills north of Highway 118 along with mapped bedrock and soil areas (Dibblee, 1991, 1992). Despite the essentially uniform distribution of pipes through most of the area, concentrated pipe breakage zones occurred primarily within alluvial soil deposits. This pipe breakage pattern suggests that ground failure was generally confined to these soil materials, and was relatively infrequent in bedrock. If significant localized tectonic deformations had occurred, a more uniform distribution of breaks through the different geologic materials would be expected. Hence, it appears that tectonic deformations did not significantly contribute to ground failure-induced damage in the Granada Hills area.

4.2.5 Northridge-Reseda-Canoga Park Area

A broad zone of ground failure occurred in the Northridge-Reseda-Canoga Park area southwest of the CSU Northridge campus as evidenced by concentrated pipe breakage (as shown in Figure 4.5) as well as widespread lateral spreading and settlement. Typical examples of pavement distress are shown in Figures 4.14 to 4.16, which show sidewalks and streets damaged by localized lateral ground movements and settlement in the Northridge area. At some locations, significant pavement distress was not accompanied by obvious ground failure, as with the heaved sidewalk with no apparent ground compression in the adjacent ground or curb shown in Figure 4.17. Sand boils were generally not observed in the area.

As evidenced by patterns of water pipe breaks, the ground failure in the Northridge-Reseda-Canoga Park area appears to have been generally well contained within a soil zone mapped as "liquefiable", as shown in Figure 4.5. Perched groundwater occurs in this area along with occasional loose, sandy stream channel deposits. These stream channel sediments are typically confined within discrete, discontinuous zones by relatively cohesive materials much less susceptible to liquefaction (Tinsley, 1994). Based on the data currently available, it appears that liquefaction may have occurred within some of the saturated, sandy stream channel deposits in the area. This mechanism of ground failure is consistent with the lack of observed sand boils, as the liquefiable deposits were generally well confined by relatively cohesive (unliquefiable) materials, and thus were less likely to vent ejecta. In addition, liquefaction of buried stream channel deposits could potentially result in "block-like" displacements and shifting of non-liquefied overlying intact sediments, thereby generating the

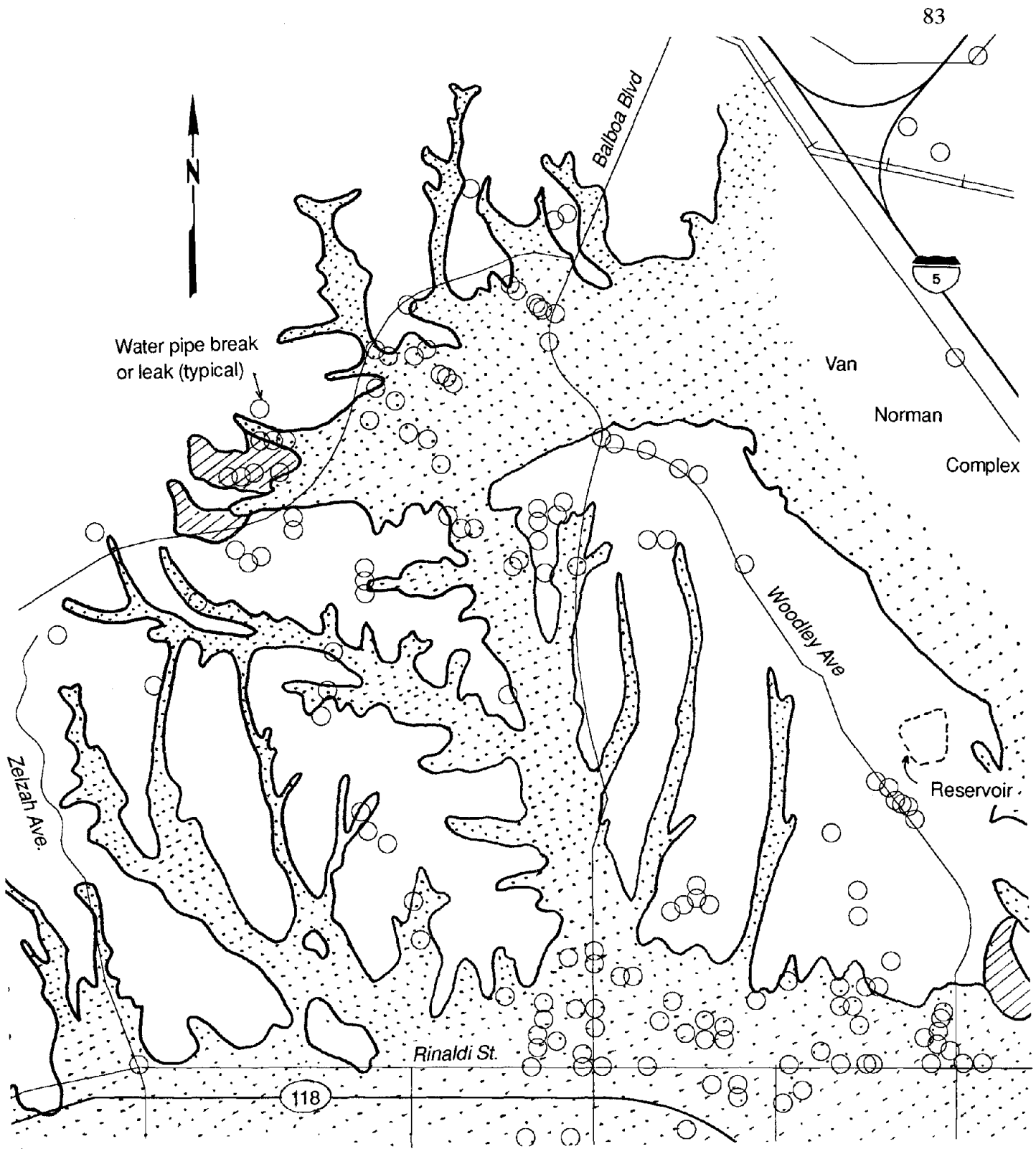


Fig. 4.13: Map of Granada Hills area north of Highway 118 showing pipe breakage and geologic conditions (pipe break data courtesy of Los Angeles Department of Water and Power; geologic conditions adapted from Dibblee, 1992)

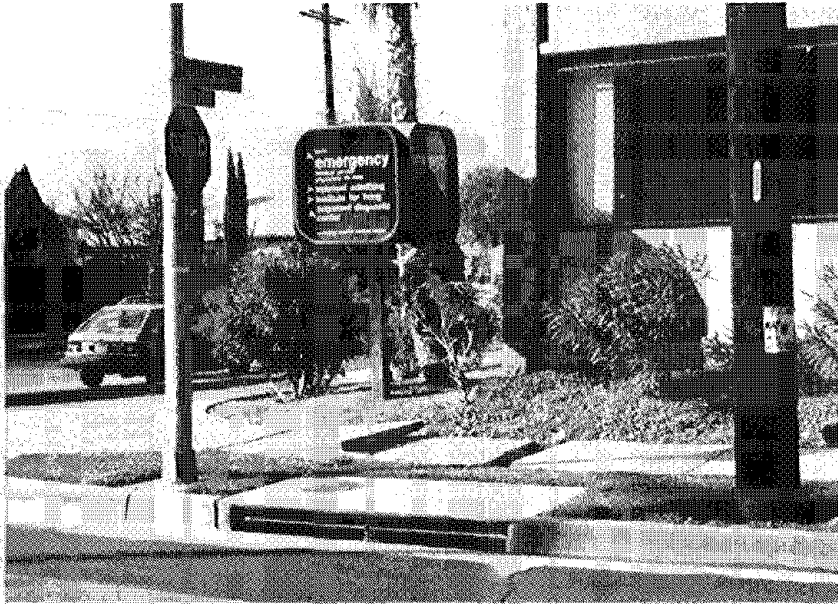


Fig. 4.14: Sidewalk buckled from lateral compression, Northridge Hospital Medical Center

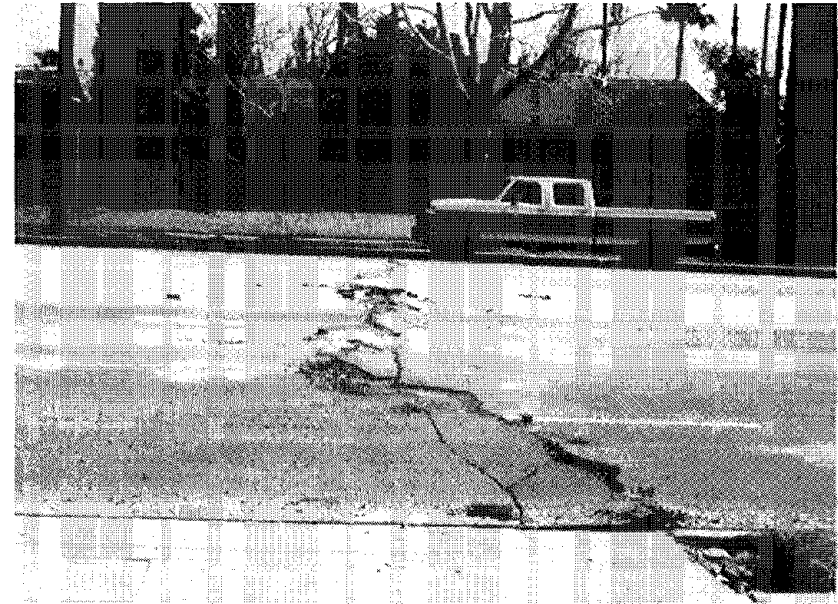


Fig. 4.15: Localized compression feature and pavement damage in Northridge

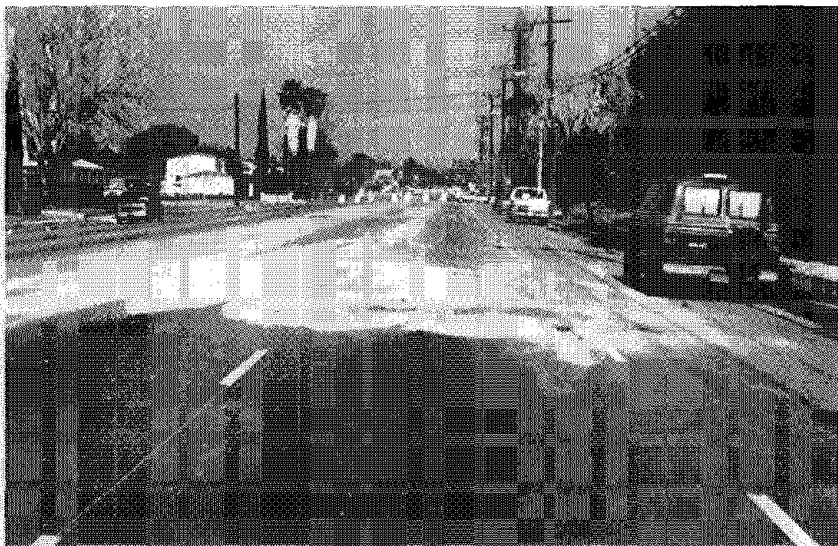


Fig. 4.16: Evidence of ground movements and sand washed onto street from utility pipe break, northeast Northridge

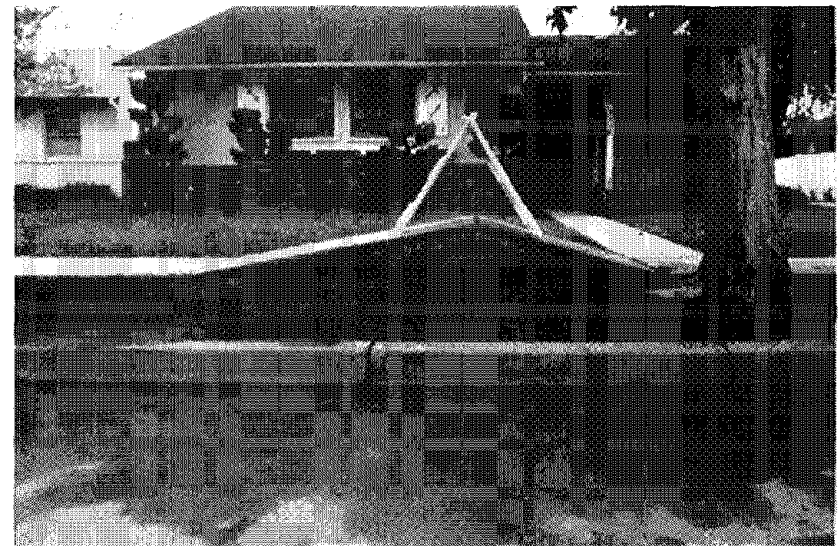


Fig. 4.17: Uplifted sidewalk in Northridge with no apparent adjacent ground failure (photo courtesy of John Tinsley, U.S. Geological Survey)

observed localized lateral compression, extension, and differential settlement features observed in the area. While the occurrence of liquefaction on a broad scale cannot be conclusively confirmed in this area due to the lack of definitive evidence such as sand boils, it appears on a preliminary basis to be the mechanism likely responsible for much of the observed ground failure in this area.

In addition to the apparent occurrence of soil liquefaction, strong shaking in the Northridge area also induced settlements in sandy fills for several bridge abutments which appear to have resulted in large part from dynamic ground compaction. Figure 4.18 shows an aerial overview of the Nordhoff Way bridge over the Southern Pacific Railroad tracks. Significant settlement of the abutments for this bridge occurred as a result of dynamic ground compaction, as shown in Figure 4.19. Numerous bridge abutments throughout the epicentral area experienced similar settlements, although the magnitude of such settlements was typically much less than that shown in Figure 4.19. A train de-railment also occurred beneath the Nordhoff Way bridge, as shown in Figure 4.20. The de-railment was probably caused by toppling of the train from inertial forces associated with strong shaking. No evidence of ground failure was observed at the de-railment site 28 hours after the earthquake, but much of the ground had been disturbed by repair efforts.

The ground failure in the Northridge-Reseda-Canoga Park region appears to have contributed relatively little to the structural damage in this area. As shown in Figure 4.6, no recognizable strong correlation between concentrations of unsafe structures and "liquefiable" soil zones exist in this area. Instead, the damage in this area appears to have generally been induced by large inertial forces associated with strong ground shaking.

4.2.6 Sherman Oaks Area

As shown in Figure 4.5, a moderate concentration of water pipe distress occurred in Sherman Oaks along the Ventura Boulevard corridor in an area mapped as "liquefiable" (Los Angeles County, 1990). Other evidence of ground failure, however, was relatively scarce as few cases of significant pavement cracking were found and no sand boils were observed. Structural damage in the area was very pervasive, however, as shown by the concentration of red-tagged structures in Figure 4.6

It appears that local geologic conditions intensified ground motions in Sherman Oaks by means of soil amplification and deep basin effects, as discussed previously in Section 3.4.1(b). These amplification effects are likely primarily responsible for the intense structural damage in the area. Based on the minimal disruption of pavements and lack of sand boils in the area, it is unlikely that pronounced liquefaction or dynamic ground compaction of shallow surficial soils occurred. However, full and/or partial soil liquefaction at moderate depths may have induced soil deformations which contributed to the observed concentrated pipe breakage. In addition, soil softening by full or partial liquefaction may have altered the soil's dynamic properties in such a way as to influence site amplification effects, and thereby contribute to the observed structural damage by affecting the characteristics of the ground motions.

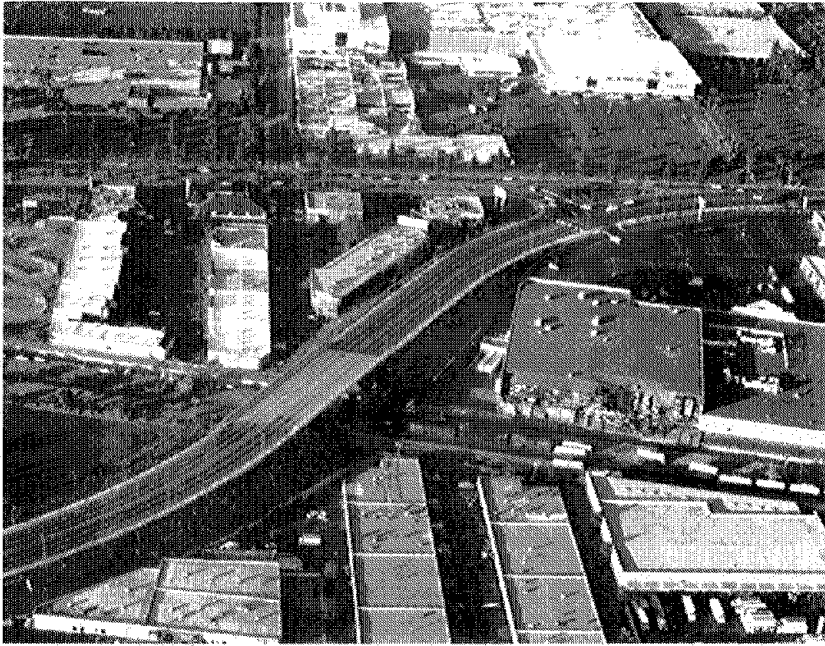


Fig. 4.18: Aerial view of Nordhoff Way bridge over Southern Pacific Railroad tracks, just south of Northridge Fashion Center. Also note train de-railment below bridge and collapsed parking garage in background.

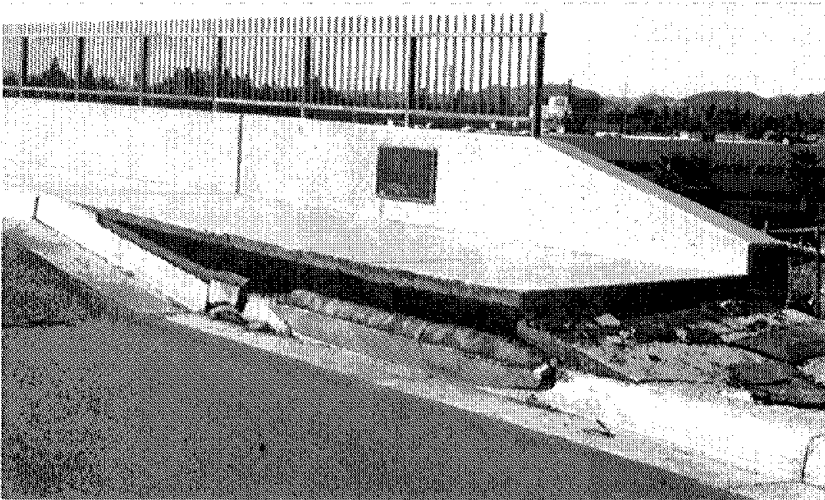


Fig. 4.19: Abutment settlement at Nordhoff Way bridge over Southern Pacific Railroad tracks

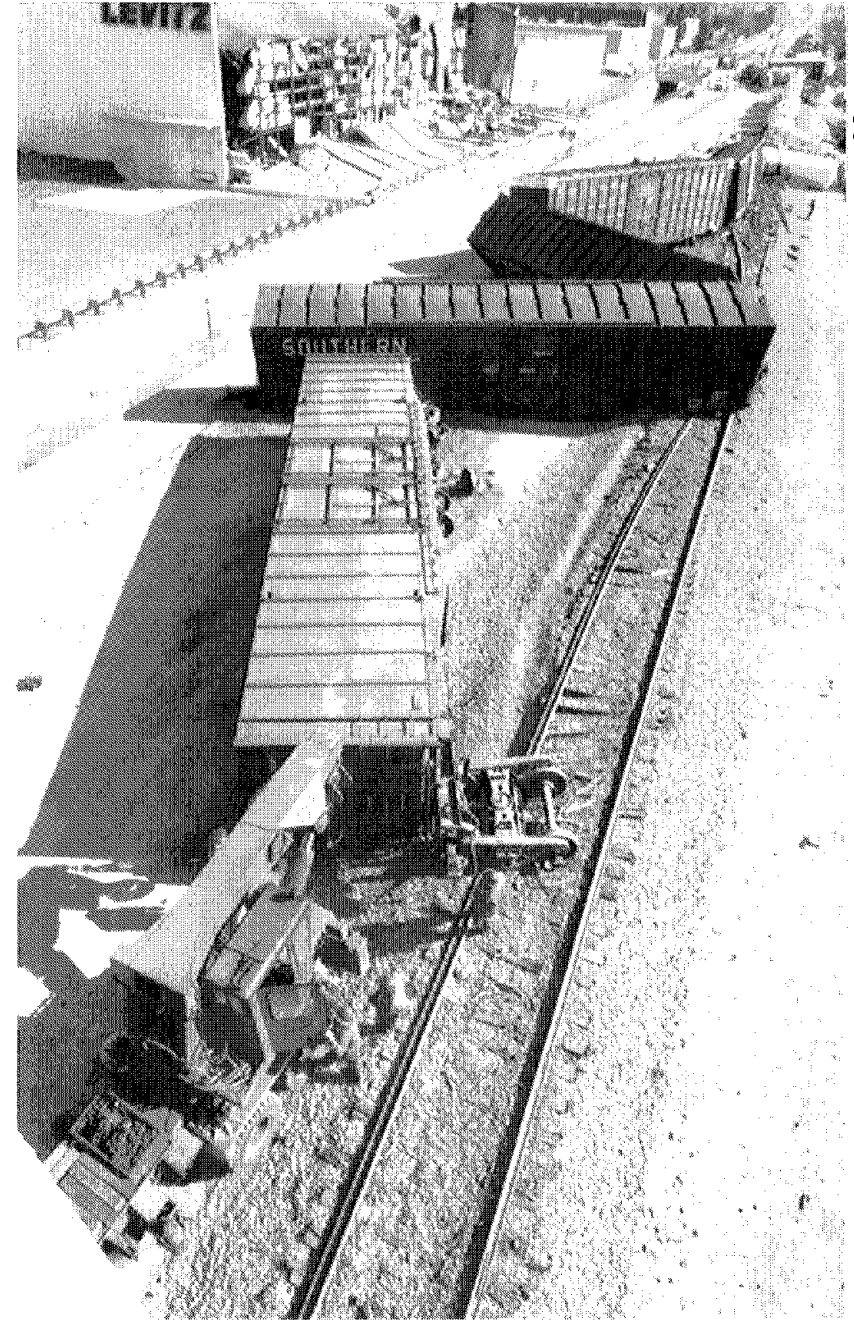


Fig. 4.20: Train de-railment beneath Nordhoff Way bridge over Southern Pacific Railroad tracks. Photo by Los Angeles Times.

4.2.7 City of San Fernando

Perhaps the most acute concentration of both pipe breaks and damaged structures in the San Fernando Valley occurred in the City of San Fernando. The area is mapped as being underlain by Holocene stream channel and dune deposits, a small section of which were delineated as "liquefiable" (due to shallow groundwater) along Maclay Avenue, as shown in Figure 4.1 (Los Angeles County, 1990). As shown in Figure 4.6, a significant concentration of structural damage occurred within this "liquefiable" zone. Detailed data on pipe break locations in the City's water distribution system were unavailable at the time this report was prepared. However, hundreds of breaks were reported in the same general location as the red-tagged structures in Figure 4.6, with relatively few breaks in other parts of the city (City of San Fernando, 1994). In addition, several breaks of an oil pipeline which traverses the city southwest of San Fernando Road occurred within the "liquefiable" zone, as shown in Figure 4.5 (California State Fire Marshall, 1994). Despite the many ruptured underground utilities in this area (including gas lines), there were relatively few fires. Hence, the distribution of building damage shown in Figure 4.6 was primarily caused by structural or foundation failure and not fire damage.

Based on the pronounced intensity of both pipeline and building damage in San Fernando, and the localization of this damage within a zone mapped as "liquefiable," it appears likely that the ground failure causing the pipe breakage also affected structures in the area. Further, due to the local geologic and groundwater conditions described above, it appears that the ground failure may have resulted from surficial soil liquefaction or partial liquefaction. As was postulated for the Sherman Oaks area, soil softening by full or partial liquefaction may have altered the soil's dynamic properties in such a way as to influence site amplification effects, and thereby contribute to the observed structural damage by affecting the characteristics of the ground motions.

In addition to the heavily damaged area near Maclay Avenue, a large zone northwest of the San Fernando city limit is mapped as "liquefiable" (Los Angeles County, 1990). As shown in Figures 4.5 and 4.6, this area experienced relatively little damage to structures or pipeline systems, suggesting that the area generally escaped significant ground failure. However, minor ground failure appears to have occurred in the vicinity of the San Fernando Valley Juvenile Hall facility, where significant liquefaction-induced lateral spreading occurred during the 1971 San Fernando Earthquake. A more detailed discussion of the ground failure near Juvenile Hall, and in the Van Norman Complex, is presented in the following section.

4.2.8 Van Norman Complex and Vicinity

The Van Norman Complex, and several surrounding areas, experienced severe damage from liquefaction during the 1971 San Fernando Earthquake. Some of the most significant damage included (1) substantial slippages in the shell materials of the Upper and Lower San Fernando Dams, including a major upstream slope stability failure and near-release of the reservoir at the Lower San Fernando Dam, (2) lateral spreading and settlement which damaged the nearby Joseph Jensen Filtration Plant, and (3) a landslide located beneath a portion of the San Fernando Valley Juvenile Hall facility and a large area downslope. Most

of these facilities were either abandoned or significantly improved between 1971 and 1994, and damage resulting from the Northridge event was relatively modest. However, widespread liquefaction occurred once again, and its effects will be discussed in this section.

The Van Norman Complex and the adjacent Juvenile Hall site are underlain by Holocene alluvial soils (Figure 3.27) which are mapped as "liquefiable" due to shallow groundwater (less than 30 feet deep) in the area, as shown in Figure 4.1 (Los Angeles County, 1990). These alluvial soils are generally stratified and layered, with some layers consisting of loose to medium dense silty sands highly susceptible to liquefaction (Marachi, 1973; Scott, 1971; Wentworth and Yerkes, 1971).

As referred to herein, the Van Norman Complex consists of facilities operated by the Los Angeles Department of Water and Power (LADWP) and the Los Angeles Metropolitan Water District (MWD). The layout of the area is shown in Figure 4.21. Since 1971, both the Upper and Lower Van Norman Reservoirs were drained and replaced by the Los Angeles Reservoir, which is operated by LADWP. The performance of these dams during the Northridge Earthquake is discussed in Section 6.2. The present section will describe the performance of other areas in and adjacent to the complex including:

- the former slide area near the San Fernando Valley Juvenile Hall facility,
- the Joseph Jensen Filtration Plant (operated by MWD),
- the San Fernando Power Plant Tailrace, located immediately north of the former Upper Van Norman Lake, and
- several other locations where liquefaction-induced damage occurred.

(a) San Fernando Valley Juvenile Hall

As a result of the 1971 San Fernando Earthquake, liquefaction-induced strength loss triggered up to 5 feet of movement of an approximately 2.5% slope below the San Fernando Juvenile Hall Facility (Youd, 1971). The slide mass was about 3900 feet long by 900 feet wide, and consisted of two segments. The eastern segment extended from the Juvenile Hall facility down to a channel on the east side of the Sylmar Converter Station, and the western segment extended from the channel to the bed of the Upper Van Norman Lake. The approximate outline of the slide is shown in Figure 4.21.

The natural soils in the general area consist primarily of sandy clay and silty sand. Recent groundwater measurements at the Juvenile Hall site indicated groundwater depths of 19 to 26 feet. Following the 1971 earthquake, several damaged buildings at the southern end of the Juvenile Hall facility were demolished. The soil underlying these former buildings was excavated to a depth of 35 feet, and a compacted buttress fill was placed, on which new structures were subsequently constructed. This buttress fill was intended to resist future seismically-induced lateral spreads beneath the buildings (Leighton and Associates, 1994).

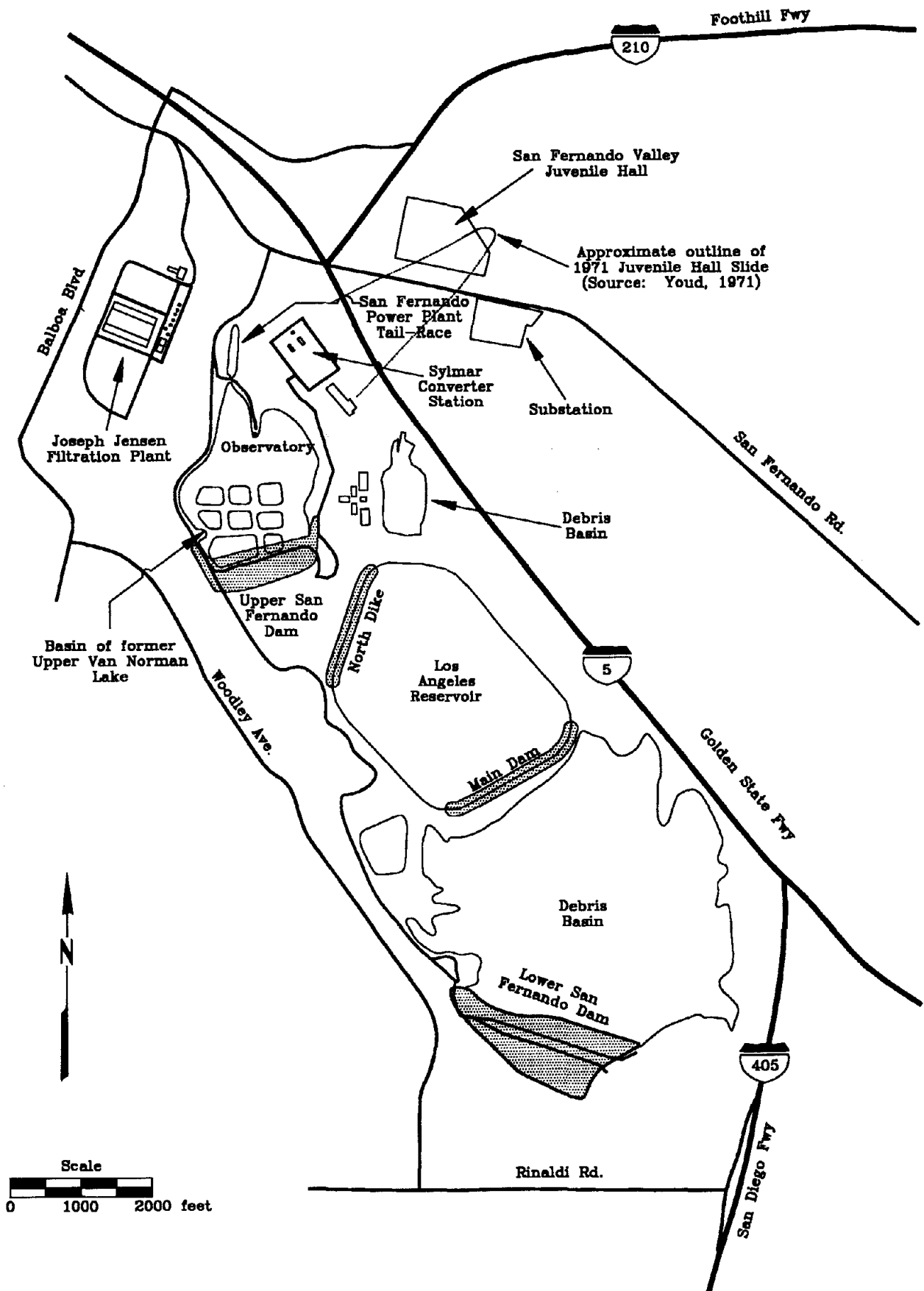


Fig. 4.21: Map of Van Norman Complex and vicinity

Following the Northridge Earthquake, ground distress patterns in the general vicinity of the 1971 landslide were observed at the Juvenile Hall facility, along San Fernando Road, and in an eastern portion of the Van Norman Complex. Crude field measurements generally indicated that the locations of this observed distress coincided fairly well with the "edges" of the 1971 displaced mass. Hence, it appears that sliding may have been partially re-activated during the 1994 Northridge Earthquake in some of the areas which experienced slide movements in 1971. However, the magnitude of the downslope lateral displacements which developed during the Northridge event were much smaller than those associated with the 1971 slide, and appear to have been on the order of 4 to 6 inches or less.

Near the top of the apparent slide feature, extensional ground movements were observed at several locations within the Juvenile Hall complex. The buttress fill underlying the southern structures at the site appeared to perform reasonably well, although some ground fissures developed outside of, and parallel to, the footings of some buildings, as shown in Figure 4.22. In addition, some structural distress to the southern Juvenile Hall buildings was observed (Figure 4.23), though this distress has not generally been attributed to ground failure (Leighton and Associates, 1994). Outside of the buttress fill, typical extensional features in the parking area included fissures up to 4 inches wide and several feet deep, as shown in Figure 4.24. According to maintenance personnel, many of these fissures in the parking area developed parallel to a large sewer line.

Downslope of the Juvenile Hall facility, evidence of ground movements was observed in the form of pavement cracking and curb buckling along San Fernando Road (Figure 4.25), 3 to 4-inch bowing of train tracks adjacent to San Fernando Road in the downslope direction, and minor ground cracking further downslope in the Van Norman Complex. Ground cracking in the east end of the Van Norman Complex was observed in a canal along the east side of the former Upper Van Norman Lake, and adjacent to foundations for a power line tower near the Sylmar Converter Stations. In addition, slide movements may have contributed to reported settlements of up to a foot around the Sylmar Converter Station (Dames and Moore, 1994). As noted previously, these distress features generally appeared to have occurred within the approximate boundary of the 1971 slide, thus suggesting that some of the original (1971) slide mass had been at least partially re-activated.

Although detailed surveys of slide movements were unavailable at the time this report was prepared, overall slope movements of the Juvenile Hall slide from the Northridge Earthquake are estimated to have been less than ½-foot based on visual observation and cumulative measurements of displacements across fissures. Hence, the recent movements were less than the 5 feet which occurred during the 1971 San Fernando Earthquake.

(b) Joseph Jensen Filtration Plant

The Joseph Jensen Filtration Plant, located in the northwest portion of the Van Norman Complex (Figure 4.21), experienced considerable damage during the 1971 San Fernando Earthquake from liquefaction-induced ground movements. The plant was again damaged by liquefaction during the Northridge Earthquake, but the damage was less severe. Nonetheless, the facility was forced to shut down for several days, affecting water service to over one



Fig. 4.22: Ground fissure with extensional movement near edge of building, Juvenile Hall facility



Fig. 4.23: Separation of walls at San Fernando Valley Juvenile Hall Facility

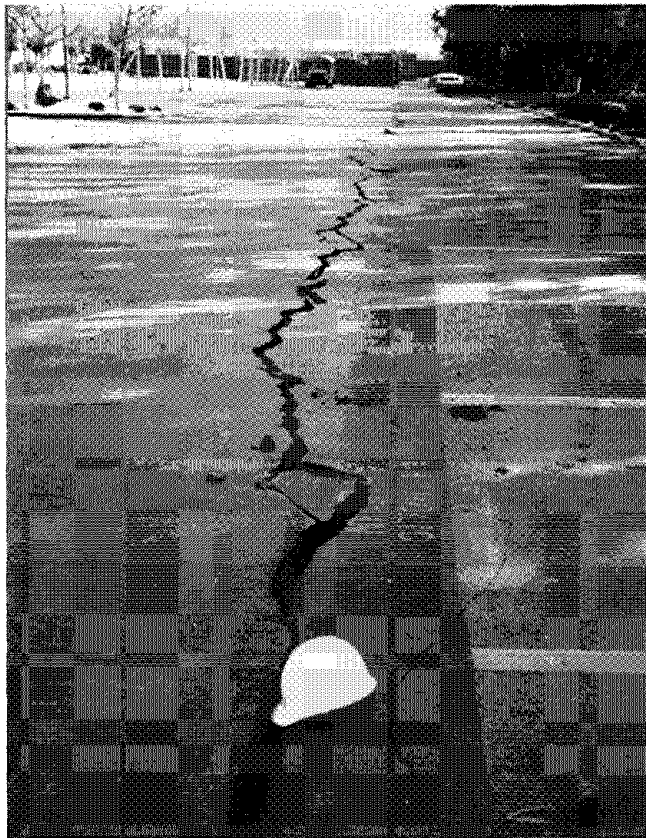


Fig. 4.24: Ground fissure from extensional movement, parking lot at Juvenile Hall facility

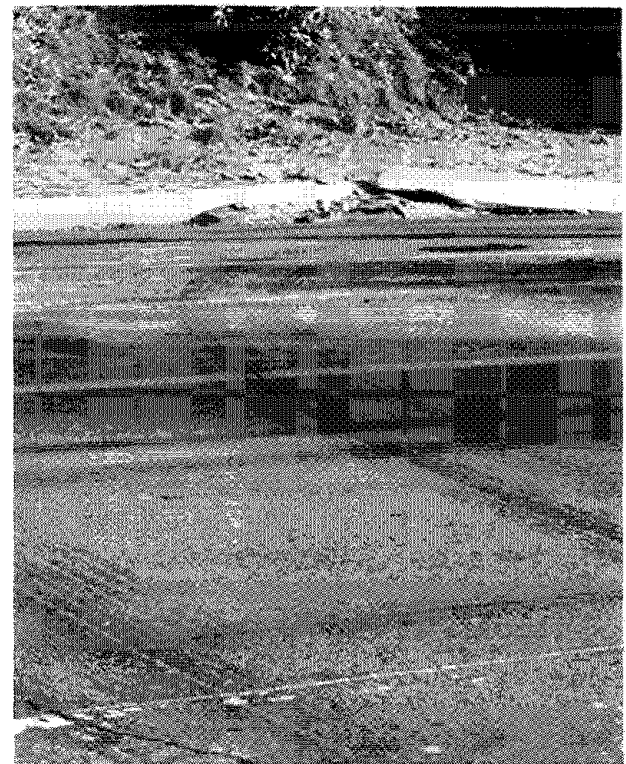


Fig. 4.25: Damage to curb on east side of San Fernando Road

million customers. The area was very strongly shaken by the Northridge event, with a peak horizontal ground acceleration of 0.98g having been recorded by a seismograph near the Generator Building at the plant (Porcella, et al., 1994).

The approximate layout of the Jensen Filtration plant site is shown in Figure 4.26. The eastern and southern portions of the site are underlain by a gently sloping alluvial plane, while the northwestern portion is located over Quaternary sedimentary bedrock of the Saugus Formation (Dibblee, 1991). The alluvial areas are generally overlain by wedge fills on the order of 40 to 50 feet thick at the east end of the facility (MWD, 1994).

During both the 1971 and 1994 earthquakes, surficial distress patterns were generally observed within the areas underlain by fill at the eastern and southern portions of the site. During the Northridge Earthquake, liquefaction of the underlying alluvial soils appears to have resulted in ground movements which propagated to the surface of the fill and damaged several facilities. Sand boils were generally not observed within the plant at the ground surface due to the considerable fill thickness; however, numerous boils and sand fissures were observed at the base of the fill slope near the San Fernando Power Plant Tailrace.

Figure 4.27 shows ground cracking in the parking lot east of the main control building, where offsets up to 3 inches wide with 8 inches of differential settlement were observed. Larger ground fissures were also observed slightly northeast of the area shown in Figure 4.27. This parking area on the east and north sides of the main control building has been improved since 1971 by the installation of over 1100 gravel columns intended to minimize pore pressure generation in liquefiable soils. The complete effectiveness of the gravel columns in mitigating the ground failure hazard might be questioned to some extent given the observed performance during the Northridge Earthquake. Nonetheless, the magnitude of the ground deformations was considerably less severe (after installation of the gravel columns) than the movements which occurred during the 1971 San Fernando event, although the pattern of the deformations appears to have been similar. Maximum observed lateral displacements near the main control building appeared to have been less than one foot during the Northridge event, whereas up to 1.7-foot displacements were measured in 1971 (Youd, 1971). Further, the largest displacements resulting from the Northridge event occurred in areas not remediated by gravel columns.

At other locations around and within the main control building, differential settlements occurred which generally resulted in movements down towards the southeast. In an underground pipeline gallery partially beneath the main control building, movements were observed across construction joints in the concrete walls, ceiling, and floor. In the pipeline gallery, grout material in concrete construction joints was exuded suddenly during the earthquake, as shown in Figure 4.28. This may have been due to sudden squeezing of the joints from shaking of the structure, or may have possibly resulted from high water pressures associated with soil liquefaction outside of the gallery.

The temporary closure of the Jensen Filtration Plant was primarily necessitated by the rupture of several buried pipes, including a break in one of two influent aqueducts north of the main control building. Figure 4.29 shows the ruptured section of an 85-inch diameter

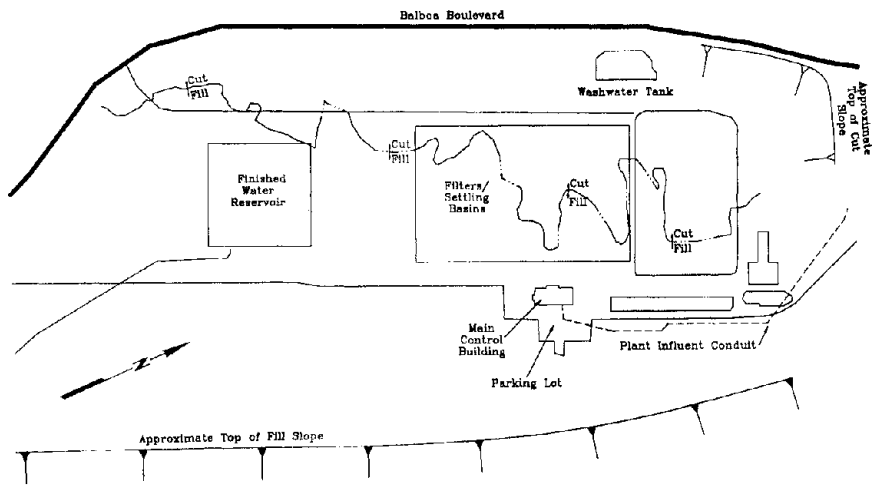


Fig. 4.26: Schematic of Joseph Jensen Filtration Plant site (adapted from Marachi, 1973)



Fig. 4.27: Ground fissure with extensional movement and differential settlement, parking lot of main control building, Jensen Filtration Plant

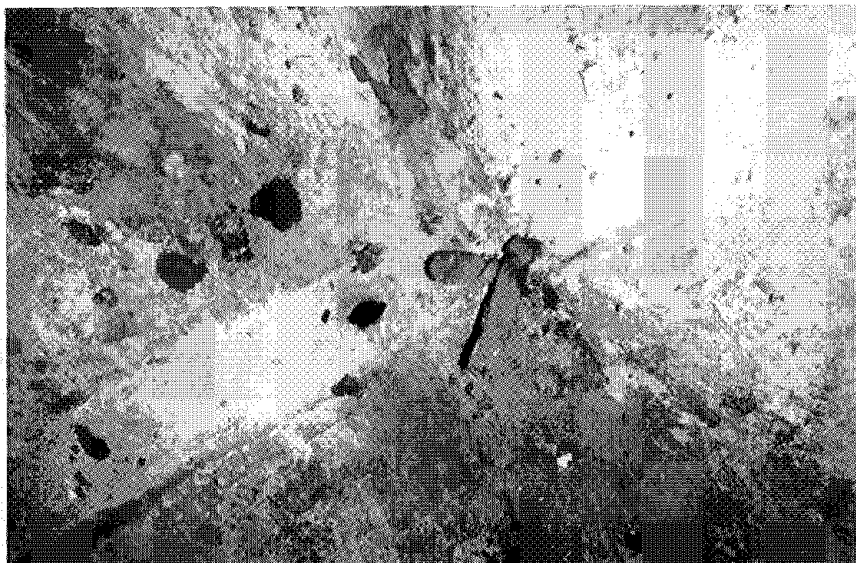


Fig. 4.28: Grout exuded from construction joint in concrete floor in pipeline gallery, Jensen Filtration Plant

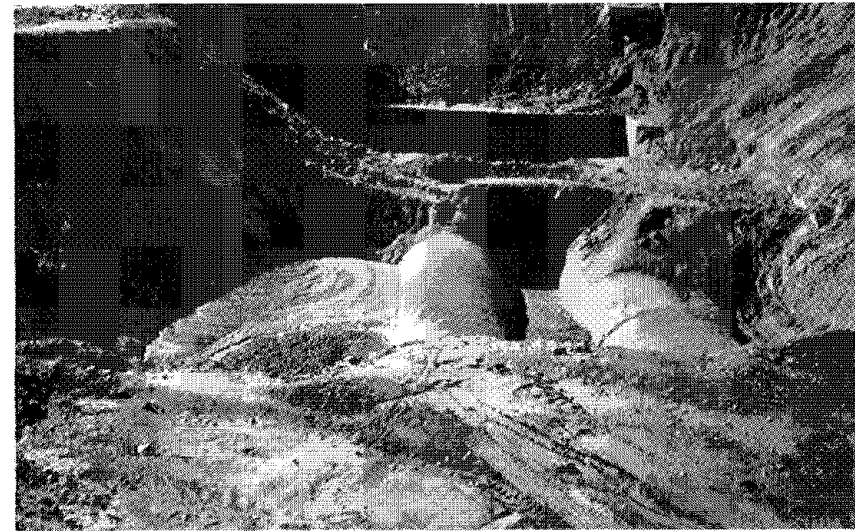


Fig. 4.29: Broken section of influent pipe during repair operations, Jensen Filtration Plant. (photo courtesy of Les Harder)

steel influent pipeline during repair operations which took about 2½ days to complete. In addition, numerous irrigation and chlorination lines were broken just south and north of the parking lot of the main control building, respectively. Towards the southern end of the facility, the fill surface around the perimeter of a 50 million gallon finished water reservoir settled approximately 2 to 4 inches relative to the reservoir. It is not known whether these movements resulted from dynamic compaction of the fill materials or re-consolidation of underlying liquefied alluvial soils. The northwestern portion of the plant, which is founded on bedrock materials, did not appear to have experienced significant ground failure during the Northridge Earthquake.

(c) San Fernando Power Plant Tailrace

The San Fernando Power Plant Tailrace is located at the base of a broad alluvial basin, situated downslope of the Jensen Filtration Plant to the west, and the San Fernando Valley Juvenile Hall to the east, as shown in Figure 4.21. The tailrace consists of an approximately 600-foot long, 110-foot wide, asphalt-lined pond retained at the south end by an approximately 15-foot tall embankment. During or shortly after the Northridge Earthquake, the embankment at the south end of the tailrace was breached, releasing the small impounded pond. The release did not appear to have caused any significant damage or flooding downstream of the tailrace.

Extensive liquefaction occurred in the vicinity of the tailrace, as evidenced by lateral spreading and sand fissures at numerous locations around the perimeter of the tailrace pond. The cracking pattern around the pond is shown in Figure 4.30 along with the location of the breach, which is also shown in Figure 4.31. On both the east and west sides of the tailrace, the lateral spreading occurred in the downslope direction towards the pond. Figure 4.32 shows buckling and compression of the gunite lining of the pond resulting from lateral spreading of the adjacent ground. Figures 4.33 and 4.34 show a typical sand fissure adjacent to the pond, and typical slumping at the top of the pond side slopes from the lateral spreading and settlement in the area, respectively. Many ground fissures adjacent to the tailrace had vertical and horizontal offsets on the order of 6 inches.

As a result of the significant lateral spreading observed in the abutment areas adjacent to the breach, it is likely that the retention embankment experienced cracking as it deformed under the imposed lateral deformations. The breach then may have ensued as water flowed through these cracks and eroded away the embankment. Although the consequences of the tailrace embankment breach were minor in this instance, the failure serves as a reminder of the potential hazards posed to earth structures by liquefiable foundation soils.

(d) Other Areas

As noted previously, the geologic and groundwater conditions in the Van Norman Complex are generally conducive to liquefaction. In addition to the areas discussed above, liquefaction also occurred at numerous other locations within the Van Norman Complex. Only some of the more notable "other" occurrences of liquefaction are discussed here.

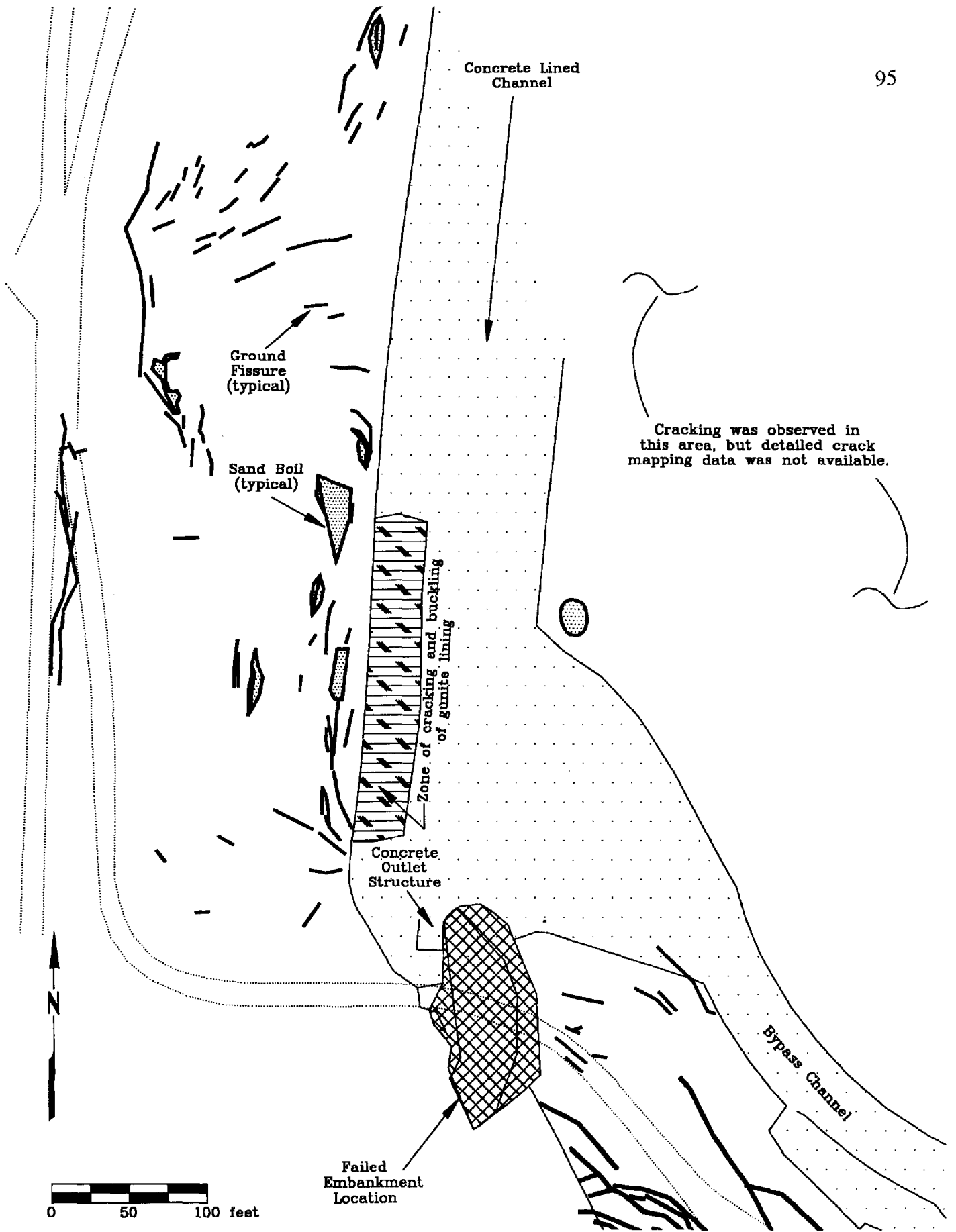


Fig. 4.30: Map of San Fernando Power Plant Tailrace facility showing locations of embankment breach and cracks induced by lateral spreading during the Northridge Earthquake. (data courtesy of Los Angeles Department of Water and Power)

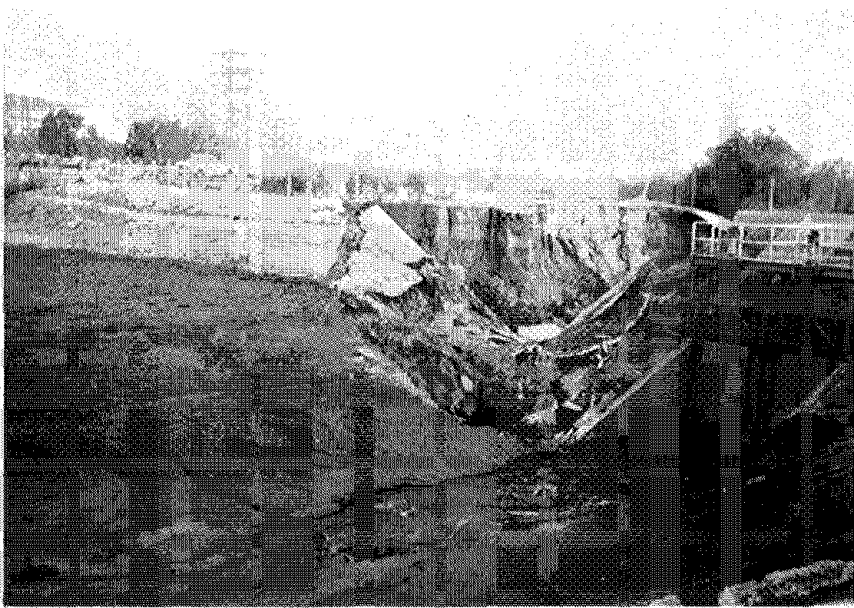


Fig. 4.31: Failed embankment section at south end of San Fernando Tailrace



Fig. 4.32: Buckling and compression of gunite pond lining, San Fernando Tailrace

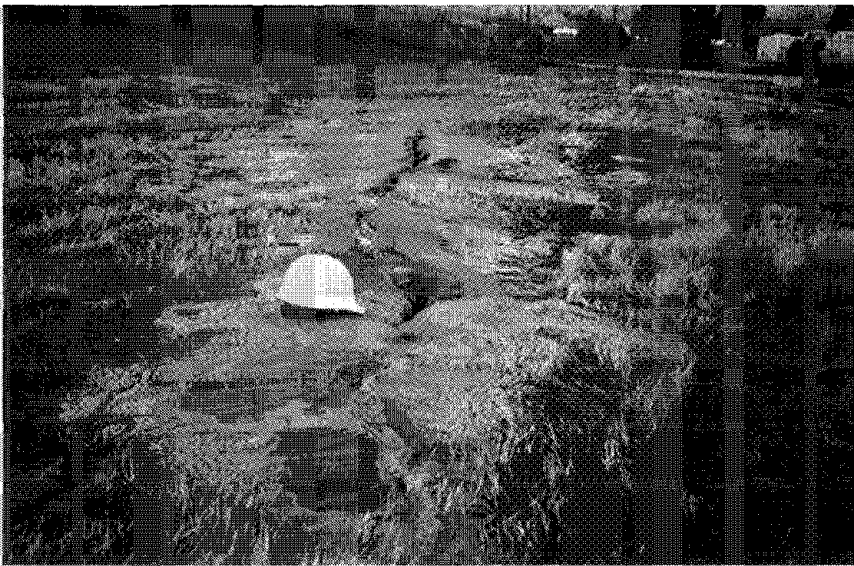


Fig. 4.33: Sand fissure at top of west slope near San Fernando Tailrace.



Fig. 4.34: Slumping of road area near top of pond side slope, San Fernando Tailrace

In the vicinity of the former Upper Van Norman Lake (shown in Figure 4.35), liquefaction affected an embankment leading to an observatory from the northern end of the lake and several small embankments impounding shallow ponds immediately upstream of the former. The locations of the observatory and the small ponds are shown in Figures 4.21 and 4.35. Figure 4.36 shows slope displacements on the order of 3 feet within the long, narrow embankment north of the observatory. This embankment suffered somewhat larger displacements on the order of 6½ feet during the 1971 San Fernando Earthquake under high water conditions for Upper Van Norman Lake, which at that time surrounded the embankment peninsula. Figure 4.37 shows a large fissure across a road immediately north of the ponds upstream of the dam. Cracks with offsets on the order of several inches to several feet were observed in the embankment fills around these ponds.

Immediately downstream of Upper San Fernando Dam, soil liquefaction appears to have been the cause of foundation pier movements for an above-ground water conduit. These movements failed several pipeline-foundation connector elements, as shown in Figure 4.38.

4.2.9 Hansen Dam Area

Hansen Dam is operated by the U.S. Army Corps of Engineers as a flood control facility, and is located southeast of the City of San Fernando in a zone mapped as "liquefiable", as shown in Figure 4.1. At the time of the Northridge Earthquake, the dam was not impounding water, but several small ponds and streams were located in the lake bed upstream of the dam. Extensive liquefaction occurred in the lake bed area as evidenced by sand boils, sand fissures, lateral spreading, and settlement. Figure 4.39 shows a road undermined by liquefaction-induced lateral spreading upstream of the dam, while Figures 4.40 to 4.42 show typical sand fissures and ground cracks from lateral spreading in this same general area. Lateral spreads of up to 3 feet with settlements of about 1 foot were found in the lake bed area along with sand boils up to 3 feet in diameter and sand fissures up to 50 feet long and 6 inches wide. The dam structure itself performed well and did not appear to have been damaged by liquefaction or strong shaking.

4.3 Simi Valley

Simi Valley, located west of the San Fernando Valley along Highway 118, experienced significant liquefaction at several locations during the Northridge Earthquake as evidenced by sand boils, lateral spreading, and settlement. As shown in Figure 3.5, recorded peak horizontal ground accelerations at rock sites south of Simi Valley were about 0.4g, although a much higher acceleration of 0.9g was recorded at a soil site near the east end of the valley (Figure 3.4).

Simi Valley is primarily underlain by alluvial soils deposited by streams emerging from the surrounding mountainous areas. These alluvial materials primarily consist of silts and clays in the eastern and western portions of the valley, although in the central region relatively sandy soils occur within an alluvial fan below Tapo Canyon (Leighton and Associates, 1972). Several natural drainage channels pass through Simi Valley, the most prominent of which is the Simi Arroyo Channel which drains from the hills to the northeast



Fig. 4.35: Overview of former Upper Van Norman Lake Area, Jensen Filtration Plant visible in background



Fig. 4.36: Slope failure in embankment near north end of Upper Van Norman Lake (photo courtesy of Les Harder)



Fig. 4.37: Ground fissure across road embankment north of pond within bed of former Upper Van Norman lake



Fig. 4.38: Failure of pipe support due to liquefaction-induced foundation movements (photo courtesy of Ross Boulanger)



Fig. 4.39: Road damaged by liquefaction-induced lateral spreading in lake bed behind Hansen Dam



Fig. 4.40: Sand fissure in lake bed behind Hansen Dam



Fig. 4.41: Close-up view of sand fissure upstream of Hansen Dam

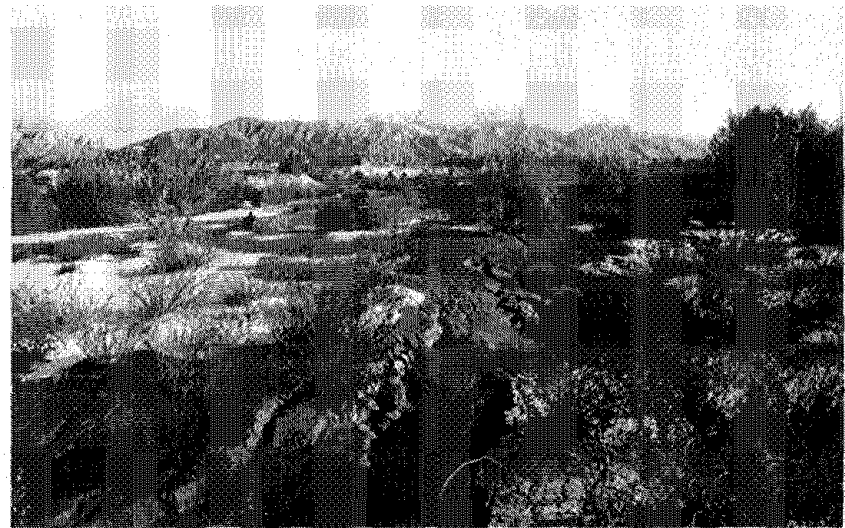


Fig. 4.42: Ground cracking and ejecta from sand fissures upstream of Hansen Dam

through the valley towards the west.

Maps of liquefaction susceptibility have not been formally prepared for the Simi Valley area; however, some insight regarding areas likely to be relatively prone to liquefaction can be gained by employing the procedure described by Youd and Perkins (1978). In this procedure, liquefaction susceptibility is evaluated by locating areas characterized by liquefiable soil type and high groundwater. With regard to soil type, sandy soils believed to be potentially susceptible to liquefaction occur in the alluvial fan area in the central portion of Simi Valley. In addition, sandy stream channel deposits might be expected in the vicinity of the streams traversing the valley. Due to the relatively cohesive nature of the soils in the remainder of the basin, the liquefaction susceptibility (regardless of ground water depth) in these areas would generally be expected to be low.

In addition to soil type, the other critical factor for assessing liquefaction susceptibility is depth to ground water. In the study of liquefaction susceptibility by Leighton and Associates for Los Angeles County (1990), susceptible soils with ground water depths less than 30 feet were considered "liquefiable", while ground water depths of 30 to 50 feet corresponded to "potentially liquefiable" conditions. Adopting these guidelines, the map in Figure 4.43 was developed to show regions having ground water depths less than 30 feet, and 30 to 50 feet. The mapping in Figure 4.43 is based on ground water table elevation maps (Leighton and Associates, 1985) and ground surface topography maps (U.S. Geological Survey, 1969). As these maps are based on data gathered about 10 years ago, they are unlikely to precisely reflect groundwater conditions at the time of the earthquake. However, they provide a reasonable basis for identifying broad zones of generally shallow groundwater. Where soils potentially susceptible to liquefaction occur within the two shallow groundwater zones, conditions may be tentatively described as "liquefiable" and "potentially liquefiable", respectively. It should be emphasized that this map is based on a very limited and somewhat dated data set, and therefore is very approximate. It is intended only to show broad zones of high groundwater, and should not be used for site-specific applications or detailed regional planning purposes.

During the Northridge Earthquake, ground failure occurred at several locations in the eastern and central portions of the Simi Valley area, causing large ground fissures, and damage to pavements and buried utility lines. Figure 4.44 shows the locations of breaks in water and sewer pipes along with the outline of high groundwater zones described above (City of Simi Valley, 1994; Southern California Water Company, 1994). Also shown in Figure 4.44 are several locations where ground cracking and pavement damage from lateral spreading and settlement were observed, although a complete inventory of ground cracking is not included. The most concentrated zone of pipe breakage and pavement distress occurred in the eastern valley area near the Simi Arroyo Channel, although notable damage also occurred north of this area along Los Angeles Avenue and Cochran Street, south-east of the channel along Kuehner Drive, and in the central portion of the valley near Tapo Street. Other damaged areas shown in Figure 4.44 are primarily mountainous, and thus were likely affected by seismically-induced fill movements or landslides in natural soils or rock.

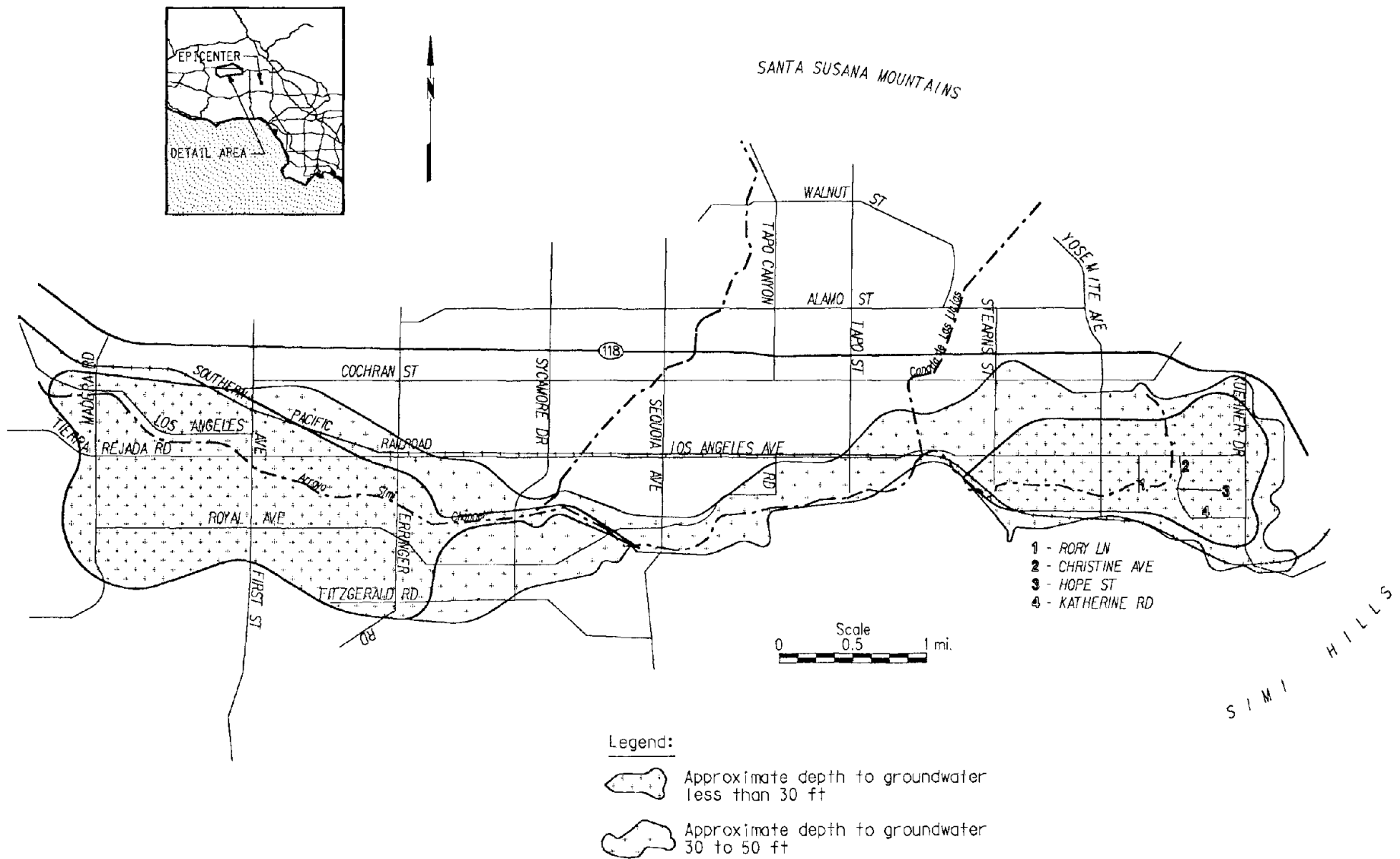


Fig. 4.43: Map of the Simi Valley region showing mapped "shallow groundwater" zones

Figures 4.45 and 4.46 show lateral spreading and settlement at Rory Lane, located near the Simi Arroyo Channel within an area in the eastern portion of Simi Valley which experienced significant ground failure. Extensive ground cracking with up to 8-inch lateral and vertical offsets developed in this area, as well as several large sand boils near the channel. This ground cracking and settlement appears to have resulted from lateral ground displacements towards the channel due to liquefaction-induced strength loss of the underlying alluvial soils. At another location near the channel, pronounced ground failure disrupted pavement and pipes at the intersection of Christine Avenue and Hope Street, just east of Rory Lane. Figure 4.47 shows warping of Christine Avenue and damage to a masonry wall at this location due to lateral spreading and settlement. Ground cracking and pavement distress in the eastern portions of Simi Valley not immediately adjacent to the Simi Arroyo Channel was generally relatively modest. A typical example of pavement buckling in these areas from lateral ground compression is shown in Figure 4.48, taken at Kuehner Drive near Katherine Road. In the central portion of Simi Valley below Tapo Canyon, very little pavement distress or ground cracking was observed.

During the Northridge Earthquake, liquefaction clearly occurred in the eastern portion of Simi Valley at several locations along the Simi Arroyo Channel. Based on the data presented in Figure 4.44, it appears ground failure also occurred in several other areas in the southeastern portion of Simi Valley along Stearns Street and Cochran Street. As the majority of the soils in this portion of the valley are cohesive according to the Leighton and Associates study (1972), any full or partial liquefaction would likely have occurred within relatively confined sandy stream channel deposits. As detailed geologic data is as-yet unavailable, no definitive conclusions on the ground failure mechanisms in these areas can be drawn.

The moderate ground failure in the central portion of Simi Valley below Tapo Canyon likely resulted from dynamic ground compaction or soil liquefaction at depth within the relatively sandy alluvial fan deposits (these mechanisms are described in Section 4.2.4). Liquefaction of shallow soils is unlikely in this area as the depth to groundwater is typically greater than 50 feet. As shown in Figure 4.44, the western Simi Valley area, despite having shallow groundwater, experienced very little pavement or pipeline distress typically characteristic of ground failure. Similar to the eastern Simi Valley area, the soils in this area are described as being primarily cohesive (Leighton and Associates, 1972), yet some liquefaction in stream channel deposits near the channel might have been expected. Due to the lack of available detailed geotechnical data, no firm conclusions can be drawn at this time in comparing the occurrence of liquefaction in the east with the non-occurrence in the west.

Figure 4.49 shows the distribution of unsafe structures as indicated by red post-earthquake inspection tags along with the outline of high groundwater zones from Figure 4.43 (FEMA, 1994). While a significant number of the red-tagged structures are located in zones which experienced liquefaction in the eastern Simi Valley area, it is not obvious to what extent liquefaction-induced ground movements may have influenced structural performance as this area also experienced relatively high ground shaking levels (Figure 3.4). In general, it appears that a majority of the structural damage in Simi Valley resulted from strong shaking and inertial forces, and was not strongly influenced by ground failure.



Fig. 4.45: Ground fissures from settlement and lateral spreading near Rory Lane, Simi Valley

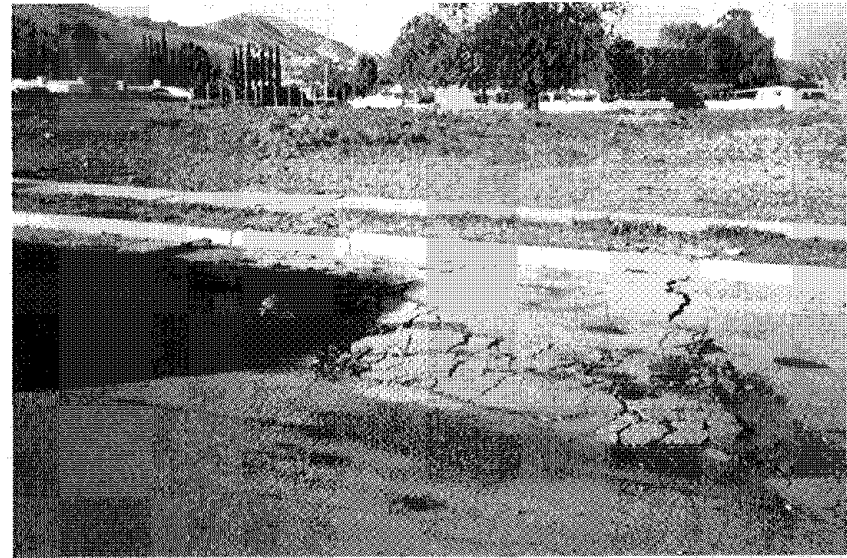


Fig. 4.46: Ground fissure from settlement and lateral spreading near Rory Lane, Simi Valley



Fig. 4.47: Damage to pavement and masonry wall from settlement and lateral spreading, Hope Street at Christine Avenue, Simi Valley



Fig. 4.48: Pavement buckling from lateral compression on Kuehner Drive near Katherine Road, Simi Valley

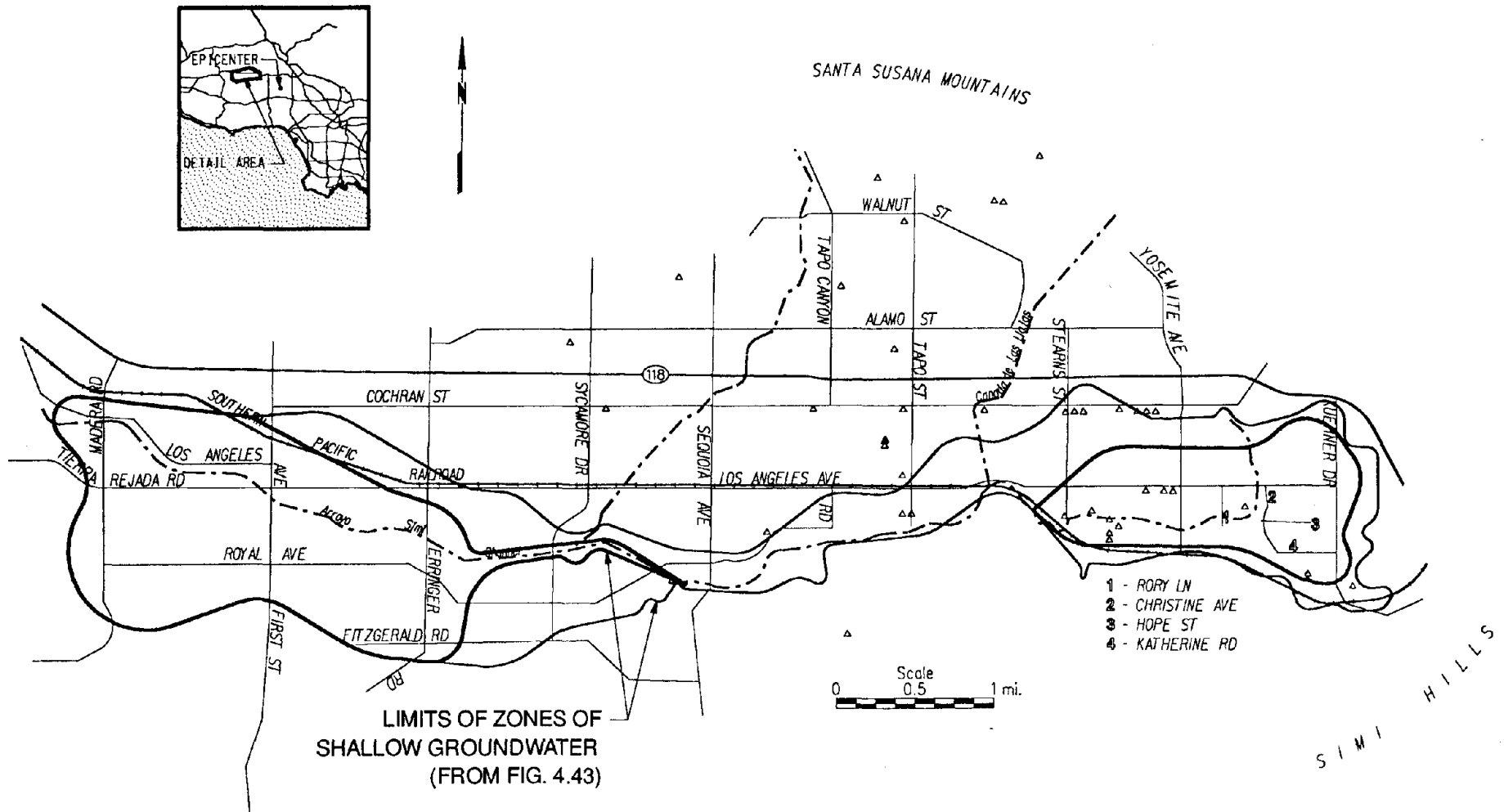


Fig. 4.49: Heavily damaged (red-tagged) structures in Simi Valley (Source: FEMA, 1994)

4.4 Santa Clara River Area

4.4.1 Introduction

The northernmost locations experiencing significant damage from ground failure during the Northridge Earthquake were in the vicinity of the Santa Clara River between Fillmore and Santa Clarita. As shown in Figure 3.4 and 3.5, recorded shaking intensities in the area varied from moderate peak horizontal ground accelerations on rock of about 0.2g to 0.4g, to relatively strong shaking levels at soils sites on the order of 0.2g to 0.6g. Massive liquefaction, ground compaction, and possible tectonic warping of bedrock in Potrero Canyon resulted in complex patterns of ground distress which received several months of study by the U.S. Geological Survey. In Santa Clarita, localized ground failures caused buckling of pavements, widespread disruption of water and other utilities, and possible structural distress. Liquefaction as evidenced by sand boils, lateral spreading and settlement occurred at several locations near the banks of the Santa Clara River near Highway 126.

It should be noted the northern-most area found to have experienced liquefaction during the Northridge Earthquake was along the banks of Gorman Creek. This area is located approximately 40 miles north of the epicenter (about 32 miles north of the northern-most extension of the fault plane), and is beyond the limits of the map in Figure 1.3. Peak horizontal ground accelerations in the area are estimated to have been less than 0.1g. Liquefaction caused numerous sand boils to form along the creek at this location as shown in Figures 4.50 and 4.51, but caused no damage as the area is undeveloped.

4.4.2 Potrero Canyon

Significant ground movements occurred within Potrero Canyon, which is a large east-west trending canyon on the northern flank of the Santa Susana mountain range. The canyon is located 6 miles west of Highway 5 and just south of State Route 126. It is approximately 18 miles from the epicenter. Based on the peak acceleration attenuation relationship for rock sites prepared by Idriss (1991), which compares well with the data from this event, it appears that the area may have experienced peak horizontal ground accelerations on rock of approximately 0.25g. A nearby strong motion station on soil recorded a peak horizontal ground acceleration of 0.46g. With the exception of a cattle ranch, the area is largely undeveloped, and little damage to structures occurred. Several gas lines and a water pipe broke, and one of the farm houses was without water for at least five days.

The fairly level ground within Potrero Canyon consists of approximately 2000 acres of alluvial and colluvial deposits. Figure 4.52 is a topographic map of the area. The approximate average slope of the canyon sediments is 2 degrees. The underlying bedrock and exposed bedrock hills in the area are part of the Pico formation, an early Pleistocene and Pliocene marine deposit of interbedded claystones, siltstones and sandstones. The small streams which drain the canyon merge with the Santa Clarita River just beyond the western end of canyon.



Fig. 4.50: Evidence of liquefaction in the form of sand boils along Gorman Creek, approximately 40 miles north of the epicenter (photo courtesy of Les Harder)

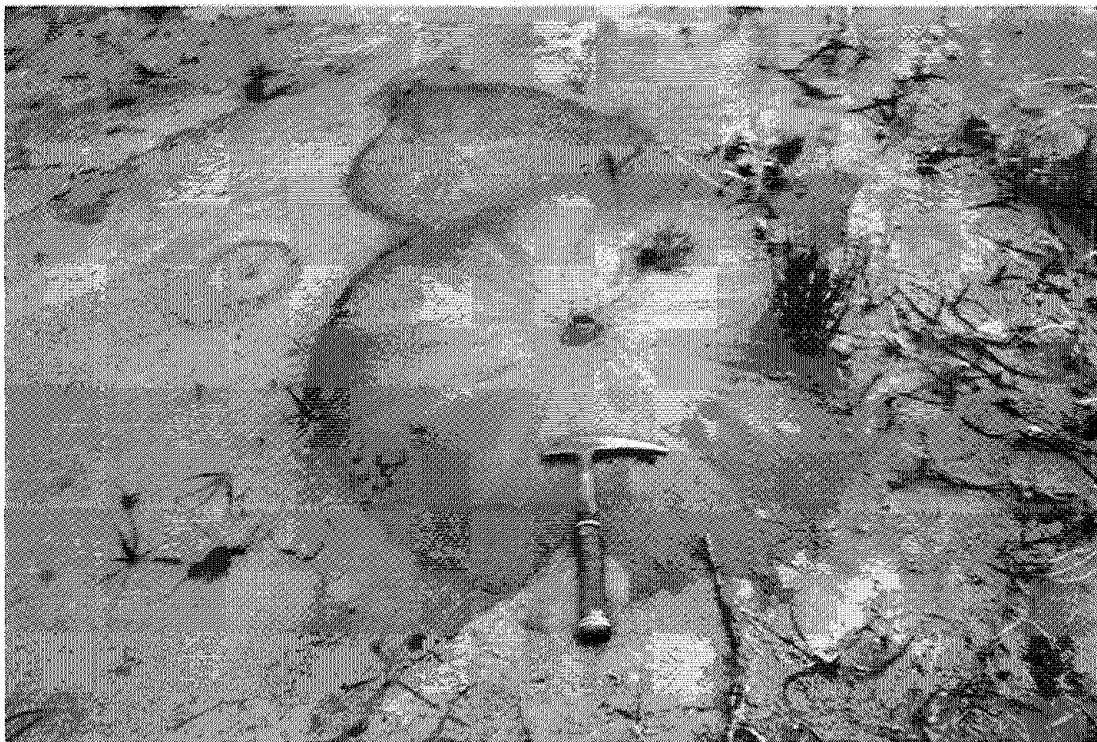


Fig. 4.51: Sand boils along Gorman Creek (photo courtesy of Les Harder)

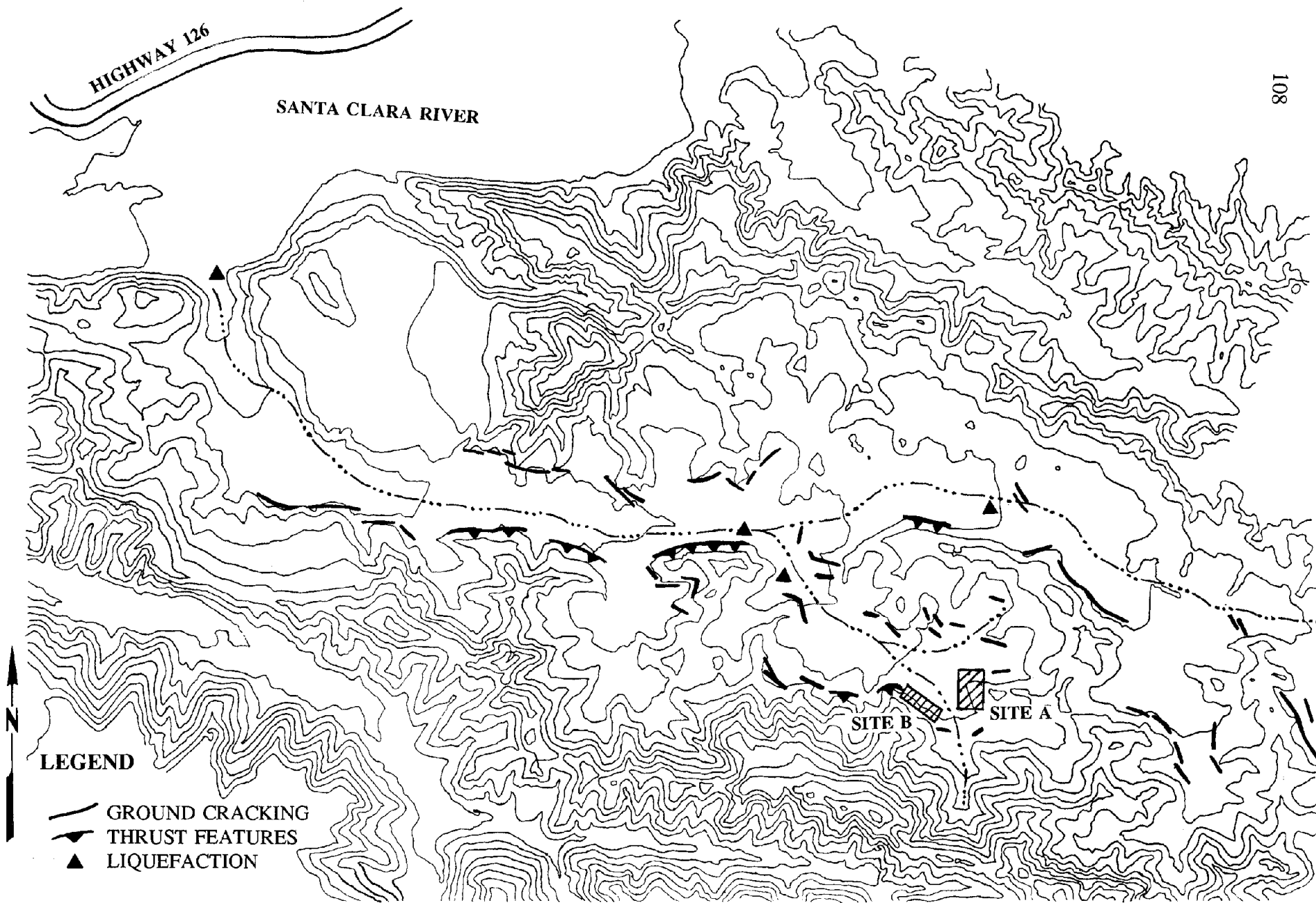


Fig. 4.52: Topographic map of Potrero Canyon. (Adapted from map provided by Newhall Land and Farming Company).

Linear ground breakage features, which are parallel to the axis of the canyon, were observed along the northern and southern margins. Sand boils were noted in several locations throughout the canyon, generally in close proximity to the stream channels (Figure 4.53). The locations of observed ground failures are plotted on the topographic map shown in Figure 4.52. In most locations, movements are distributed over wide zones of ground cracking. An aerial view of typical deformations along the base of a hill within the canyon is shown in Figure 4.54. Deformations appeared to be more pronounced at the base of small hills along the margins of the main canyon walls, and in many locations the cracks follow the contours around the toe of the hill. However, the dense grasses and other vegetation inhibited mapping of cracks in several small swale areas between hills. Where ground deformation features could be mapped through these swales, the cracks cut across the alluvial deposits at the toe of the swale linearly, remaining approximately parallel to the overall trend of the canyon.

Along the northern margin of the canyon, fractures are primarily extensional, with substantial differential vertical offsets and minor right lateral offsets. Multiple ground fractures within zones 5- to 50-foot wide accommodate as much as two feet of vertical movement. A zone of parallel extension cracks with almost two feet of relative vertical displacement is shown in Figure 4.55. Typical right-lateral ground deformation is shown in Figure 4.56.

Along the southern margin of the canyon, linear features are both compressional and extensional, with minor left lateral offsets. In numerous locations, compression was characterized by shallow thrusting along distinct shear surfaces that dip to the south at approximately 30 to 40 degrees with up to 8 inches of dip-slip displacement. Trenches across these features revealed that slippage of the A soil horizon occurred, held together by grass roots. The shear surfaces dipped south, into the hills, only for a short distance before curving upward and becoming parallel with the surface of the hill. Head scarps above these features could not be found. However, it would not take a large amount of extension across the height of the hills to account for the 8 inches of thrusting at the bases. Figure 4.57 shows measurement of a thrust feature.

Compressional features were also noted at the entrance to many of the smaller valleys within the canyon. These features are also largely linear, but extend outward from the margins to the center of the valley (Figure 4.58). This is consistent with lateral spreading of the sediments downslope. Compressional features develop as these sediments ride up on the sediments in the main canyon. In one location the ground surface was raised more than 4 inches relative to the surrounding ground. A similar feature was found where the canyon narrows. Evidence of localized compression within one of these valleys at the east end of the canyon was demonstrated by the movement of the pipe shown in Figure 4.59. The pipe was pushed up and to the right due to a shortening of 5 inches along its length.

Landslides were observed along the northern flank of the Santa Susana Mountains. However, none of these deep-seated landslides were found to be related to the compressional features in Potrero Canyon.

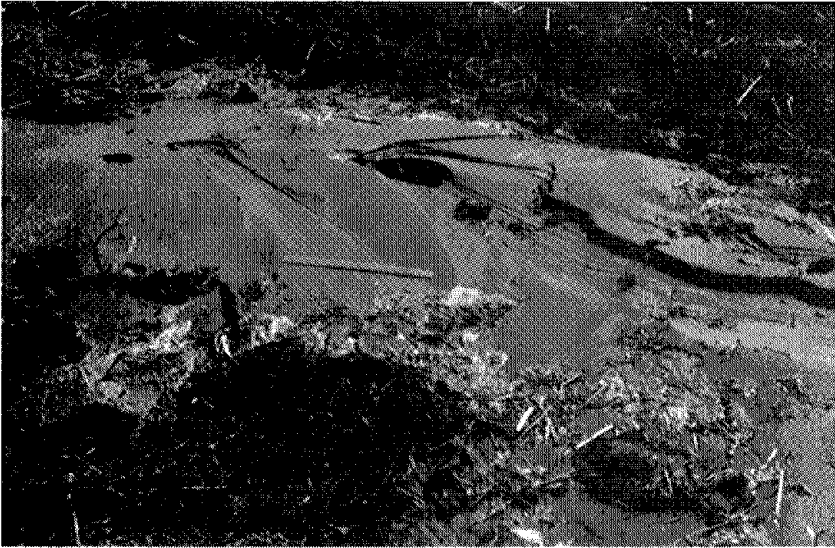


Fig. 4.53 Sand boil within Potrero Canyon



Fig. 4.54: Aerial view of cracking along the southern margin of Potrero Canyon



Fig. 4.55: Wide zone of extension cracks at the soil to bedrock contact in Potrero Canyon



Fig. 4.56: Example of right lateral displacement along the northern margin of Potrero Canyon

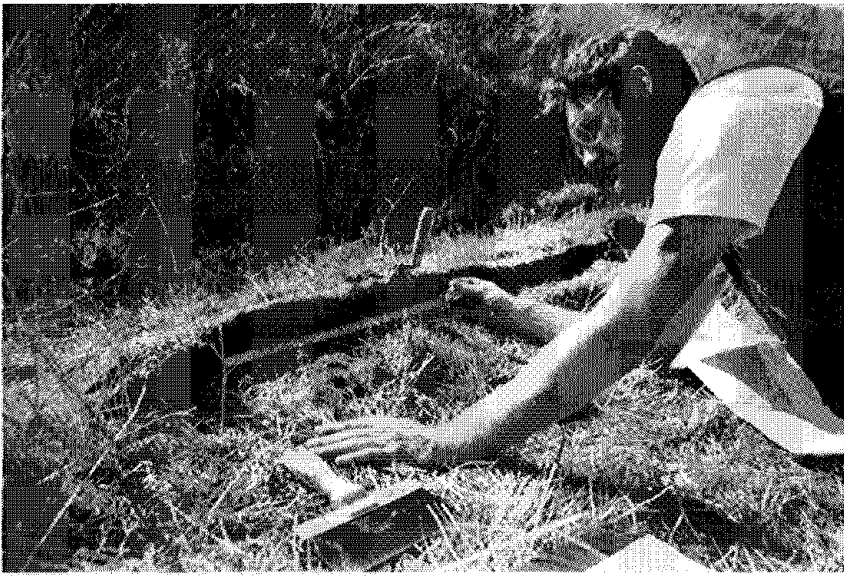


Fig. 4.57: Shallow thrusting of A soil horizon



Fig. 4.58: Compression feature where canyon narrows



Fig. 4.59: Evidence of localized compression. Note that originally straight pipe was pushed up and laterally; shortening across its length was 5 inches

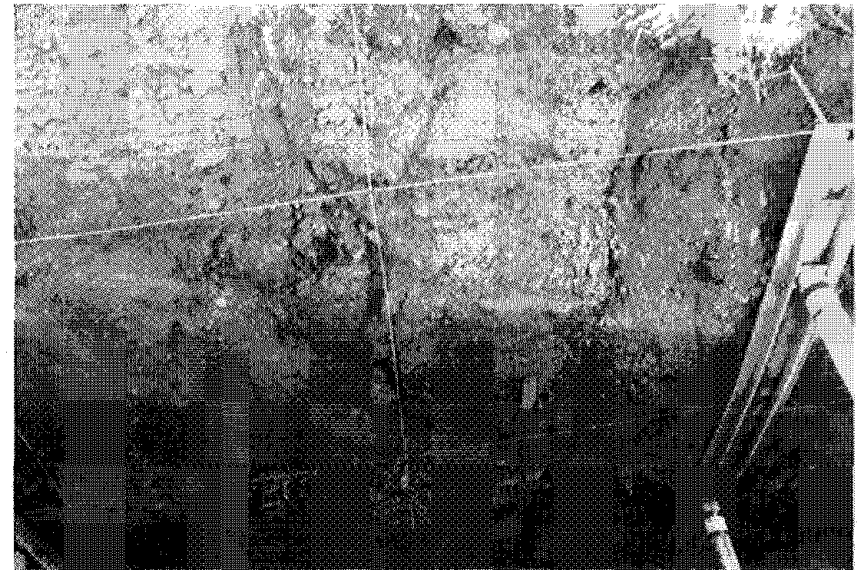


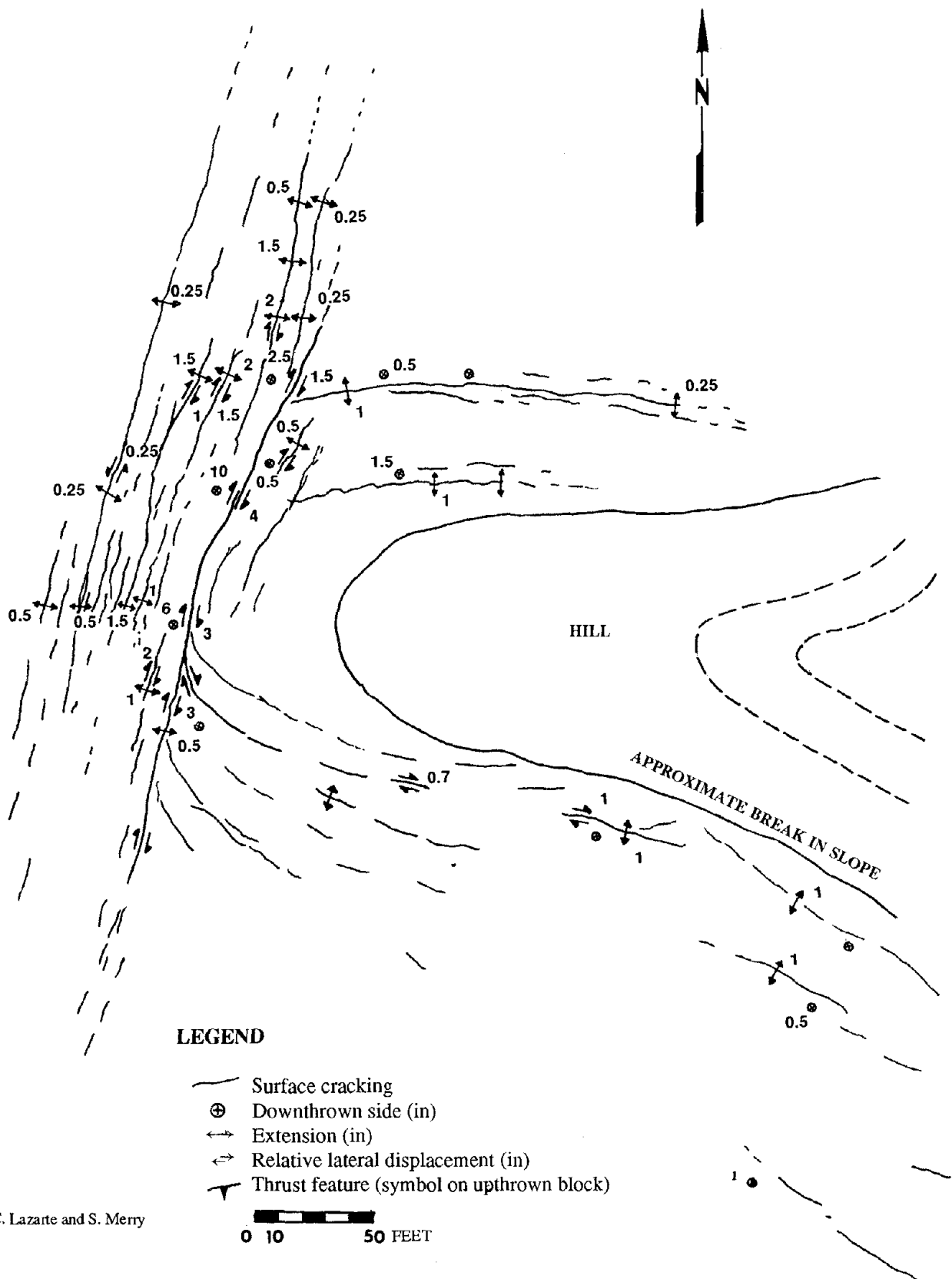
Fig. 4.60: Trench on the southern margin of Potrero Canyon. Note the vertical cracks and the contact between the darker, lower unit and the lighter, upper unit

Several small areas were mapped in detail, with the orientations and offsets on individual cracks measured. These detailed maps indicate the pattern of cracking typical throughout the canyon. Figure 4.61 is a map of the area labeled in Figure 4.52 as Site A. General ground movements at this location are to the west, with a small component to the north. These are consistent with the overall slope of the ground surface. The hill appears to influence the cracking pattern very little, as the majority of fractures remain linear. Figure 4.62 is a map of Site B shown in Figure 4.52. This site is along the southern margin of the valley. The complex pattern of cracking includes both extensional and thrust features. It should be noted that the zone of cracking is often more than 75 feet wide, extending from the bottom of the hill out into the nearly flat valley. The terrain in this zone slopes down to the north at an approximate slope angle of 8 degrees.

Potrero Canyon overlies the northern projection of the southerly dipping reverse fault rupture plane for the Northridge Earthquake. Hence, the widespread ground breakage within the canyon is being investigated for possible evidence of surface fault rupture. It appears, however, that much of the observed ground breakage can be explained by dynamic compaction of the alluvial and colluvial deposits and large scale lateral spreading resulting from liquefaction of primarily sandy and silty sandy deposits. The lateral offsets along the margins are consistent with an overall movement of the valley deposits to the west, which is downslope.

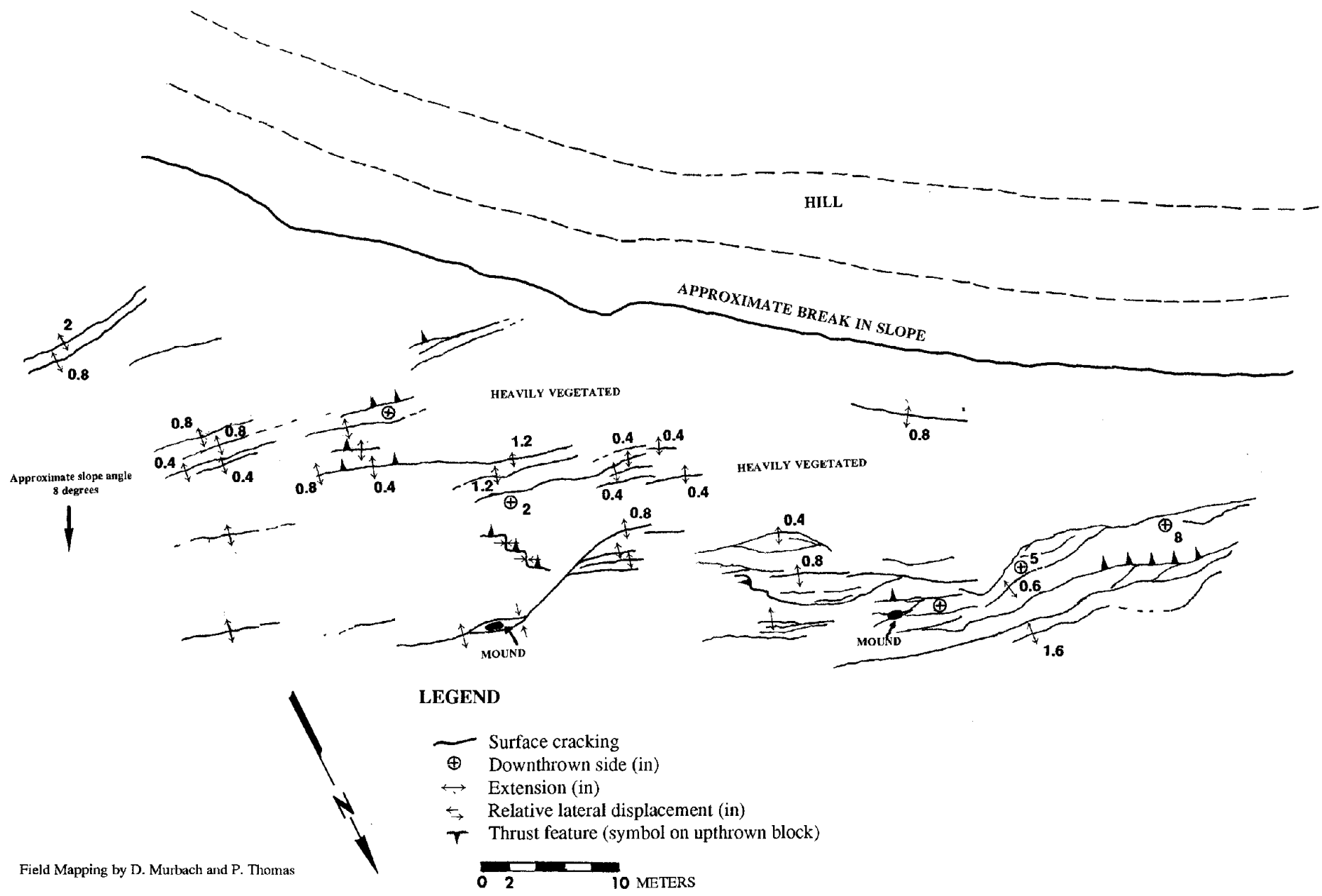
The United States Geological Survey (USGS) has completed extensive mapping and trenching of the canyon (David Schwartz, 1994). Trenching on the southern margins of the canyon exposed vertical cracks extending into bedrock and bedding plane shears whose orientations support dynamic compaction. Figure 4.60 shows vertical cracks in a trench on the southern margin of the canyon. The crack just to the right of the shoring accommodated a few inches of slip, as can be seen by the offset of the contact between the darker, lower unit and the lighter, upper unit. Bedrock offsets and infilled cracks reveal two prior tectonic events which produced approximately the same magnitude of vertical offsets. These events are being dated, and preliminary results indicate that the most recent event occurred approximately 1200 years ago, and the earlier event occurred during late Holocene.

The ground movements observed in Potrero Canyon following the Northridge Earthquake are not unique. Similar movements were observed on the southern flank of the Santa Susana Mountains following the 1971 San Fernando Earthquake. Lateral spreading of a large area on a slope of less than 3 degrees occurred at the Juvenile Hall site discussed in section 4.2.8. It should be noted that the Potrero Canyon site is currently being planned for future residential and commercial use, which serves to illustrate the importance of determining whether this type of deformation over such a vast area could have been anticipated and accounted for in design. Numerous sites with similar geologic conditions exist which have yet to be developed or have already been developed. Thus, Potrero Canyon presents an excellent case study of seismically induced ground breakage and the geotechnical considerations required in land development projects in seismically active regions.



Field Mapping by C. Lazarte and S. Merry

Fig. 4.61: Detail map showing crack patterns at Site A from Figure 4.52



LEGEND

- Surface cracking
- ⊕ Downthrown side (in)
- ↔ Extension (in)
- ↔ Relative lateral displacement (in)
- ▲ Thrust feature (symbol on upthrown block)

0 2 10 METERS

Field Mapping by D. Murbach and P. Thomas

Fig. 4.62: Detail map showing crack patterns at Site B from Figure 4.52

4.4.3 Santa Clarita

Santa Clarita is located near the Santa Clara River between Interstate Highway 5 and Highway 14. Ground failure at several locations within the city disrupted numerous underground pipeline systems which interrupted utility service to residents for days. Ruptures in an oil pipeline which traverses the southwestern portion of the city allowed oil to spill into the Santa Clara River. The area was also the site of numerous structural failures, the most vivid example of which was the collapse of several sections of the Interstate Highway 5 crossing over Gavin Canyon at The Old Road. As shown in Figure 3.4, recorded peak horizontal ground accelerations at soil sites in Santa Clarita varied from about 0.5 to 0.6g, with the strongest motions apparently occurring nearest the epicenter at the south end of the city.

The morphology of the Santa Clarita area consists of a series of low-lying valleys amidst mountainous ridgeline areas. Geologic materials in the valleys consist of Quaternary, fine to coarse-grained alluvial soil deposits, while regions of higher relief are underlain by uplifted and faulted Plio-Pleistocene marine and nonmarine rocks (Los Angeles County, 1990). As shown in Figure 4.63, the major drainage through Santa Clarita is the Santa Clara River, which flows west through Soledad Canyon. The river banks are relatively flat and broad in the east and west ends of the city, but towards the center of town the river flows through a somewhat narrower canyon area. Notable streams and canyons tributary to the Santa Clara River include San Francisquito, Bouquet and Mint Canyons north of the river, as well as Sand Canyon and the South Fork of the Santa Clara River to the south. In turn, canyon areas tributary to the South Fork of the Santa Clara River include Placerita, Wiley, Lyon, Pico, and Gavin Canyons. Of these canyon areas, extensive development has occurred in Buoquet Canyon, Pico Canyon east of Tournament Road, along the South Fork of the Santa Clara River north of the inlet from Lyon Canyon, Placerita Canyon west of Highway 14, and along the Santa Clara River in Canyon Country. Development has encroached upon hilly terrain bounding these valley areas in several locations as well.

In a seismic hazard study for the City of Santa Clarita, several of these basin/canyon areas were mapped as being susceptible to liquefaction during strong earthquake shaking (City of Santa Clarita, 1991). As shown in Figure 4.63, susceptible areas include a long zone generally following the alignment of the Santa Clara River, a relatively broad zone along the South Fork of the Santa Clara River north of Wiley Canyon Road, and portions of San Francisquito and Bouquet Canyons. This liquefaction susceptibility mapping was performed using the general procedure originally set forth by Youd and Perkins (1978), wherein zones characterized by high groundwater and potentially liquefiable soil types are considered susceptible to liquefaction. In the mapping of Santa Clarita liquefaction susceptibility, Holocene alluvial soils with depths to groundwater less than 30 feet were considered to be "liquefiable" (Los Angeles County, 1990). Numerous developed alluvial basins within Santa Clarita were not mapped as "liquefiable" according to these criteria, namely Mint Canyon, Pico Canyon east of Tournament Road, Placerita Canyon west of Highway 14, and an area adjacent to the South Fork of the Santa Clara River south of Wiley Canyon Road. The low liquefaction susceptibility assigned to these areas resulted from the mapping of a relatively deep (greater than 30 feet) groundwater table (Los Angeles County, 1990).

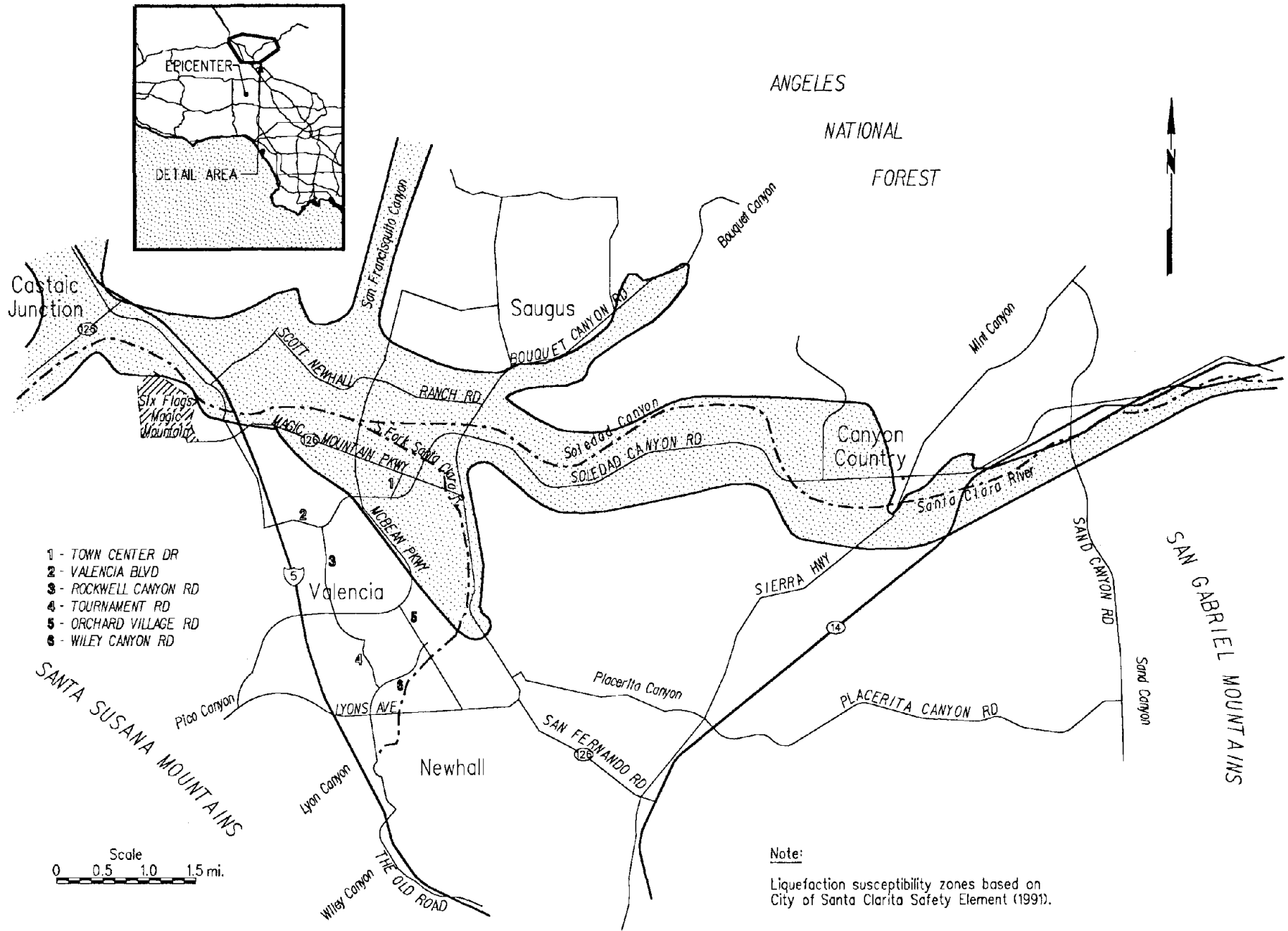


Fig. 4.63: Map of Santa Clarita showing mapped "liquefiable" zones

During the Northridge Earthquake, ground failure in Santa Clarita caused lateral spreading, settlement, and severe damage to pavements and buried utility pipes. Figure 4.64 shows the locations of water pipe breaks within the city along with the mapped "liquefiable" zones from Figure 4.63 (Newhall County Water District, Santa Clarita Water Company, Valencia Water Company, 1994). Also shown in Figure 4.64 are breaks in an oil pipeline which traverses the city approximately along a line between the Highway 126 intersections with Highway 14 and Interstate Highway 5 (California State Fire Marshall, 1994). As shown in Figure 4.64, areas experiencing ground failure, as evidenced by concentrated occurrences of pipe breaks, include alluvial basins between McBean Parkway and Wiley Canyon Road east of Interstate Highway 5, a portion of McBean Parkway just north of Pico Canyon west of Interstate Highway 5, a relatively broad zone south of Lyons Avenue, and several areas near the Santa Clara River (near Interstate Highway 5 and Country Canyon). It should be noted that the occurrence of ground failure as inferred from concentrated pipe break zones is only valid in developed areas with extensive pipe networks. Several additional but only sparsely developed areas along the Santa Clara River also experienced ground failure as evidenced by lateral spreading, settlement, and associated ground cracking.

Figure 4.65 shows the locations of severely damaged structures as indicated by red post-earthquake inspection tags along with the outline of "liquefiable" soils (FEMA, 1994). Structural damage was fairly severe in the area, with both residential and non-residential structures being significantly affected by the strong shaking, and in some cases possibly by ground failure. Examples of damage to non-residential structures include the collapse of a water storage tank east of Highway 5 at Valencia Boulevard (Figure 4.66), a distressed portion of the Los Angeles Aqueduct near Saugus (Figure 4.67), and the collapse of a freeway section at the Interstate Highway 5 crossing over Gavin Canyon.

It may be seen by comparing Figures 4.64 and 4.65, that several ground failure zones (as indicated by concentrated pipe breaks) also experienced high concentrations of structural damage. These areas of combined structural and pipeline damage concentrations include the area between McBean Parkway and Wiley Canyon Road west of Interstate Highway 5, two areas west of Interstate Highway 5 at Lyon Canyon and Pico Canyon, and two areas along the Santa Clara River near Interstate 5 and Canyon Country. Where these damage correlations are strong, ground failure may have contributed to structural damage. The concentrated structural damage along San Fernando Road near Lyons Avenue was not accompanied by a particularly high concentration of pipe breakage, suggesting that ground failure is relatively less likely to have been a significant contributor to structural distress in this area.

As shown in Figure 4.64, the highest concentration of pipeline distress occurred in two alluvial basin areas located in the vicinity of the Pico Canyon creek between Tournament Drive and Wiley Canyon Road, and along the north bank of the South Fork of the Santa Clara River north of Lyons Avenue. A narrow northeast-trending finger ridge separates these two alluvial areas west of the merge of Pico Canyon creek with the South Fork of the Santa Clara River, as shown in Figure 3.34. The highest concentrations of pipe breaks occurred in alluvium adjacent to the ridge, while the pipe breakage pattern on the ridge itself was considerably more dispersed. As the ground failure appears to have primarily occurred within

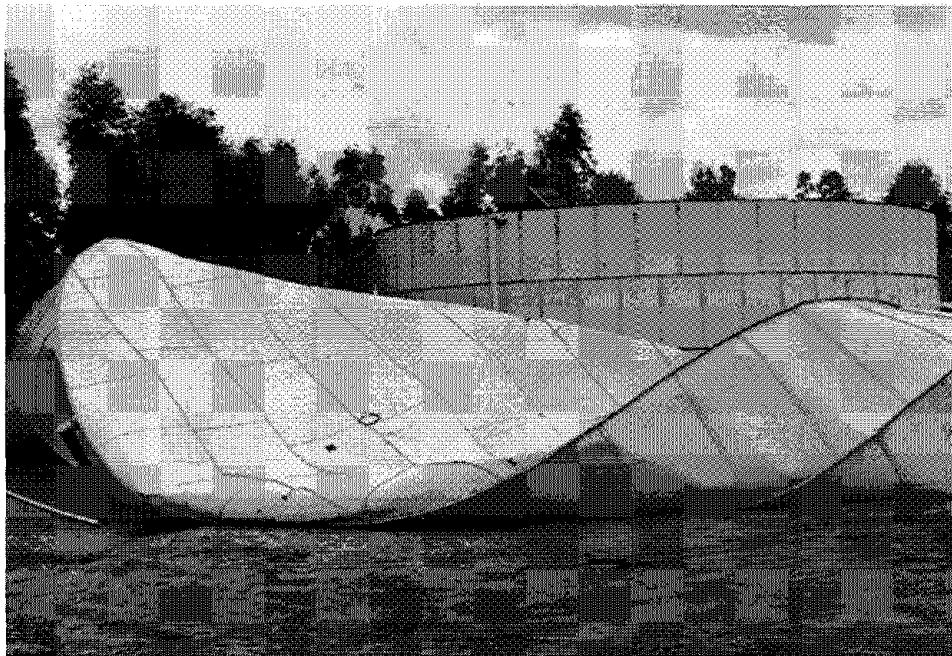


Fig. 4.66: Failed water storage tank, Santa Clarita (photo courtesy of Valencia Water Company)

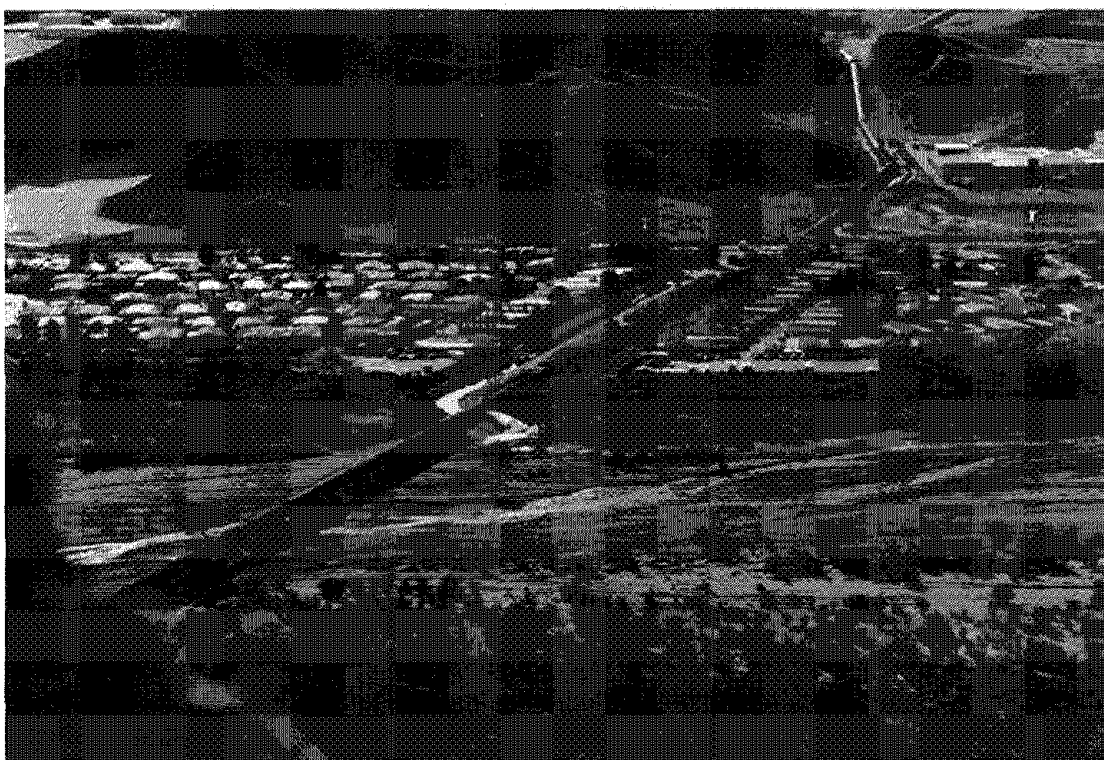


Fig. 4.67: Bleeding of water from the Los Angeles Aqueduct just west of Saugus

unconsolidated sediments, the likely culprit mechanisms are liquefaction and dynamic ground compaction. No detailed ground-level surveys by the authors were performed immediately following the earthquake in this area; hence, data providing conclusive evidence of soil liquefaction (such as sand boils) is not available. However, pipe break descriptions provided by field repair crews indicate that the pipes typically either "mashed together" in compression or "pulled apart" in extension (Valencia Water Company, 1994). These descriptions suggest that pronounced lateral ground movements occurred, which, in a relatively flat area, would typically be associated with liquefaction-induced lateral spreading. This possible occurrence of liquefaction in the area suggests that actual ground water elevations along at least the impacted portions of Pico Canyon creek and the South Fork of the Santa Clara River may have been somewhat higher than what is indicated on published depth to groundwater maps (Los Angeles County, 1990).

Pronounced lateral ground movements and settlements also occurred in other valley areas of Santa Clarita. A small developed area west of Interstate Highway 5, just north of Lyons Canyon experienced significant, though very localized, damage to structures, pavements and buried pipes. Figure 4.68 shows a water meter and sidewalk damaged by lateral compression at this location, while Figure 4.69 shows a water pipe damaged by localized lateral movements and settlement slightly northwest of this area at Larwin Tank. Further northwest near Pico Canyon, a concentration of structural and pipeline damage occurred along McBean Parkway. Many of the housing developments in these areas are constructed over large fills, and the observed ground failure may have resulted from dynamic compaction of the fill soils.

Near the Santa Clara River, settlement and lateral spreading caused numerous pipe breaks, including the rupture of an oil pipeline which led to contamination of the adjacent river area. Figure 4.70 shows a typical example of lateral spreading near the river banks, where a concrete slab at a water well was buckled by lateral compression. Due to the shallow groundwater and recent soils near the river bank, the ground failure in this area likely resulted from soil liquefaction.

In conclusion, liquefaction in Santa Clarita during the Northridge Earthquake appears to have occurred at several locations near the Santa Clara river, resulting in lateral spreading and localized settlements. While this area near the river had previously been mapped as "liquefiable", other areas which clearly also experienced ground failure had not been so designated. These impacted areas (excluding the areas expected to have been damaged by fill movements) are primarily underlain by recent alluvial deposits, but were mapped with a low liquefaction susceptibility based on suspected groundwater depths greater than 30 feet. Due to the lack of field observation data obtained to date, it cannot yet be conclusively determined whether this mapping is erroneous and shallow ground water enabled soil liquefaction to occur, or whether another ground failure mechanism such as dynamic ground compaction was responsible. However, based on the apparent occurrence of significant lateral spreading in these areas (as inferred from reports by field repair crews), and the presence of adjacent natural streams (which might be expected to provide locally high ground water), liquefaction appears to be a likely culprit mechanism to explain the observed damage. Further study of the liquefaction susceptibility of these areas would appear to be warranted in light of the ground failure which occurred there during the Northridge Earthquake.

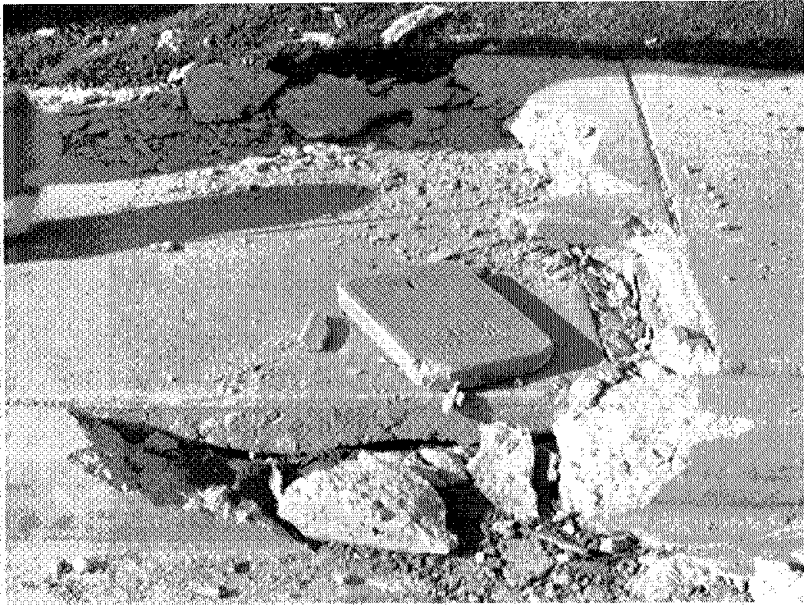


Fig. 4.68: Crushed water meter and sidewalk from lateral ground compression, Wintergreen Court, Santa Clarita (photo courtesy of Valencia Water Company)

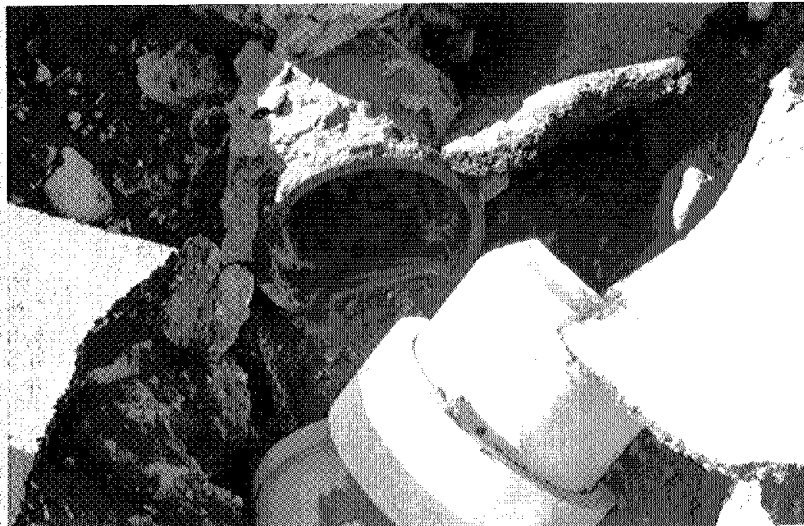


Fig. 4.69: Broken water pipe near Larwin Tank, Santa Clarita (photo courtesy of Valencia Water Company)



Fig. 4.70: Slab at water well buckled by lateral spreading near the Santa Clara River, Santa Clarita (photo courtesy of Valencia Water Company)

4.4.4 River Bank Areas Between Santa Clarita and Fillmore

Several areas along the banks of the Santa Clara River, between Santa Clarita and Fillmore, experienced liquefaction during the Northridge Earthquake. These areas are generally very sparsely populated and undeveloped, and hence very little damage appears to have resulted from the observed ground failures.

Fillmore was heavily impacted by structural distress during the Northridge Earthquake, as shown by the concentration of red-tagged structures in Figure 3.23. However, no significant evidence of ground failure in the form of ground cracking or major pipe breakage was observed in field reconnaissance of the area. It is likely that much of the severe structural damage in the area resulted from strong shaking overwhelming a number of inadequately designed structures, as shown in Figure 4.71.

Near the Highway 23 crossing over the Santa Clara River, sand boils were observed near a bridge pier for an overcrossing under construction, and cracks induced by lateral spreading were found approximately 15 feet away from the pier. The ground cracking and sand boils observed at this location are shown in Figures 4.72 and 4.73. This liquefaction in the river bank area caused no apparent damage to the bridge structure.

Further east, liquefaction was reported by a local resident at a site along the Santa Clara River near Potrero Canyon. Based on the reports of this individual, sand boils emerged during both the main shock and a rapid sequence of two, approximate magnitude 5 aftershocks on January 18, 1994. However, an aftershock on the day of the earthquake of magnitude 5.7 did not appear to liquefy this site, according to this individual. Using the attenuation relationship for rock sites developed by Idriss (1991), which has been shown to provide generally good predictions of ground motions from this event, mean accelerations on rock during these aftershocks are predicted to have been about 0.04g to 0.06g. Somewhat higher ground surface accelerations may have occurred at the ground surface due to soil amplification effects. The occurrence of liquefaction in the January 18 aftershock sequence likely resulted from the increased duration of the double event relative to the single aftershock event on January 17. Having thus bracketed the shaking conditions wherein liquefaction occurred, this site may represent an interesting case history against which to calibrate liquefaction analysis procedures.

4.5 Coastal Areas

4.5.1 Introduction

Ground failure during the Northridge Earthquake occurred in a number of coastal areas including Santa Monica, Marina del Rey, Redondo Beach, and the Port of Los Angeles. Santa Monica and Marina del Rey generally experienced relatively minor, localized, and undamaging liquefaction in beach areas, although several inland portions of Marina del Rey appear to have experienced moderate ground softening as evidenced by pipe breakage. In a mole for the King Harbor area of Redondo Beach, liquefaction-induced settlement and lateral spreading of loose sandy fill materials ruptured a number of utility lines and led to the failure

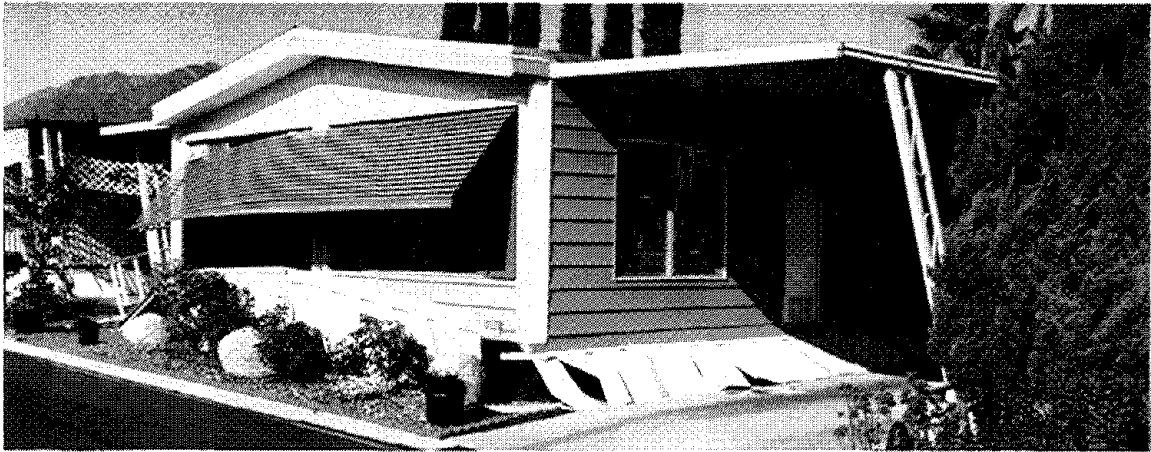


Fig. 4.71: Damaged mobile home in Fillmore. Numerous structures were severely damaged in Fillmore in the absence of any apparent large-scale ground failure.



Fig. 4.72: Ground cracking from lateral spreading in river bed area near Highway 23 crossing over Santa Clara River



Fig. 4.73: Sand boil near bridge pier, Highway 23 crossing over Santa Clara River

of a bulkhead wall. One of the southern-most areas which experienced ground failure was the Port of Los Angeles, where liquefaction caused moderate lateral spreading, settlement, and large sand boils.

4.5.2 Santa Monica and Marina del Rey

Santa Monica and Marina del Rey, located south of the Santa Monica Mountains approximately 12 to 16 miles southeast of the epicenter, experienced moderate, though generally relatively undamaging, ground failure during the Northridge Earthquake. Portions of Santa Monica appear to have been very strongly shaken during the earthquake. Recorded peak horizontal ground surface accelerations on soils sites in Santa Monica were on the order of 0.3 to 0.9g, as shown in Figure 3.4. The southern portions of Santa Monica and Marina del Rey, however, experienced relatively moderate shaking levels on the order of 0.2 to 0.3g. Significant structural damage occurred in Santa Monica north of Interstate Highway 10, though south of the freeway structural damage was relatively sparse.

As shown in Figure 3.35, most of Santa Monica is underlain by Pleistocene fine- to medium-grained alluvial or marine terrace deposits, though a tongue of more recent Holocene-age, medium to coarse-grained soils extend towards the coast from inland areas north of Interstate Highway 10. Further south at Marina del Rey, the soils are mapped as Holocene fine to medium-coarse grained alluvial, flood plain, and dune deposits. Ballona Creek, which serves as the drainage for much of the central Los Angeles area, discharges to Santa Monica Bay just south of the marina at Marina del Rey, and much of the recent alluvial and stream channel deposits in the area appear to have been deposited near its banks. Based on the soil and groundwater conditions in the area, liquefaction susceptibility maps have been compiled for this region as part of the Los Angeles County Safety Element. Figure 4.74 shows the zones having the highest liquefaction susceptibility in Santa Monica and Marina del Rey based on this mapping (Los Angeles County, 1990). As shown in Figure 4.74, these areas include a portion of West Los Angeles along Santa Monica Boulevard, and a wide zone encompassing Marina del Rey roughly bound by Rose Avenue to the north and Jefferson Boulevard to the south.

Relatively minor ground failure occurred in the Santa Monica-West Los Angeles-Marina del Rey areas during the Northridge Earthquake. Figure 4.75 shows the distribution of pipe breaks in the area along with the outline of "liquefiable" soil zones from Figure 4.74 (City of Santa Monica, City of Los Angeles, and Los Angeles County Water Works, 1994). Also shown in Figure 4.75 are the locations of observed liquefaction features such as sand boils, sand fissures, and lateral spreads. In Santa Monica, liquefaction occurred at several beach areas, but generally was notably absent from inland areas. Figure 4.76 shows an overview of a parking lot near the Santa Monica Municipal Pier where sand fissures, lateral spreading and settlement occurred. A large sand fissure from the parking lot is shown in Figure 4.77. Pavement cracking in the parking lot occurred subparallel to the coastline with horizontal and vertical offsets on the order of 1½ to 5 inches. Minor lateral spreading was also observed further north in a beach area near San Vicente Boulevard, though no sand fissures or boils were observed at this location.

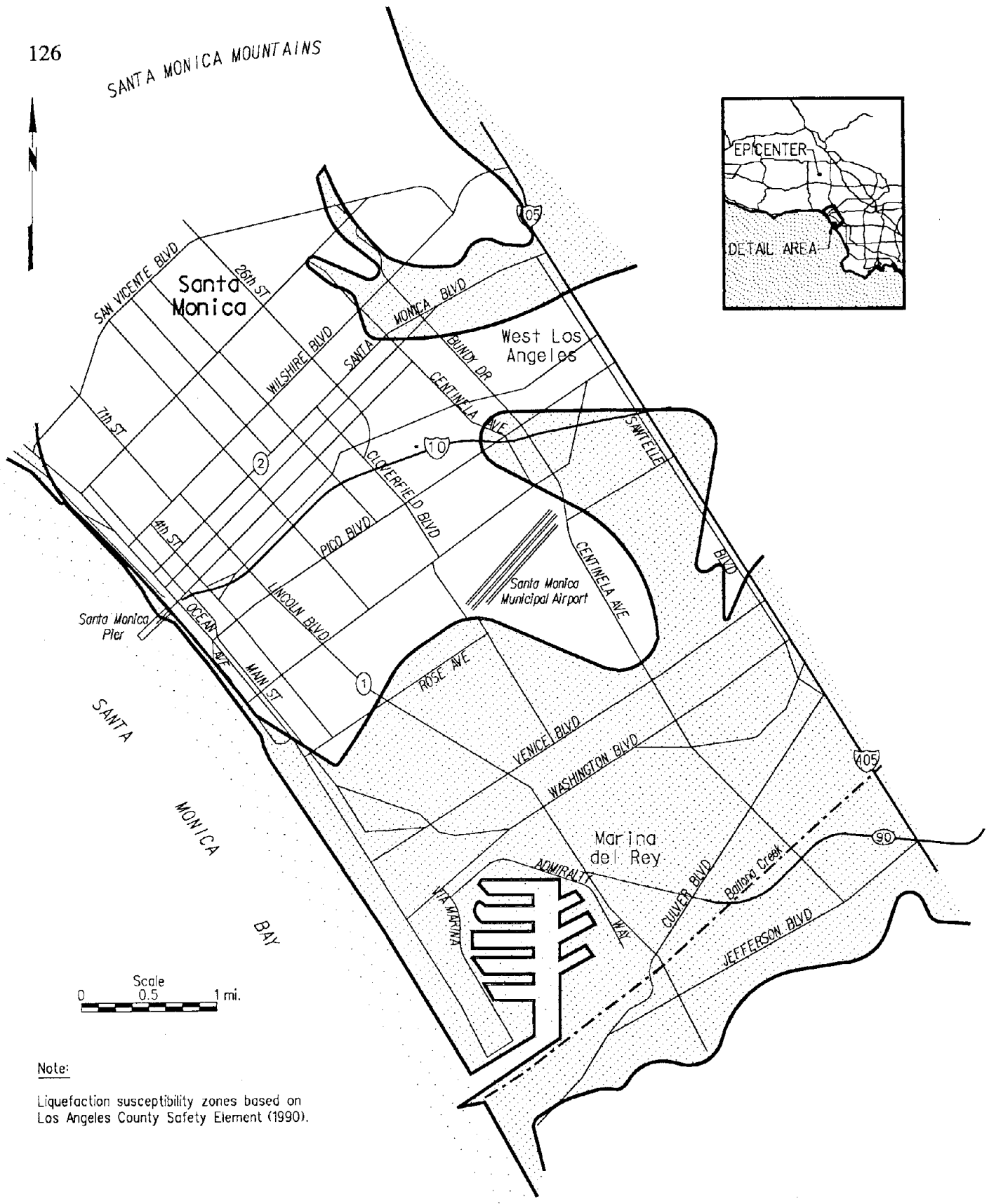


Fig. 4.74: Map of the Santa Monica-Marina del Rey region showing mapped "liquefiable" zones

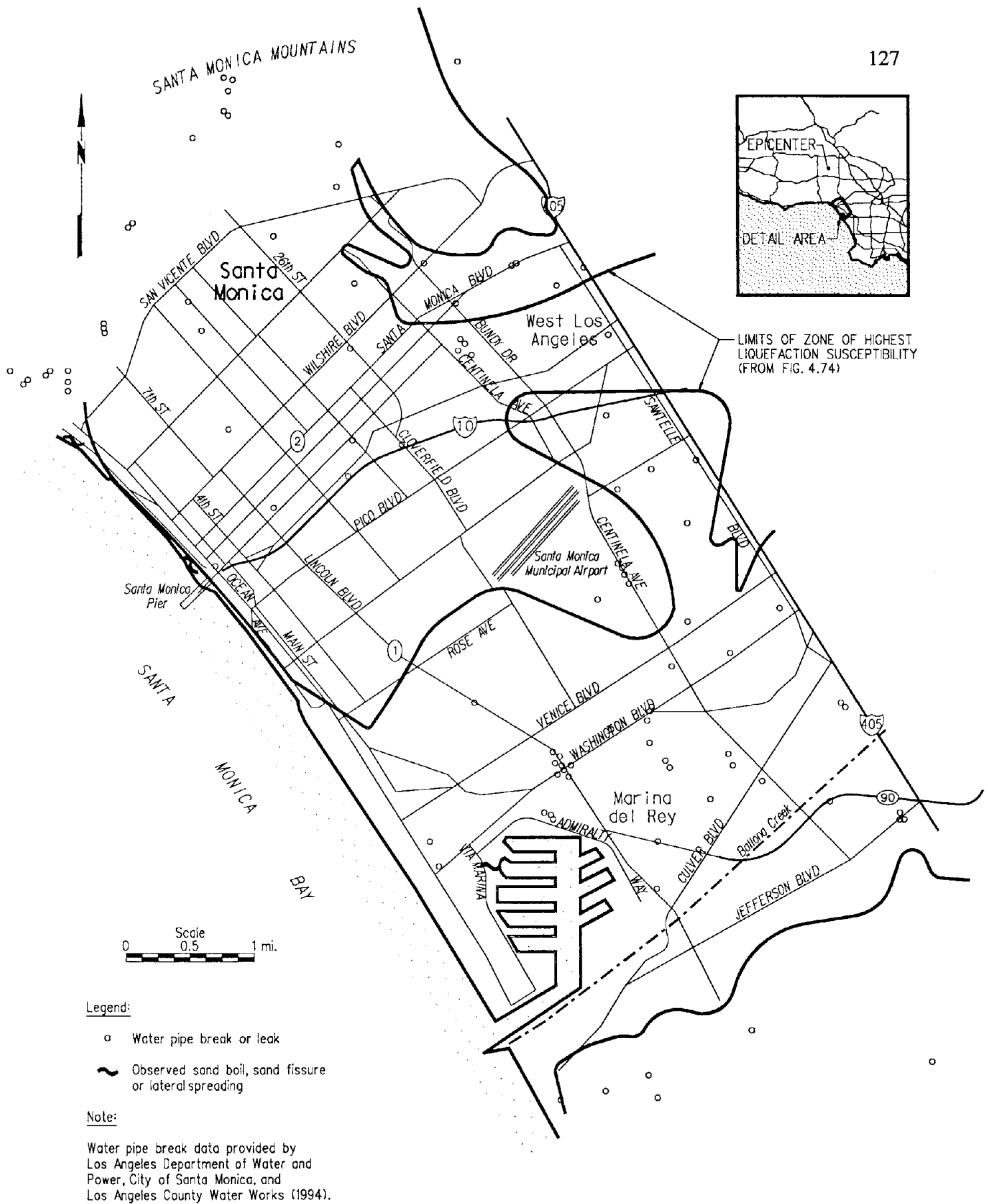


Fig. 4.75: Pipe breakage in the Santa Monica-Marina del Rey region



Fig. 4.76: Overview of parking lot with numerous sand fissures near Santa Monica Municipal Pier



Fig. 4.77: Sand fissure in parking lot near Santa Monica Municipal Pier

Further south, at Marina del Rey, a modest concentration of pipe breakage occurred northeast of the marina between Washington Boulevard and Culver Boulevard, as shown in Figure 4.75. This area is known to have fairly recent soil deposits and relatively high groundwater, and hence might have been expected to show more substantial evidence of liquefaction. However, the moderate local ground shaking levels appear to have only produced minor ground softening possibly due to partial soil liquefaction. More substantial liquefaction may have occurred in an artificial beach area at the marina near the intersection of Via Marina and Admiralty Way where a large sand fissure was reported (Los Angeles County, Department of Harbors and Beaches, 1994).

Figure 4.78 shows the locations of severely damaged structures, as indicated by red post-earthquake inspection tags, along with the outline of "liquefiable" soils from Figure 4.74. As shown in Figure 4.78, numerous structures were damaged in Santa Monica north of Interstate Highway 10, although relatively little damage occurred south of this freeway. Based on the lack of pipe break concentrations or ground cracking in the heavily damaged portions of Santa Monica, as well as the geologic conditions in the highly damaged zones, ground failure does not appear to have been a significant contributor to the large concentration of structural damage in the area.

4.5.3 Redondo Beach

One of the most notable examples of soil liquefaction caused by the Northridge Earthquake was approximately 26 miles southeast of the epicenter in the coastal community of Redondo Beach. Liquefaction occurred in a mole area within a marina causing movement of a bulkhead wall, as well as significant pipe breakage within the mole. In addition, liquefaction at a nearby recreational aquatic facility known as Seaside Lagoon destroyed the system's pipe network and concrete lining. The expected cost of re-building and stabilizing these areas has been estimated at approximately three million dollars (City of Redondo Beach, 1994).

The following information on the recent history and geologic conditions at the King Harbor area in Redondo Beach is based on a report prepared by M&T Agra, Inc. (1994). This firm has served as the geotechnical consultant on the repair and reconstruction of the damaged mole area.

The current King Harbor facility at Redondo Beach was constructed between 1956 and 1962 to house a marina. A large breakwater provides protection for three earthen moles which extend into the marina to provide berths for recreational boats. The middle mole, known as Mole B, is located over a former beach area which was significantly eroded due to the construction in 1938 of a breakwater to the north, which displaced longshore currents offshore and cut off the southward migration of replenishing sand. Fill materials for Mole B were obtained from nearby dunes and beach deposits. The sandy fill materials were placed by end dumping the soil from trucks, and spreading the material into place with bulldozers. Only the top several feet of fill above the harbor water levels received mechanical compaction. Construction of the mole was completed by placement of coarse rock materials on the slopes of the sand fills (to minimize washout and erosion of the sand), and the

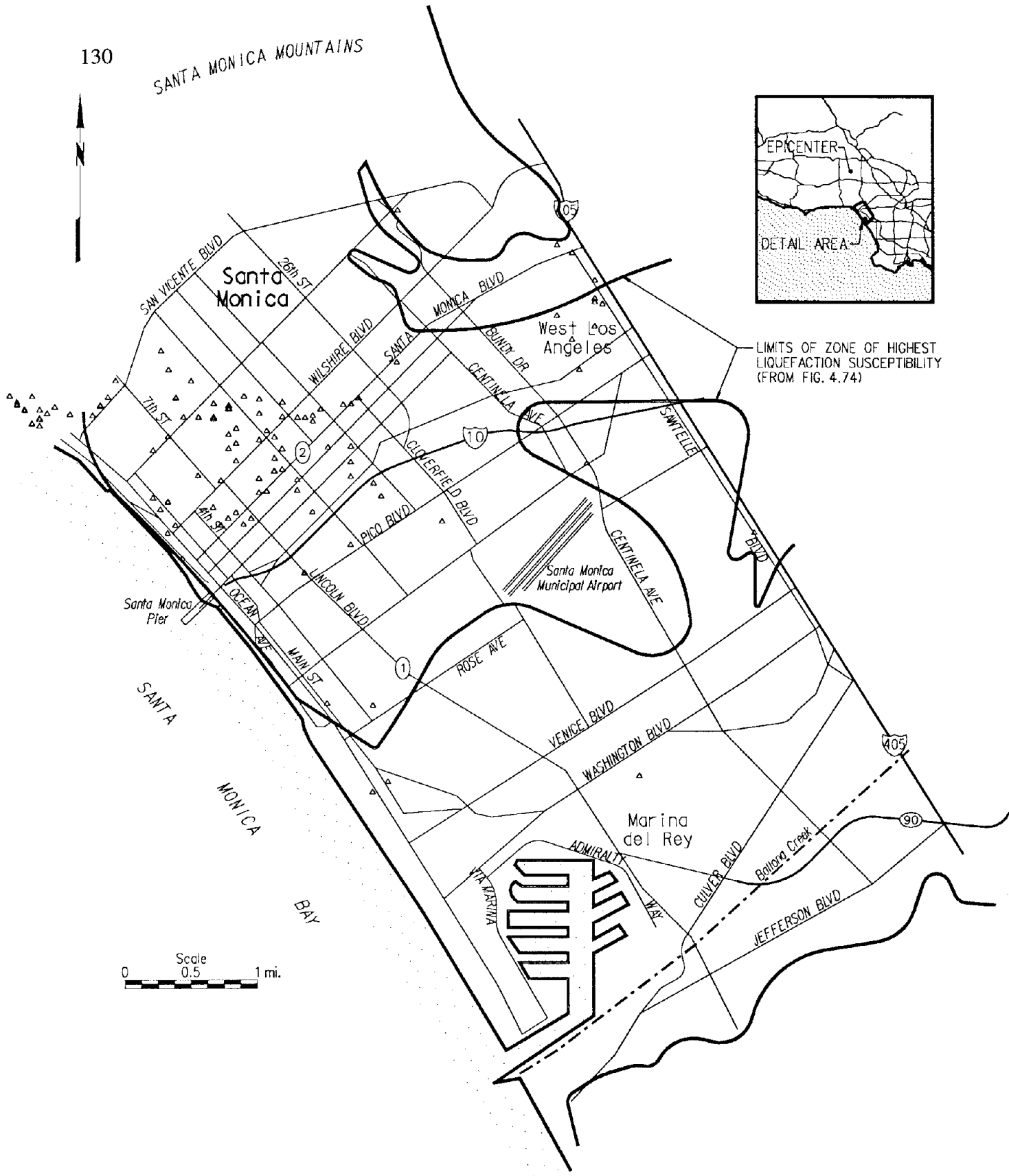


Fig. 4.78: Heavily damaged (red-tagged) structures in the Santa Monica-Marina del Rey region (Source: FEMA, 1994)

construction of a 5-foot tall, cast-in-place concrete retaining wall atop the rocky materials. The finished mole surface was graded to about elevation +10 to +11 feet Mean Sea Level (MSL), whereas the top of wall and water elevations are +7 feet MSL and +2 to +4 feet MSL, respectively. Since the original construction of the Mole B area, several feet of settlement have occurred in the area.

As shown in Figure 4.79, the fill soils at Mole B consist of loose to very loose sands which extend to depths of 21 to 23 feet in the failure area. These fill soils are underlain by interbedded very soft to soft silty lagoonal deposits and loose to dense sandy beach deposits of Holocene age which extend to depths of approximately 25 to 35 feet. The upper portion of the original beach deposits appeared to have been eroded following the construction of the breakwater in 1938. The lagoonal and beach deposits are in turn underlain by fluvial and/or marine deposits consisting of relatively uniform sands having a dense to very dense consistency. The soil consistencies given for the various soil units were determined on the basis of the standard penetration test.

The Northridge Earthquake caused liquefaction of the sandy fill materials at Mole B, and possibly of the underlying beach and lagoonal deposits as well. Liquefaction-induced strength loss in the fill materials resulted in significant lateral spreading and settlement which caused up to 17 feet of displacement of the south wall of Mole B into the marina, as well as several feet of settlement of the mole surface, as shown in Figure 4.79. In addition, numerous utility pipes in the mole were broken, pavements were disrupted, and several small buildings on the mole were damaged. Figures 4.80 and 4.81 show an overview of the Mole B area including the damaged bulkhead wall and parking area. Figure 4.82 shows damage in a parking area behind the displaced wall section near the location of a ruptured utility pipe. Virtually every utility pipe located behind the failed wall section was reported to have been broken by the lateral spreading and settlement in the area (City of Redondo Beach, 1994). The liquefaction-induced strength loss of soils underlying the parking lot caused "bearing capacity" failures to occur beneath several cars as shown in Figure 4.83. Figure 4.84 shows a close-up view of the wall near the maximum displacement section.

Re-construction of the Mole B area is planned in conjunction with remedial efforts to reduce the liquefaction susceptibility of the sandy soils underlying the mole. Currently, proposed remediation techniques include the installation of stone columns through the fill materials and underlying beach and lagoonal deposits, and vibrocompaction of the remaining fill soils underlying the mole (M & T Agra, Inc., 1994).

In a southern portion of King Harbor, liquefaction of sandy fill materials severely damaged a recreational aquatic facility known as Seaside Lagoon. The facility was used for recreational swimming and consisted of a contoured sandy bowl with a concrete bulkhead along one side of the facility, as shown in Figure 4.85. Liquefaction of the underlying sandy materials in the area resulted in differential settlements, lateral spreading, and sand boils. Figures 4.86 and 4.87 show ground cracking from lateral spreading adjacent to the lagoon and a sand boil in the lagoon area, respectively. Liquefaction resulted in differential settlement of the bulkhead wall on the order of 18 inches, and breakage of numerous 4 to 10-inch water pipes serving the facility (City of Redondo Beach, 1994).

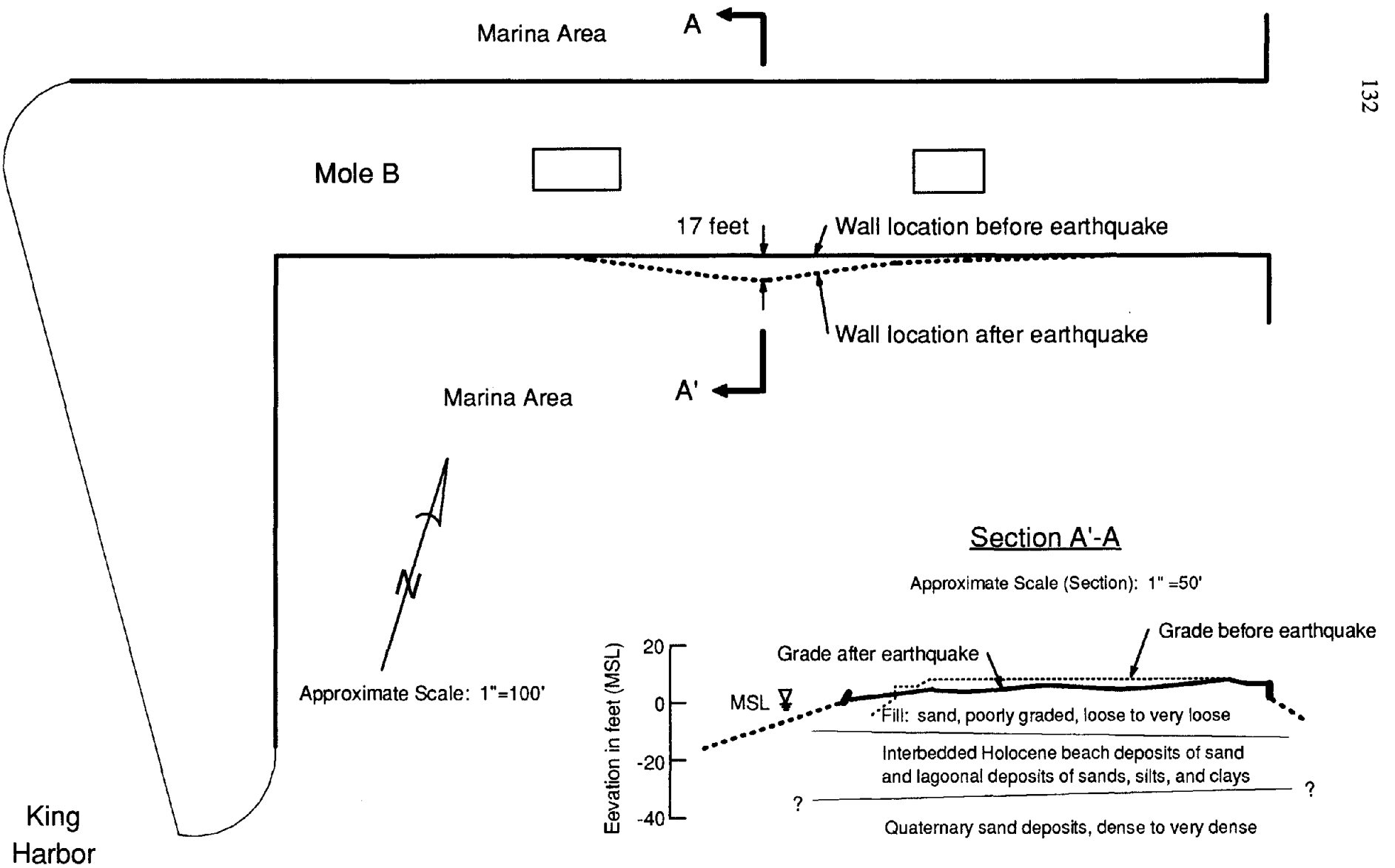


Figure 4.79: Plan view and section for Mole B at King Harbor, Redondo Beach showing wall movement. Reference: M&T Agra, Inc. (1994)

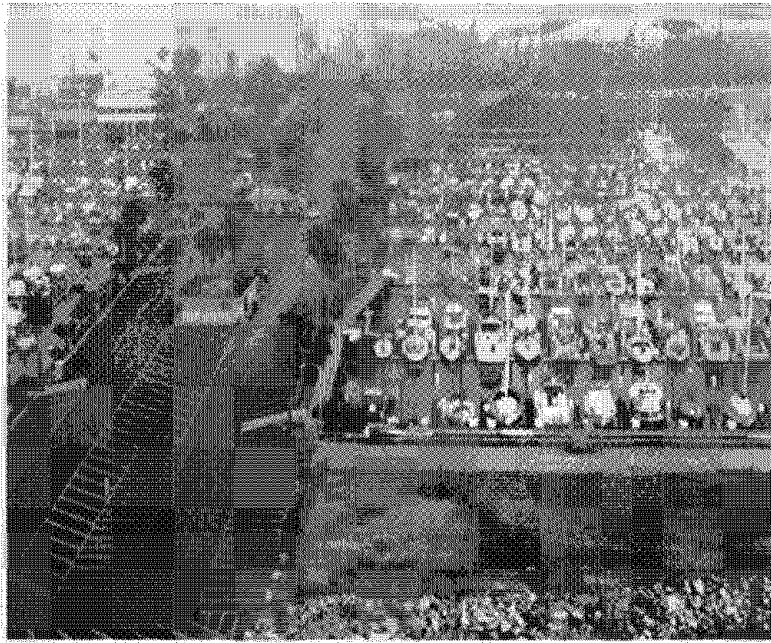


Fig. 4.80: Overview of Mole B at King Harbor, Redondo Beach
(photo courtesy of John Tinsley, U.S. Geological Survey)

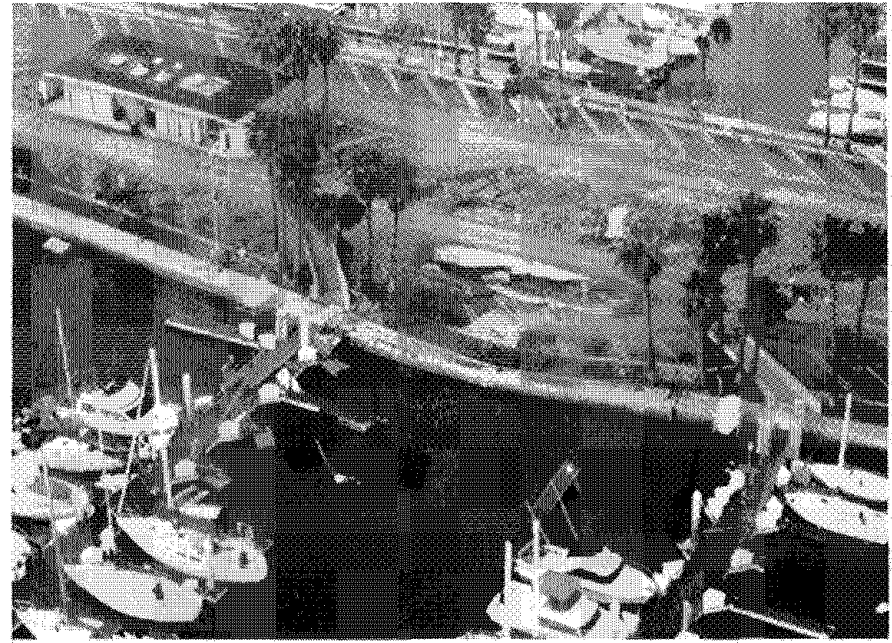


Fig. 4.81: Overview of wall failure and distress in parking area,
Mole B at King Harbor, Redondo Beach
(photo courtesy of John Tinsley, U.S. Geological Survey)



Fig. 4.82: Damage in parking area behind failed wall section at Mole B



Fig. 4.83: Liquefaction-induced bearing capacity failures
beneath cars in parking lot at Mole B. Photo by
Los Angeles Times.



Fig. 4.84: View of failed retaining wall near maximum displacement section at Mole B

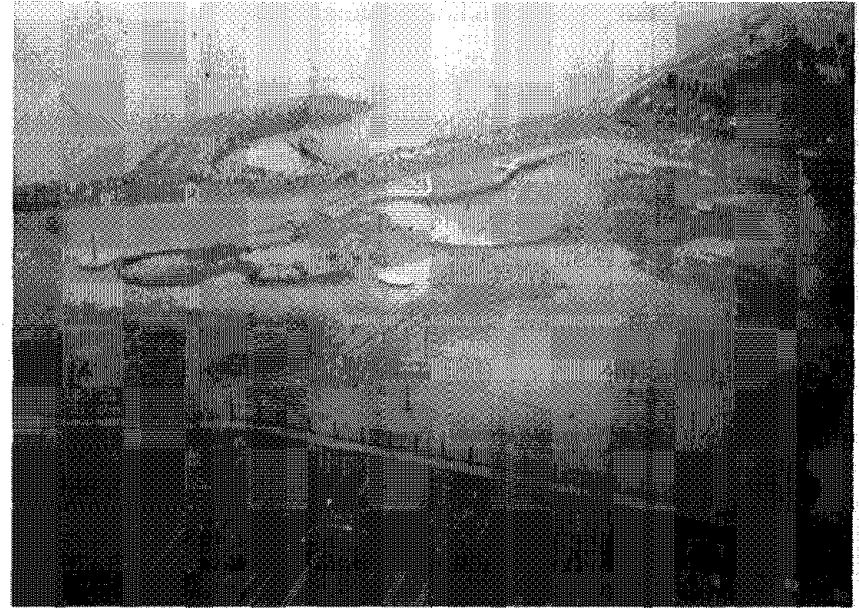


Fig. 4.85: View of Seaside Lagoon area in south arm of King Harbor, Redondo Beach (photo courtesy of John Tinsley, U.S. Geological Survey)



Fig. 4.86: Ground cracking from lateral spreading adjacent to Seaside Lagoon

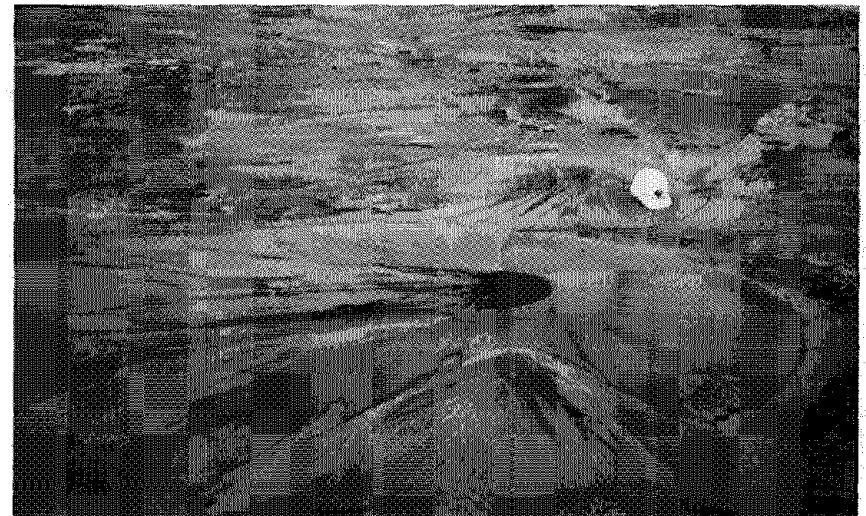


Fig. 4.87: Sand boil within Seaside Lagoon

4.5.4 Port of Los Angeles

The southern-most area known to have experienced significant damage from liquefaction was at the Port of Los Angeles, located on the south side of Los Angeles near Interstate Highway 110 as shown in Figure 1.3. Peak horizontal ground accelerations on the order of 0.1g to 0.2g were recorded at most soil sites in the vicinity of the port (Figure 3.4), with the nearest station at the Vincent Thomas Bridge (approximately 5000 feet from the site) recording a relatively large acceleration of 0.25g. The port is primarily constructed on hydraulic fills with pile-supported wharves extending over revetment slopes (Hayden, 1994).

Liquefaction at the port resulted in a variety of damage including bending and breakage of crane rail systems, architectural damage to several structures, disruption of utilities providing water and power to the area, and ground surface cracking from lateral spreading and settlement (Hayden, 1994). The overall effects of this damage was relatively minor, however, as the port facilities were repaired within 5 days of the earthquake and repair costs only totaled about \$50,000 (Port of Los Angeles, 1994).

The most significant occurrences of liquefaction at the port were near Berths 121 to 126 and at Pier 300. At Berths 121-126, a paved area 200 feet in diameter behind a dike and wharf experienced lateral spreading and settlement from liquefaction of the underlying loose, silty and sandy fill soils. Cone penetration testing performed after the earthquake indicated the fill soils in this area had relative densities on the order of 20 to 50 percent, based on penetration resistance correlations with relative density. Some of the damage and clean-up operations in this area are shown in Figures 4.88 to 4.90. Lateral spreading in the area caused 2 to 3 inch movements of the wharf structure, and several 1 to 2-inch wide cracks 500 to 600 feet in length behind the wharf. Settlements of 6 to 8 inches occurred to pavements, and approximately 10 cubic yards of sand emerged from large boils which penetrated the 7-inch thick asphalt in the area (Hayden, 1994).

Pier 300 consists of an undeveloped fill constructed fairly recently (in the last 5 years). The central portion of the pier had been pre-loaded prior to the earthquake to densify clayey soils underlying the fill, but no ground densification measures had been employed to densify the sandy fill materials (Port of Los Angeles, 1994). During the Northridge Earthquake, lateral spreading of 4 to 6 inches occurred in the pier's east dike (based on visual observation), but caused minimal damage due to the lack of development in the area (Hayden, 1994). A small graben and sand fissure associated with these movements are shown in Figure 4.91.

4.6 Central Los Angeles Area

Portions of the central Los Angeles area, from Hollywood in the north to the Culver City-West Adams area in the south, suffered significant and very well publicized structural damage from the Northridge Earthquake. Significant, though less publicized, ground failure also occurred in the area, as evidenced by hundreds of pipe breaks within several relatively well defined zones. As shown in Figure 3.4, recorded shaking levels on rock and soil sites in this region varied from peak horizontal accelerations of 0.3 to 0.4g north of Interstate Highway 10, to approximately 0.2 to 0.3g south of the freeway.



Fig. 4.88: Sand ejecta in parking area adjacent to Berths 121 to 126, Port of Los Angeles (photo courtesy of Doug Thiessen, Port of Los Angeles)



Fig. 4.89: Sand ejecta in parking area adjacent to Berths 121 to 126, Port of Los Angeles (photo courtesy of Doug Thiessen, Port of Los Angeles)

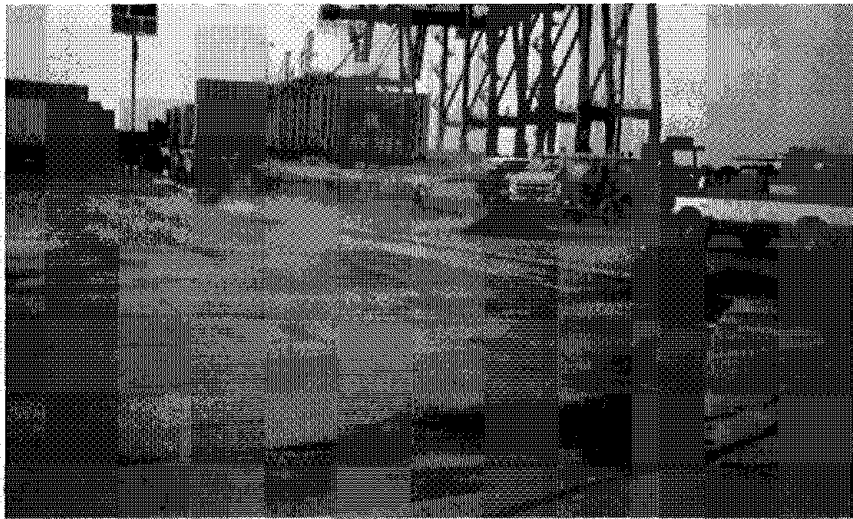


Fig. 4.90: Clean up of sand ejecta at Port of Los Angeles (photo courtesy of Doug Thiessen, Port of Los Angeles)

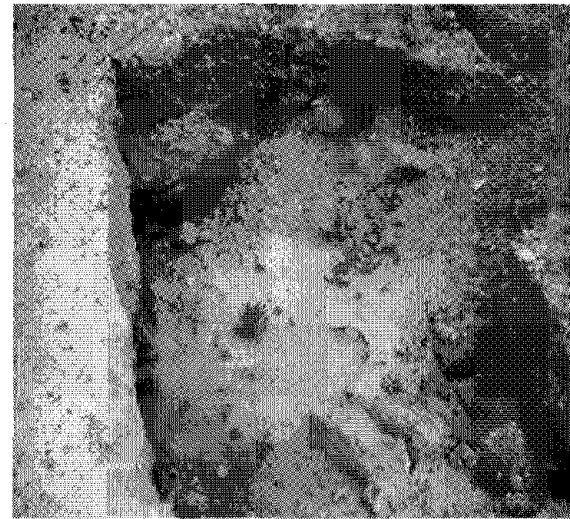


Fig. 4.91: Ground fissure and sand boil, Pier 300, Port of Los Angeles (photo courtesy of Doug Thiessen, Port of Los Angeles)

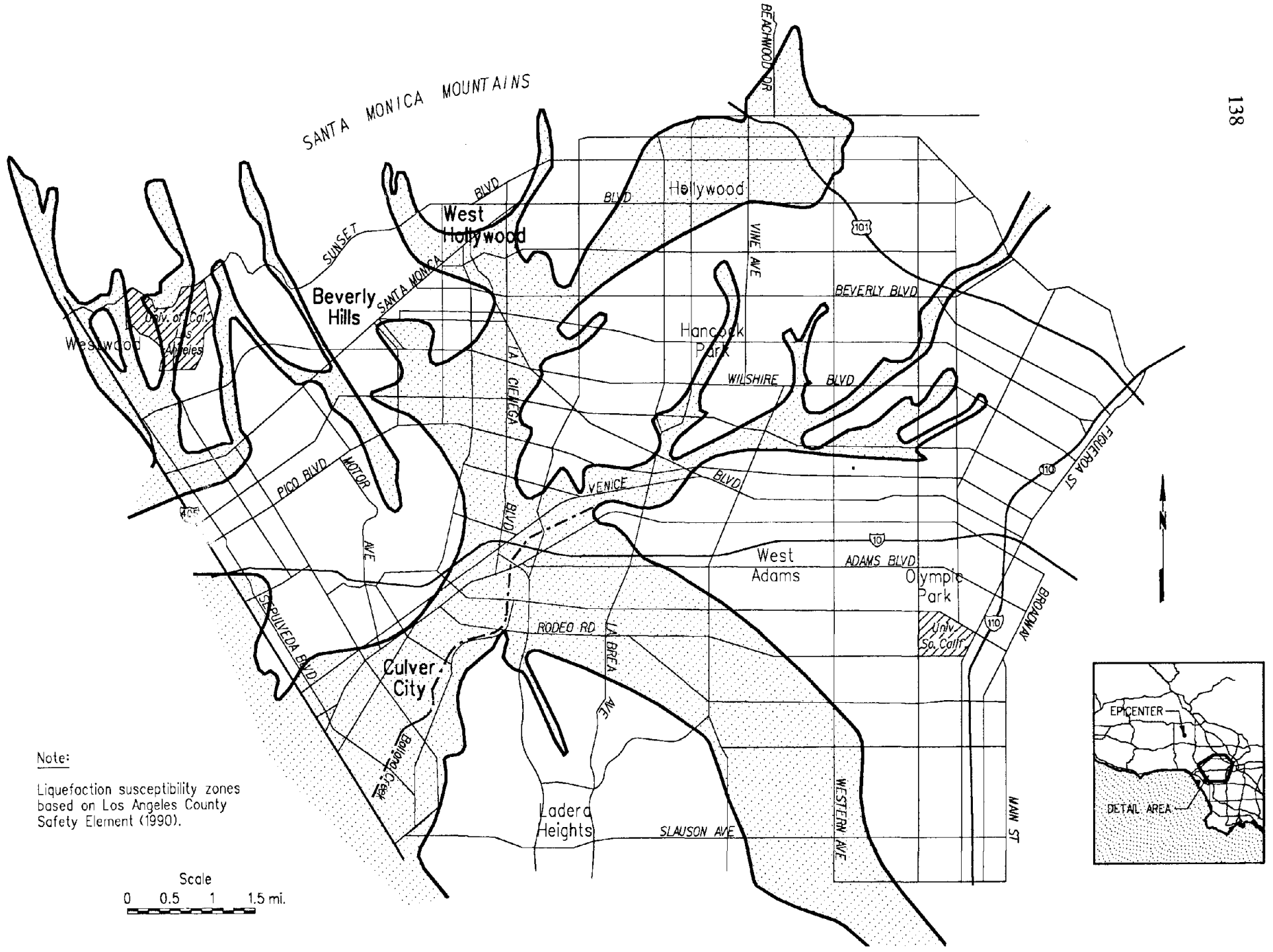
The geology of the central Los Angeles region consists of lobes of Pleistocene soil and rock materials overlain in some basin areas by fine- to coarse-grained Holocene sediments of various thickness, as shown in Figure 3.30. Areas where these Holocene soils coincide with regions of shallow groundwater (less than 30 feet below the ground surface) have been mapped as "liquefiable", and are shown in Figure 4.92 (Los Angeles County, 1990). It may be seen from Figure 4.92 that "liquefiable" zones appear to follow the pattern of a series of streams tributary to Ballona Creek, which is the only significant active stream in the area. The "liquefiable" zones shown in Figure 4.92 encompass wide portions of Hollywood, Culver City, and an area southwest of West Adams, as well as portions of West Hollywood, Beverly Hills, Hancock Park, and Westwood.

During and immediately after the Northridge Earthquake, over 450 pipe breaks occurred within the central Los Angeles region. Figure 4.93 shows the distribution of pipe breaks and leaks in the area along with the outline of mapped "liquefiable" soil zones from Figure 4.92 (City of Los Angeles, City of Beverly Hills, City of Culver City, and California American Water Company, 1994). Based on the pipe breakage patterns shown in Figure 4.93, ground failures appear to have occurred in the vicinity of La Cienega Boulevard at Interstate Highway 10 (near the collapsed highway bridge structures), at a portion of Motor Avenue south of Pico Boulevard, in the Beverly Hills-West Hollywood area southeast of Santa Monica Boulevard, in Hollywood between Sunset and Beverly Boulevards, southwest of the West Adams area, and throughout the Santa Monica Mountains north of Sunset Boulevard. It should be noted that detailed data on pipe break locations east of Western Avenue was not available for inclusion in Figure 4.93 at the time this report was prepared, but that relatively few pipe breaks or leaks were reported to have occurred in the area (City of Los Angeles, 1994).

Other than the distress to the water distribution system shown in Figure 4.93, relatively little evidence of ground failure in the central Los Angeles area was found. Reconnaissance of the area revealed very little ground or pavement cracking from settlement or lateral spreading, and no sand boils or sand fissures are known to have occurred.

Figure 4.94 shows the distribution of structural damage as indicated by red post-earthquake inspection tags along with the outline of "liquefiable" soil zones from Figure 4.92. As was discussed previously in Section 3.4.1(d), very concentrated structural damage occurred just west of West Adams along Adams Boulevard and in Hollywood along Sunset Boulevard. Significant, though less concentrated, distress also occurred in southeast Beverly Hills and south of the University of Southern California. As may be seen by comparing Figures 4.93 and 4.94, the correlation between concentrated pipe breakage and structural damage zones is very poor, suggesting that the ground failure responsible for the damage to the water distribution system likely had relatively little impact on structural damage patterns.

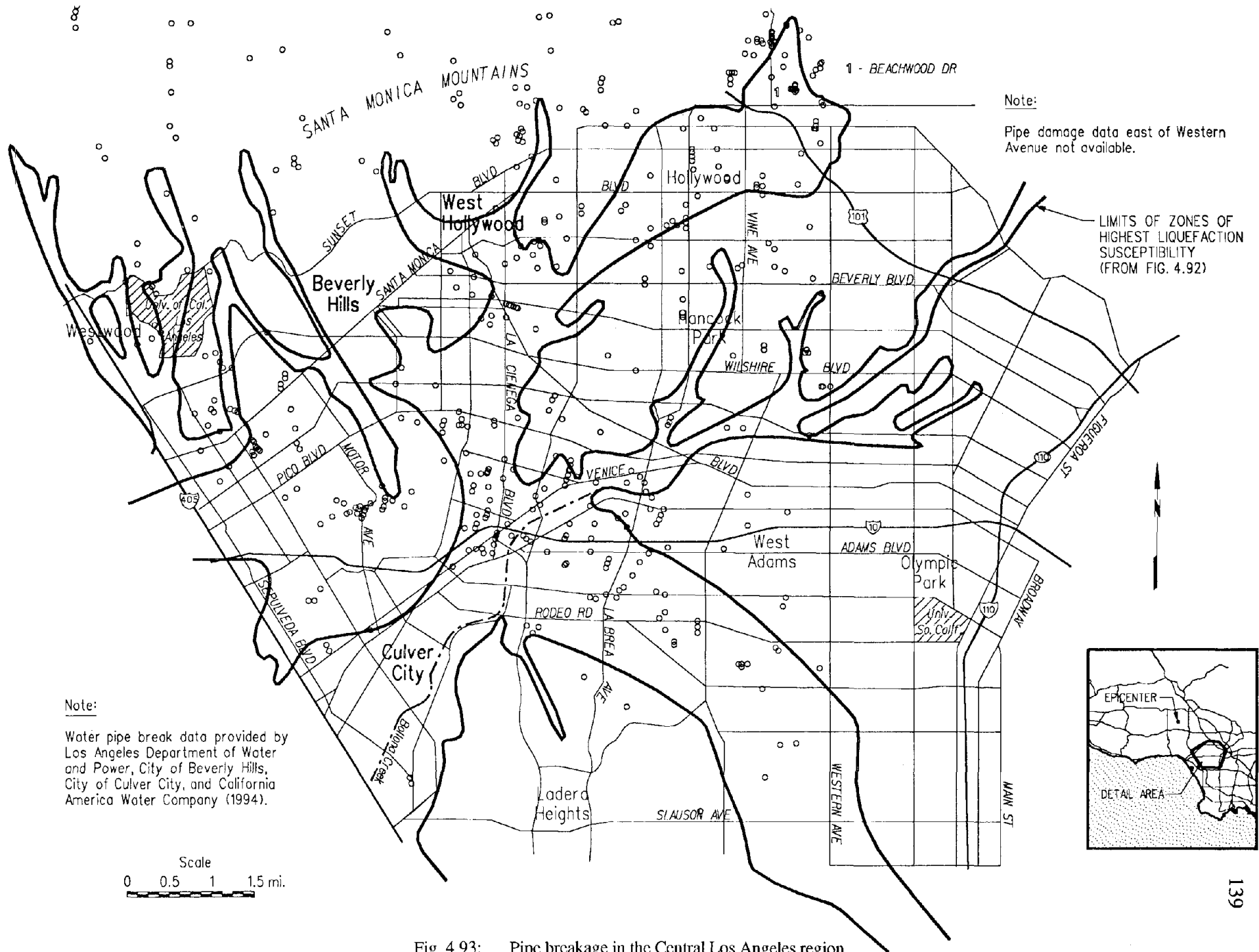
Based on available data on damage characteristics and patterns in the central Los Angeles area, ground failure generally appears to have occurred at several locations, but to have been of relatively moderate consequence to the engineered infrastructure. The occurrence of ground failure, as evidenced by concentrated patterns of pipe distress, was most typically within soil deposits mapped as "liquefiable". The soils in these ground failure zones may



Note:
 Liquefaction susceptibility zones
 based on Los Angeles County
 Safety Element (1990).

Scale
 0 0.5 1 1.5 mi.

Fig. 4.92: Map of the Central Los Angeles region showing mapped "liquefiable" zones



Note:
Pipe damage data east of Western Avenue not available.

LIMITS OF ZONES OF HIGHEST LIQUEFACTION SUSCEPTIBILITY (FROM FIG. 4.92)

Note:
Water pipe break data provided by Los Angeles Department of Water and Power, City of Beverly Hills, City of Culver City, and California America Water Company (1994).

Fig. 4.93: Pipe breakage in the Central Los Angeles region

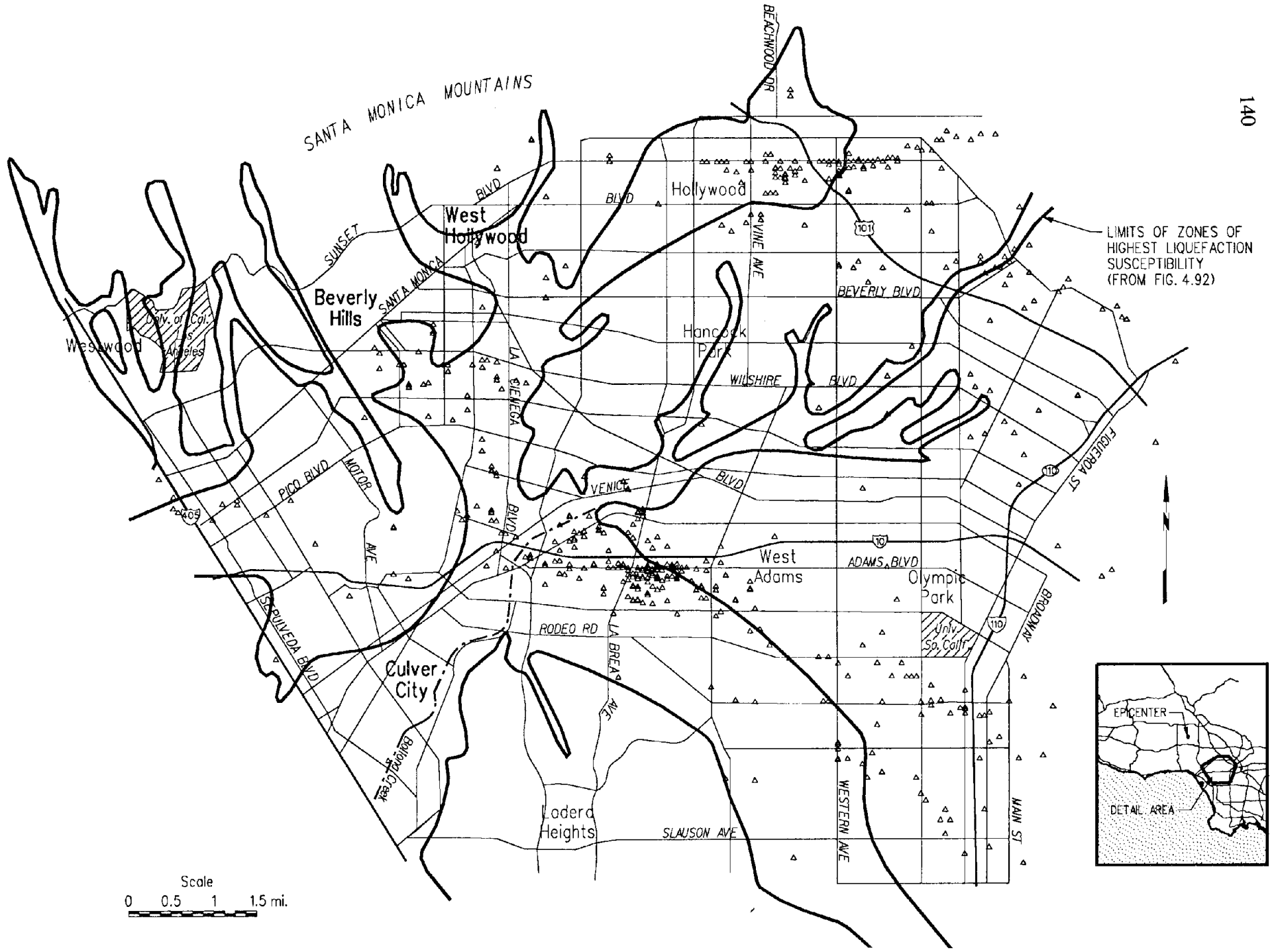


Fig. 4.94: Heavily damaged (red-tagged) structures in the Central Los Angeles region (Source: FEMA, 1994)

have experienced moderate pore pressure increase during the earthquake shaking, with subsequent drainage and re-arrangement of the soil matrix producing residual deformations. Such deformations may have been sufficiently large to rupture or crack old and brittle buried pipes, but were clearly of little consequence to the relatively ductile wood frame structures most typically found in the area. Apparently, ground failure-induced surface deformations were also of insufficient magnitude to produce significant pavement distress which could readily be attributed to the earthquake.

The only significant exceptions to the trend of concentrated pipe breakage occurring primarily within mapped "liquefiable" soil deposits occurred in the Santa Monica Mountains and at Motor Avenue south of Pico Boulevard. In the Santa Monica Mountains, most of the pipe breakage likely resulted from seismically-induced landsliding or fill movements. The damaged area at Motor Avenue occurred within shallow, Quaternary-age, marine sediments consisting of sand, pebbly sand, gravel, and silt (Dibblee, 1991). The depth to groundwater in the area is poorly established on published maps, and the area is not mapped as "liquefiable" or "potentially liquefiable" (Los Angeles County, 1990). The distressed zone is located near a minor topographic knob above a swale to the east. The series of pipe breaks immediately east of the bend in Motor Avenue are likely due to seismically-induced landsliding or fill movements above the relatively steep banks of the adjacent swale. The concentration of breaks along, and west of, Motor Avenue, occurred in relatively flat terrain and are unlikely to have been caused by landsliding in the absence of significant strength loss in the soils. The more likely culprit mechanisms for this distress include settlement and/or lateral ground deformations induced by dynamic ground compaction or liquefaction. Insufficient data is currently available to conclusively establish which, if either, of these phenomena may have occurred at this location.

4.7 Miscellaneous Topics

4.7.1 Ground Failure Effects on Deep Foundations

To date, no cases have been reported of ground failure resulting from the Northridge Earthquake causing severe distress to deep foundations such as piles or piers, although it should be noted that such distress would be intrinsically difficult to observe. At several locations, however, structural inertial forces were found to have induced permanent displacements of pile/pier caps. One such case was at the Highway 14-Interstate Highway 5 interchange, where several collapses of bridge structures occurred. This interchange is located in steep terrain with shallow bedrock. Several columns for the bridge structures were observed to have suffered residual lateral displacements in the downslope direction, as shown in Figure 4.95. These displacements are believed to have resulted from permanent distortion of the foundation elements under seismically-induced inertial forces from the bridge superstructure, and do not appear to be associated with ground failure or landsliding. It is not known to what extent these movements of the pile/pier cap may have influenced the structural collapse.



Fig. 4.95: Ground cracking and graben formation behind bridge column due to downslope movement of pile/pier cap, Highway 14 - Interstate Highway 5 interchange

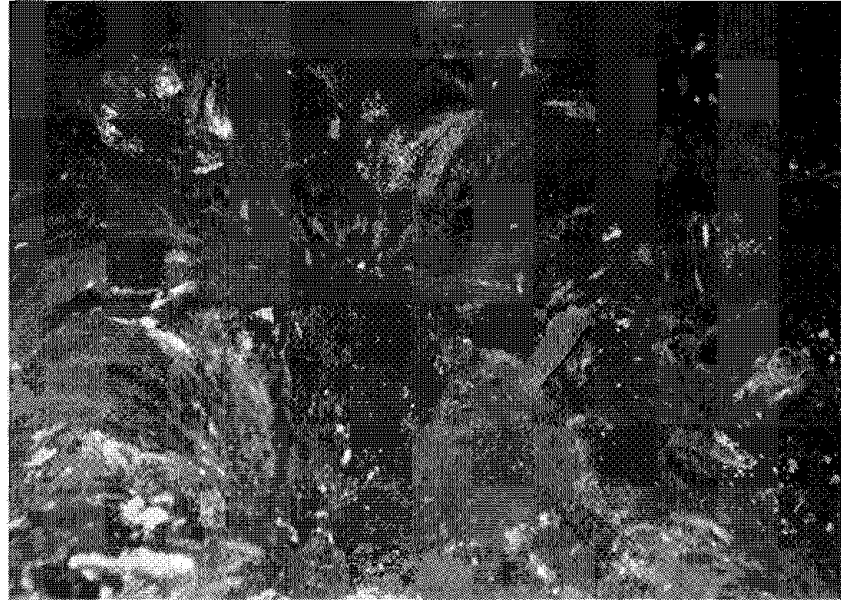


Fig. 4.96: Sand boil with salt streamers. Scale of photograph is about 2 feet across

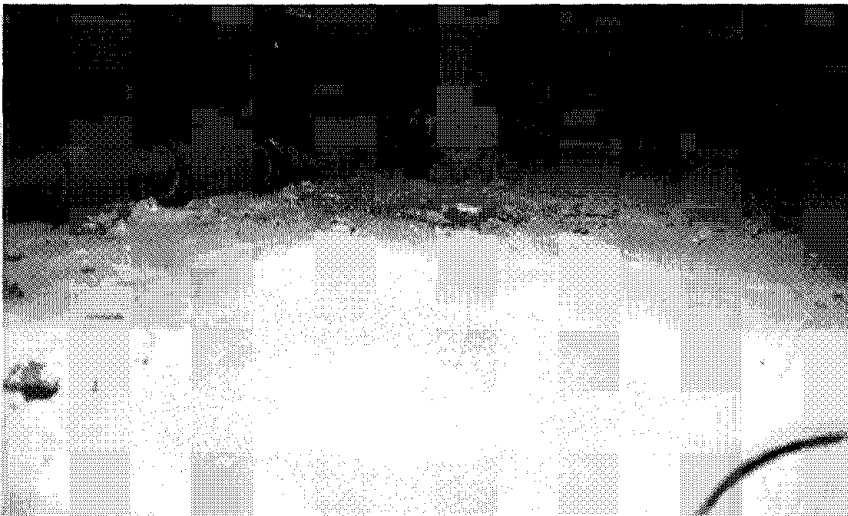


Fig. 4.97: Ejecta from sand fissure beneath residence in Woodland Hills. The ejecta at this location consisted almost exclusively of salts



Fig. 4.98: Close-up view of salt ejecta from Figure 4.97 showing coarse sand-sized particles and fine 2-inch "plaster" block. The plaster was originally found beneath the coarse material.

4.7.2 Liquefaction of Evaporite Bearing Deposits

(contributed by David J. McMahon and Terence L. Jenkins)

The presence, and potential involvement, of evaporite bearing sediments were noted in two cases of liquefaction beneath single family residences with raised foundation systems. One such residence is located between the Santa Monica and Hollywood Faults in the City of Santa Monica. The site is underlain by alluvium of late Pleistocene age (Dibblee, 1991) and appeared to have shallow groundwater. The shallow groundwater could be perched between local fault splays or above a less permeable soil horizon, or could be due to irrigation or leaks in the plumbing system. Liquefaction ejecta was found adjacent to linear fissures which may have been pre-existing shrinkage cracks or could have formed during the earthquake. The observed ejecta at the site had streamers of white evaporite crystals (Figure 4.96) which were found to have emerged from intersections of the linear ground fissures. The type of evaporite mineral(s) in the ejecta have not yet been determined. Liquefaction at this site may have been caused by earthquake-induced collapse of salt-cemented soils, although an alternate possibility is that the liquefaction could have occurred in loose sands and silts, with the evaporite deposits possibly becoming incorporated into the ejecta as it flowed along pre-existing shrinkage cracks where these mineral(s) had been previously concentrated by evaporation.

The second site where liquefaction of evaporite salts was found is in Woodland Hills and is founded on a ridge of commonly gypsiferous, diatomaceous sandstone/siltstone/claystone within the Modelo Formation. Shallow groundwater occurs in the area, likely due to a perched aquifer on relatively impermeable claystones. Liquefaction at the site was observed in the form of boils which contained a significant salt content. In one location, the ejecta was comprised almost exclusively of salts, as shown in Figure 4.97. The salt particles were generally of coarse sand-size, although a finer-grained "plaster-like" material was observed to have segregated from the coarser particles. This "plaster-like" material (shown in Figure 4.98) exhibited flow features on its surface and appeared to have dried as a result of its proximity to a hot water pipe beneath the house. In this case, liquefaction is believed to have resulted from the collapse of crystalline gypsum veins, commonly found along bedding and joints in the Modelo Formation.

Field identification of liquefaction influenced by the presence of salts can be complicated by the relatively high solubilities of the salts involved. Highly soluble salts tend to wash away due to landscape watering or rainfall. At both of the sites discussed above, the ejected salts were well preserved in sheltered areas beneath the raised foundations of the residences. At the time of the site visits several weeks after the earthquake, no signs of salt in ejecta were observed around the exteriors of either residence.

4.8 Summary

Ground failure by soil liquefaction and dynamic ground compaction occurred over a widespread area as a result of the Northridge Earthquake. Limited ground failure by these mechanisms affected sites up to approximately 35 miles south and north of the epicenter at the Port of Los Angeles and Gorman Creek, respectively. The locations at which liquefaction and/or dynamic ground compaction occurred can generally be grouped by dividing the affected region into five zones as follows:

1. The San Fernando Valley: Liquefaction and ground compaction occurred over large portions of the San Fernando Valley in the southwestern valley communities of Northridge-Reseda-Canoga Park, north of the epicenter in Granada Hills, near the foot of the Santa Monica Mountains in Sherman Oaks, in the City of San Fernando, within the Van Norman Complex, and in the lake bed behind Hansen Dam. Soil conditions at these sites typically consist of Holocene, fine- to coarse-grained alluvial or dune deposits. The groundwater was generally believed to be located at relatively shallow depths (less than 30 feet) in the affected areas, with a significant exception being Granada Hills where the phreatic surface is much deeper. The mode of ground failure in some of these areas appeared to have been liquefaction or partial liquefaction of shallow soils, though in several cases, full or partial liquefaction of soils at depth may have led to "blocky" movements of unsaturated and relatively intact overlying surficial soils. In Granada Hills, dynamic ground compaction of relatively loose, unsaturated, near-surface sandy materials also may have contributed to the observed ground failure. Damage resulting from both liquefaction and dynamic ground compaction primarily consisted of pipe breakage and pavement distress. However, at several locations including the City of San Fernando and Granada Hills, liquefaction-induced settlement and lateral spreading may have contributed to localized structural distress patterns.
2. Simi Valley: Liquefaction and partial liquefaction of alluvial and stream channel deposits occurred within the strongly shaken eastern portion of Simi Valley. The resulting lateral spreading and settlement damaged underground utilities and surface pavements, but appears to have had relatively little impact on structural distress patterns. In the central Simi Valley area, soil liquefaction at depth and/or dynamic ground compaction appears to have occurred in sandy alluvial fan deposits south of Tapo Canyon, resulting in moderate damage to utility pipes.
3. Santa Clara River Area: Liquefaction and dynamic ground compaction occurred at several locations near the Santa Clara River including Potrero Canyon, Santa Clarita, and numerous riverbank areas between Santa Clarita and Fillmore. With the exception of Santa Clarita, damage resulting from ground failure was limited by relatively sparse development in these areas. Within Santa Clarita, however, ground failure in several developed basin and canyon areas appears to have caused significant pipe breakage and pavement distress. In some cases, it appears these occurrences of ground failure also contributed to structural damage patterns.

4. Coastal Areas: Liquefaction occurred at several coastal areas including Santa Monica, Marina del Rey, Redondo Beach, and the Port of Los Angeles. Site conditions in most of these areas generally consisted of natural dune sands, lagoonal deposits inboard of the beach faces, or loose, artificial sandy fills. Very little damage resulted from liquefaction in the Santa Monica-Marina del Rey areas. In Redondo Beach, however, liquefaction-induced lateral spreading within saturated sandy fills resulted in fairly costly damage to a mole facility. Liquefaction of poorly compacted sandy fills also occurred at the Port of Los Angeles, although the consequent damage was relatively inexpensive to repair.
5. Central Los Angeles: Ground failure potentially due to partial soil liquefaction of Holocene alluvial and dune deposits resulted in widespread distress to buried utility pipes. However, there is little evidence to suggest that ground failure significantly damaged other components of the infrastructure such as pavements and structures. The widespread structural distress in the area has generally been attributed to the effects of local geologic conditions on ground motions such as soil amplification and deep basin effects.

A number of important observations can be made regarding the occurrence of ground failure resulting from the Northridge Earthquake, namely:

- Several relatively well-defined patterns of ground failure emerged following the earthquake, and appear to consist of: (a) widespread liquefaction in strongly shaken areas characterized by Holocene sandy materials and shallow groundwater, (b) the general lack of liquefaction in areas underlain by older Pleistocene soils, and (c) damaging ground deformations due to soil liquefaction at depth, combined in some cases with near-surface dynamic ground compaction, in very strongly shaken areas with moderately deep groundwater and significant depths of Holocene materials.
- On a regional scale, damage resulting from soil liquefaction and dynamic ground compaction generally consisted of pipe breakage and pavement distress. However, in several areas such as Santa Clarita, Granada Hills, and the City of San Fernando, ground failure appears to have also contributed to patterns of regional structural distress.
- The apparent occurrence of partial soil liquefaction in many areas serves to highlight the influence of shaking duration on damage resulting from soil liquefaction. A longer duration earthquake might have caused full liquefaction and resultant larger ground deformations over a much broader area than what was observed following the Northridge Earthquake, and consequently induced significantly higher damage intensities in these areas.
- Data collected since the earthquake has provided evidence that cost-effective regional liquefaction microzonation techniques can provide reasonably good insight on seismic ground failure hazards. This finding is especially significant given the limited data on which the mapping for Los Angeles County was based. Liquefaction susceptibility

for the county was primarily estimated with the use of regional geologic and groundwater maps, with a general lack of relatively costly site specific data (such as penetration resistances measured by Standard Penetration or Cone Penetration Tests). However, this "simple" regional mapping effort was less than fully successful, suggesting a need to continue to refine mapping efforts of this type, possibly by means of obtaining more detailed field data (e.g. boring logs from geotechnical investigations, standard penetration resistance values, etc.)

- Ground failure by the mechanisms of soil liquefaction at depth and/or dynamic ground compaction appears to have occurred at several locations during the Northridge Earthquake. Localized differential ground deformations associated with these mechanisms have often been thought to be relatively small, and hence not to represent a significant hazard to structures or other components of the infrastructure. This reasoning was tested to some degree during the Northridge Earthquake. While surface deformations believed to have resulted from these mechanisms were typically only of moderate consequence to structures, damage to critical "lifeline" systems such as buried pipelines was often relatively severe. Hence, these mechanisms would appear to represent a potential hazard to developed areas on a regional scale, although the local hazard (i.e. to a particular residence) may be relatively modest in many cases.

In conclusion, it is clear from the observations made following the Northridge Earthquake that significant seismic ground failure hazards continue to exist in the basin and coastal areas in and around Los Angeles. These hazards can be quantified approximately on a regional scale using established microzonation techniques (Youd and Perkins, 1978), and even more reliably on a site-specific basis using well-known, simplified penetration resistance techniques (e.g. Seed, et al., 1985). Further, once sites potentially vulnerable to ground failure by liquefaction or dynamic ground compaction have been identified, the risk can be effectively mitigated at some cost. Hence, the technology exists within the earthquake engineering community to minimize the effects of ground failure from future earthquakes; what is now needed is the will on the part of policy makers to recognize and suitably address this risk.

Chapter Five: Landslides

by Gretchen A. Rau, Jorge G. Zornberg, and Nicholas Sitar

5.1 Introduction

The young and tectonically active Transverse Ranges rimming the Los Angeles Basin are characterized by high relative relief, deep dissection, and very steep slopes. In many areas, average slope gradients exceed 60-70% (Cooke, 1984). Along the coast, active uplift has produced extensive marine terrace deposits which are characterized by steeply eroded slopes along the beaches and along canyons extending inland. Given this geomorphic setting, landslides in the Los Angeles area are a relatively common phenomenon, necessitating careful planning for development and for emergency repairs after major storms and earthquakes. Most landslide damage comes with large storms. Major rainstorms in the Los Angeles region occurred in 1969, 1978, 1980, and 1992; the debris and mudflows associated with these storms caused nearly 30 fatalities and extensive damage to residential development, small businesses, and agriculture (Gath, 1992).

Historically, earthquake-induced landslides have also had a significant impact. Both the 1971 San Fernando Earthquake, and the 1991 Sierra Madre Earthquake caused hundreds of shallow surficial failures, rockfalls, small slumps, and debris slides, and reactivated several large deep-seated landslides, in the affected regions.

The Northridge Earthquake caused hundreds of scattered rockfalls and landslides throughout Los Angeles and Ventura Counties. The landslides were distributed across an area radiating approximately 25 kilometers from the epicenter, including the Simi Hills, Big Mountain, the Santa Monica, San Gabriel, and Santa Susana Mountains, and along the marine terrace bluffs in Santa Monica and the Pacific Palisades. The seismically-induced failures occurred for the most part in areas of known susceptibility to landsliding, as can be seen by comparing Figures 5.1 and 5.2. Impact of these landslides included road closures, homes damaged and destroyed, and increased susceptibility to debris flows during subsequent storms. No fatalities directly related to the landslide activity were reported. The predominant modes of failure were shattered ridges, shallow surficial slides and rockfalls, and rockslides. Figure 5.3 is an oblique view of shallow failures along a ridge in the Santa Susana Mountains. The numerous rockslides and landslides activated in the mountainous areas by the mainshock and aftershocks were visible from large distances in the form of rising dust clouds, as seen in Figure 5.4.

5.2 Marine Terrace Deposits: Santa Monica and the Pacific Palisades

The Pacific Palisades is a stretch of steep cliffs along the Pacific Coast Highway (Highway 1). The soils are poorly consolidated sediments of Cretaceous to Quaternary age, and the area has experienced intermittent and serious slope failures for many years. There are over 50 major active landslides, together with historic and pre-historic slides throughout the area. Notable landslides of the twentieth century include the Via de Los Olas (or Flagg's Restaurant) slide in 1956-58, which blocked the Pacific Coast Highway in 1958, and the

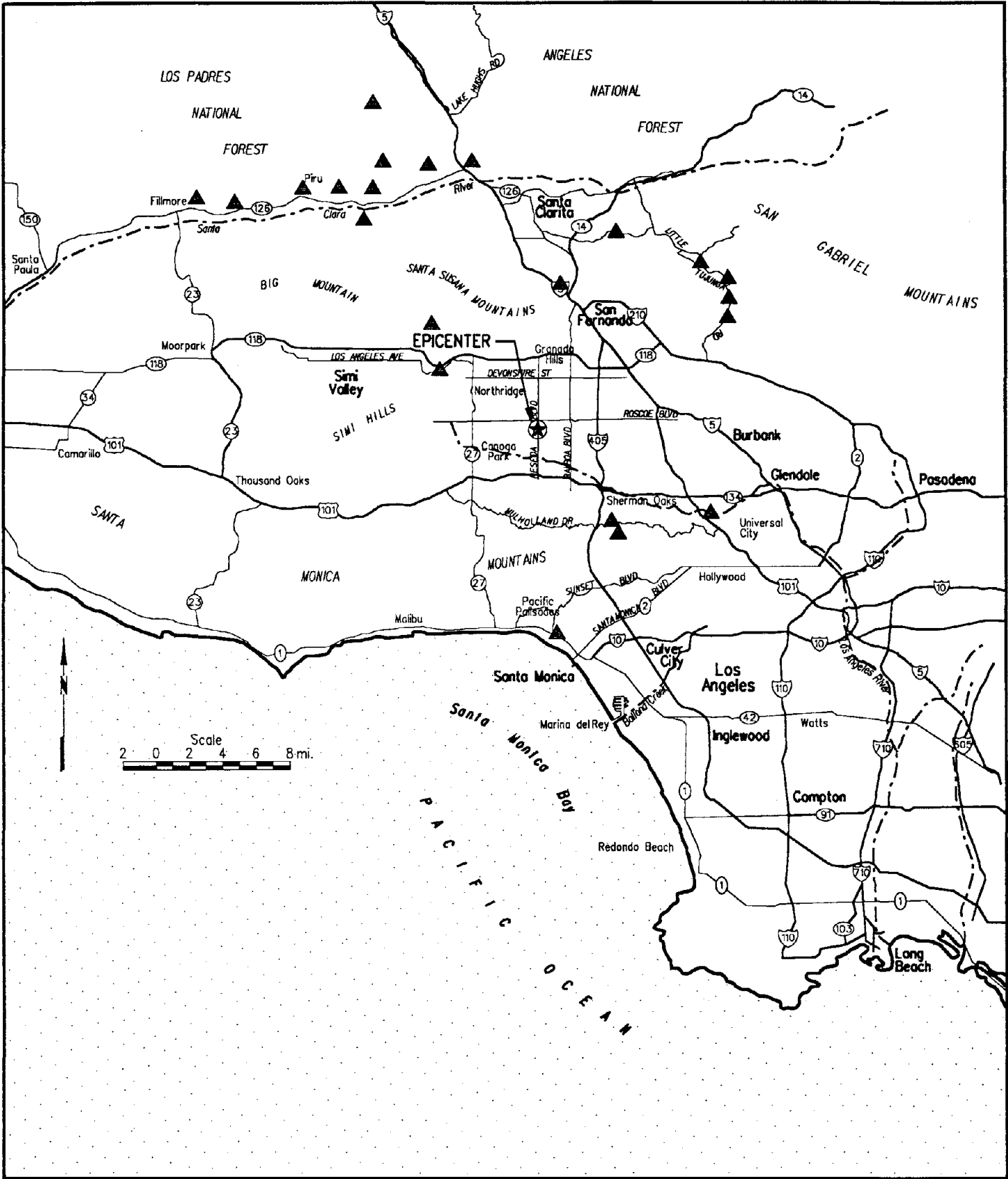


Fig. 5.1: Principle areas affected by slope instability during the Northridge Earthquake.

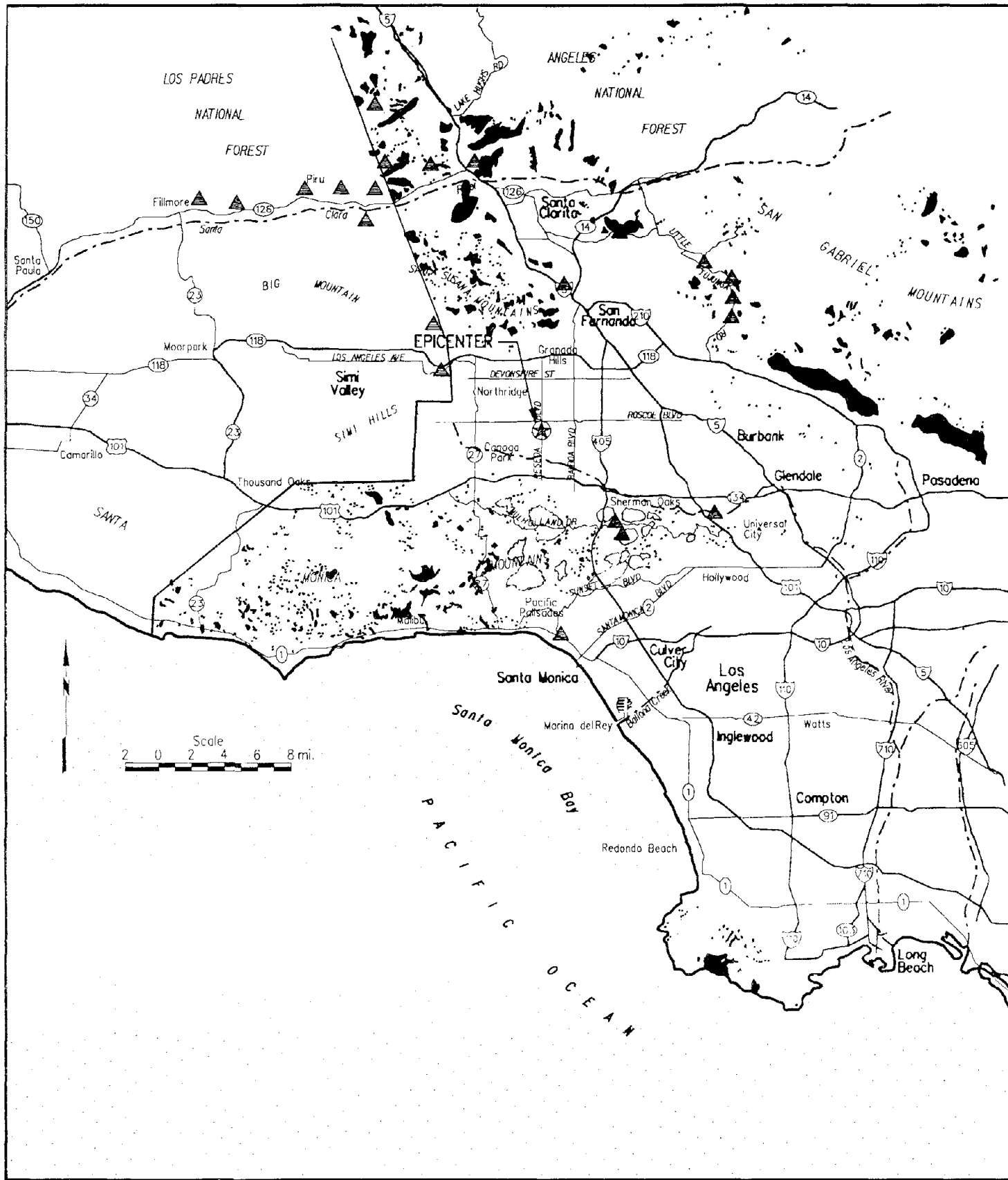


Fig. 5.2: Landslide inventory for the County of Los Angeles. Adapted from the County of Los Angeles, Department of Regional Planning, 1990.

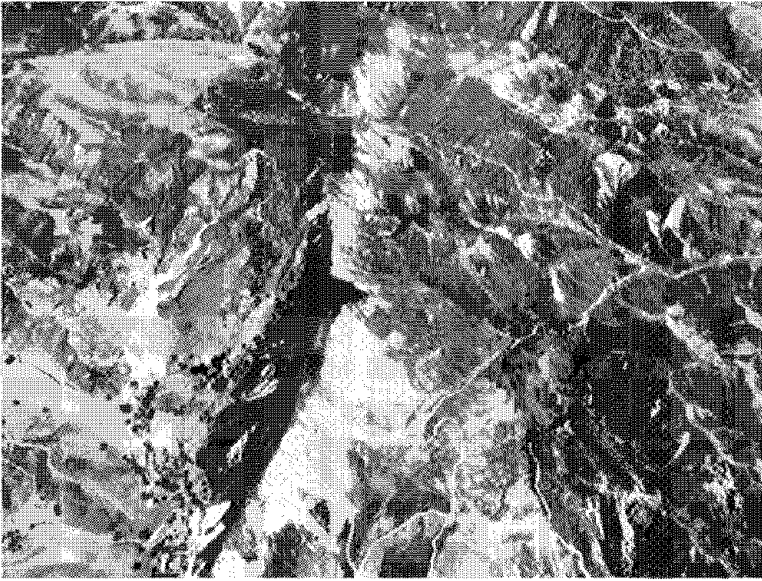


Fig. 5.3: Oblique view of shallow failures along ridgeline, Santa Susana Mountains, north of Simi Valley (photo courtesy of NASA-Ames Research Center, C-130 program)

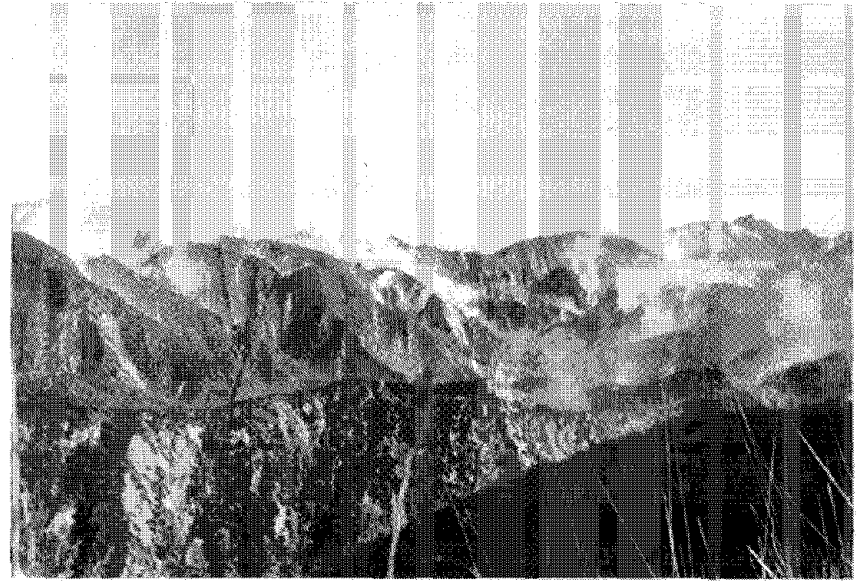


Fig. 5.4: Rising dust clouds during an aftershock. (photo courtesy of D.O. Shumway, California Division of Mines and Geology)



Fig. 5.5: Aerial view of landslide at the Pacific Palisades.

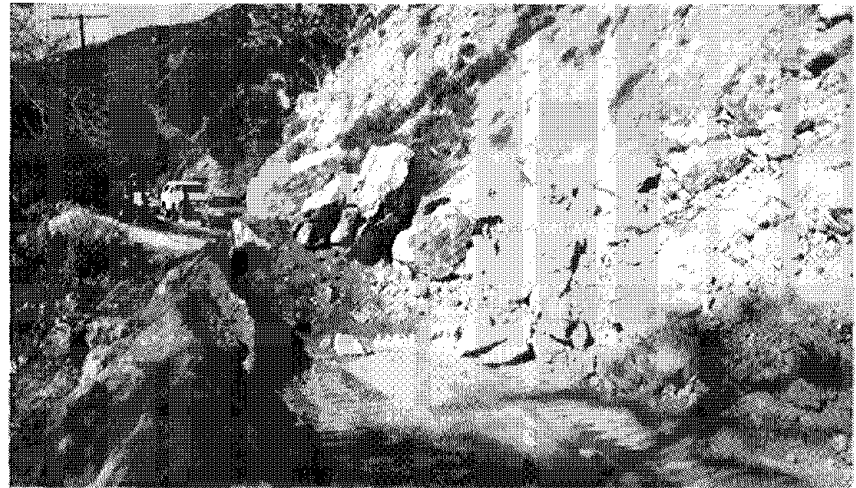


Fig. 5.6: Road closure at Dillon Divide, Little Tujunga Road. (Photo courtesy of Ray Salehpour, County of Los Angeles Department of Public Works)

slides of 1965 which caused over a million dollars in damage (Cooke, 1984).

Four large landslides, along with several smaller slides, closed the northbound lanes of the Pacific Coast Highway between Temescal Canyon Road and Chautauqua Boulevard for at least 4 days following the Northridge Earthquake. The most damaging of these landslides occurred just north of Chautauqua Boulevard on the Pacific Coast Highway (Figure 5.5). The slide carried a portion of a house down the slope, and on adjacent properties, shallow concrete piers and H-piles were observed to be hanging in mid-air near the crest of the slope. Three homes at the crest of the bluff were condemned. The bluffs consist of Quaternary age deposits of weakly cemented sand and are on the order of 120 to 200 feet in height. The slopes on which the failures occurred are moderately steep (between 45 and 60 degrees), and the failure masses tended to be only a few yards deep, subparallel to the slope, and had widths on the order of 300 feet. The slide debris was predominantly loose sand.

Clear evidence of topographic amplification of shaking was also observed in this residential development. The most severe damage to homes occurred near the crest of the bluffs, and the amount of damage decreased rapidly within one slope height of the crest. The major damage consisted of toppled chimneys, toppled appliances and water heaters, and toppled masonry garden walls.

Further south, in Santa Monica, shallow raveling occurred along steep slopes at the edge of the marine terrace above the beach and the Pacific Coast Highway. The slopes in this area are underlain by poorly sorted, poorly consolidated Quaternary fanglomerates. The slopes are approximately 150 feet high, and new tension cracks were observed as much as one half of the slope height behind the crest. In one location, a paved path along the crest was undermined, but it must be noted that similar failures have been occurring during each rainy season.

5.3 San Gabriel Mountains

Numerous earthquake-induced landslides were observed in the Angeles National Forest of the San Gabriel Mountains. Some of the slides encroached into the Little Tujunga Road, which links Interstate 210 and Highway 14. These slides had to be cleared by heavy equipment, causing the road to be closed to traffic until January 20. Road crews also reported a major rockslide along Placerita Canyon Road. Many rockslides and extensive dry raveling occurred during aftershocks.

More than ten rock slides were observed along Little Tujunga Road. One of the largest rockslides in this area occurred in a roadcut through fractured granitic rocks at Dillon Divide. The volume of debris and the large size of the fallen rocks kept the road closed for four days (Figure 5.6). Granitic rocks exposed in the roadcut are extensively jointed, forming boulder-sized blocks. About 2,000 cubic yards of debris and boulders were estimated to have been removed from this site. Once reopened, this road served as a main alternative access to Santa Clarita.

Also in the Angeles National Forest, extensive pavement cracks, indicating deformation of the road embankment, were observed along the Little Tujunga Road at Bear Canyon and Sand Canyon. These hemispherically shaped fresh cracks were up to 1-1/2 inches wide, with up to 2 inches of vertical offset. Transverse fractures extending from the middle of the road to the outboard margin were also common. These features are generally indicative of poor performance of small "wedge" fills placed to support the outboard edges of the roadways.

5.4 Santa Susana Mountains, Big Mountain, and Simi Hills

Numerous landslides occurred in the mountains north of the Simi and San Fernando Valleys. Perhaps the largest landslide caused by the Northridge Earthquake is the Del Valle landslide, shown in an aerial view in Figure 5.7, and as observed from an adjoining ridge in Figure 5.8. This landslide encompassed an area approximately one quarter of a square mile, and caused an offset of a fireroad approximately 20 feet vertically and 40 feet horizontally.

Another landslide occurring in the Ramona oil field about a mile from the Del Valle slide is shown in Figure 5.9. This landslide buried one oil well and disrupted the road access to others. The earthquake apparently triggered an incipient landslide, as tension cracks were observed around the oil well (Figure 5.10) in the days prior to the earthquake.

Large landslides also occurred at Castaic Junction, just northeast of the Interstate Highway 5/ State Highway 126W intersection, and on Interstate Highway 5, north of the Interstate Highway 5/ State Highway 14 interchange. An apparent bedding plane slip occurred just west of this interchange in the Santa Susana Mountains, causing a large offset of a fireroad. Several other rockslides and rockfalls were also noted in the Santa Susana Mountains (e.g.: Figure 5.11).

A section of the Santa Susana Pass Road, a two-lane roadway that parallels Highway 118 and connects the San Fernando Valley with Simi Valley, was closed due to slides. The road is approximately 5 miles from the epicenter and is cut into cemented sand and weak sandstone canyon walls that slope at 2H:1V and greater. Slope failures and landslides occurred both downslope and upslope of the road, and varied from 25 feet to more than 100 feet in height (Figure 5.12). Debris from upslope failures was generally large enough to block the near-slope lane of the road. Blocks as large as 5 feet in diameter were noted, and at least one of the slides appeared to be a failure along intersecting joint planes. Downslope failures created extensional cracks 10 to 30 feet away from the edge of the slope and parallel with the road. One larger slide caused vertical differential subsidence of 5 inches in the roadway and an additional 12 to 18 inches along the shoulder.

Several shallow rockslides were also observed along the hills on the north side of Highway 126 between Fillmore and Interstate 5 (Figure 5.13). At least one of these failures occurred in weathered sandstone.

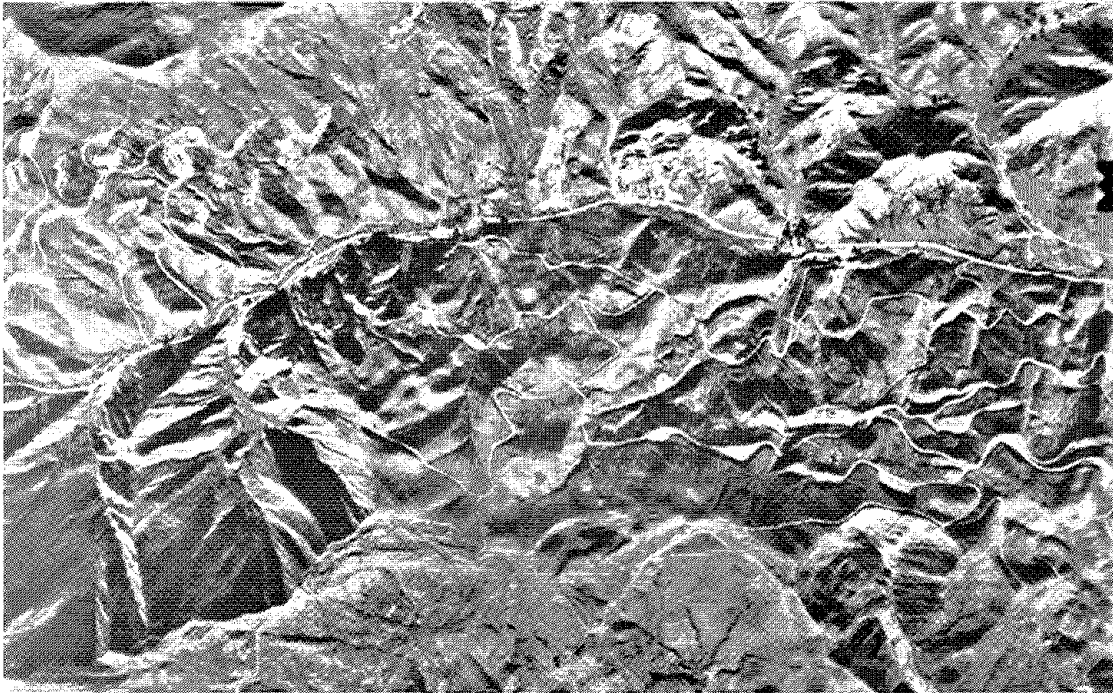


Fig. 5.7: Vertical aerial view of San Martinez Grande Canyon showing landslide at Del Valle. (photo courtesy of NASA-Ames Research Center, C-130 Program)



Fig. 5.8: View of Del Valle landslide headscarp, looking east. (Photo courtesy of T. McCrink, California Division of Mines and Geology)

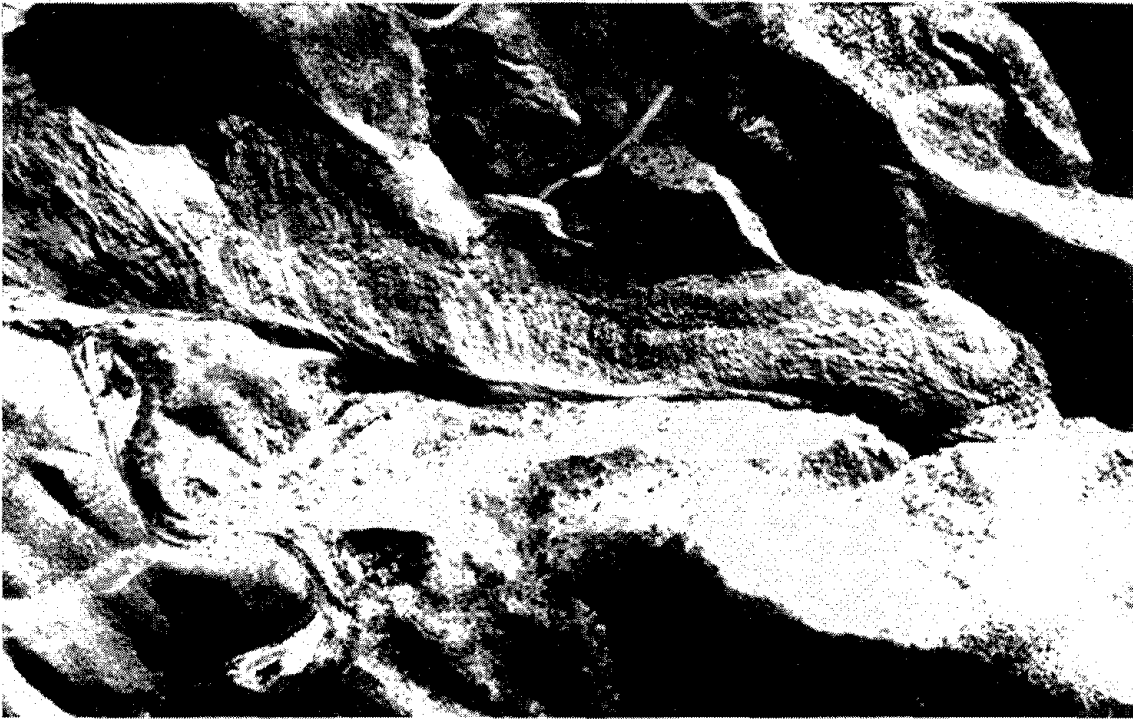


Fig. 5.9: Aerial view of landslide at Ramona Oil Field. (Photo courtesy of USAF - Beale AFB, 9th ISS)



Fig. 5.10: Oil well at headscarp of landslide at Ramona oil field. (Photo courtesy of T. McCrink, California Division of Mines and Geology)

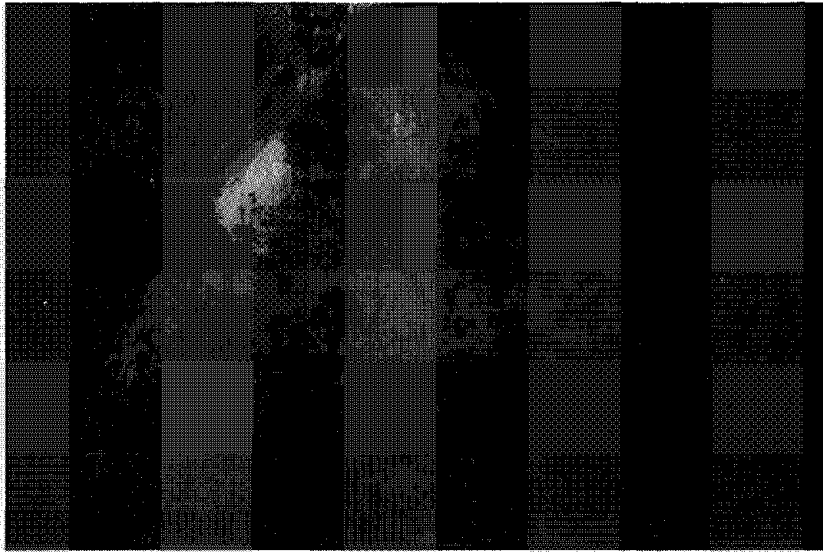


Fig. 5.11: Rockfall, Santa Susana Mountains.

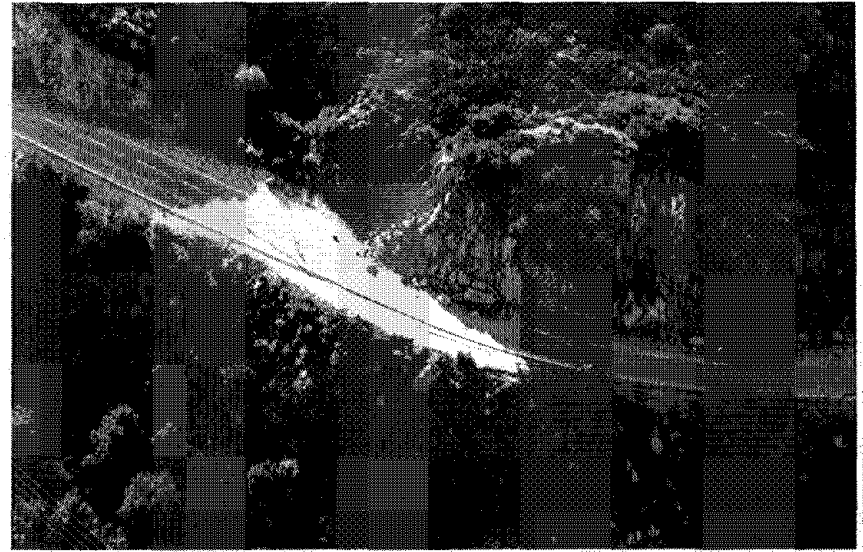


Fig. 5.12: Rockslide along Santa Susana Pass Road, near the pass.

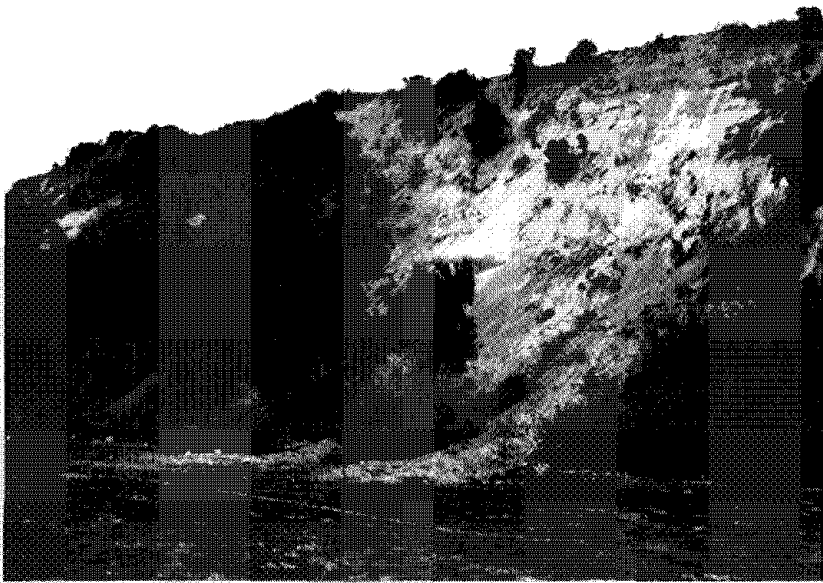


Fig. 5.13: Raveling along Highway 126, near the Santa Clara River.

5.5 Urban Los Angeles

In more populated areas, earthquake-induced landsliding was observed in Universal City, where a 24-foot high landslide occurred on Cahuenga Blvd. On Angelo Drive in Beverly Glen, fractures with horizontal and vertical movements were reported in a residential neighborhood built on a pre-existing landslide. At this point it is not clear whether the cracking represents reactivation of the landslide, or settlement of the fill overlying the landslide.

Another landslide occurred on Mulholland Drive in Sherman Oaks, approximately one mile west of Beverly Glen Blvd. Seven or eight breaks in four water mains resulted from this slide, and the road was closed temporarily. The landslide was approximately 1,200 to 1,400 feet wide, and the maximum vertical offset at the headscarp was on the order of a couple of feet. No toe or sidescarps were identified, and slope indicators installed after the earthquake showed no further movement. The slide material included the Modelo sandstone bedrock and some fill from the original construction of Mulholland Drive. Further east on Mulholland Drive, a brittle failure of shotcrete created a hazard along a slope approximately 35 feet high and a couple hundred feet long, and caused a brief road closure.

Chapter Six: Performance of Geotechnical Structures

by Jonathan P. Stewart, Leslie F. Harder, Jr., Anthony J. Augello,
Ellen M. Rathje, Jorge G. Zornberg, Alan L. Kropp, David J. McMahon,
Jonathan D. Bray, Raymond B. Seed, Nicholas Sitar, and Michael Riemer

6.1 Introduction

Numerous geotechnical structures such as dams, hillside structural fills, earth retaining structures, and solid waste landfills were strongly shaken by the Northridge Earthquake. Most of these structures performed very well, but there were several notable cases of failure and poor performance. This chapter is organized according to the type of geotechnical structure, and will present data obtained from post-earthquake reconnaissance of these structures and subsequent investigations. The performance of dams is discussed in Section 6.2, while Section 6.3 describes the failure of a tailings dam located north of the Simi Valley area. Sections 6.4 and 6.5 present the performance of hillside structural fills and earth retaining structures, respectively. Finally, Section 6.6 addresses the performance of solid-waste landfills.

6.2 Performance of Dams

6.2.1 General

There are 117 dams located within Ventura and Los Angeles counties (88 earth- and rock-fill dams, 29 concrete dams), and approximately 65 of these dams are within 25 miles of the Northridge epicenter (see Figure 6.1). Many of these structures are operated as debris dams and had little active reservoir storage at the time of the Northridge Earthquake. However, there are also a number of large dams in this area that were retaining significant reservoirs at the time of the earthquake, including Castaic, Santa Felicia, and Encino Dams.

Most of the dams in these two counties were inspected by the California Division of Safety of Dams and/or Federal inspectors within a few days after the earthquake. There were no dam failures, and with the exception of Pacoima Dam, all dams performed reasonably well. Observed damage generally consisted of limited cracking and a few shallow slides. Although some news reports on the day of the earthquake initially indicated that Santa Felicia Dam was on the brink of failure and that people downstream were being evacuated, this rumor was false. In no case was public safety considered to be in immediate jeopardy due to a possible uncontrolled reservoir release.

Several of the dams warrant further discussion despite the generally good performance of these structures. This is because of damage sustained (e.g. Pacoima Dam), their historical importance to geotechnical engineering (e.g. Lower San Fernando Dam), the need to document good behavior of major dams (e.g. Castaic Dam), and/or the fact that important strong motion data was acquired at these sites during the Northridge Earthquake. The dams which will be discussed further in the forthcoming sections are:

- Pacoima Dam
- Lower San Fernando Dam
- Upper San Fernando Dam
- Los Angeles Reservoir Dam
- Castaic Dam
- Santa Felicia Dam
- Encino Dam
- Stone Canyon Dam
- Upper Stone Canyon Dam
- Lower Franklin No. 2 Dam
- Upper Franklin Dam

6.2.2 Pacoima Dam

Pacoima Dam is a 365-foot-high variable arch concrete dam. The dam was completed in 1929 and is owned and operated by the Los Angeles County Department of Public Works to provide flood control and limited storage for ground water recharge. The dam is located in very steep terrain within the San Gabriel Mountains and was originally intended to be approximately 10 feet higher. However, the left side of the arch abuts a relatively narrow ridge of fractured gneissic granite-diorite, and not enough competent material was found to build the dam to its original design height. In order to complete the dam to its actual height, a thrust block of mass concrete was placed on the rock ridge and serves as part of the left abutment (see Figures 6.2 through 6.4).

Pacoima Dam is well known among earthquake engineers for the 1.25g peak horizontal acceleration recorded at a station on the left abutment during the 1971 San Fernando Earthquake. This record included a long period lurch or "fling" motion near the beginning of the shaking and has been used in modified forms for seismic reanalyses of many critical structures. The instrument location for this motion is on the narrow rock ridge on the left abutment just below a water tank (see Figure 6.3). There has been considerable speculation over the years regarding whether or not topographic amplification effects contributed strongly to the very high peak acceleration recorded in 1971.

During the 1971 San Fernando Earthquake, the dam experienced some distress, particularly in the form of cracking in the thrust block in the left abutment. This was attributed to a downstream movement of two blocks of rock within the left abutment and resulted in a ½ degree tilt of the seismograph on the left abutment towards the northwest (downstream). To stabilize this movement, 35 steel tendons were drilled into the left abutment and tensioned to provide additional resistance.

Pacoima Dam is located approximately 11 miles northeast of the epicenter of the 1994 Northridge Earthquake. The fault rupture propagated up towards the dam and may have extended to within 8 miles of the dam site (distance being measured from the fault rupture surface to the dam site, not from the surface projection of the rupture). This rupture propagation towards the dam may have resulted in "directionality effects" (concentration of wave energies) which may have led to increased levels of shaking at the dam site. Since

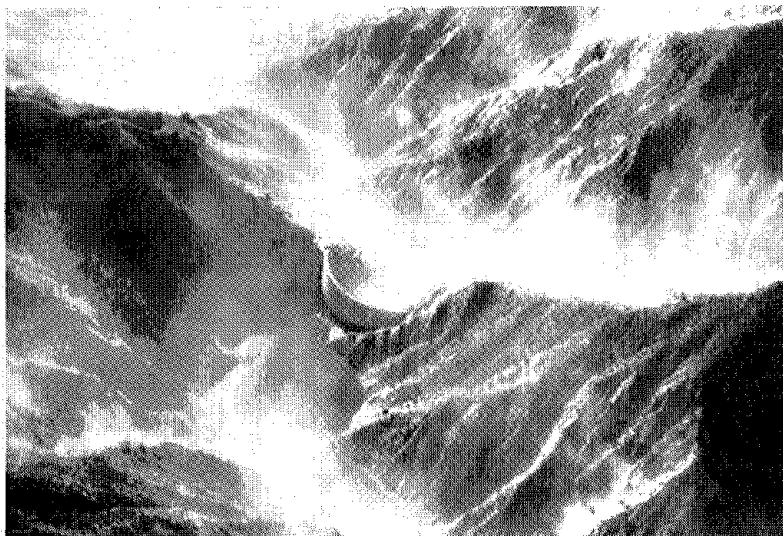


Fig. 6.2: Aerial photograph of Pacoima Dam taken January 17, 1994 (photo courtesy of U.S. Air Force)

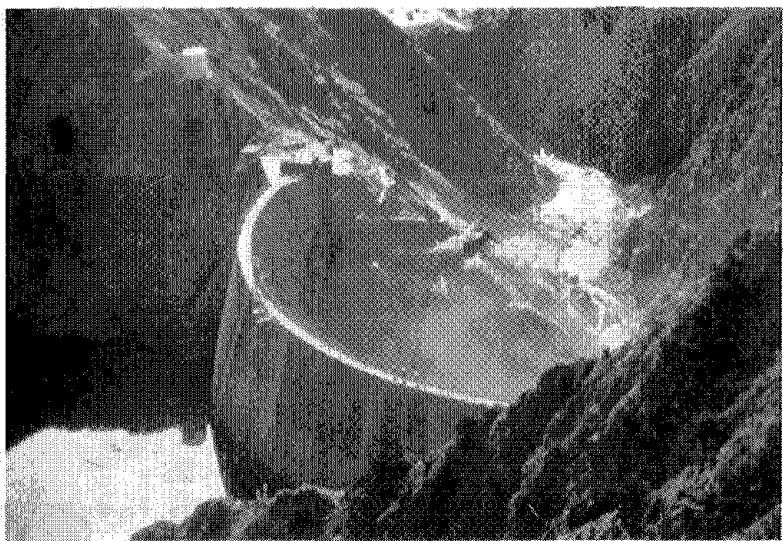


Fig. 6.3: Aerial photograph of Pacoima Dam taken January 18, 1994 (photo courtesy Lloyd Cluff, Geoscience Dept., Pacific Gas and Electric Company)

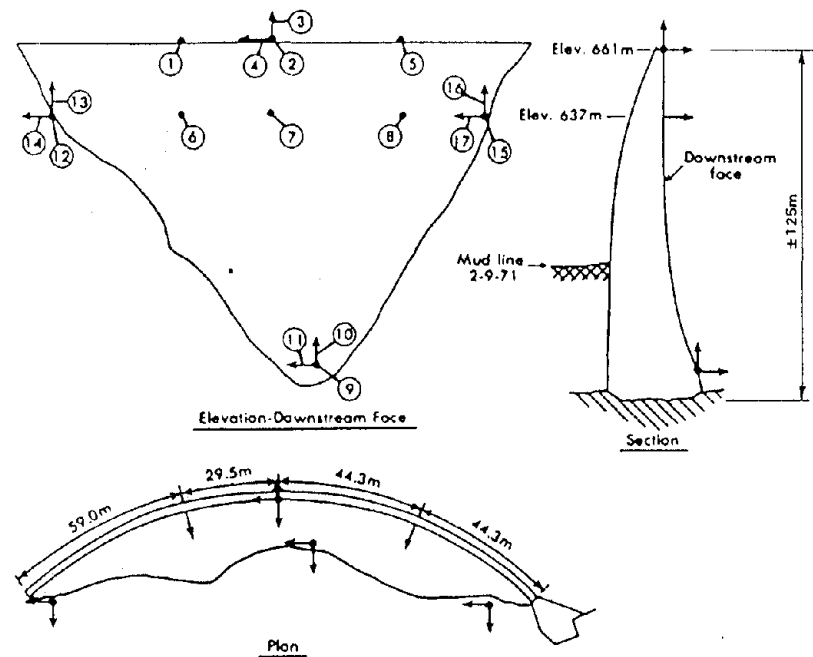


Fig. 6.4: Schematic views of Pacoima Dam (Source: California Division of Mines and Geology, 1994)

1971, several additional seismographs had been added to the dam, its foundation, and abutments (see Figure 6.4). The measured peak horizontal and vertical accelerations in the channel bottom immediately downstream of the dam were 0.44g and 0.20g, respectively. The upper left abutment seismograph recorded a peak horizontal acceleration of 1.53g and a peak vertical acceleration of 1.39g. Several accelerometers on the dam itself recorded peak accelerations in excess of 1g, with one instrument on the crest recording a peak horizontal acceleration of about 2.3g. These results showed that topographic/geometric effects strongly influenced the levels of shaking sustained at different locations.

Following the 1994 Northridge Earthquake, additional fracturing of the rock on the steep abutments developed and there were numerous rock falls. Figure 6.2 presents an aerial photograph taken a few hours after the Northridge earthquake which shows some of the dust from rock falls produced in the vicinity of the dam as a result of aftershocks. The rock falls caused significant damage to walkways (see Figure 6.5) and partially filled the spillway chute. In addition to the rock falls, many of the shotcrete-covered rock slopes in the vicinity of the dam suffered extensive fracturing and cracking. Fissures several inches in width were commonly found in the shotcrete cover, along with buckled and shattered blocks of shotcrete in some areas (see Figure 6.6). A timber tramway leading up to the top of the dam on the left abutment suffered extensive damage due to foundation movements and consequent lack of support.

The most significant damage appeared to be related to movements of the left abutment relative to the dam (see Figure 6.7). A $\frac{1}{4}$ to $\frac{1}{2}$ inch wide crack in the thrust block ran diagonally up the block to merge with the vertical joint between the block and the concrete arch (see Figures 6.8 through 6.10). In addition, there were also diagonal hairline cracks extending several feet into the concrete arch from the joint near the thrust block crack. The vertical joint also opened up and widened towards the crest of the dam. At the dam crest, the joint had opened to a width of about 2 inches (see Figure 6.11). The thrust block side of the joint was also offset about $\frac{1}{2}$ inch downstream and $\frac{3}{4}$ of an inch down relative to the concrete arch. Thus, apparently the left abutment had moved away and downstream relative to the arch. This distress and behavior was similar to what had happened following the 1971 San Fernando Earthquake, but was more severe following the 1994 event.

During both the 1971 and the 1994 earthquakes, the reservoir level was relatively low, and it is uncertain how much more damage would have been sustained had the reservoir been full. However, it is important to point out that this structure has probably been twice subjected to some of the highest peak seismic loads ever experienced by a dam. Since the Northridge earthquake, the reservoir elevation has been restricted to about $\frac{2}{3}$ the height of the dam pending the results of more thorough investigations. Surveys, crack mapping, and drilling explorations (see Figure 6.12) are being performed in order to assess the effects of the movements and to determine what remedial measures are warranted.

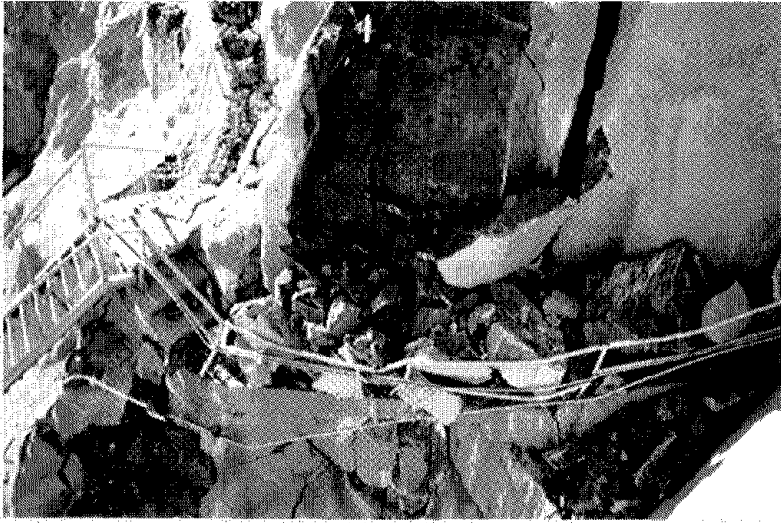


Fig. 6.5: Photograph of Pacoima Dam right abutment walkway (photo courtesy Division of Safety of Dams)

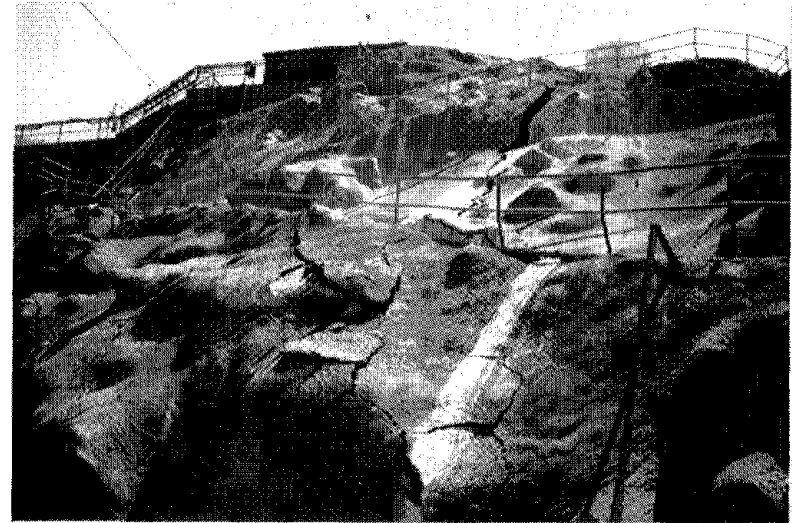


Fig. 6.6: Photograph of Pacoima Dam left abutment looking up at thrust block

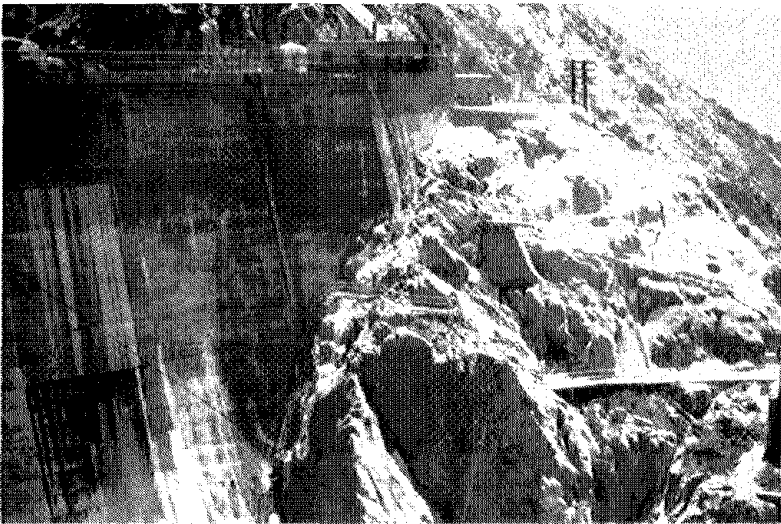


Fig. 6.7: Photograph of Pacoima Dam left abutment thrust block



Fig. 6.8: Photograph of cracking in Pacoima Dam thrust block (photo courtesy Division of Safety of Dams)

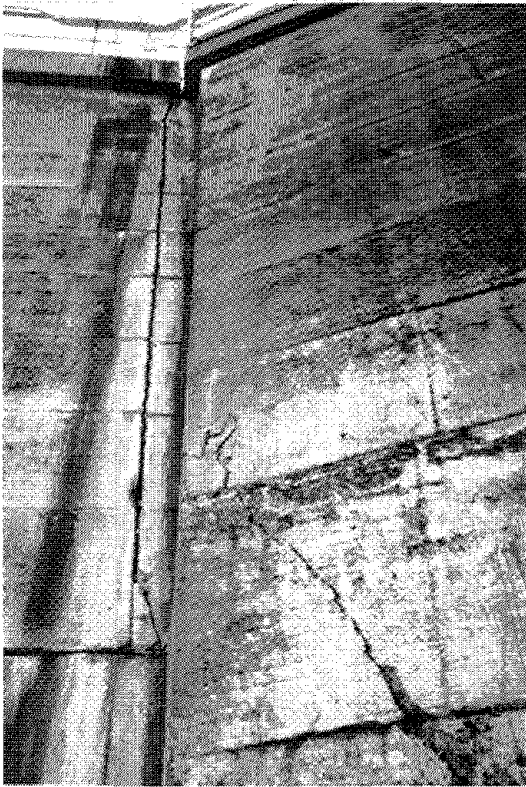


Fig. 6.9: Photograph of vertical joint between Pacoima Dam arch and left abutment thrust block



Fig. 6.10: Close-up photograph of cracking in Pacoima Dam thrust block

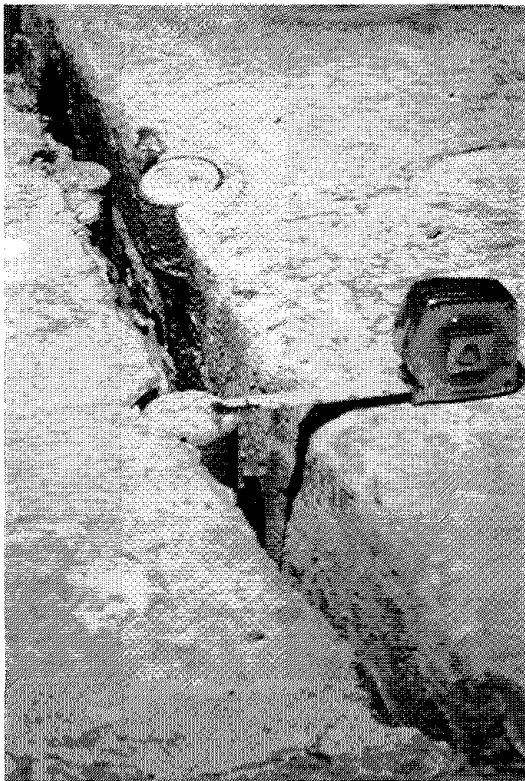


Fig. 6.11: Close-up photograph of opened thrust block vertical joint on Pacoima Dam crest

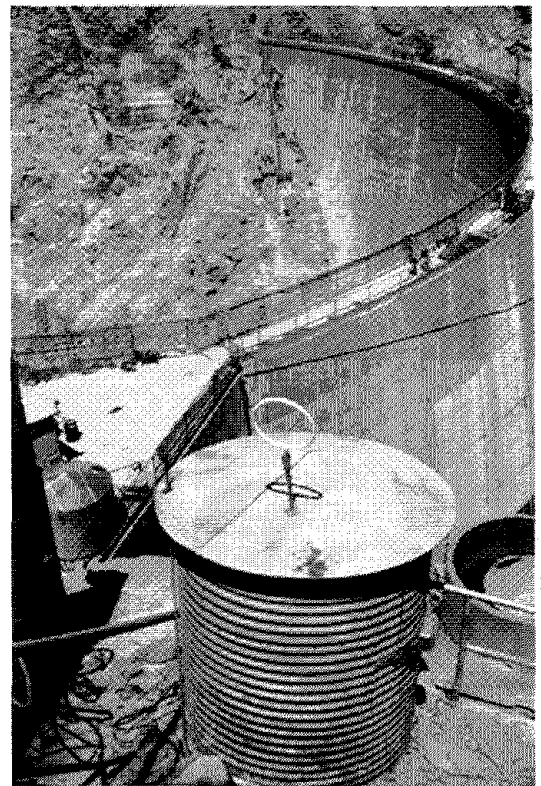


Fig. 6.12: View of Pacoima Dam from left abutment. Note seismograph in foreground and lift joint water stains on upstream slope caused by water testing in boreholes

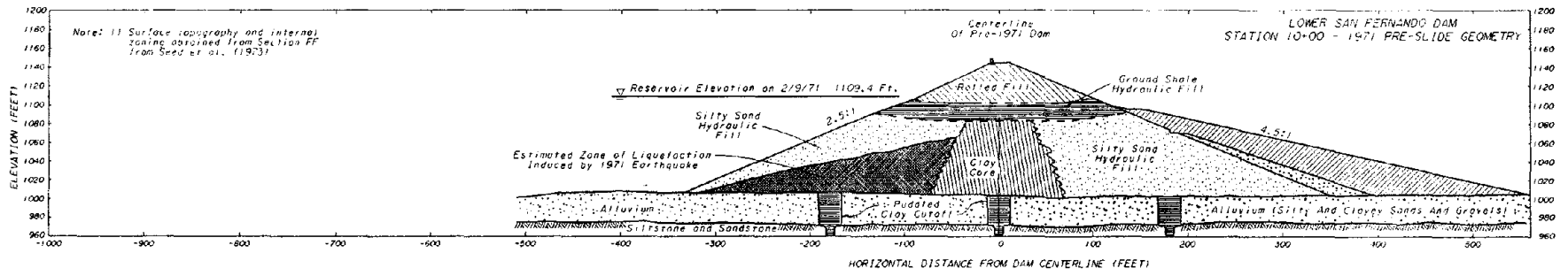
6.2.3 Lower San Fernando Dam

The performance of the Lower San Fernando Dam following the 1971 San Fernando Earthquake is one of the most important case histories in geotechnical earthquake engineering. The Lower San Fernando Dam was originally built to provide water storage for the City of Los Angeles as part of the Van Norman Reservoir Complex. A major portion of the dam was composed of sandy hydraulic fill discharged from starter dikes on the upstream and downstream edges of the embankment as it was raised. This led to a more or less symmetric fill with materials ranging from coarse sands near the outside edges, grading to a clayey core in the middle. This operation continued between 1912 and 1915. In 1916, a 10 to 15-foot thick layer of hydraulic fill containing ground-up shale was added to the initial hydraulic fill. Between 1916 and 1930, various rolled fills were added to complete the dam to a maximum height of approximately 145 feet. Between 1929 and 1930, a sloping drain zone of shale and gravel was added to the downstream face to help control seepage and increase stability. In 1940, another downstream buttress of rolled fill was added to increase stability. The dam is founded on relatively dense silty and clayey sands and gravels overlying sedimentary rock.

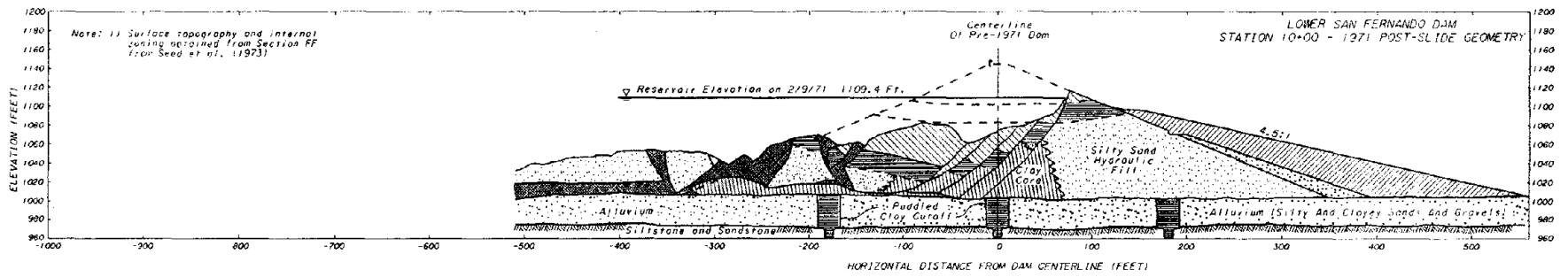
During the 1971 San Fernando Earthquake, the dam site experienced a peak ground acceleration of about 0.55g. As a result of the strong ground motions, a portion of the upstream hydraulic fill liquefied, resulting in a major upstream slide approximately 20 to 30 seconds after the earthquake. Shown in Figures 6.13(a) and 6.13(b) are cross sections of the dam at Station 10+00 before and after the slide took place. Shown in Figure 6.13(a) as a dark wedge upstream of the core is the zone of sandy hydraulic fill that was estimated by Seed et al. (1973) to have liquefied. As a result of the liquefaction, intact blocks of fill slid out into the reservoir, riding on top of the liquefied material (see Figure 6.13(b)). Following the earthquake, portions of the upstream toe of the dam were found to have slid out into the reservoir by as much as 200 feet. Several researchers have used the performance of this dam to calibrate various methods of analysis and exploration tools for use in assessing other dams. It comprises a particularly useful case history because the upstream and downstream hydraulic fill sections are only marginally different, yet one failed and the other did not.

Following the 1971 earthquake, the city of Los Angeles decided to replace both the Upper and Lower San Fernando Dams with a new dam and reservoir, Los Angeles Reservoir Dam. However, the Lower San Fernando Dam was retained in modified form to provide flood control. The modifications consisted of removing and recompacting a wedge of the slide near the center of the dam (see Figure 6.13(c)). In addition, irregular grades within the slide mass and the crest were smoothed out to provide more uniform slopes. The resulting reconstructed dam has a 60-foot wide crest and a maximum height of about 115 feet. In addition, a new outlet pipe composed of 8-foot diameter corrugated metal pipe was installed to connect the remaining portion of the old outlet pipe to an intake within a small pond upstream of the dam.

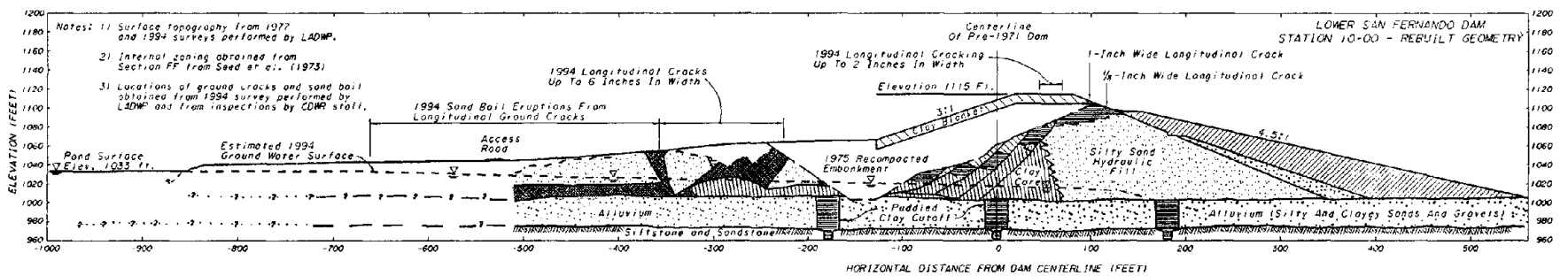
The Lower San Fernando Dam is located approximately 6 miles northeast of the epicenter of the 1994 Northridge Earthquake, and about 6 miles away from the estimated fault rupture plane. The estimated peak ground acceleration at the dam site during the 1994 event was between 0.4g and 0.6g. As a result of the shaking, the reworked slide mass liquefied again,



a) Cross section immediately before 1971 slide



b) Cross section after 1971 slide



c) 1994 cross section

Fig. 6.13: Cross sections of Lower San Fernando Dam at Station 10+00

which resulted in lateral spreading upstream towards the small pond. The lateral spreading resulted in widespread longitudinal cracking running hundreds of feet. On the dam crest, cracks were generally less than about 2 inches in width (see Figure 6.14). Upstream of the recompacted portion, longitudinal cracks had widths as much as 6 inches, together with vertical offsets of several inches (see Figure 6.15). Additional cracking further upstream towards the lower access road and pond was accompanied by numerous sediment boils (see Figures 6.16 and 6.17). These sediment boils were generally composed of silty sands. The locations of significant cracks and sediment boils were mapped by staff of the City of Los Angeles Department of Water and Power and are shown in Figure 6.18.

Monuments aligned in three rows along the dam were surveyed in January 1993 and again in April 1994. Results indicated that the crest of the dam experienced a maximum settlement of 0.66 feet near Station 10 as a result of the earthquake. The maximum horizontal movement measured was 0.57 feet upstream. This upstream movement was also recorded at Station 10, but on a separate monument on the rebuilt upstream slope and upstream of the longitudinal cracking observed on the crest.

The most serious distress sustained by the rebuilt Lower San Fernando Dam consisted of a sinkhole which developed near the right edge of the upstream cracking (see Figures 6.18 and 6.19). This sinkhole had a width (parallel to the dam axis) of 26 feet, a length (normal to the dam axis) of about 42 feet, and a maximum depth of about 13 feet. The sinkhole was later found to be centered on the corrugated metal pipe connecting the old outlet pipe to the upstream pond. The corrugated metal pipe was excavated in May 1994 and found to have sustained near complete lateral collapse, presumably due to increased lateral pressures caused by the earthquake (see Figures 6.20 and 6.21). During the excavation, additional sinkholes were discovered. Apparently, erosion caused by the water flowing through the partially collapsed pipe removed soil which entered through tears in the pipe, thus causing the sinkholes. Following the replacement of the outlet pipe and perhaps regrading of some of the cracks, the dam is expected to resume its function of providing limited flood control.

6.2.4 Upper San Fernando Dam

The Upper San Fernando Dam is an 82-foot high hydraulic fill embankment that was completed in 1921. As with the original Lower San Fernando Dam, the Upper San Fernando Dam is part of the Van Norman Complex and provided water storage for the city of Los Angeles. The majority of the dam was constructed using the "semi-hydraulic" fill method. This construction method generally consisted of placing material in dikes at the upstream and downstream toes and spreading the fill material in between by sluicing it with jets of water. As with the Lower San Fernando hydraulic fill, finer material tended to be deposited in the middle of the dam to form the core, and the coarser material remained near the outer portions of the dam to form the embankment shells. Although the original design called for adding hydraulic fill to make a dam over 100 feet high, this plan was changed part way through construction. Instead, the dam was completed only to Elevation 1200 feet using the semi-hydraulic fill method. The upper 18 feet of dam consisted of a parapet rolled fill placed on the upstream portion of the semi-hydraulic fill (see Figure 6.22).



Fig. 6.14: Photograph of 2-inch wide longitudinal crack on crest of Lower San Fernando Dam

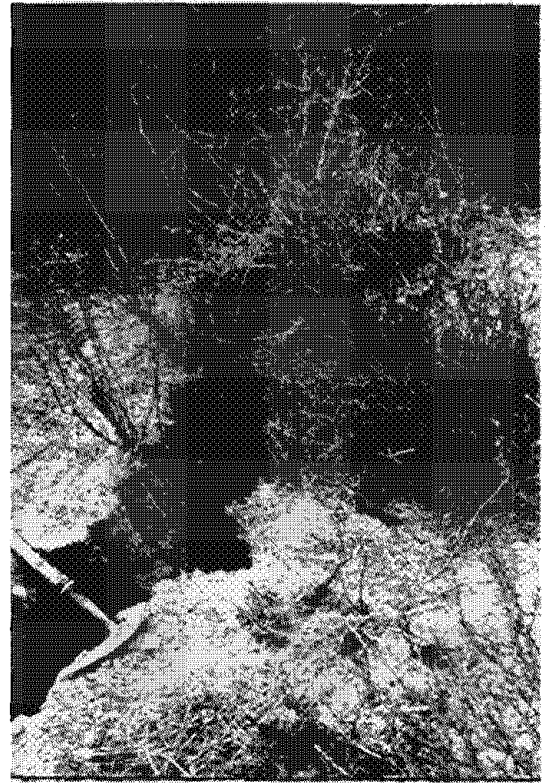


Fig. 6.15: Photograph of 6-inch wide longitudinal crack upstream of rebuilt Lower San Fernando Dam crest



Fig. 6.16: Photograph of sediment boil at Lower San Fernando Dam located on old slide downstream of lower access road



Fig. 6.17: Photograph of sediment boil at Lower San Fernando Dam on old slide upstream of lower access road

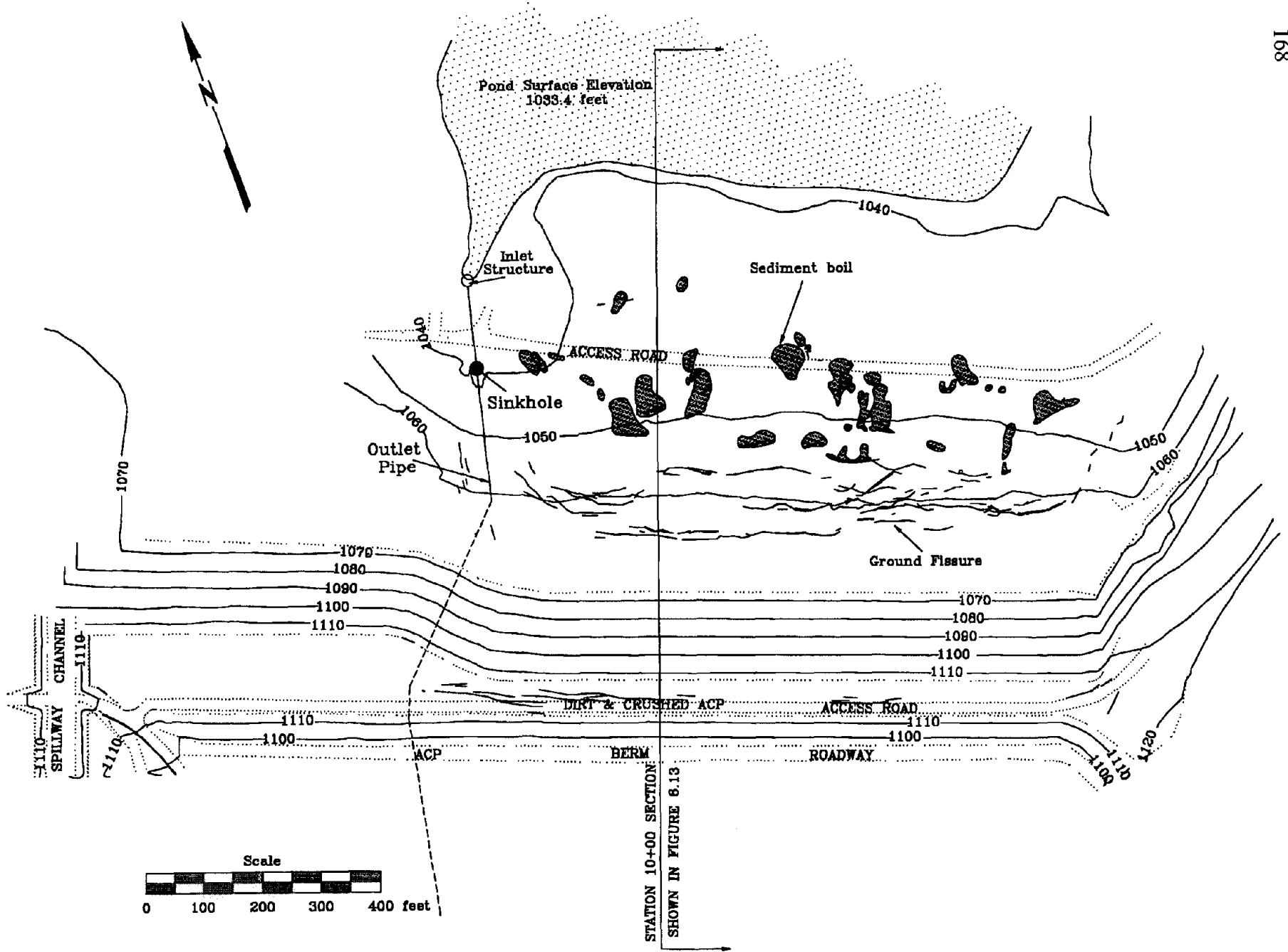


Fig. 6.18: Plan view of Lower San Fernando Dam showing locations of cracking and sediment boils (data courtesy Los Angeles Department of Water and Power)

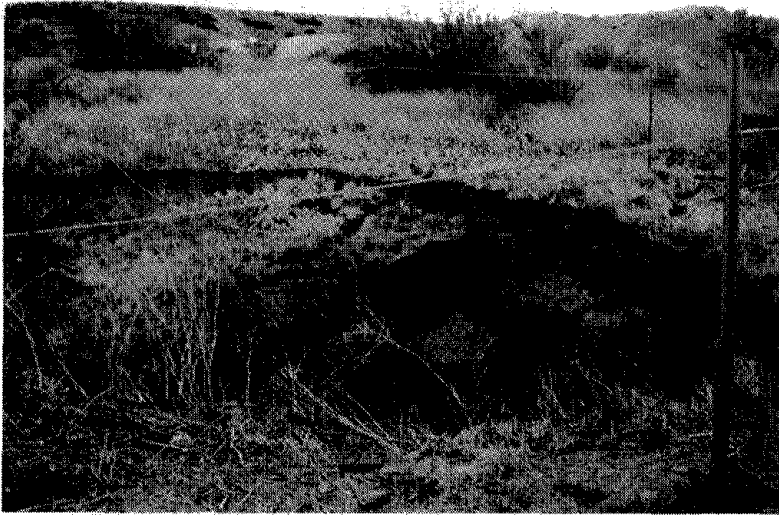


Fig. 6.19: Photograph of sinkhole at Lower San Fernando Dam

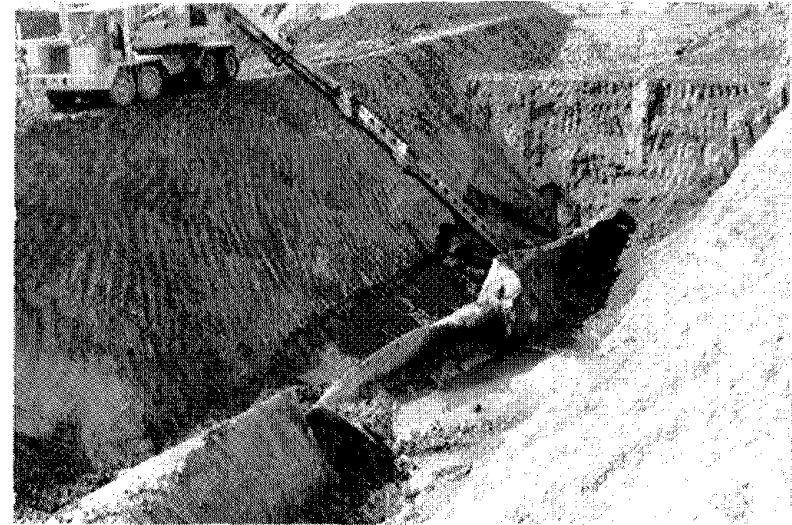


Fig. 6.20: Photograph of collapsed CMP outlet pipe at Lower San Fernando Dam

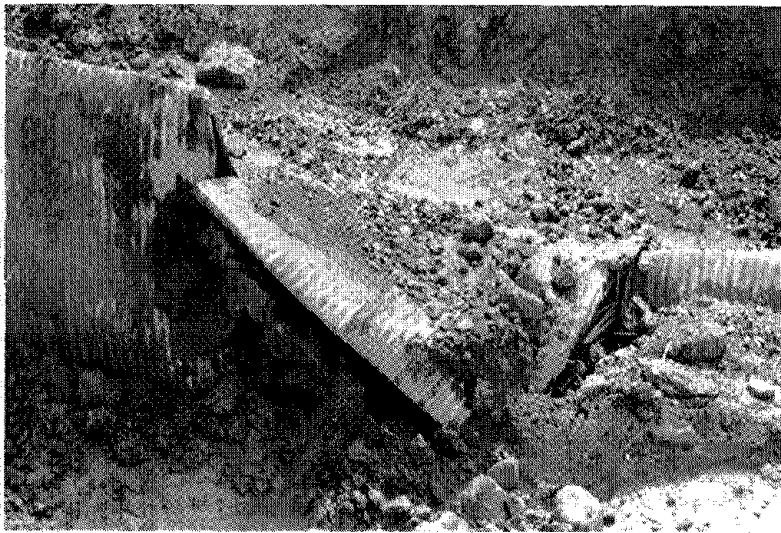


Fig. 6.21: Photograph of portion of collapsed CMP directly beneath sinkhole at Lower San Fernando Dam

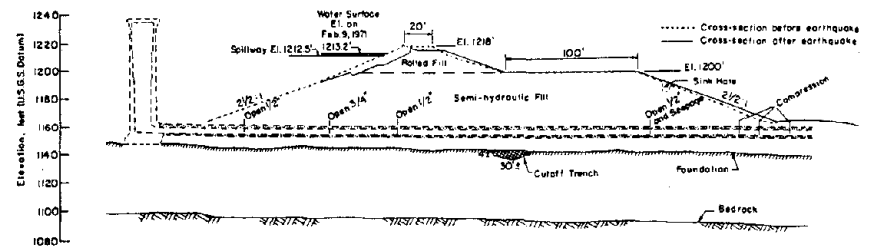


Fig. 6.22: Cross section of Upper San Fernando Dam following 1971 San Fernando Earthquake (Source: Seed, et al. 1973)

During the 1971 San Fernando Earthquake, this dam also developed liquefaction-induced distress. Although no flow slides resulted, the dam sustained significant settlements and downstream movements. The downstream movement of the dam was in the form of lateral spreading and led to the development of several longitudinal cracks along the upstream slope of the dam. According to Seed et al. (1973), the upstream cracks appeared to be multiple shear scarps. Maximum crest movements caused by the 1971 earthquake were 3.2 feet of settlement and about 5 feet of horizontal downstream movement. However, monuments along the outlet pipe on top of the semi-hydraulic fill recorded downstream horizontal movements as high as 7 feet. The lateral movements induced cracking in the concrete outlet pipe and resulted in a sinkhole within the semi-hydraulic fill above the outlet pipe (see Figure 6.22).

Following the 1971 earthquake and the construction of the new Los Angeles Reservoir Dam, the Upper San Fernando Dam received minor remediation in the form of regrading and some grouting along the outlet pipe. As with the Lower San Fernando Dam, the Upper San Fernando Dam now serves to provide limited flood control at the Van Norman Complex. In addition, the reservoir area has been diked to provide filtration ponds for the City of Los Angeles.

The Upper San Fernando Dam is located approximately 6½ miles northeast of the epicenter of the 1994 Northridge Earthquake, and about 6½ miles away from the estimated fault rupture plane. The estimated peak ground acceleration at the dam site during the 1994 event was between 0.4g and 0.6g. The shaking caused limited liquefaction, and sediment boils were observed in the dikes surrounding the filtration ponds in the old reservoir area. Sediment boils were also found near the left upstream toe of the dam near the spillway. The latter boils suggest the possibility that the base of the semi-hydraulic fill may have been saturated and liquefied again.

Post-earthquake surveys indicated that the parapet crest settled and spread laterally upstream towards the filtration ponds as a result of the shaking. Maximum crest settlement was approximately 1.4 feet, and maximum horizontal crest movement was about 0.6 feet upstream. These movements led to 2 to 3-inch wide transverse/oblique cracking near both abutments, and numerous longitudinal cracks on both the parapet and semi-hydraulic fill surfaces (see Figure 6.23). The 1994 distress is significant, but the lateral movements are much less than the damage sustained during the 1971 earthquake. This is presumably because a much lower proportion of the semi-hydraulic fill was saturated and because there was no reservoir present to provide a downstream driving force. The dam is now being investigated to assess the damage and to determine what, if any, remediation is necessary.

6.2.5 Los Angeles Reservoir Dam

The Los Angeles Reservoir Dam was completed in 1977 to replace the water storage elements of the Upper and Lower San Fernando Dams at the Van Norman Complex. The reservoir is located directly between the two San Fernando reservoirs and is in the shape of a bowl (see Figure 6.24). Two dams, the Main Dam and a northern auxiliary dam known as the North Dike, are zoned embankments founded on rock and serve to enclose the reservoir.

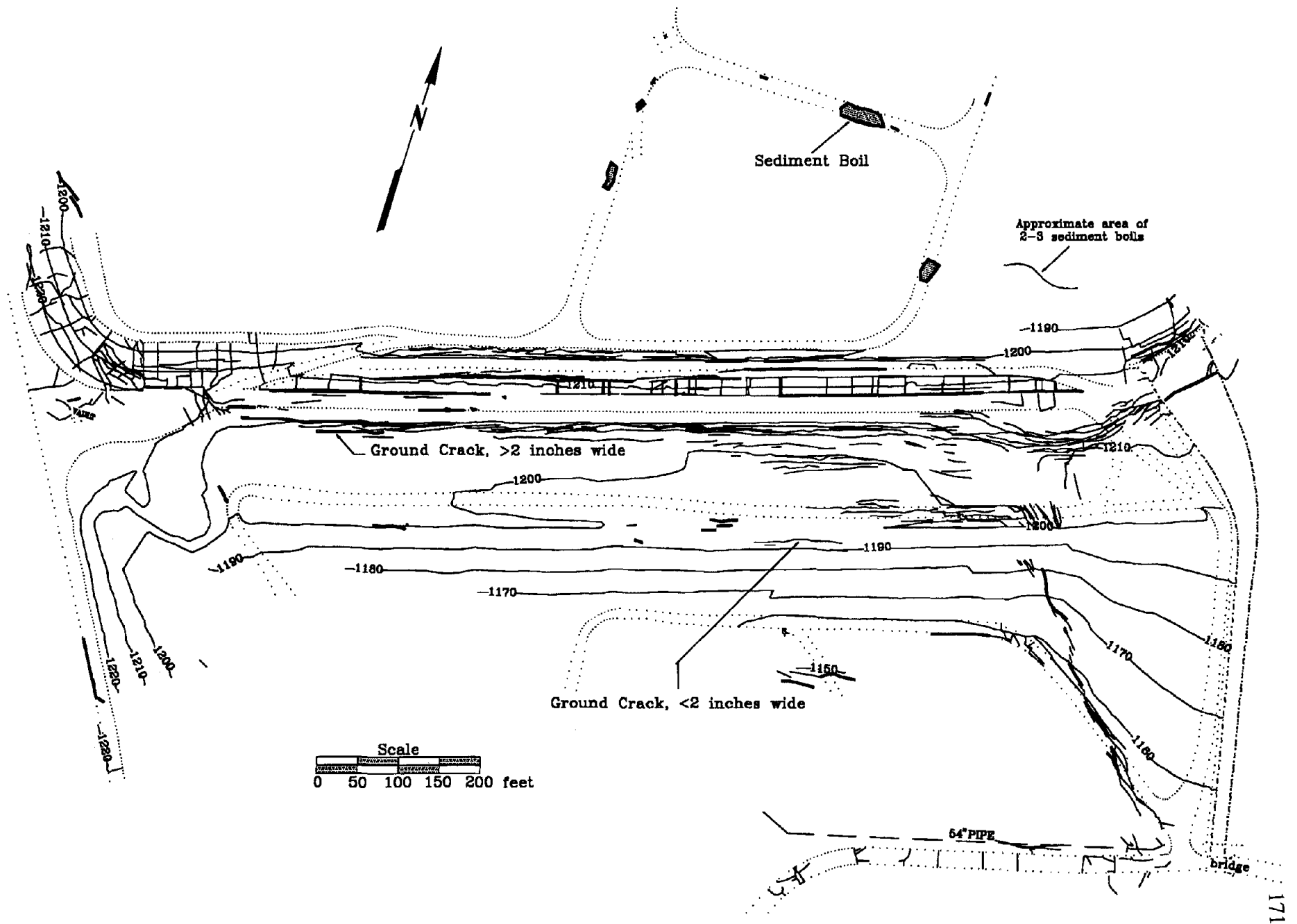


Fig. 6.23: Plan view of Upper San Fernando Dam showing locations of cracking and sediment boils (data courtesy Los Angeles Department of Water and Power)

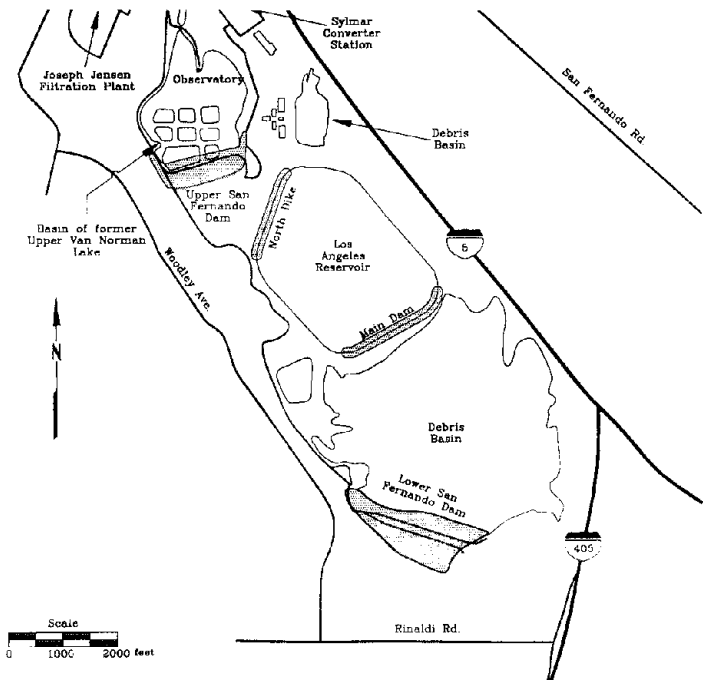


Fig. 6.24: Plan view of southern portion of Van Norman Complex



Fig. 6.25: Aerial photograph of Los Angeles Reservoir (photo courtesy Yoshi Moriwaki, Woodward-Clyde Consultants)

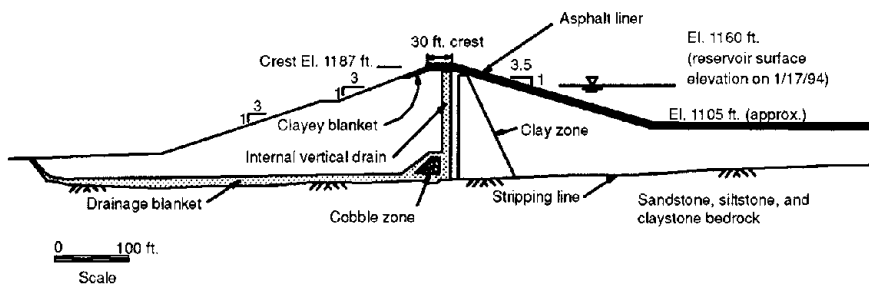


Fig. 6.26: Cross section of Los Angeles Reservoir Main Dam (data courtesy Los Angeles Department of Water and Power)

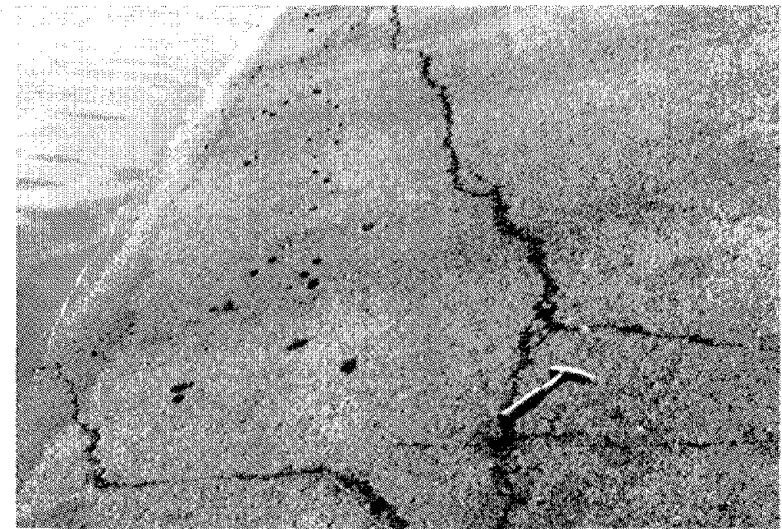


Fig. 6.27: Cracking of upstream asphalt concrete slope protection on Los Angeles Reservoir North Dike

The remaining portions of the reservoir bowl enclosure are in cut. Figure 6.25 presents an aerial photograph of Los Angeles Reservoir. The 80-foot high North Dam is in the right center of the photograph. In the background behind the outlet tower is the 130-foot high Main Dam (Note that the Upper San Fernando Dam with its filter ponds is in the right foreground). Both the Main Dam and the North Dike incorporate a compacted clay core upstream of the centerline. Downstream of the core is a vertical filter drain which connects to a horizontal blanket drain (see Figure 6.26). Seepage from the blanket drains is discharged into collection vaults where it is pumped out.

The Los Angeles Reservoir was about 27 feet below the crest of the dam when the 1994 Northridge Earthquake occurred. Preliminary results show that the seismograph on the right abutment of the Main Dam recorded a peak horizontal acceleration of 0.43g during this event. Seismographs on the crests of the Main Dam and North Dam recorded peak accelerations of 0.56g and 0.65g, respectively. In addition, a downhole seismograph at the foundation contact beneath the crest of the Main Dam recorded a peak horizontal acceleration of 0.35g.

The 1994 Northridge Earthquake induced settlements of about 3.5 inches at the Main Dam and about 1 inch at the North Dike, along with fairly extensive cracking of the upstream asphalt concrete slope protection (see Figure 6.27). The largest of these cracks was about 1-inch wide. There was also a ¼-inch wide transverse crack across the crest of the North Dike near its left abutment (see Figure 6.28). This crack extended across a 30-inch deep pre-existing utility trench and was only about a hairline in width at the bottom of the trench.

Seepage also increased after the earthquake, particularly at the North Dike. Although most drains recorded relatively small increases, the seepage flows from the west drain of the North Dike increased from 68 gallons per minute before the earthquake to 240 gallons per minute one day after the earthquake. In the weeks that followed, seepage slowly decreased back towards its pre-earthquake magnitude. Some of the piezometers downstream of the core within the North Dike also showed increased water levels for a limited time period after the earthquake, but this was interpreted to be a result of pumps within the seepage vaults shutting down and allowing seepage water to back up above the blanket drain. After new pumps were installed to pump out the vaults, the piezometric levels came back down to about their pre-earthquake levels.

The Los Angeles Reservoir has a large reinforced concrete outlet tower near the Main Dam. A seismograph within the tower recorded a peak horizontal acceleration of 1.3g. As a result of the shaking and differential movements of the tower and bridge piers, the northern end of one of the walkway spans to the tower shook loose from its restraints and displaced laterally about 16 inches on the pier.

In light of the relatively high levels of shaking, the Los Angeles Dam can be considered to have performed reasonably well. The cracking appears to be of minor significance. The staff of the Los Angeles Department of Water and Power plan to patch some of the cracks, remedy the displaced walkway of the outlet tower, and to closely monitor the seepage at the North Dike.

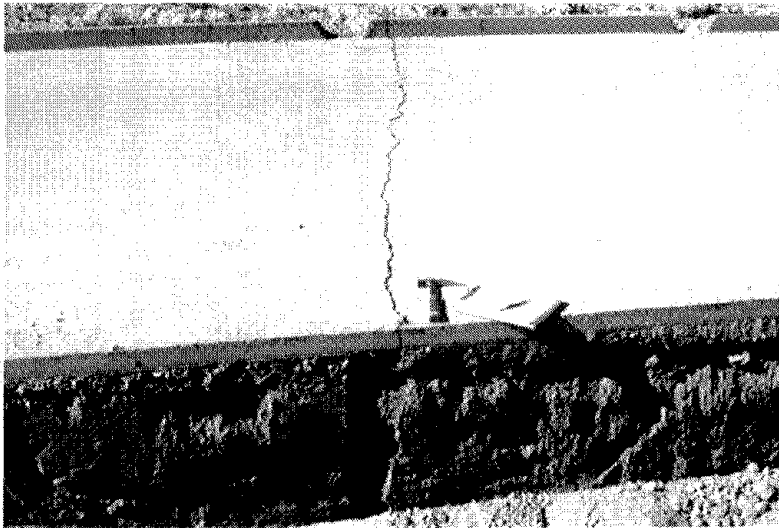


Fig. 6.28: Photograph of transverse crack on crest of Los Angeles Reservoir North Dike near its left abutment



Fig. 6.29: Photograph of Castaic Dam looking towards the right abutment

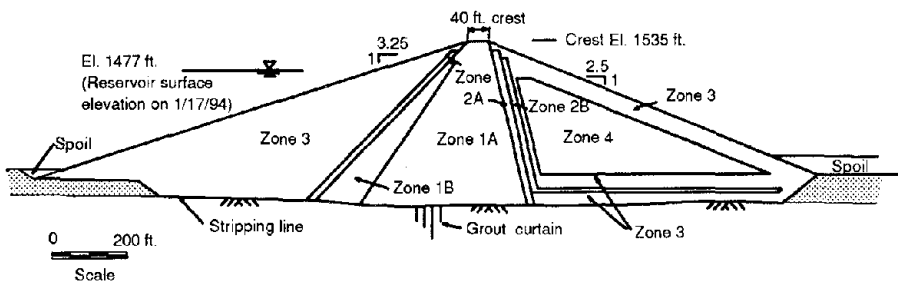


Fig. 6.30: Cross section of Castaic Dam (data courtesy of California Department of Water Resources)

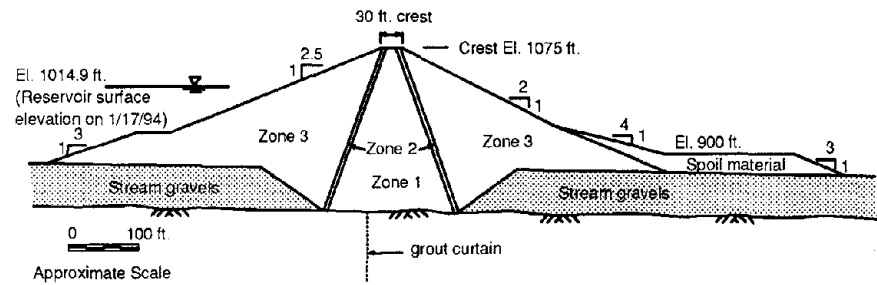


Fig. 6.31: Cross section of Santa Felicia Dam (data courtesy of United Water Conservation District)

6.2.6 Castaic Dam

Castaic Dam and Reservoir are owned and operated by the California Department of Water Resources to provide water supply as part of the State Water Project. The dam was completed in 1973 as a zoned embankment with a maximum height of 340 feet (see Figure 6.29). The dam has a central compacted clay core that is flanked by filter zones and dense gravelly shell zones (see Figure 6.30). Most of the dam is founded on sedimentary rock. However, a portion of the embankment near the left abutment is partially founded on landslide material which was not feasible to remove completely during construction.

The dam is located approximately 21 miles north of the epicenter of the 1994 Northridge Earthquake, and about 13½ miles away from the estimated fault rupture plane (see Figure 6.1). At the time of the earthquake, the reservoir surface was approximately 58 feet below crest elevation. Seismographs at the downstream toe and crest recorded peak horizontal accelerations of 0.23g and 0.35g, respectively. The dam performed well for this moderate level of shaking with the only observed distress consisting of new hairline extensions of old cracks on the crest of the dam and on its soil cement upstream slope protection.

There is also a large reinforced concrete outlet tower at Castaic Dam. A seismograph within the tower measured peak accelerations of about 0.8g in both horizontal directions. No significant damage to the tower itself was reported, although there was some limited pounding damage at the end of the bridge deck leading to the tower. However, a small crane located on the top of the tower that was used to raise and lower fish screens in front of the intakes did collapse. In addition, one of the reinforced concrete piers supporting the bridge decks providing access to the tower appears to have permanently shifted laterally towards the tower by about 3 to 4 inches, causing one of the steel bridge decks to slip off its roller bearings and fall on the edge of the bearing seats. Plans call for this deck to be jacked up and fitted with new bearings and bearing seats.

6.2.7 Santa Felicia Dam

Santa Felicia Dam impounds Lake Piru and is owned and operated by the United Water Conservation District to provide water supply. The dam was completed in 1955 as a zoned embankment with a maximum height of 213 feet. The dam has a central compacted clay core that is flanked by filter zones and densely compacted shell zones (see Figure 6.31). Most of the dam is founded on dense stream bed gravels. However, the core and filter zones were carried down to sedimentary rock.

The dam is located approximately 21 miles northwest of the epicenter of the 1994 Northridge Earthquake, and about 13½ miles away from the fault rupture (see Figure 6.1). This dam had previously sustained a peak horizontal acceleration of 0.24g at the downstream toe during the 1971 San Fernando Earthquake without experiencing any significant damage. At the time of the 1994 Northridge Earthquake, the reservoir surface was approximately 60 feet below crest elevation. Seismographs on the right abutment and on the crest recorded peak horizontal accelerations of 0.27g and 0.30g, respectively. The dam performed excellently for this moderate level of shaking. There was no sign of recent cracking

anywhere on the dam itself, including a 3-foot high masonry parapet wall on the upstream edge of the crest. However, there was a 1/8 inch wide transverse crack in fill placed to connect an access road to the crest of the dam at the left abutment.

During the day of the Northridge Earthquake and for several days later there were both television and newspaper reports stating that the safety of Santa Felicia Dam was in jeopardy and that the town of Fillmore downstream was being evacuated. These accounts were incorrect and Santa Felicia Dam appears to have performed as well as any other dam during this earthquake. It is not certain how the incorrect rumor was started. However, the water district was releasing 132 cfs through its outlet on the morning of the earthquake. It has been speculated that news media flying over in a helicopter mistook this routine discharge as a symptom of serious distress.

6.2.8 Encino Dam

Encino Dam and Reservoir are owned and operated by the Los Angeles Department of Water and Power to provide domestic water storage. Encino Dam was originally completed as a 118-foot high rolled fill in 1924. Seepage problems developed almost immediately after first filling, and a downstream filter and buttress was added to the dam between 1949 and 1950. Between 1960 and 1962, the upstream portion of the original dam was removed, the alluvium upstream was completely stripped to sedimentary rock, and rolled fill was placed upstream to create a new dam with a maximum height of 168 feet (see Figure 6.32). There are also four additional embankments or dikes to help enclose the reservoir and/or to serve as debris basins.

Encino Dam is located approximately 4.5 miles south of the epicenter of the 1994 Northridge Earthquake, and about 11 miles away from the estimated fault rupture plane (see Figure 6.1). This dam had previously sustained a peak horizontal acceleration of about 0.15g at its base during the 1971 San Fernando Earthquake without experiencing any significant damage. Preliminary results indicate that the seismograph on the left abutment measured a peak horizontal acceleration of 0.23g during the 1994 Northridge Earthquake. Similar to its previous performance, there was no significant damage observed at Encino Dam following the Northridge Earthquake. Distress observed following the 1994 event was limited to random hairline cracking on the asphalt concrete on the crest. There was also a new hairline crack in the asphalt concrete surface on the access road running up the downstream slope. This latter crack ran transversely across the road, approximately halfway up the slope. These cracks were considered minor.

6.2.9 Stone Canyon and Upper Stone Canyon Dams

Stone Canyon and Upper Stone Canyon Dams are owned and operated by the Los Angeles Department of Water and Power to provide domestic water supply. Stone Canyon Dam was originally completed in 1924 to a maximum height of 166 feet using hydraulic filling techniques. Despite the use of a 50-foot deep clay cutoff trench through the foundation alluvium, Stone Canyon Dam experienced significant seepage problems in the years following its initial construction. Between 1954 and 1956, the dam was rebuilt to a slightly larger

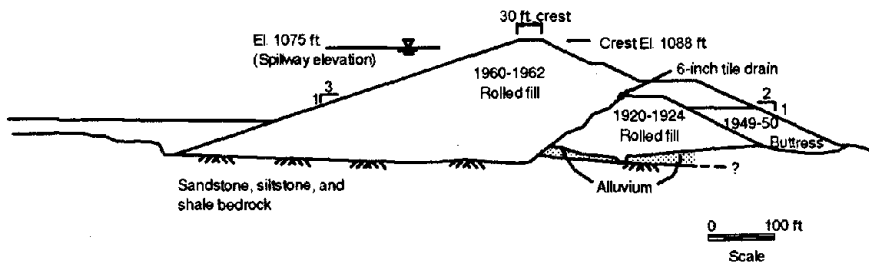


Fig. 6.32: Cross section of Encino Main Dam (data courtesy Los Angeles Department of Water and Power)

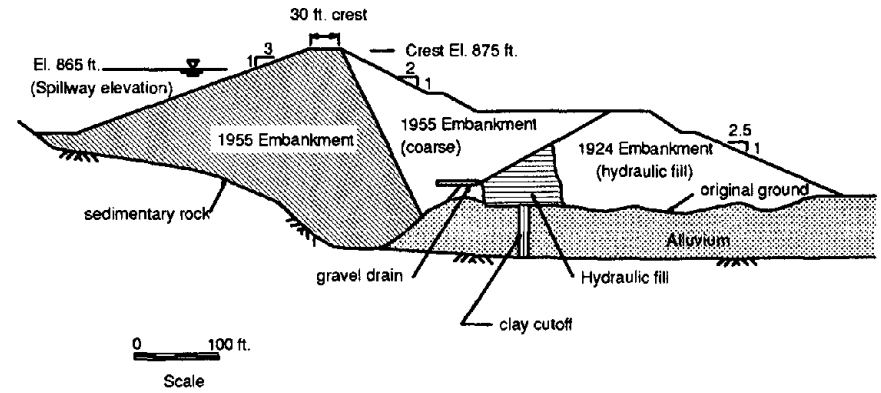


Fig. 6.33: Cross section of Stone Canyon Dam (data courtesy Los Angeles Department of Water and Power)

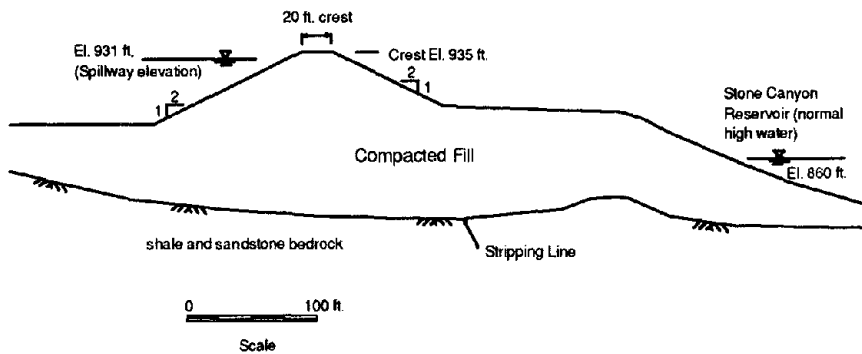


Fig. 6.34: Cross section of Upper Stone Canyon Dam (data courtesy of Los Angeles Department of Water and Power)

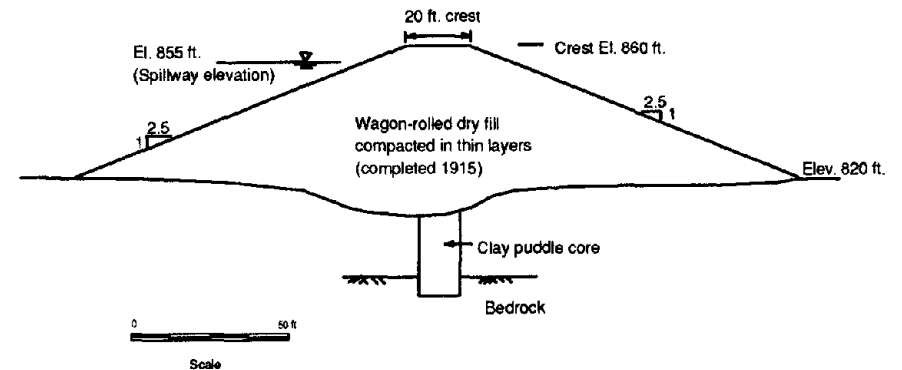


Fig. 6.35: Cross section of Upper Franklin Dam (data courtesy of Los Angeles Department of Water and Power)

height. This construction consisted of removing the upstream portion of the existing dam and overlying alluvium and then constructing a rolled fill to reach a maximum height of 185 feet. There was an attempt to place the coarser portion of the rolled fill in the downstream half of the new embankment (see Figure 6.33). The Upper Stone Canyon Dam was completed in 1954 as a homogeneous rolled fill. It is founded on sedimentary rock and has a maximum height of 111 feet (see Figure 6.34).

The Upper Stone Canyon and Stone Canyon Dams are located respectively 8 and 9 miles southeast of the epicenter of the 1994 Northridge Earthquake (see Figure 6.1). These dams have previously sustained peak horizontal ground accelerations of about 0.15g during the 1971 San Fernando Earthquake without experiencing any significant damage. Preliminary estimates indicate that these dams sustained peak horizontal ground accelerations on the order of 0.3g to 0.4g during the 1994 Northridge Earthquake. The only distress observed at these two dams were new hairline extensions of old cracks on the crests of the dams. The good performance of the downstream hydraulic fill within Stone Canyon Dam may be due to the fact that previous observations have indicated that it is not saturated downstream of the core.

6.2.10 Upper Franklin and Lower Franklin No. 2 Dams

The Upper Franklin Dam is owned and operated by the Los Angeles Department of Water and Power to regulate flow from a power plant. It has a maximum height of 50 feet and was completed in 1915 as a uniform wagon rolled fill. The dam is founded on alluvium and has a 25-foot deep clay cutoff down to rock (see Figure 6.35). Observation wells have indicated a high phreatic line within the dam.

The Lower Franklin No. 2 Dam is also owned and operated by the Los Angeles Department of Water and Power, but is used to provide domestic water supply. The dam is a homogeneous earthfill completed to a maximum height of 49 feet in 1982 as a replacement for the old Lower Franklin Dam which was constructed using hydraulic fill techniques. The Lower Franklin No. 2 Dam is founded on sedimentary rock and incorporates a vertical and horizontal internal drain.

The Upper Franklin and Lower Franklin No. 2 Dams are located respectively 10 and 11 miles southeast of the epicenter of the 1994 Northridge Earthquake (see Figure 6.1). The Upper Franklin Dam sustained a peak ground acceleration of about 0.15g during the 1971 San Fernando Earthquake and performed reasonably well. Preliminary results indicate that seismographs at the foundation and at the crest of the Lower Franklin No. 2 Dam measured peak horizontal accelerations of 0.22g and 0.42g, respectively, during the 1994 Northridge Earthquake. Both dams performed well and the only distress noted was a hairline transverse crack in the asphalt surface of the crest of Lower Franklin No. 2 Dam. This crack was located near Station 30+90 near the dam's left abutment.

6.2.11 Miscellaneous Embankment Dam Performance

There was also cracking observed in several small dams which serve to retain debris basins. These dams are generally less than 50 feet in height and the cracking was considered minor. Some of the cracking observed was along backfilled utility trenches. One small dam, Porter Estate Dam, was located about 3 miles northeast of the Northridge epicenter. Although the reservoir was empty at the time of the earthquake, the dam sustained longitudinal cracking and shallow slides with scarps up to 6 inches in height. The dam was completed in 1888 and has a maximum height of only 41 feet.

6.2.12 Summary

Several dams of various sizes were shaken by moderate to strong ground motion from the 1994 Northridge Earthquake. With the possible exception of Pacoima Dam, all dams performed reasonably well, and no significant damage was sustained to any earth dams. This continues the general good performance of earth dams noted after other recent earthquakes. However, the movements sustained at the partly saturated Upper and Lower San Fernando Dams remind us of how poorly hydraulic fills can perform during strong shaking. One of the major incidents during the 1971 earthquake was the near failure of the Lower San Fernando Dam due to liquefaction-induced upstream sliding. If that dam had failed, approximately 80,000 people would have been within the inundation zone of the resulting flood and it would in all likelihood have been the largest natural disaster in U.S. history. The City of Los Angeles appears to have learned the lessons of the 1971 San Fernando Earthquake and can take some measure of credit for replacing these and other hydraulic fill dams with more competent structures.

6.3 Failure of Tapo Canyon Tailings Dam

6.3.1 General

The only significant flow slide to occur as a result of the 1994 Northridge Earthquake involved the failure of a small tailings dam and pond in Tapo Canyon near Simi Valley. The tailings dam was approximately 80 feet high and was located approximately 13 miles from the Northridge epicenter. However, the fault rupture extended somewhat closer, to approximately 8½ miles away from the site (see Figure 6.36). The peak horizontal ground acceleration near the tailings pond was estimated to have been between 0.4g and 0.6g. As a result of the earthquake, large and relatively intact blocks of the dam slid downstream over a hundred feet, allowing the tailings to flow out through the breach and travel several hundred feet downstream. Portions of the tailings impounded behind the failed embankment ended up in an adjoining creek and flowed several thousand feet downstream within the creek channel.

Ground cracking from lateral spreading was observed in other retention embankments within Tapo Canyon as well, although no flow slides or debris release developed in these instances. In addition, sand boils were observed within retained debris at one of ponds upstream of the failed tailings pond.

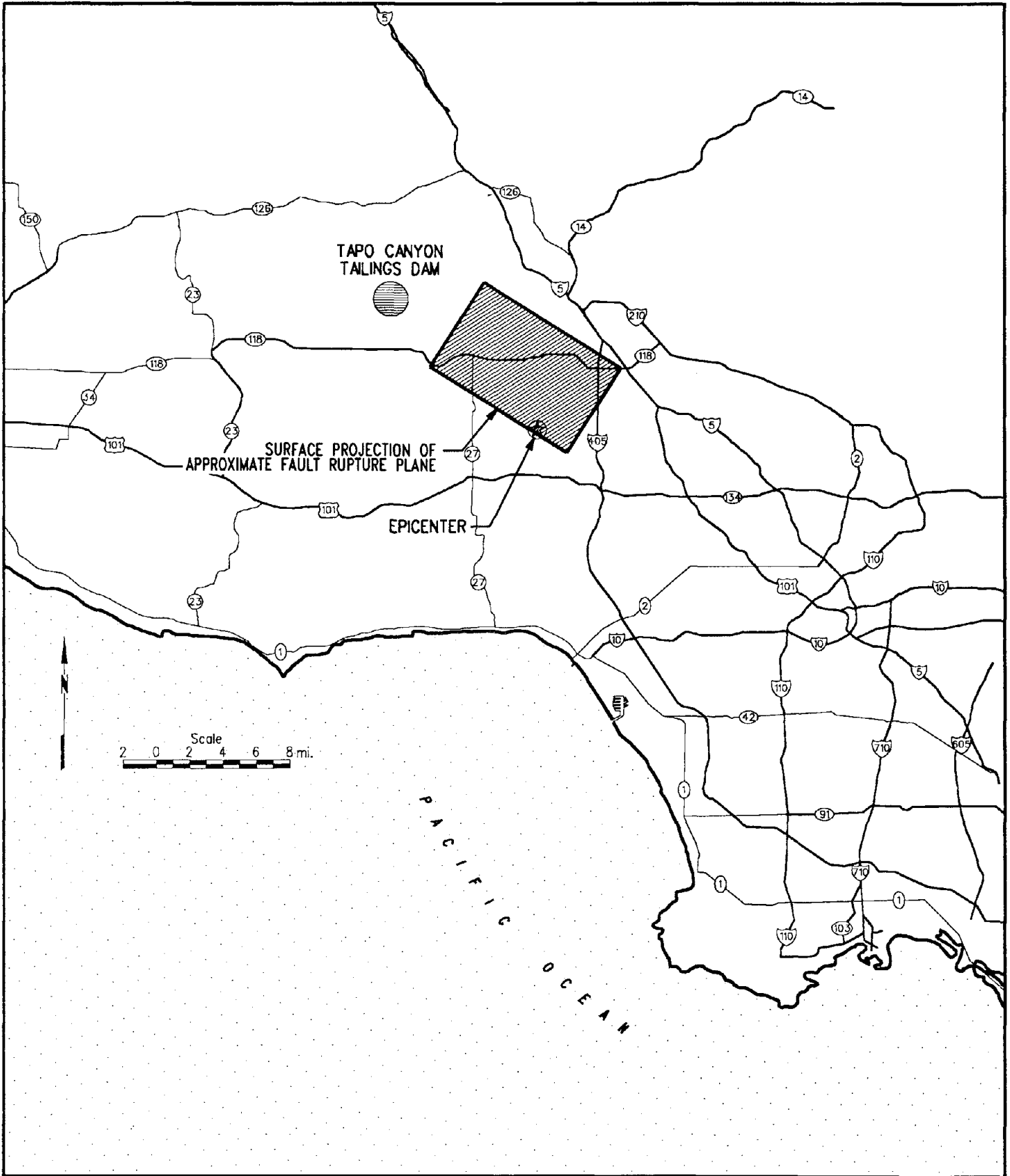


Fig. 6.36: Location of Tapo Canyon Tailings Dam site

6.3.2 Construction History

The tailings dam and pond are owned by the P. W. Gillibrand Company as part of a sand and gravel aggregate mining operation. This particular pond, known as Pond No. 6, is one of several ponds on the property that have been used over several decades to settle waste from the aggregate mining operation. According to the owner, Pond No. 6 was located partially within a former hill which had been excavated and mined out in the 1970's for aggregate prior to the construction of the pond. The former hill occupying the pond site was composed of weak rock materials of the Pico and Monterey formations. These formations are Tertiary marine sandstones, conglomerates and shales of Pliocene and late Miocene age. The mining operations apparently hollowed out part of the hill, causing it to look very much like a natural bowl with natural rock ridges and piles of mine waste forming the enclosure. A gap in the rock ridge and mine waste piles was excavated on the southwestern side to allow ground water to run out by gravity flow to the adjoining creek during the later stages of the mining excavation.

According to the owner, much of the available aggregate within the pit was becoming exhausted by about 1980 and ground water was making further excavation difficult. Consequently, mining was stopped and the pit was converted for use as a settling pond. As with several other ponds on the property, Pond No. 6 was used to settle out fines washed out of the sand and gravel aggregate obtained during the mining process. The fines were conveyed in suspension by water flowing in trenches to the pond site. Within the pond, the fines would settle out and the water would be reclaimed for further use by means of pumps floating on rafts. Most of the fines and resulting tailings were apparently smaller than the No. 140 sieve size. However, examinations of the tailings exposed near the surface of Pond No. 6 showed the presence of sandy soils as well. The tailings apparently consisted of stratified layers of soils ranging from fat clays with plasticity indices as high as 30 to 50 to non-plastic sandy silts and silty sands.

The information currently available indicates that much of the retention for the early stages of the pond could have been provided by the natural sedimentary rock ridges remaining after excavation of the original hill. Rock ridges and cut slopes appear to have formed the early pond enclosure on the northern side, southeastern side, and southern corner of the pit. On the southwestern side, mine waste was apparently spoiled or piled in the dry to make wide embankments to form the early portion of the enclosure on this side of the pit. The only opening in this early enclosure would have been the gap excavated on the southwestern side to remove ground water during the mining phase. This gap would have required a retention embankment at the beginning of the ponding stages. As the pond filled up with tailings over the years, additional embankment stages were apparently added within the rock gap and, eventually, on top of the rock ridges and mine waste embankments as well in order to contain additional tailings. The owner indicated that the embankment stages may have been placed using the upstream method, but that substantial material was added in each stage. The upstream method consists of constructing retention embankments in stages with each stage being founded on top of the previous embankment stage and on portions of the retained tailings. Thus, the centerline of the retention embankment moves "upstream" as the height of the embankment increases.

The tailings pond eventually took the shape of a triangle in plan view, with the northern side being approximately 1,000 feet long and entirely in cut. The southwestern and southeastern sides are both about 900 feet long with retention slopes approaching 80 feet in height. In 1987, an approximate 600-foot long buttress was added to the outside slope of the southwestern retaining embankment along the creek in order to provide additional stability. Unlike the other two sides, the southwestern side appears to be composed mainly of fill. According to the owner's engineer, the buttress was approximately 60 feet wide and incorporated an internal drain to collect seepage. The drain consisted of a 6-inch perforated pipe placed within a gravel trench. The material used to construct the buttress appears to have been primarily a gravelly, silty sand. On the outside of the buttress along the creek, riprap was added to provide slope protection. For portions of this reach, the creek channel had to be relocated outward (downstream) to provide space for the buttress.

The dam was eventually filled with sediment by about 1992, at which time ponding of waste material was halted. Over the next two years, the eastern half of the pond was used by a nearby concrete batch plant as a spoil area for waste concrete. Concrete trucks would be driven onto the eastern pond surface and operators would wash out the waste concrete from their trucks, an operation which continued even after the Northridge Earthquake. This resulted in a discontinuous surface layer of waste concrete across the eastern half of the pond surface to a depth of about 4 to 6 feet. The western half of the pond was apparently not used for this purpose, perhaps because water was sometimes still ponded on this half of the facility. It is uncertain as to the exact source of the water that was ponding in this half, but it may have been due to leakage from conveyance ditches and ponds located immediately to the north. Figure 6.37 shows an aerial photograph of the completed pond taken in April 1993. This photograph clearly shows ponded water in the western half of the facility.

6.3.3 Description of Flow Slide

The flow slide resulted from the failure of an approximately 200-foot long section of the tailings dam near the southwest part of the pond. In this area, the dam slid out and broke up into at least two pieces which were found approximately 200 and 300 feet downstream of their original positions, respectively. The breach of the tailings dam occurred in the same area where available information indicates that a gap was created in the natural rock ridge and mine waste embankments left from mining of the original hill. This is the location of the highest fill and is the only location where the pond was apparently being retained by the later retention embankments alone. Following the failure of the tailings dam, some of the retained tailings flowed out of the breach in a viscous flow which travelled over 600 feet downstream. Within the pond, the surface of the remaining tailings sloped down concentrically towards the breach in a manner similar to a viscous fluid passing through a funnel. The surface layer of waste concrete on the eastern pond surface broke up into large blocks and spread apart. Figures 6.38 through 6.51 present photographic, topographic and schematic information describing the behavior of the flow slide.

In addition to the dam failure, the remaining portion of the southwestern dam was extensively damaged. Portions of the dam on this side settled as much as 10 feet and spread laterally in both the upstream and downstream directions. The large displacements resulted



Fig. 6.37: Aerial photograph of Pond No. 6 in Tapo Canyon before the Northridge Earthquake.
(Photo by I.K. Curtis, Inc., April, 1993)

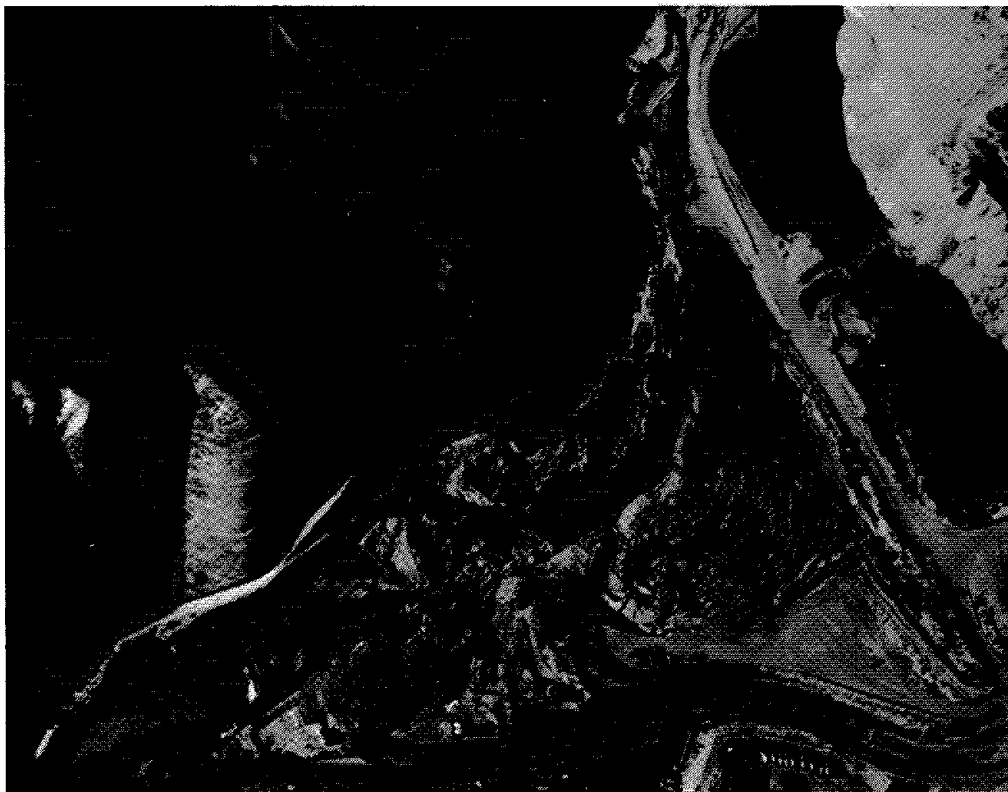


Fig. 6.38: Aerial photograph of Tapo Canyon Tailings Dam on day of Northridge Earthquake.
(photo courtesy of U.S. Air Force)

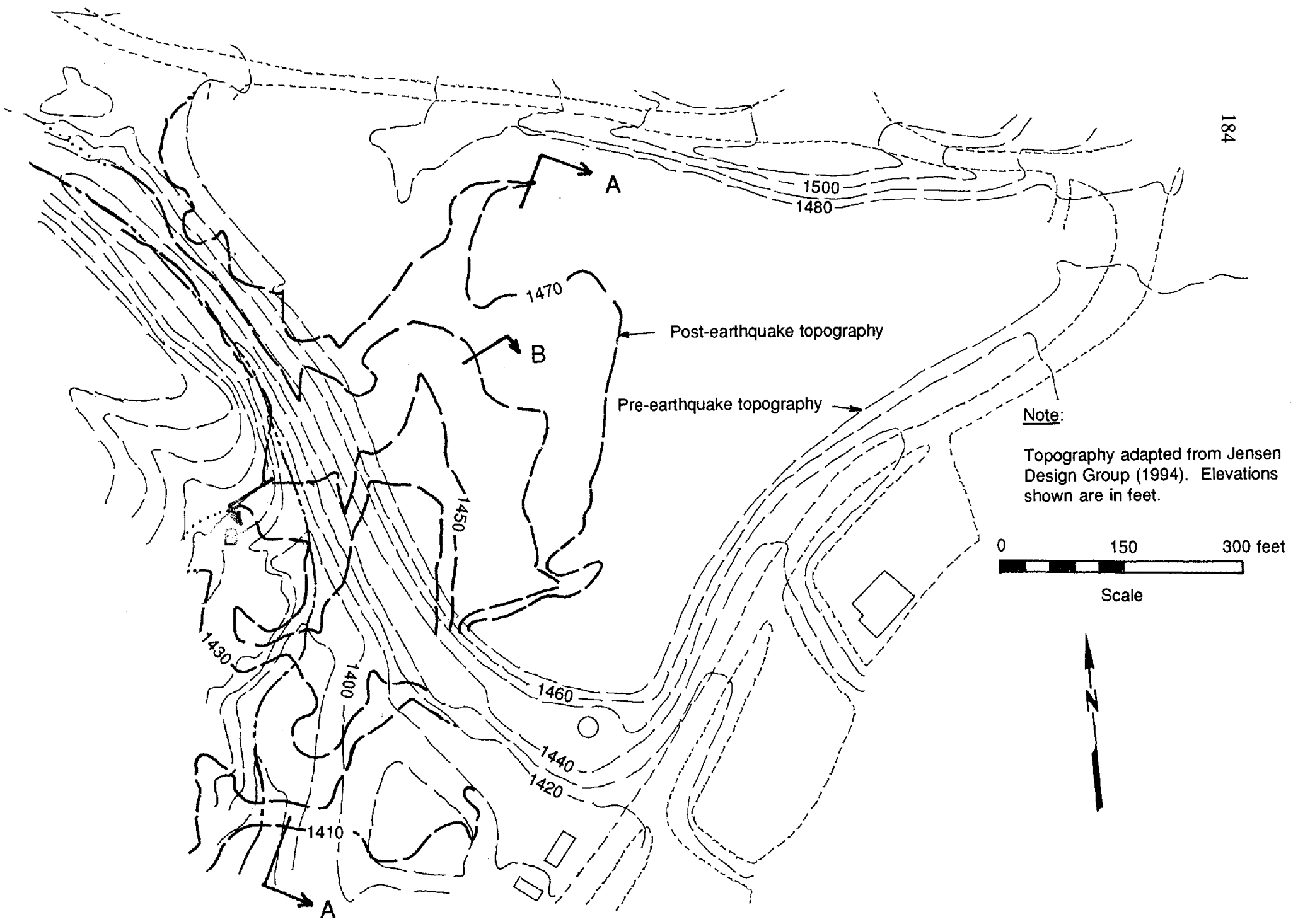


Fig. 6.39: Topography at Tapo Canyon Pond No. 6 prior to and following the Northridge Earthquake

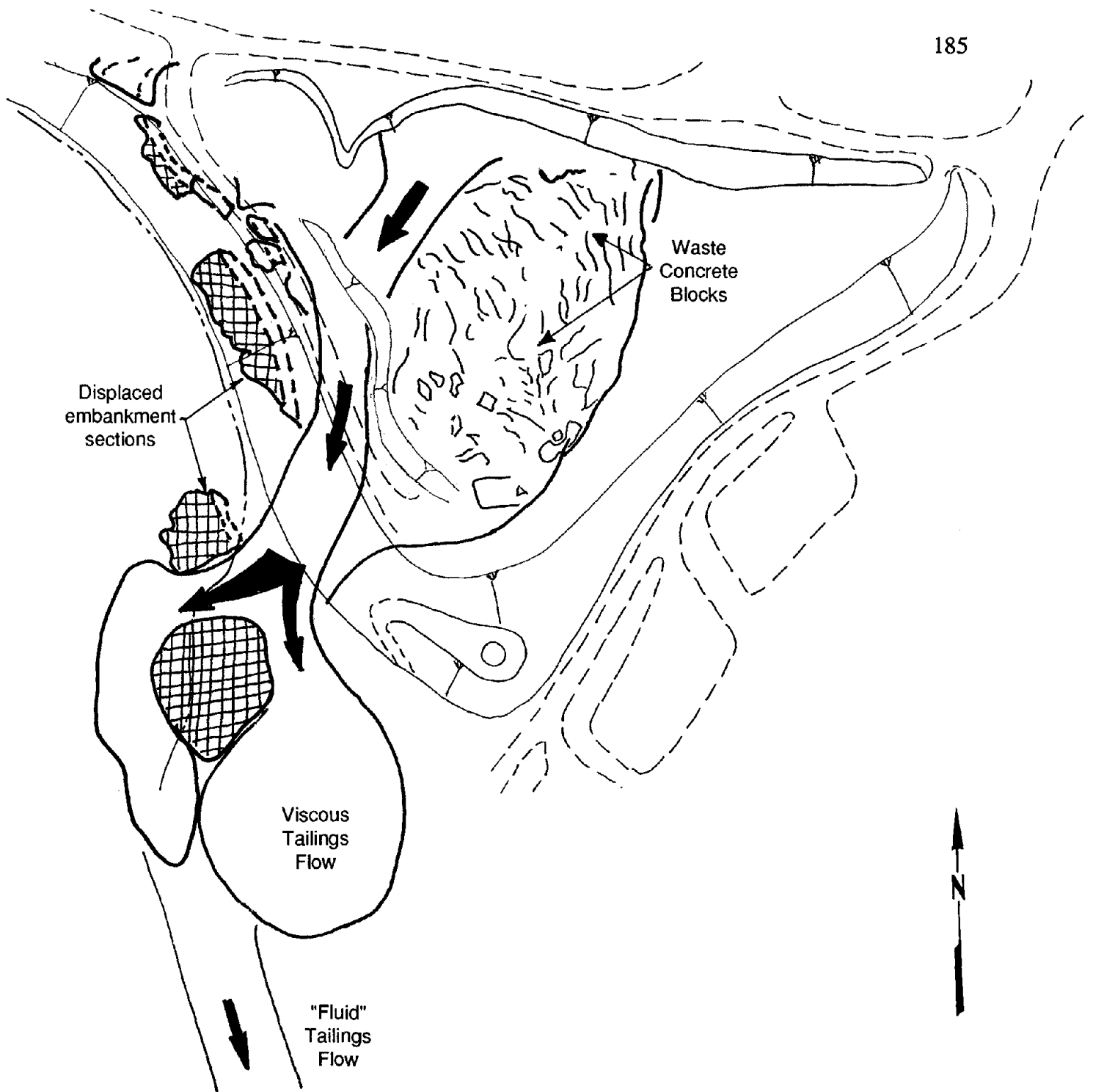


Fig. 6.40: Schematic of Tapo Canyon Tailings Dam failure and resulting flow slide

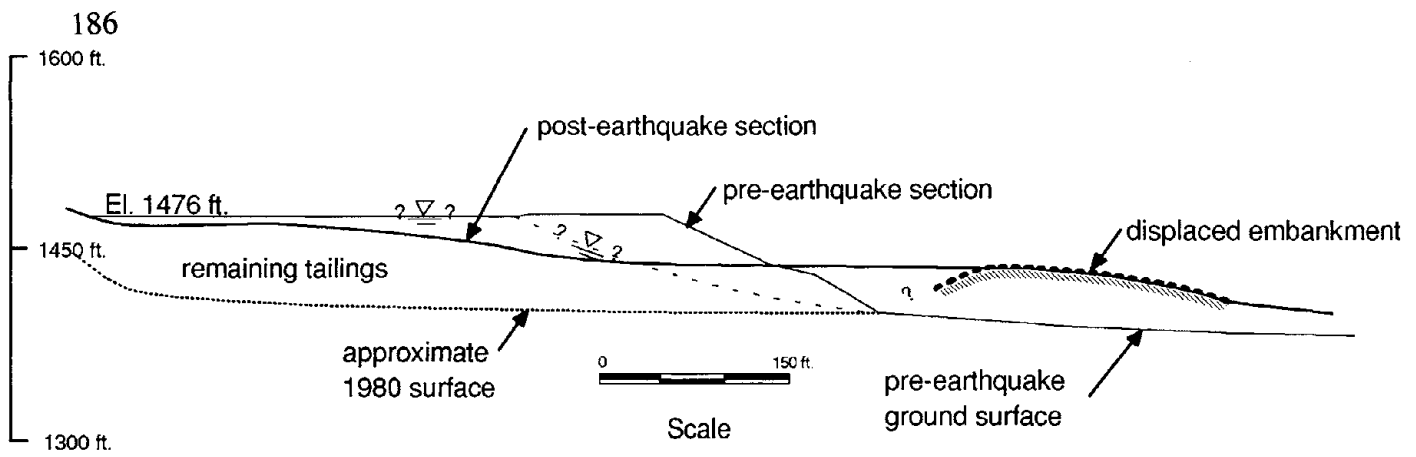


Fig. 6.41: Section A-A from Figure 6.39, showing failed tailings dam and resulting flow slide.

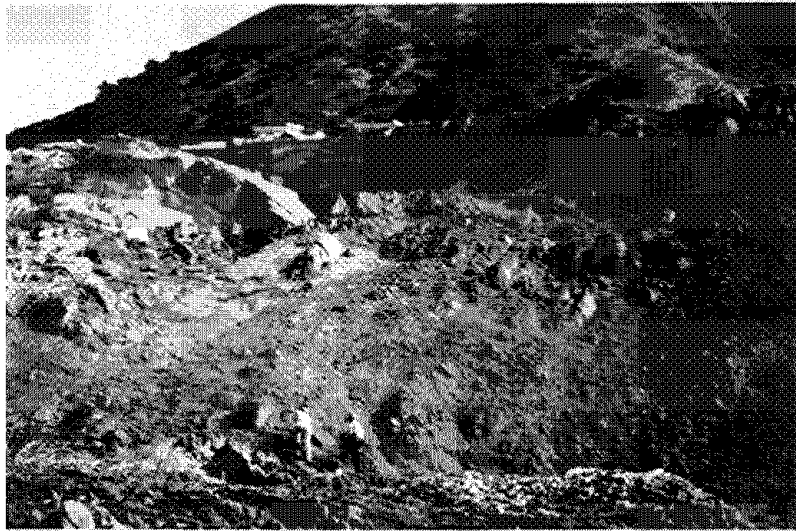


Fig. 6.42: View looking east across flow slide within breach towards southeast embankment

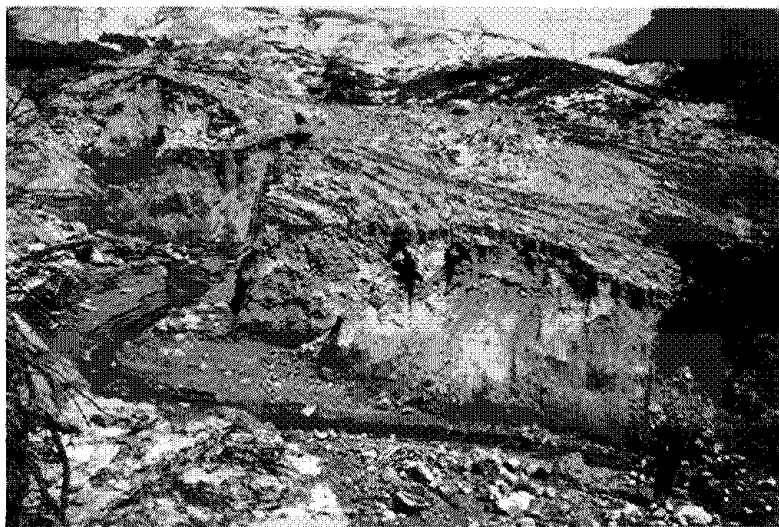


Fig. 6.43: Edge of lobe of viscous tailings flow near creek, photograph taken 600 feet downstream of the failed pond, looking north.

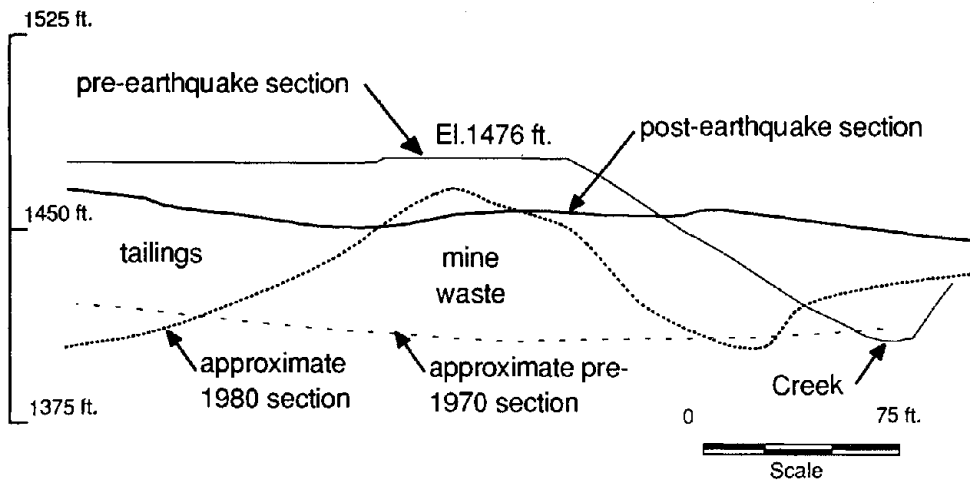


Fig. 6.44: Section B-B from Figure 6.39, failed embankment section northwest of breach

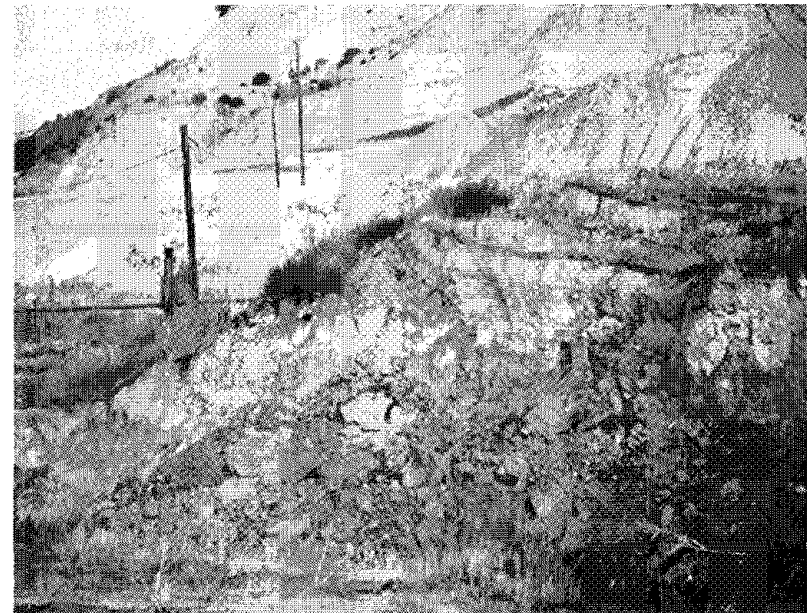


Fig. 6.45: Offset in roadway on north portion of southwest embankment



Fig. 6.46: "Split" crest area of failed southwest embankment

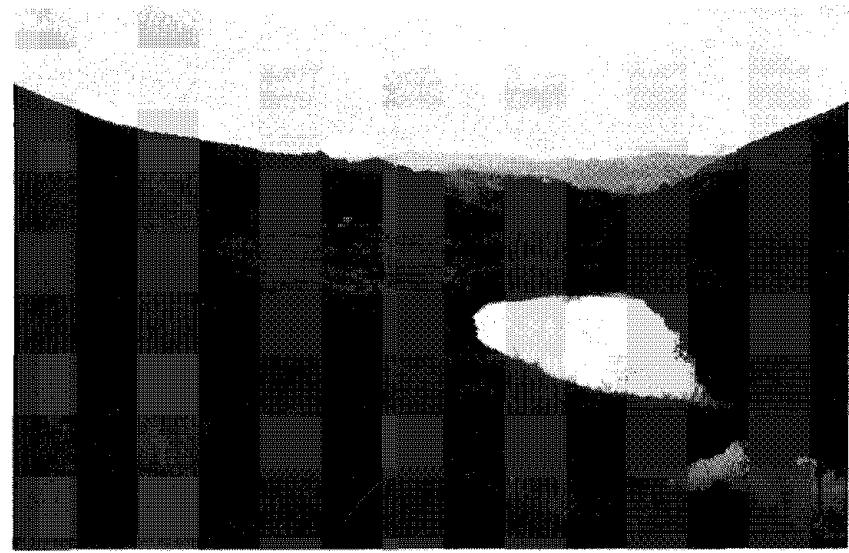


Fig. 6.47: Portion of failed southwest embankment blocking creek, forming small lake.

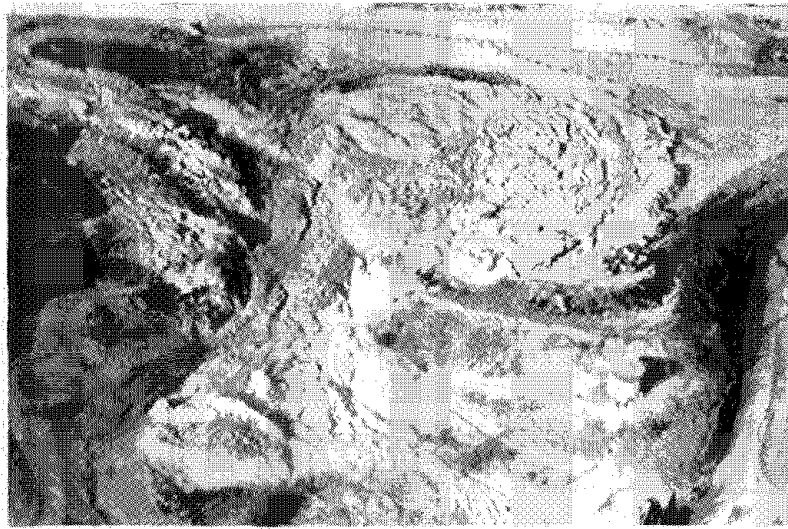


Fig. 6.48: Aerial view of tailings dam failure (photo courtesy of Yoshi Moriwaki, Woodward Clyde Consultants)

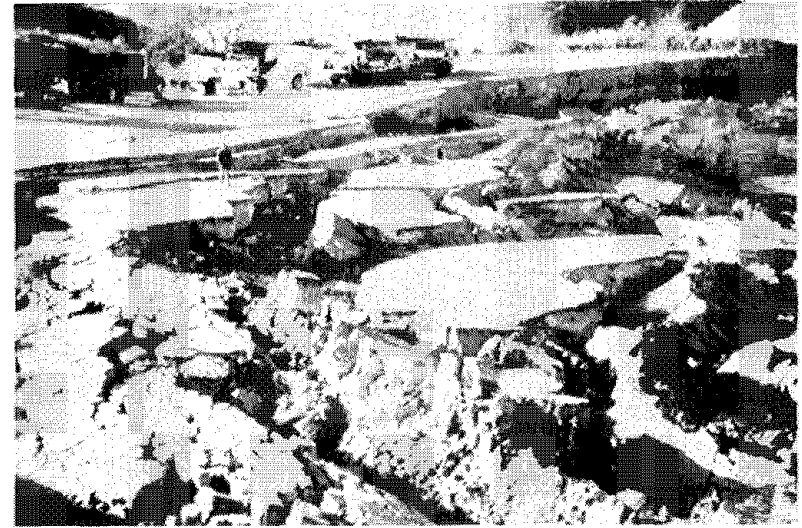


Fig. 6.49: Photograph of displaced concrete blocks on pond surface

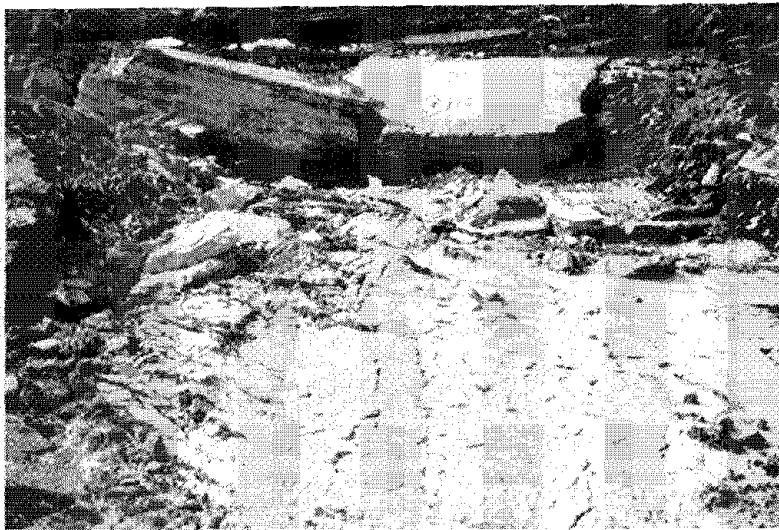


Fig. 6.50: Photograph of pair of concrete blocks which traveled 84 feet across pond surface

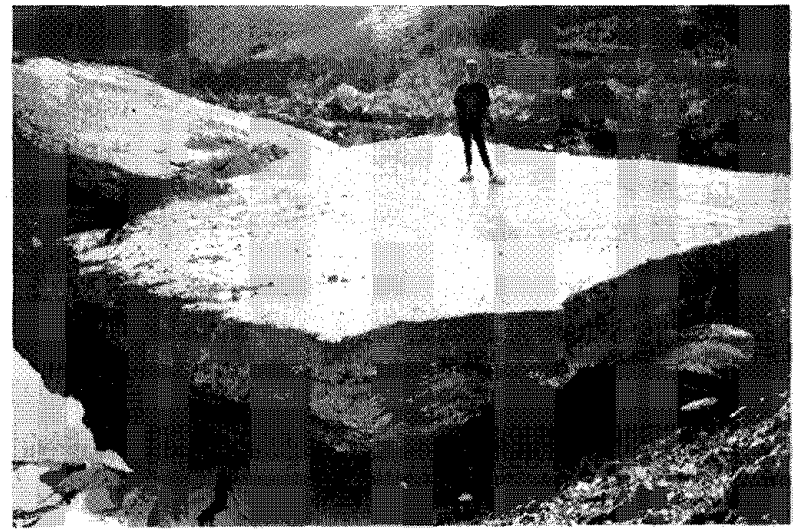


Fig. 6.51: Close-up photograph of 200-ton concrete block

in extensive cracking with crack dimensions exceeding several feet in both vertical and horizontal directions. Portions of the buttress and riprap added in 1987 ended up on the opposite (western) side of the creek from where they had been constructed (see Figures 6.44 through 6.46). For a while, the creek was partially dammed up in this area by the displaced dam and tailings (see Figure 6.47). The fact that this portion of the dam did not experience a complete flow failure, and the nature of the observed lateral spreading, are probably due to the presence of the mine waste piles and possible rock ridges underlying the retaining dam in this area (see Figure 6.44). Some of the displacements of the southwestern dam may also have been limited by the presence of the opposite, or western, creek bank.

The southeastern side of the dam did not appear to have been significantly damaged. This may be due to a lesser amount of saturation within the tailings on this side of the pond, or may be due to the fact that the rock ridge forming the base of the retaining embankment is higher on this side.

Downstream of the principal, relatively viscous flow slide, more "fluid" tailings were found to have splashed up across the creek and against the adjacent hillside. The splashed material appears to be composed predominantly of clayey soils. Further downstream, tailings entered the creek channel, filling much of the channel to unknown depths, and flowed thousands of feet downstream. Trees were found in the channel surrounded by tailings with "splashes" running several feet up the upstream side of their trunks.

One of the more notable features of the flow slide was the fact that some of the blocks of concrete waste on the eastern surface of the pond exhibited significant surface displacements (see Figures 6.48 and 6.49). These blocks, typically 4 to 6 feet thick and weighing hundreds of tons, were found to have moved directly across the pond surface as the surface sloped down towards the breach. Figure 6.49 shows a portion of the broken concrete surface and the displacements between blocks (note person and trucks in background for scale). Track marks left in the surface of the tailings could be found behind the displaced blocks. Shown in Figures 6.50 and 6.51 are photographs of a pair of blocks which slid over 84 feet down the sloping pond surface following the breach of the tailings dam. Each block is approximately 24 feet across and weighs over 200 tons. The surface across which the blocks travelled has a slope of approximately 12.5 degrees from the horizontal. The blocks' lateral movements were apparently halted by either reaching the bottom of the slope, as in the case with the pair in Figure 6.50, or by the buildup of tailings material ahead of the block (note waves of pushed up material in Figure 6.49).

During an interview nine days after the earthquake, a neighbor indicated that rumbling/rushing noises were heard a few minutes after the main shock, and the neighbor believed that this was the beginning of the flow slide. The neighbor estimated that the elapsed time between the main shock and the rumbling noises was less than 10 minutes.

The failure and flow slide were caused by earthquake-induced liquefaction of the tailings, and perhaps, portions of the retaining embankments. Two sediment boils were found on an inspection nine days after the earthquake. The boils were found in tailings, one near the northeast portion of the pond and the other one near the western edge of the flow near the

creek and one of the displaced pieces of embankment. Both boils consisted of non-plastic silty sand with the upper boil containing about 47 percent non-plastic fines and the lower boil containing about 16 percent non-plastic fines.

6.4 Hillside Structural Fills

In the years since World War II, substantial development of hillside regions in the Santa Monica, San Gabriel, and Santa Susana mountains has occurred. Associated with this development has been the construction of fills to create level building pads for houses and other structures. These fills can generally be characterized as being either deep canyon fills, sometimes over one hundred feet thick at their deepest points, or smaller "wedge" type fills used on the faces of slopes. When these fills have been constructed according to accepted modern standards, they are generally well-compacted due to concerns regarding long term static compression and settlements.

During the Northridge Earthquake, many structures constructed on hillside fills experienced significant distress. Damage was noted in both modern and older construction, and in some cases was observed in the absence of any apparent large-scale shear failure in the fill soils or foundation materials. Some of the damaged fills had been constructed as recently as one month prior to the earthquake, apparently in conformance with current standards and practices. In all, these failures have resulted in millions of dollars of damage to hillside structures.

A preliminary map illustrating the locations of a number of damaged modern hillside fills is presented in Figure 6.52. The locations of fill damage shown in this figure were compiled from civil engineers, geotechnical engineers, geologists, engineering geologists and public agencies involved in investigations of fill damage. It should be noted that Figure 6.52 represents only site location data collected to date, and that additional data may become available. Numerous other locations of fill damage occurred in modern fills, but are not shown due to concerns about client confidentiality. In addition, there were numerous fill failures in older roads where the fills had not been keyed, benched or compacted in accordance with modern practices. Failures in old fills were common along Mulholland Drive, Santa Susana Pass Road, Topanga Canyon Boulevard (Highway 27), and other smaller residential roads that were first graded prior to World War II.

One particularly recent fill damaged by the Northridge Earthquake is located along Highway 126 just west Interstate Highway 5. A new post office which was not yet occupied is located in the vicinity of this fill and was severely damaged by the earthquake. It is not known whether the post office was underlain by the fill soils or a natural rock ridge. However, the fill does underlie an access road to the post office which experienced several inches of lateral and vertical ground movements, as shown in Figures 6.53 and 6.54.

In general, fill damage was observed throughout the hillside areas surrounding the epicenter. While there appear to be concentrations of fill damage in some areas, it is not yet known whether these concentrations are due to similar age of construction (and standards of practice), types of underlying earth materials, site orientation with respect to the epicenter,



Fig. 6.53: Pavement cracking due to movements of underlying fill, access road for Newhall post office.



Fig. 6.54: Pavement cracking from fill movements below Newhall Post Office

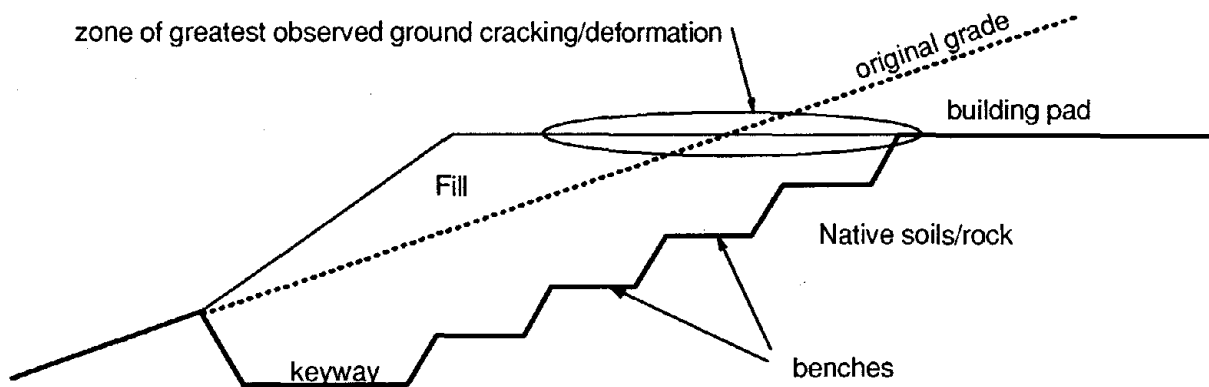


Fig. 6.55: Schematic of typical "wedge" fill geometry

or other factors. Additional data may shed some light on these trends as more detailed second phase investigations are carried out.

Many of the damaged hillside homes were constructed on "wedge" fills having geometry similar to that shown in Figure 6.55. Typical damage to hillside homes on these fills are shown in Figures 6.56 to 6.59. Localized vertical and horizontal soil displacements of several inches were observed in many instances within the fill portions of the building pads. Significant structural distress occurred when these movements developed within the building envelope. In addition, cracks resulting from these movements could collect surface runoff and thereby contribute to future static slope instability. In many cases, the areas closest to the tops of slopes were most severely damaged, possibly due in part to topographic/geometric amplification effects which may have locally increased the severity of ground shaking and resultant inertial forces in these locations.

Several failure mechanisms are believed to be responsible for the observed fill damage, including:

1. Underlying Ground Failure: Several ground failure mechanisms may have occurred in foundations soils beneath fills including (a) the reactivation of older landslides in the foundation materials, (b) flexural slip along bedrock bedding planes or other geologic features due to regional-scale warping, and (c) settlement and lateral spreading induced by liquefaction, partial liquefaction, or dynamic compaction of loose alluvial or colluvial foundation soils.
2. Differential Dynamic Response: For "wedge" fills, differential ground shaking levels may have occurred between the cut and fill portions of the building pads, possibly resulting in part from amplification of the ground motions in the fills.
3. Dynamic Compaction of Fill Soils: In unsaturated fills composed of cohesionless soils, strong shaking may have induced settlement and lateral ground movements, particularly if the fills were poorly compacted. These deformations may also have occurred in fills composed of unsaturated cohesive soils compacted "dry" of optimum moisture content and characterized by discrete "clods" of soil separated by void space. In some cases, these deformations may have resulted in some deviatoric "slumping" of the fills leading to crest settlements and associated toe/face bulging. Similarly, it is also possible that the seismic shaking may, in some cases, have exacerbated deformations which had been developing over time under static (non-seismic) conditions.

The seismically-induced deformation mechanisms of differential dynamic response and dynamic compaction have not generally been widely recognized as potentially significant issues in the design and construction of residential fills in this region.

The poor performance of modern "wedge" fills during the Northridge Earthquake is of considerable importance to the geotechnical engineering profession. The standards of practice in the construction of these fills have evolved considerably since World War II to address



Fig. 6.56: Structure damaged by movements in "wedge" fill, view is along top of fill slope



Fig. 6.57: Evidence of extensional ground movements near back of structure shown on Figure 6.56

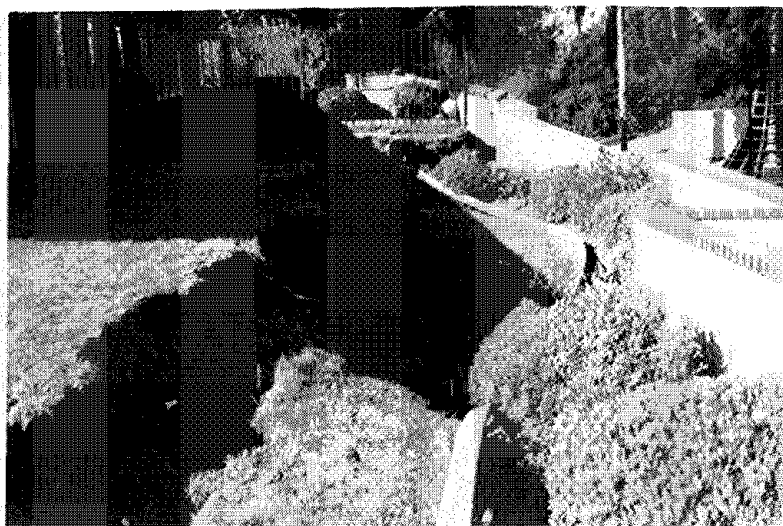


Fig. 6.58: Slumping near top of "wedge" fill slope



Fig. 6.59: Extensional ground cracking near cut-fill interface of "wedge" fill. Note extension of crack into structure and resulting damage.

troublesome static failure, or long term static distress, mechanisms such as landsliding and settlement. Modern design and construction practices in this region typically include compaction specifications, keying, benching, geologic mapping, subsurface and surface drainage provisions, and construction observation under the direction of a licensed civil engineer. While these practices have generally improved the static performance of fills, the potential for poor dynamic performance has not been widely recognized. With the data collected following the Northridge Earthquake, it appears that further evolution of the standards of practice may be necessary for the proper design and construction of "wedge" fills in seismically active areas.

6.5 Earth Retaining Structures

While there is consensus that seismic shaking causes at least transient increases in the lateral pressures acting against earth retaining structures, relatively few cases of seismically-induced failures of walls located above the water table have occurred. However, it is not clear whether the small number of failures is necessarily indicative of a lack of wall movements (Seed and Whitman, 1970).

The state-of-practice for seismic design of earth retaining structures is to perform a conventional pseudo-static analysis. A dynamic horizontal thrust is assumed to be exerted by the retained fill, and the magnitude of this pseudo-static thrust is most commonly estimated using either the Mononobe-Okabe approach, or derivatives of this method. This approach is not only used in the seismic design of conventional retaining structures, but its use has been extended to the design of more recently developed retaining systems, namely reinforced soil structures. To date, the performance of properly designed and constructed reinforced soil walls during earthquakes has been excellent (Mitchell and Christopher, 1990). Qualitative assessments have been made on the seismic performance of reinforced soil walls and slopes that have experienced earthquake excitation during the 1989 Loma Prieta earthquake for the case of structures reinforced with either extensible (Collin et al., 1992) or inextensible inclusions (The Reinforced Earth Company, 1992). No significant signs of structural distress or movements were noted in these field assessments. Because of the flexible nature of these structures, they are generally believed to perform well when subjected to horizontal ground accelerations. However, examination of structures that have actually experienced earthquake excitation remains essential since this constitutes the only true confirmation that the design and performance of these structures is in fact satisfactory.

A general visual inspection of various types of retaining structures in the affected region was carried out following the Northridge Earthquake. Specific close inspection of structures under the jurisdiction of Caltrans was performed along U.S. Highway 101, Interstate Highway 10 and California State Highway 2. The inspected structures included reinforced soil structures, soil nailed walls, and crib walls. The map in Figure 6.60 shows the locations of the different retaining structures discussed in this section. In general, conventional retaining walls and particularly reinforced soil structures performed well during the Northridge earthquake. Some distress was observed, however, in several reinforced concrete crib retaining walls.

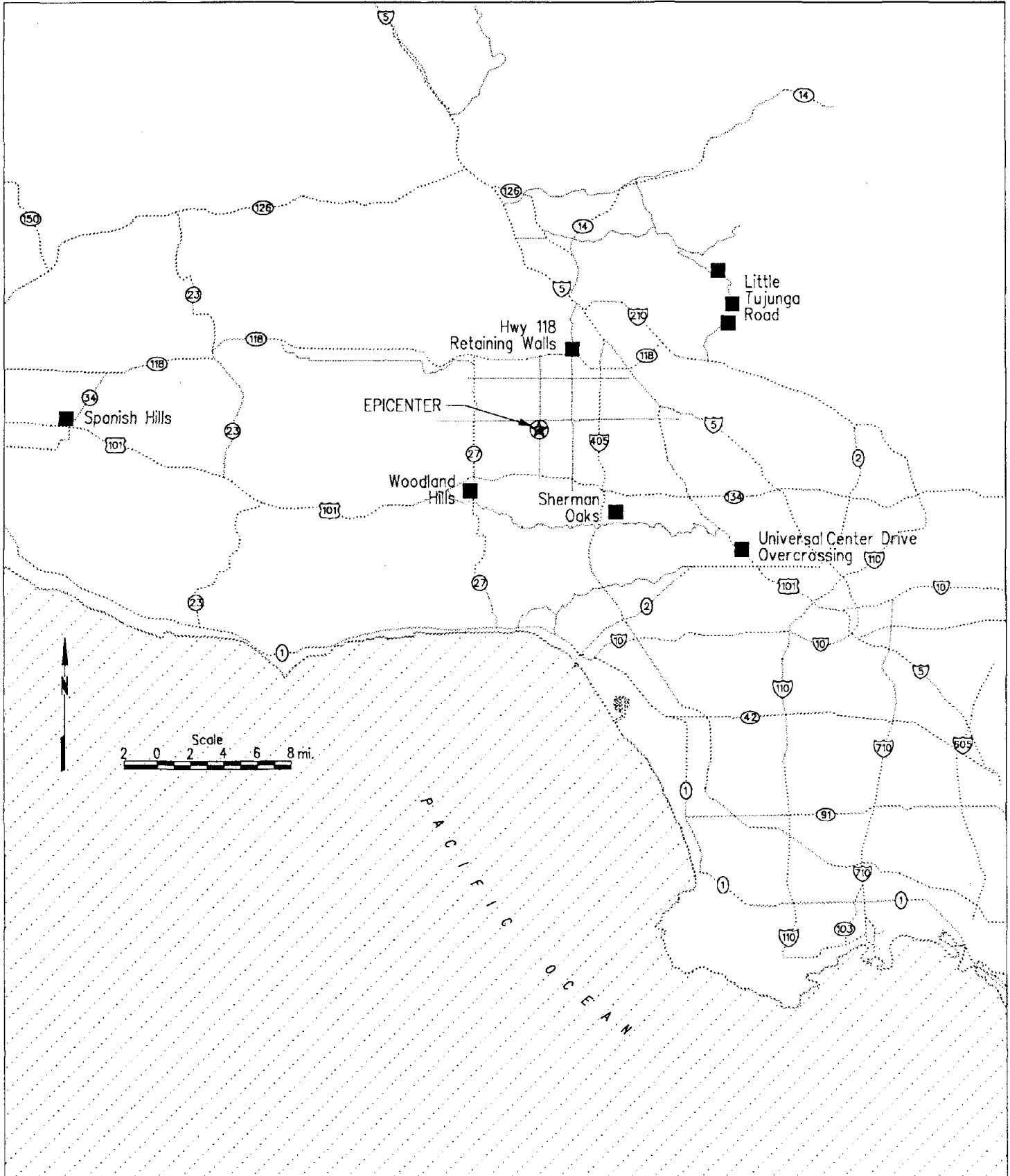


Fig. 6.60: Map showing the locations of earth retaining structures discussed in this report

The inspected mechanically stabilized earth walls and soil nailed walls showed no signs of structural distress. This good performance of reinforced soil structures during seismic events has been attributed to their simple and regular shape, and to the flexibility of the system that promotes redistribution of earthquake forces. Los Angeles County has only recently begun to allow construction of mechanically stabilized retaining structures and, consequently, most of the inspected reinforced soil structures were located in Ventura County, west of the epicentral region. Of particular interest was the Spanish Hills project, a major hillside development in Camarillo, located approximately 46 km (29 miles) from the epicenter of the Northridge earthquake. Estimated horizontal ground acceleration at this site was 0.2g. This landform contour grading project included over 13,000,000 m³ of earthwork and over 430,000 m² of geogrid reinforcement, including a 24 m (80 ft) high 1:1 geogrid reinforced slope. Visual observations made of several of the geogrid reinforced slopes after the earthquake indicated that these structures performed very well, with no physical distress, cracking, sloughing or erosion problems on the slopes having been observed. To monitor the lateral deflection along the alluvium foundation material, a slope inclinometer was installed at the toe of this geogrid reinforced slope. No lateral movement of the slope, resulting from the ground shaking generated by the Northridge Earthquake, was indicated by inclinometer readings taken one week after the event (Leighton and Associates, 1993).

Several earth retaining walls were inspected along the Little Tujunga Road in the Angeles National Forest. The retaining structures were either metallic or reinforced concrete crib walls, often battered (inclined), and up to 6 m (20 ft) high. Maximum horizontal ground accelerations in this area are estimated to have been on the order of 0.4g. Although the seismic excitation in this region caused major rockslides, visual inspections of these structures did not indicate any signs of distress, or cracks on the paved road over the retained fills. A typical metallic crib wall along the Little Tujunga road is shown in Figure 6.61. Even though a slide was triggered by the earthquake next to this wall, no signs of distress were observed in this structure.

Similarly, no damage was observed in large (approximately 6 m high) reinforced concrete retaining walls built along California State Highway 118, and located only 12 km (8 miles) from the epicenter. These retaining structures appear to have been subjected to maximum horizontal ground accelerations of approximately 0.8g, based on recordings from nearby seismographs.

Signs of earthquake-induced distress were found on structures located in Universal City along Highway 101 at the Universal Center Drive Overcrossing. Three large, up to 12 m (40 ft) high crib walls with segmental concrete facing units have been privately built at this location. The walls are located approximately 19 km (12 miles) from the epicenter of the earthquake. Based on data from nearby stations, the estimated peak horizontal ground acceleration at the site appears to have been approximately 0.35g. The southern-most wall at this location showed evidence of distress and movements during the earthquake, as shown in Figure 6.62. Continuous cracks more than 25 mm (1 inch) in width were observed on the paved surface, parallel and approximately 1.5 m behind the wall facings. Settlements of the backfill of up to 50 mm in relation to the retaining structure occurred along the cracks (Figure 6.63). A second set of cracks, also parallel to the facing, were located approximately 6 m



Fig. 6.61: Typical reinforced concrete crib wall in the Angeles National Forest. The scarp on the top left side of the picture is from a landslide induced by the earthquake.

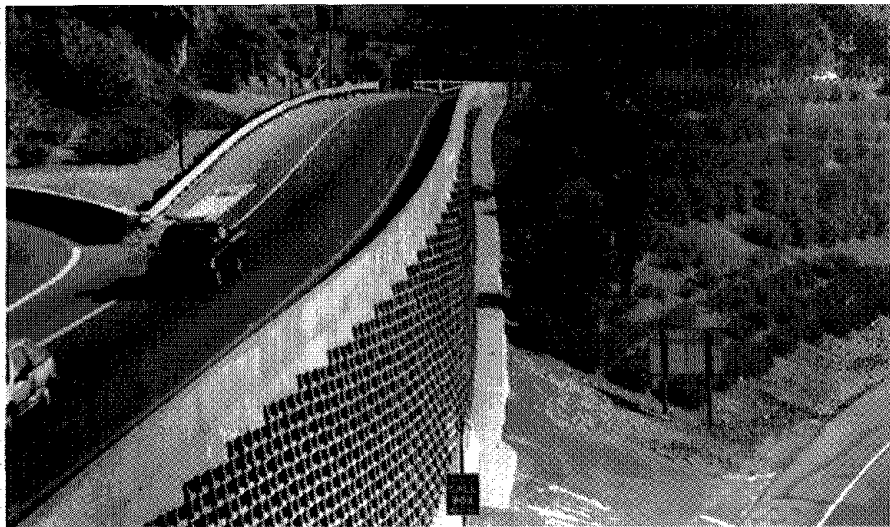


Fig. 6.62: Southern-most crib wall at University Center Drive Overcrossing. Note pavement cracking parallel to wall.

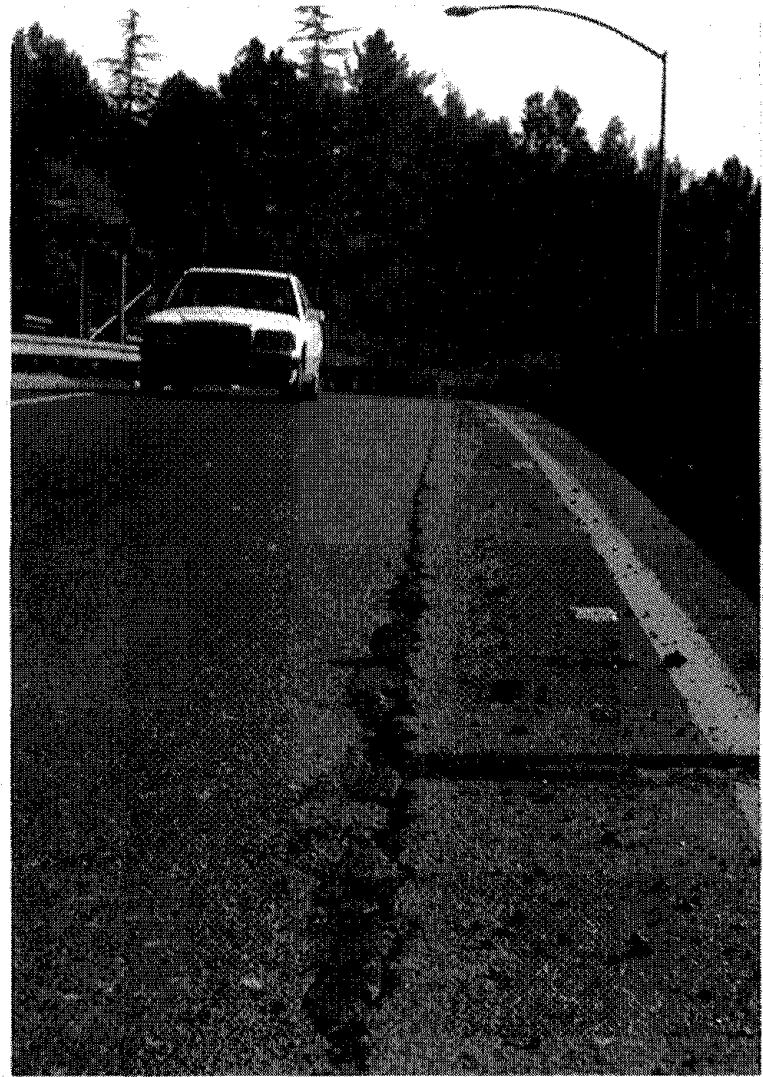


Fig. 6.63: Close-up of crack behind the southern-most crib wall at Universal Center Drive Overcrossing

behind the wall. These cracks occurred at a location where the wall foundation transitions from natural ground to an engineered fill slope. This foundation transition occurs at the highest section of the structure, and it is not clear whether the localization of cracking was influenced by the fill height, the foundation transition, or both. Analysis of the cross section of the reinforced concrete crib wall shows that the location of the continuous line of cracking near the wall corresponds to the inboard end of the concrete crib. The vertical differential settlements likely resulted from either earthquake-induced compaction of the retained fill or, most probably, lateral deflection of the crib wall which resulted in settlement of the retained backfill.

A second crib wall at the Universal Center Drive Overcrossing, the highest of the three crib walls at this location, also showed signs of structural distress. Although no cracks were observed on the paved surface above the wall, damage was observed after the earthquake in structural elements of the retaining structure. The signs of distress were observed in the connections between the stretchers and headers near the base of the wall. Numerous vertical cracks, as well as concrete crushing, occurred at the section of maximum height of the wall, raising potential concerns about the structural adequacy of the concrete elements of the wall.

Significant damage was also reported for approximately 9 m (30 ft) high battered concrete crib walls located in Woodland Hills. Additionally, complete failure was reported for approximately 5 m high conventional reinforced concrete retaining walls located at Sherman Oaks. These walls were subjected to maximum horizontal accelerations on the order of 0.6g.

Although further investigation of the performance of the earth retaining structures that experienced structural distress should be pursued, it appears that both conventional retaining structures as well as reinforced soil systems generally performed well during the Northridge event. An exception to this appears to be the distress observed to several reinforced concrete crib wall systems, suggesting that rigid and massive structural elements, such as concrete crib walls, may not perform as well as more flexible retaining wall systems during seismic events.

6.6 Solid Waste Landfills

6.6.1 Introduction

Federal Regulations ("Subtitle D") effective October 9, 1993, require that municipal solid waste (MSW) landfills located in seismic impact zones be designed to resist earthquake hazards. The seismic response of waste repositories is of concern because dynamic loads may produce relative movements within the waste, bottom liner system, cover system, foundation and their interfaces. These movements could damage either the top or base liner systems, with a consequent loss of sealing, and/or disrupt the function of the leachate and surface gas collection systems.

Seismic design procedures for MSW landfills have been developed, however, largely without the benefit of well-documented case histories. Consequently, established design procedures for evaluating the seismic performance of waste fills largely rely upon unverified

assumptions about waste properties and waste fill dynamic behavior. Given the profession's experience and relative confidence with the procedures developed to analyze the seismic stability of earth embankments, these procedures have been applied, with some modifications, to waste fills. However, the applicability of these procedures to waste fills requires investigation. Waste containment liner and cover systems employed in landfills are often constructed with layers of vastly dissimilar materials, such as high density polyethylene (HDPE) geomembranes and compacted clay liners. Waste materials are inherently heterogeneous, and their physical properties are difficult to assess through field or laboratory testing. Irregular landfill configurations may not be amenable to one- and two-dimensional dynamic response analyses. Hence, waste landfill seismic design procedures may need to evolve from procedures initially developed for conventional earth structures in order to adequately address these concerns.

The 1994 Northridge Earthquake provides important observational data on the response of MSW landfills to strong levels of earthquake shaking. Nine waste landfills which experienced strong levels of shaking (the Operating Industries, Inc., Chiquita Canyon, Sunshine Canyon, Lopez Canyon, Simi Valley, Calabasas, Scholl Canyon, Mission Canyon and Puente Hills landfills), including two with geosynthetic liner systems, were inspected immediately after the event. The location of these MSW landfills (except Puente Hills, which is 6 km east of OII) as well as six other MSW landfills of interest (the Toyon Canyon, Bradley, Penrose, Burbank, Palos Verdes and Terra Rejada landfills) are shown in Figure 6.64.

In general, the performance of solid waste landfills, several of which appear to have been subjected to peak bedrock accelerations of 0.2 to over 0.5g, was good. None of these landfills showed any signs of major instability, although several experienced minor levels of damage (cracking). Many of these landfills experienced a temporary shutdown of the gas flare system due to the loss of power after the earthquake. One impacted landfill, the Operating Industries Inc. (OII) landfill, is well-instrumented with survey monuments, inclinometers and a pair of strong motion recording stations. Because of the difficulties associated with laboratory evaluation of the dynamic properties of waste materials (dynamic strength, moduli and damping), these full-scale field case histories present an invaluable opportunity to study the dynamic response characteristics and performance of waste landfills, and to back-calculate bounding values for key properties and parameters of these fill systems.

In this section, the observed seismic performance of nine MSW landfills will be discussed. Four landfills which are particularly noteworthy will be described in detail, and these landfills are the OII, Chiquita Canyon, Sunshine Canyon and Lopez Canyon landfills. The performance of the other five landfills, which were also inspected immediately after the earthquake event, will be summarized at the end of this section.

6.6.2 Operating Industries Inc. Landfill

(a) General

The Operating Industries Inc. (OII) landfill is located in the city of Monterey Park, approximately 48 km southeast of the epicenter. The landfill was split into two separate parcels by the construction of the Pomona Freeway (Highway 60). The south parcel, which is the primary landfill unit, is shown in Figure 6.65. It is bordered by Highway 60 to the north and a residential development to the south. The north parcel, located north of Highway 60, was operated for only a limited number of years and is not a major waste fill unit. For that reason, this report will focus on the south parcel of the OII landfill. Figure 6.64 shows the location of the landfill with respect to the surface projection of the fault rupture plane. The OII Landfill is located approximately 44 km from the zone of the energy release.

The OII landfill is approximately 76 ha (190 acres) in size and was constructed by filling in a former gravel pit. The landfill stopped receiving waste in 1984 and is currently awaiting final closure as a Superfund Site. The landfill was constructed without a compacted liner system, and currently has an interim soil cover. As previously mentioned, the OII landfill is well instrumented with survey monuments, inclinometers and a pair of strong motion recording stations (one on top of the waste fill, and one adjacent to the toe of the fill). The location of the recording stations are shown in Figure 6.65 and 6.66. The base accelerograph (SS-1) recorded a peak ground acceleration of approximately 0.24g (longitudinal or east-west direction) and the top station (SS-2) recorded a peak ground acceleration of approximately 0.25g (longitudinal direction). The OII landfill presents a unique opportunity to back-calculate the dynamic properties of the waste fill as several earthquake events, with different levels of excitation and occurring at different epicentral distances, have now been recorded at this site. The Northridge strong motion records will be discussed in detail in the next section.

The maximum thickness of the waste fill is approximately 100 m at the center and the top of the landfill is between 20 to 70 m above the adjacent ground (Anderson et al., 1992). Side slopes range from 3H:1V to as steep as 1.3H:1V (Figure 6.66). The berm roads were constructed along the side slopes by building up a wedge-shaped fill using the cover soil. Thus, the thickness of the cover soils varies from less than 1 m along the slope to as much as 4.5 to 6 m thick at the outboard edges of some of the berm roads.

Minor cracking occurred at a number of locations on the faces of the slopes of the OII landfill, mainly but not exclusively at or near to the berm roads. Figure 6.67 is an air photo showing some of the cracks observed along the slope of the north face at the OII landfill three days after the earthquake. Figure 6.68 and 6.69 show typical cracks along the berm roads on the north face of the landfill. The cracks were generally on the order of 5 to 15 cm or less at their widest point, and post-earthquake trenching indicated that surficial cracks did not appear to extend fully through the soil cover system into the underlying waste at this landfill. The cracking appeared to represent brittle cracking of the stiffer compacted soil veneers overlying the more ductile waste fill and did not appear to represent any threat of incipient instability. However, cracking of the cover veneers can provide pathways for the

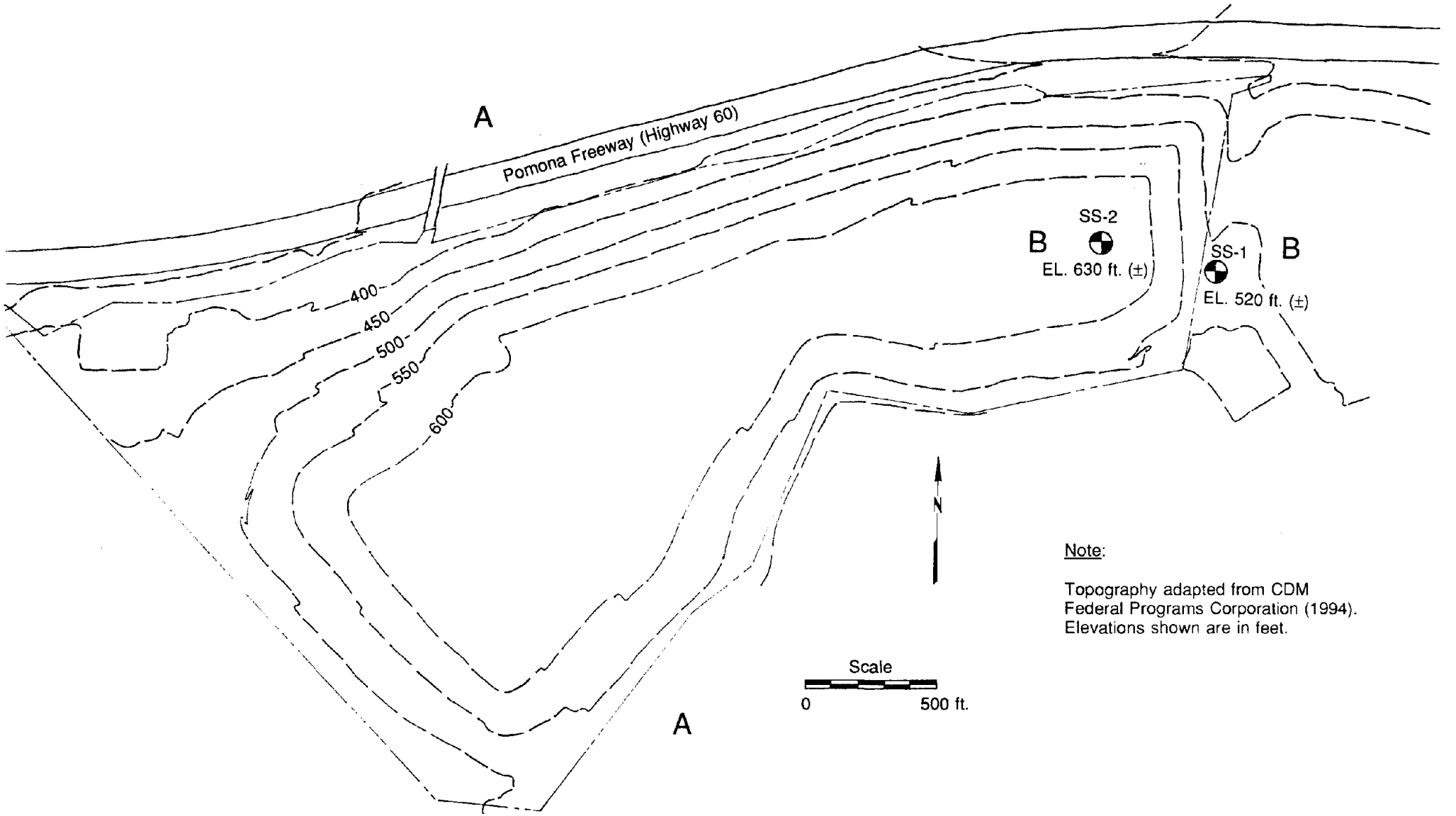


Fig. 6.65: Plan View of Oil Landfill showing contours of waste fill (adapted from CDM Federal Programs, 1994)

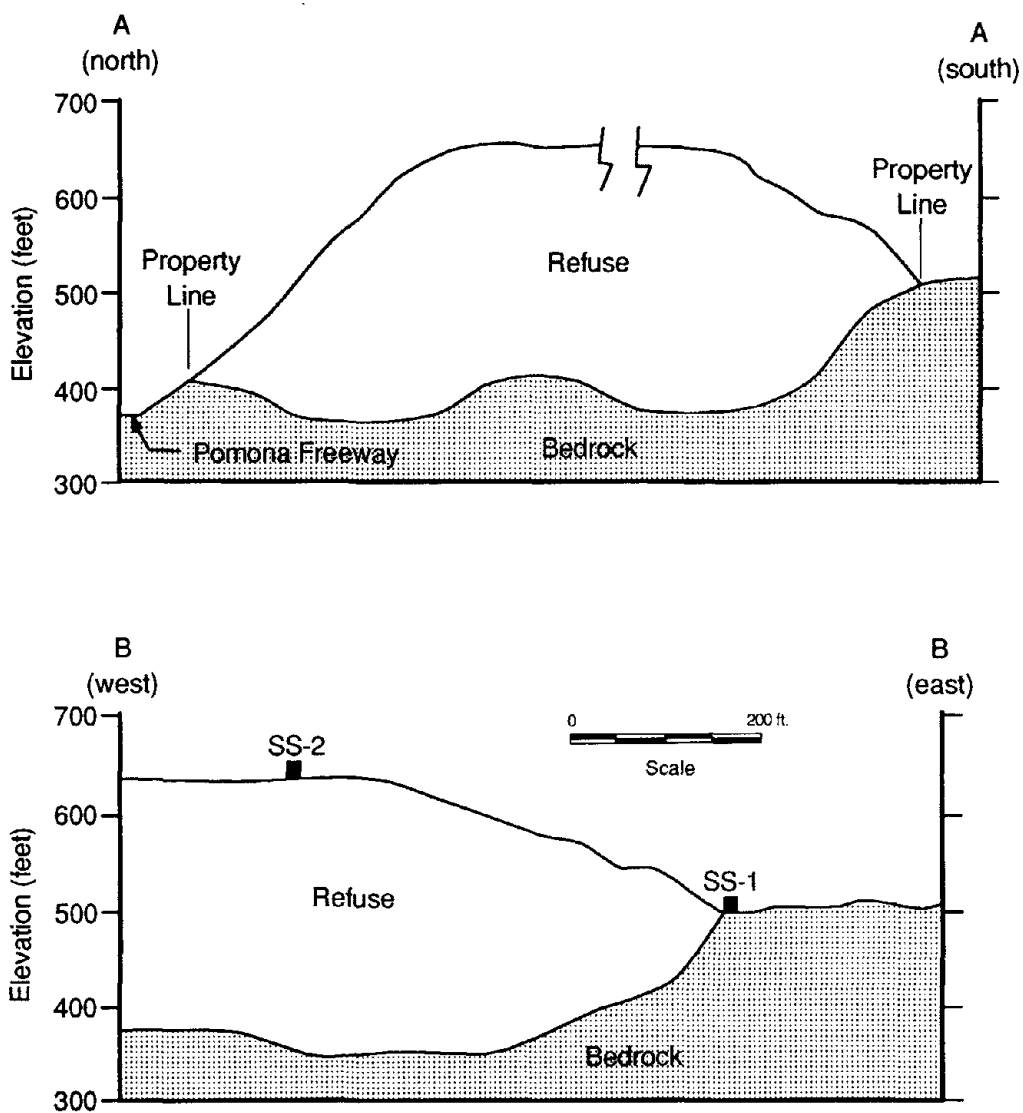


Fig. 6.66: Cross sections of the Oil Landfill
 (adapted from CDM Federal Programs, 1994)

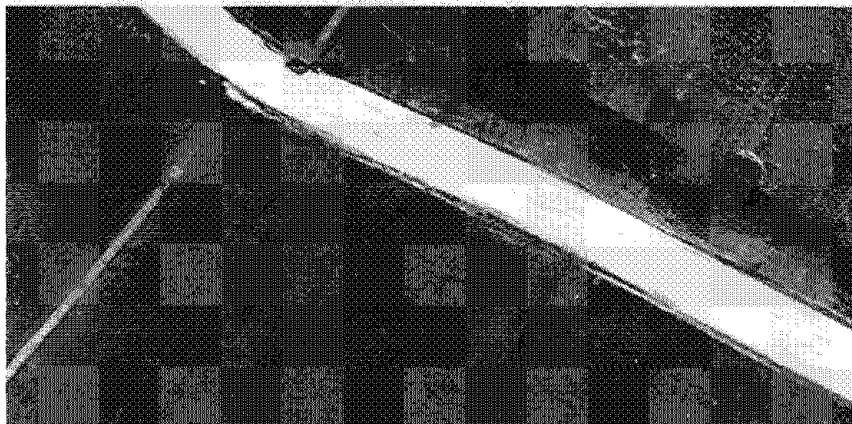


Fig. 6.67: Crack along north side slope near to a berm road at the OII Landfill

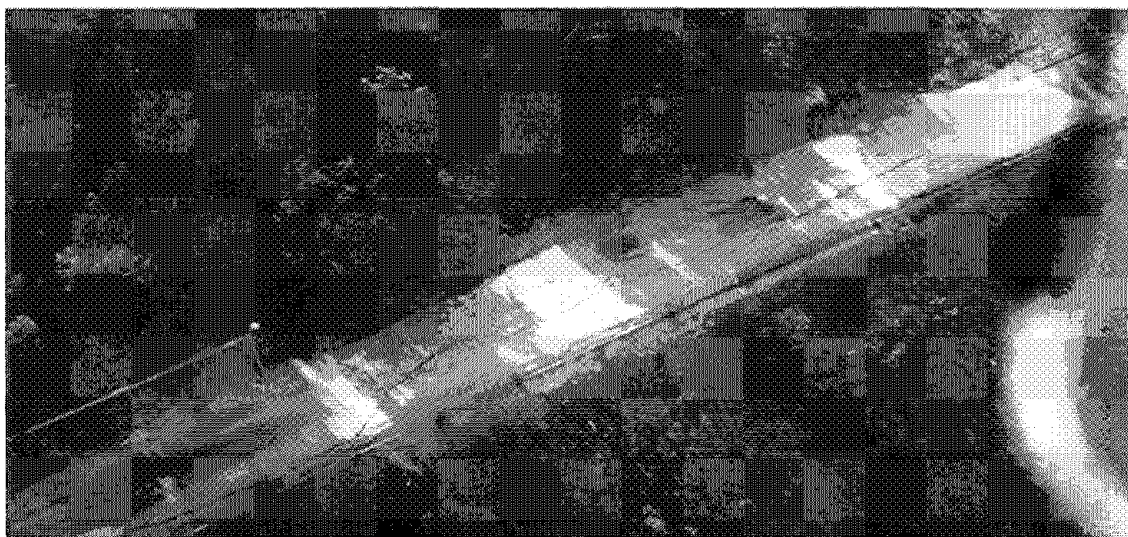


Fig. 6.68: Crack along berm road north side of the OII Landfill



Fig. 6.69: Crack along berm road, north side of the OII landfill

escape of landfill gas. Instrumentation data will be useful in assessing the effects of the Northridge Earthquake ground shaking in more detail.

(b) Strong Motion Records:

The strong motion station situated at the base of the landfill is located on native ground. This material varies from a very hard clayey silt - silty clay to siltstone and claystone (Anderson et al., 1992). The other station is situated a little more than a hundred meters to the west on top of nearly 75 m of refuse. Additional information about the monitoring system is summarized by Hushmand et al. (1990), and general site characteristics have been summarized by Siegel et al. (1990).

The acceleration-time histories recorded at these two stations are shown in Figure 6.70, along with the maximum horizontal accelerations (MHA) and mean square frequencies. The base longitudinal and transverse acceleration-time histories are similar in frequency content (both have mean square frequencies of 3.8 Hz.) and in intensity with MHA's of 0.24 g and 0.225 g, respectively. The Idriss (1991) rock attenuation relationship, which has been shown in Chapter 3 to represent the Northridge data well, would predict a mean MHA of 0.1 g and a mean plus two standard deviations MHA of 0.25 g at a distance of 44 km for a $M_w=6.7$ event. Hence, the recorded MHA values at the base of the OII landfill fall just below the mean plus two standard deviation value. Based on this observation and the site data provided by Anderson et al. (1990), it is not clear if the OII base station can be considered a true bedrock station.

The horizontal acceleration-time histories at the top of the landfill show that the waste fill filters out some of the high frequency motions and amplifies the long period motions. The mean square frequencies of the top longitudinal and transverse motions have decreased to 2.0 Hz. and 2.9 Hz., respectively. Previous measurements by Hushmand Associates (1994) indicate that the fundamental period of the OII landfill for small magnitude earthquakes is between 0.8 and 1.2 seconds. The fundamental period of the landfill would be expected to increase for stronger levels of excitation (like Northridge) as the dynamic stiffness of the refuse degrades with increasing shear strain. Thus, this landfill would be expected to filter out the high frequency motions and amplify the motions close to its fundamental period.

Acceleration response spectra for the longitudinal and transverse motions are shown in Figure 6.71. For both records, there was attenuation in the high frequency range, but at periods beyond approximately 0.6 seconds, there was amplification of the motions from the base to the top. This is most pronounced in the longitudinal direction at periods of 1 to 1.25 seconds, where the amplification was on the order of three. Figure 6.72 shows the Fourier amplitude ratios (top/base ratios) for the longitudinal and transverse motions. The amplification functions indicate that the fundamental period of the OII landfill is approximately 1.2 seconds in both the longitudinal and transverse directions, and that the landfill responds primarily in its first mode.

Preliminary analyses were performed to ascertain whether one dimensional wave propagation analyses could capture the recorded motions at the top of the landfill given the

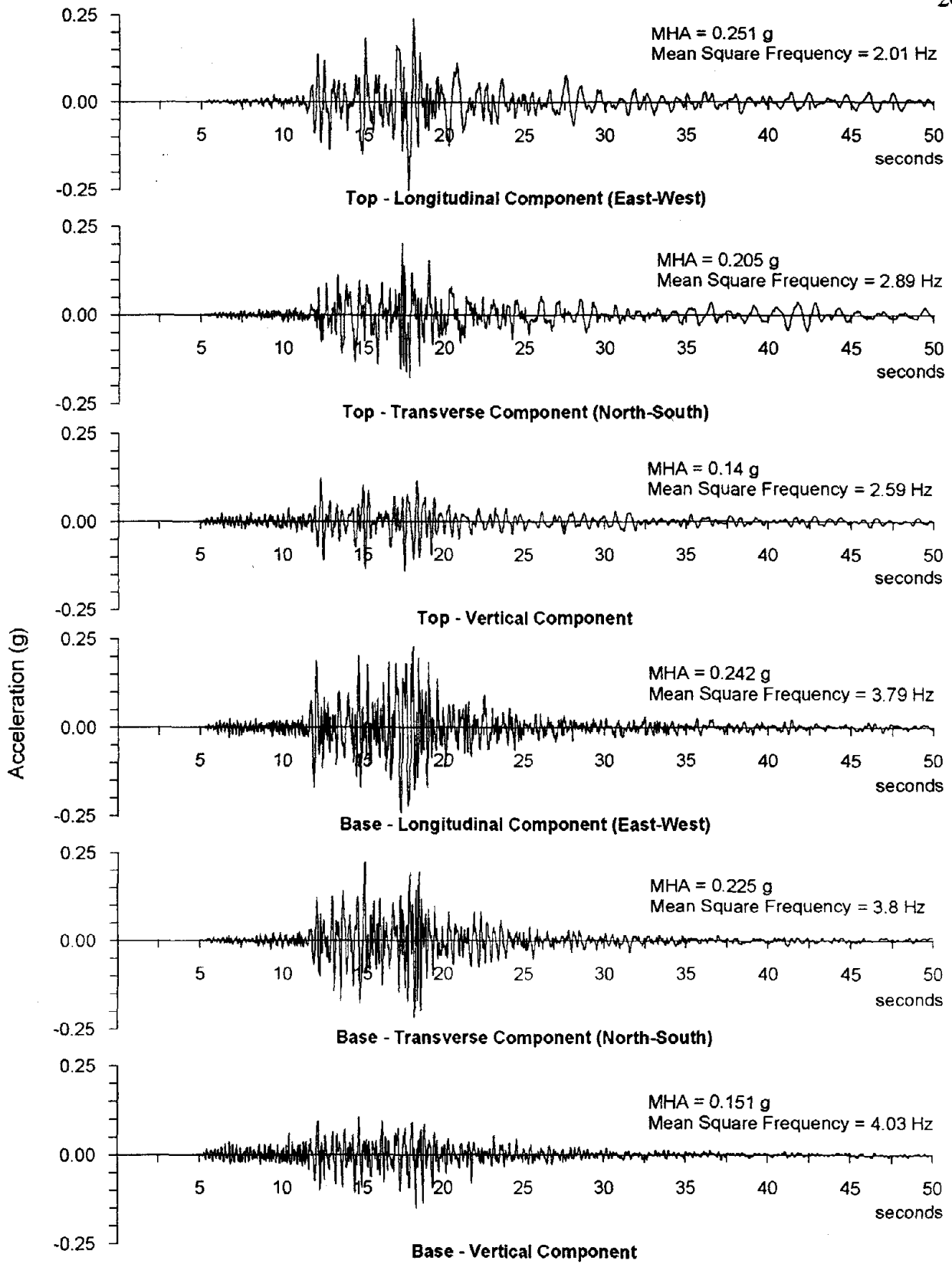


Fig. 6.70: Recorded acceleration-time histories at the OII Landfill

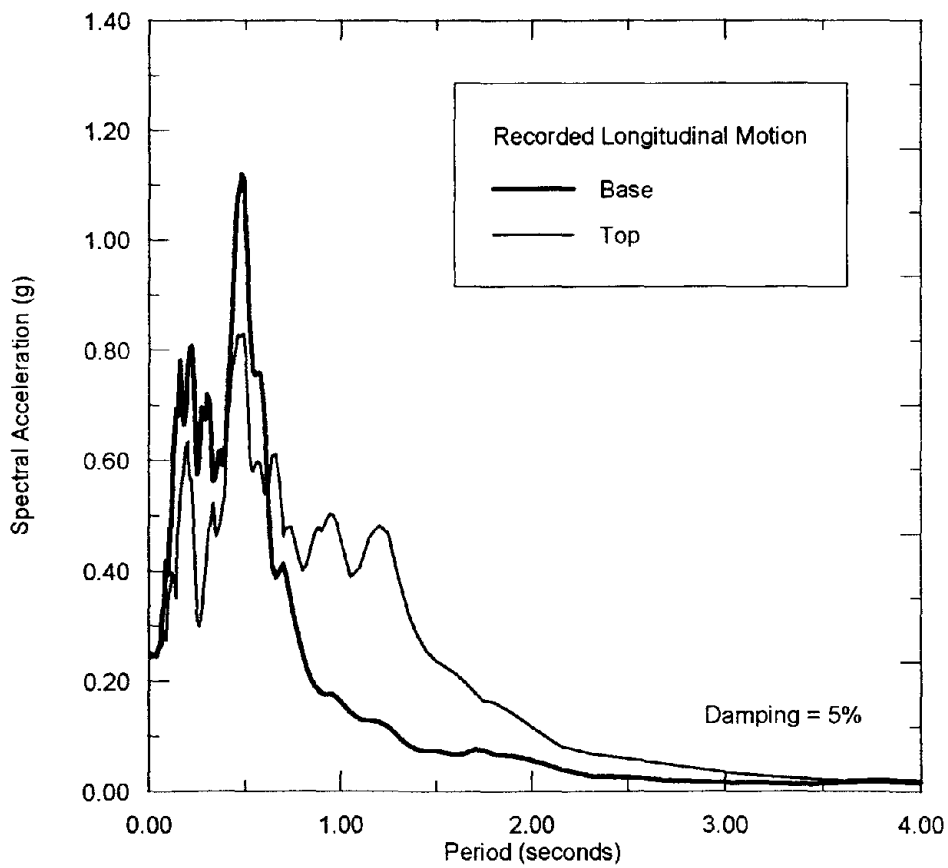
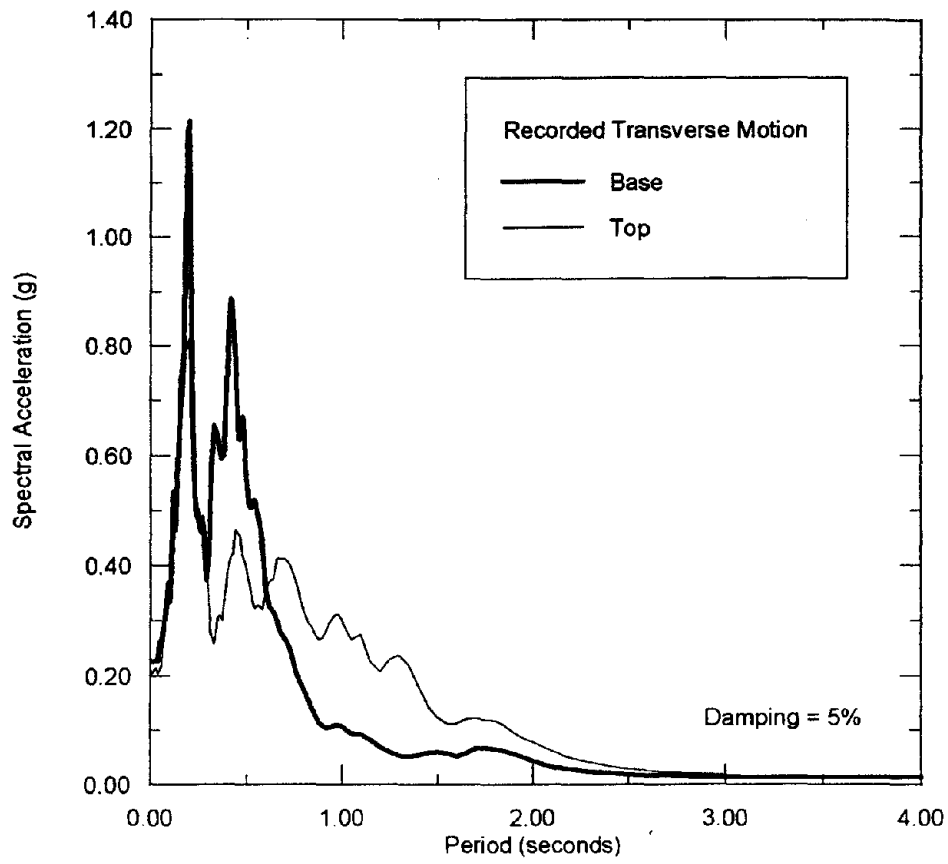


Fig. 6.71: Acceleration response spectra from the recorded motions at the OII Landfill

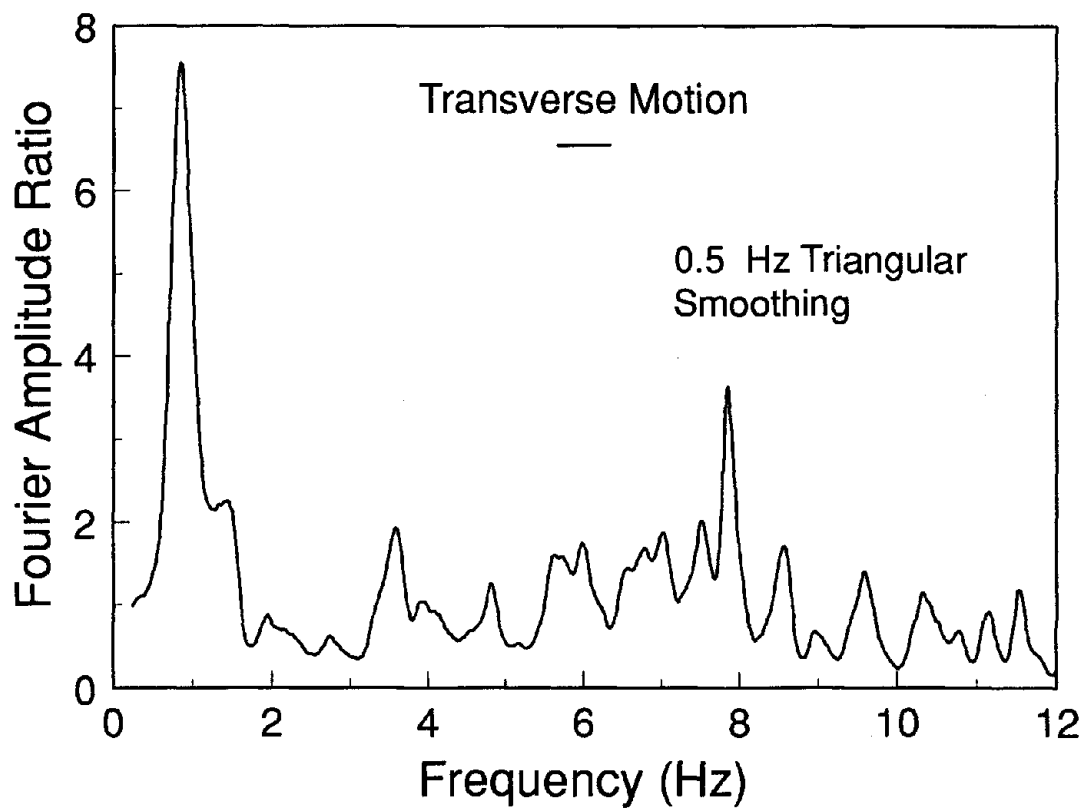
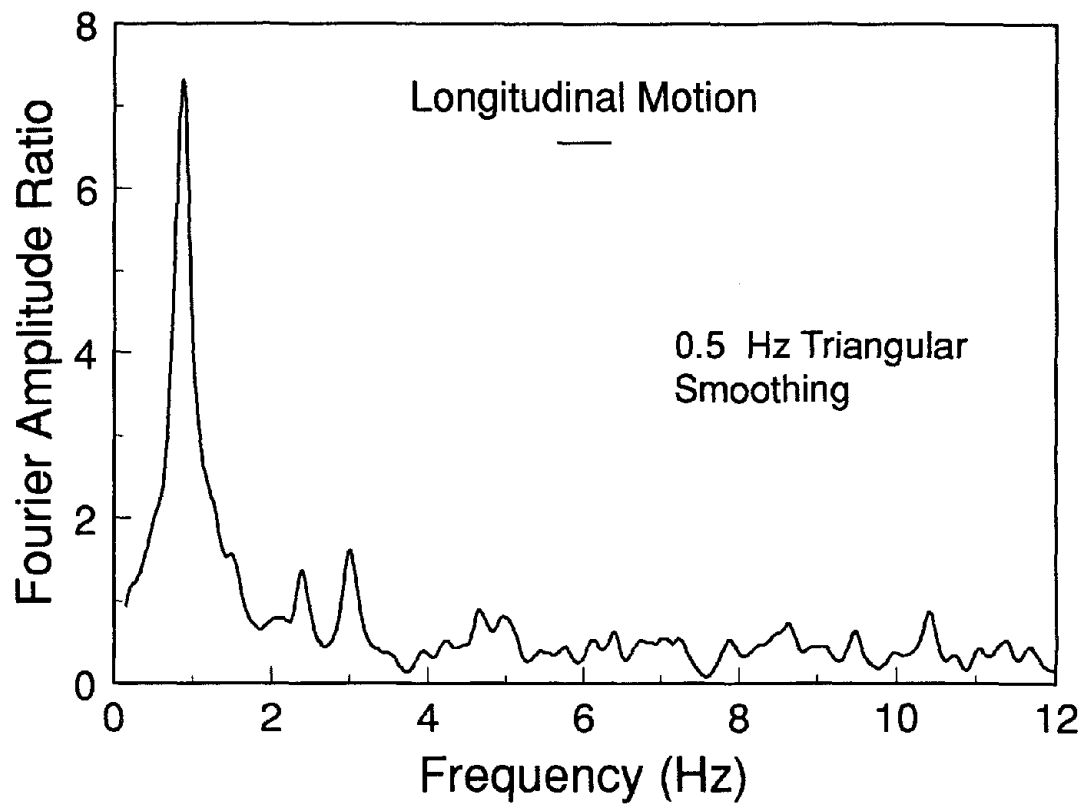


Fig. 6.72: Fourier amplitude ratios for the recorded motions at the OII landfill

input base motions. The program SHAKE91 (Idriss and Sun, 1992), which uses the equivalent linear model, was used for these analyses. The landfill was modeled as 75 m high with an unit weight varying linearly from 6.3 to 12.6 kN/m³ (40 to 80 pcf). The shear wave velocity was assumed to vary from 91 m/s (300 ft/s) at the top of the landfill to 366 m/s (1200 ft/s) near the bottom. The resulting model had an average shear wave velocity of 238 m/s (780 ft/s) and a period of 1.2 seconds. These values are consistent with the average shear wave velocities of between 204 and 244 m/s (670 and 800 ft/s) developed from seismic surveys of the OII landfill by Woodward Clyde Consultants (1982) and the Hushmand Associates (1994) measurements of the OII landfill's fundamental period at small strains of between 0.8 and 1.2 seconds. Other reasonable waste shear wave velocity profiles (i.e. $V_s = 91-244, 152-366, 152-455$ m/s) were used in the study to evaluate the sensitivity of the results to this parameter. Various shear modulus degradation and damping curves were also used in the SHAKE91 analyses. These included the curves proposed for waste by Singh and Murphy (1990), those proposed for clay with a plasticity index between 20 and 40 by Vucetic and Dobry (1991), and the shear modulus degradation curves proposed for sand by Iwasaki et al. (1976). These curves are shown in Figure 6.73. The ratio of the equivalent uniform shear strain to maximum shear strain (the SHAKE91 parameter "n") was taken to be $n = 0.5$ in most analyses. Although the equation given by Idriss and Sun (1992) in the SHAKE91 manual would recommend a value of 0.57 for the $M_w = 6.7$ earthquake, a value of 0.5 was chosen because of the relatively short duration of the earthquake and the few cycles at or near the maximum horizontal ground acceleration.

The analyses using the Singh and Murphy (1990) modulus degradation and damping curves provided the best match to the recorded motions at the top of the OII landfill, and the results from the SHAKE91 analysis of the baseline case using these curves are shown in Figure 6.74. In the longitudinal direction, the calculated acceleration response spectrum agreed well with the recorded motion in the period range of 0.4 to 0.9 seconds, but it under-predicted the motion in the high frequency range and under-predicted the spectral ordinate near the fundamental period of the landfill. In the transverse direction, the calculated acceleration response spectrum matched the recorded motion near the landfill's fundamental period, but again under-predicted the high frequency motion. Also, SHAKE91 predicted a larger than observed amplification of the spectral accelerations near the periods of 0.5 and 1.75 seconds. In both directions, the maximum horizontal acceleration was slightly under-predicted. The recorded MHA's were 0.25 g and 0.20 g in the longitudinal and transverse directions, respectively, while SHAKE91 predicted MHA's of 0.19 g and 0.16 g, respectively. The clay and sand modulus degradation and damping curves gave results that amplified the bedrock MHA and over-predicted the spectral response. Using higher and lower ranges of waste fill shear wave velocities did not improve the results. These results are preliminary, and more detailed analyses need to be performed to back-calculate the properties of the landfill and gain further insight into the landfill's seismic response.

6.6.3 Chiquita Canyon Landfill

At the Chiquita Canyon landfill, a moderate amount of damage occurred as a result of the earthquake. This damage includes cracks in the soil cover systems, tears in the geosynthetic liner system and a temporary shutdown of the gas removal system due to a loss

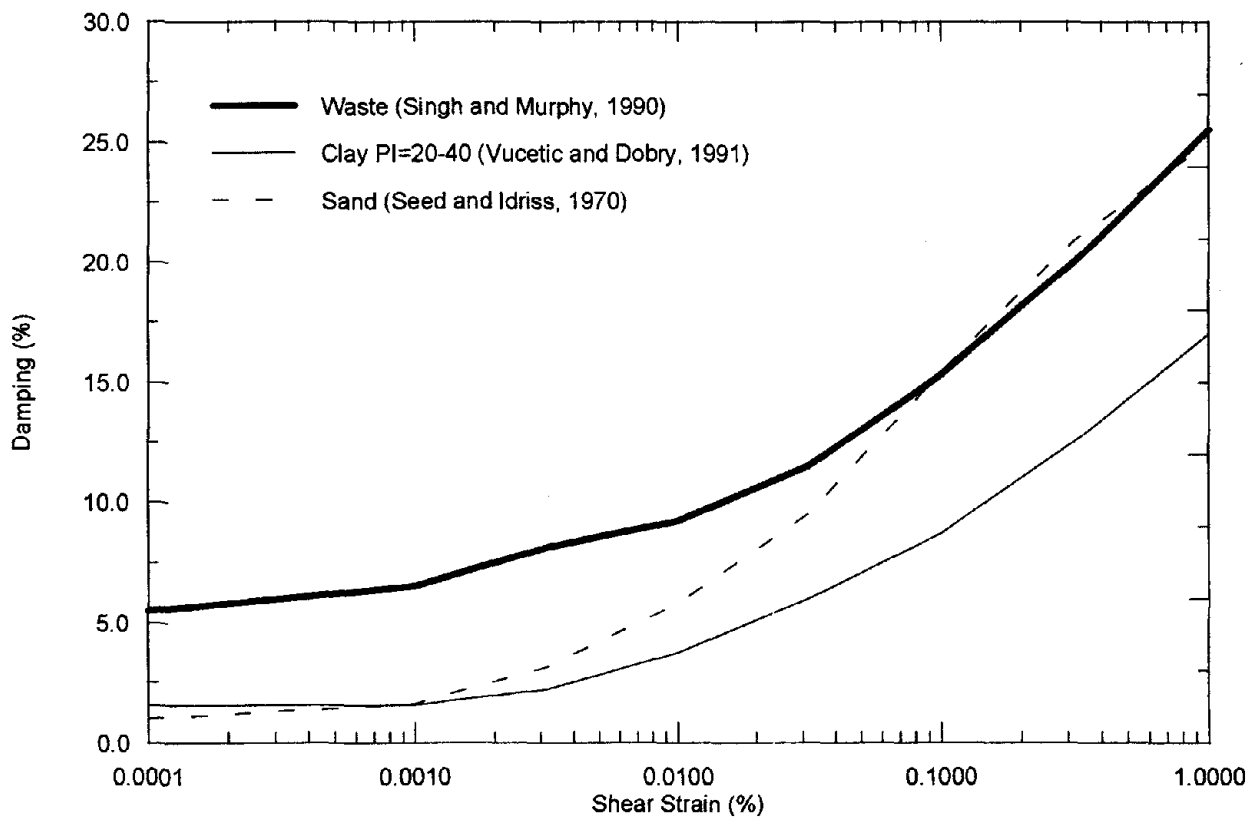
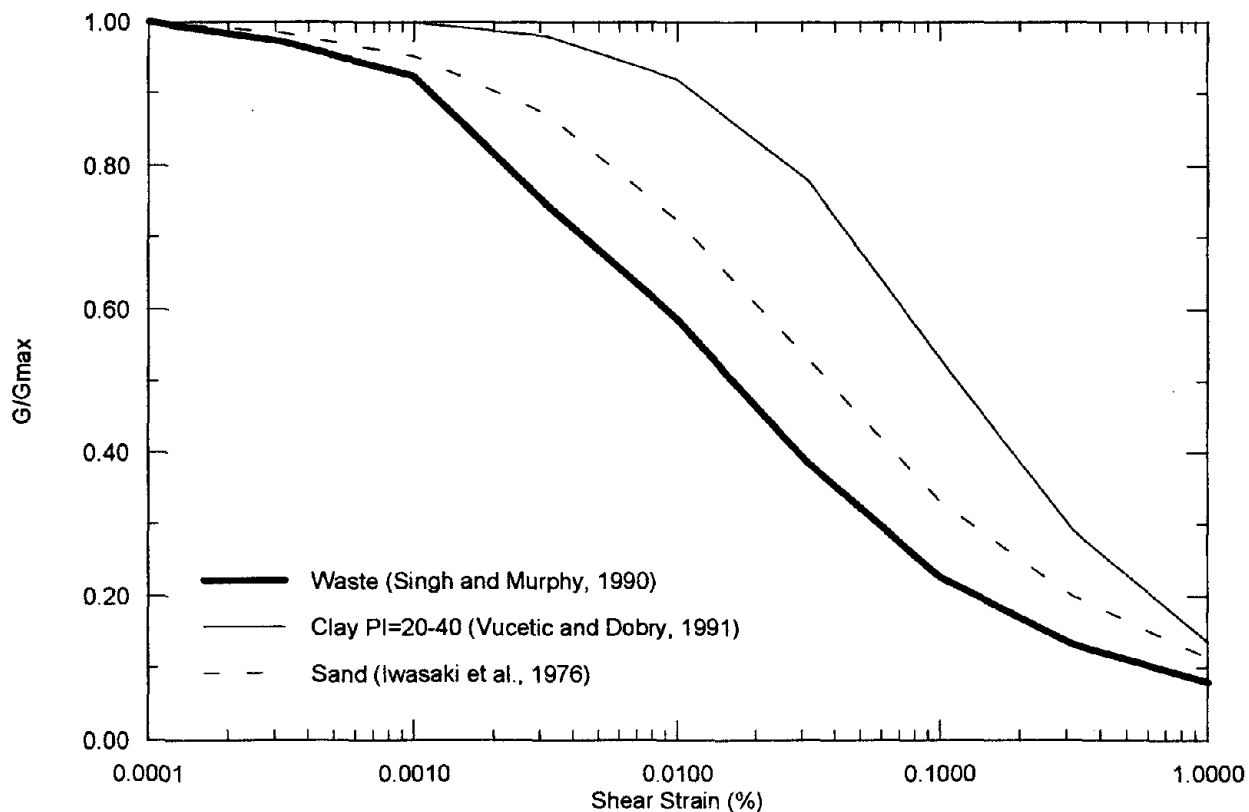


Fig. 6.73: Shear modulus degradation and damping curves used in SHAKE91 analyses

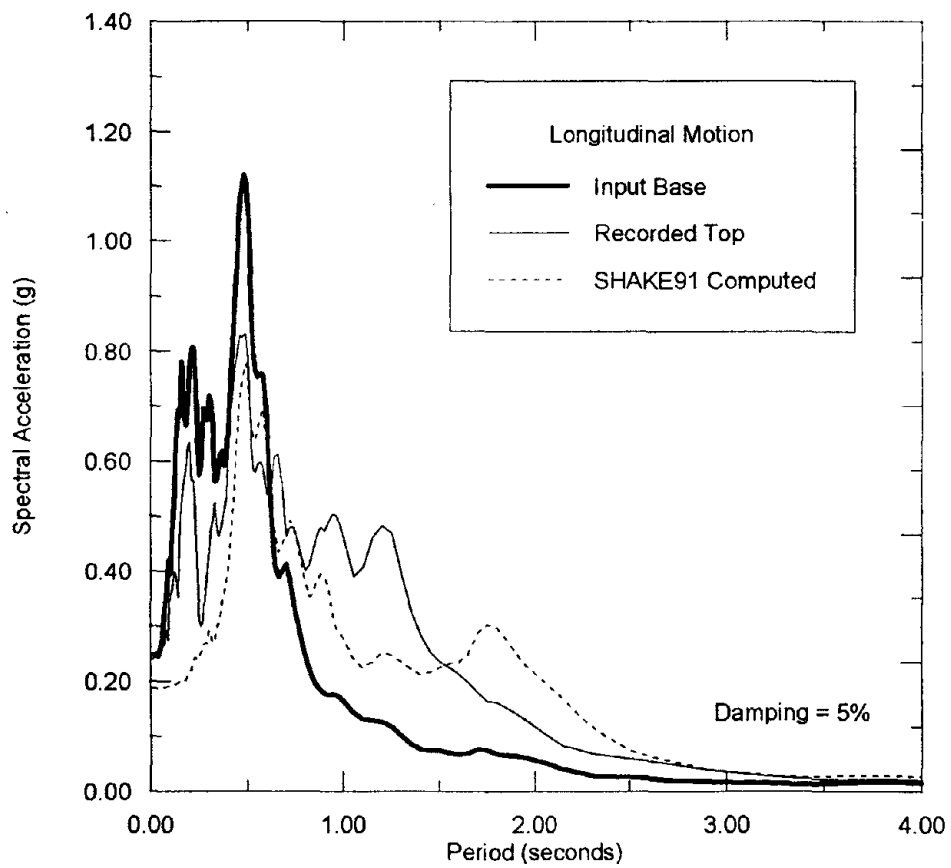
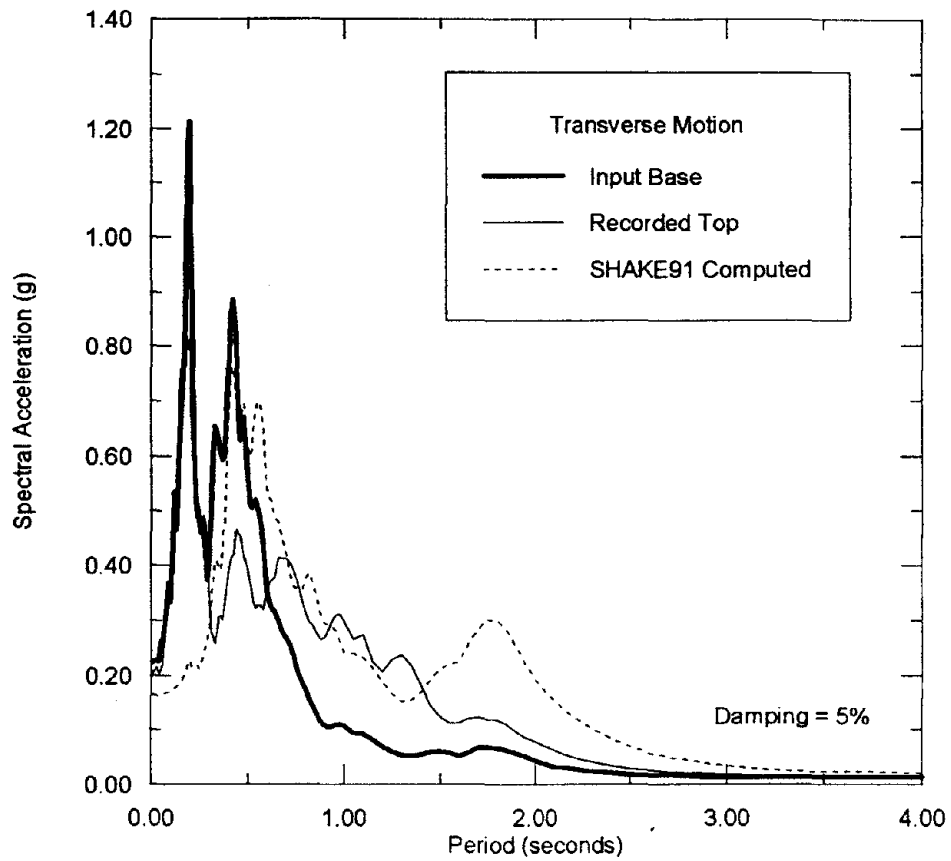


Fig. 6.74: Comparison of SHAKE91 results and recorded motions ($V_s = 91 - 366$ m/s, unit weight = $6.3 - 12.6$ kN/m³, $n = 0.5$) using Singh and Murphy (1990) shear modulus reduction and damping curves

of external power. The landfill is located in the city of Valencia just northwest of the Interstate Highway 5 / Highway 126 interchange, approximately 25 km north of the epicenter. Figure 6.64 shows the location of the landfill with respect to the surface projection of the fault rupture plane. The Chiquita Canyon Landfill is approximately 16 km from the zone of energy release, and California Strong Motion Instrumentation Program (CSMIP) seismograph stations in the area recorded peak ground accelerations on the order of 0.4g. The Idriss (1991) attenuation relationship for rock predicts a mean peak ground acceleration of approximately 0.3g at the Chiquita Canyon site for a Magnitude 6.7 earthquake event.

This MSW landfill is separated into several cells some of which are separated by canyons. Figure 6.75 is a plan view of the entire landfill. Figure 6.76 is an air photo of the landfill looking south towards the entrance of the landfill. The primary canyon, which is the original landfill unit, started operating in 1972 and stopped receiving waste in 1988. This area of the landfill has no liner system. Area (Cell) A was constructed with a 60-mil high density polyethylene (HDPE) single base liner system. Some of Canyon B was constructed with a 60-mil HDPE single base liner system, and the rest of this area has a single compacted soil/bentonite liner. Area C began accepting waste in 1991 and is the only area of the landfill currently accepting waste. At the time of the earthquake, portions of Area C were being excavated for use as daily cover for the section of Area C currently being filled (Phase 1, Cell C). The basal side slopes of Cell 1 are lined with a 60-mil smooth HDPE geomembrane single liner system. The base of this cell has a composite single liner system constructed with a 0.61 m-thick bentonite admix underlying a single-sided, textured HDPE geomembrane (textured side down). Figure 6.77 shows filling operations in Cell C four days after the earthquake. Figure 6.78 is a plan view of Cell C showing the contours of the waste fill. These contours were determined from a survey conducted 5 days after the earthquake. The slope in this area was graded at approximately 2H:1V. Area D, which is lined with a 60-mil HDPE, started receiving waste in 1989 and stopped receiving waste in 1991.

After the earthquake, cracks were observed in all cells of the landfill. Immediately after the earthquake, longitudinal cracks were observed at the top of the landfill along the interface between the landfill liner and the waste fill in Phase 1, Cell C. The cracks were approximately 30 cm wide at their widest, with a vertical offset of 15 to 30 cm, causing a localized tear in the geomembrane in one area of Cell 1. The tear, which occurred at the top of the slope near the anchor trench, was approximately 4 m long and 23 cm wide. Figure 6.79 shows the tear in the geomembrane liner at Chiquita Canyon. This tear occurred close to the anchor trench where the largest static (pre-seismic) stresses in the HDPE geomembrane would be expected as a result of the settlement and compaction of the waste fill.

Minor cracking was observed in the Primary Canyon and Canyon B. In areas A and D, cracks parallel to the top of the slope were observed in the soil cover. In area A, typical cracks were on the order of 15 cm wide with approximately 13 cm of vertical offset. Figure 6.80 shows the cracking along the top of the slope in Cell A. The cracks in Cell D were somewhat more pronounced. These cracks were as wide as 30 cm, with 20 cm of vertical offset exposing the HDPE liner in some areas. Figure 6.81 shows the type of cracking observed in Cell D where the liner system was exposed liner system. The California Integrated Waste Management board was notified in February 1994 that a second tear in the

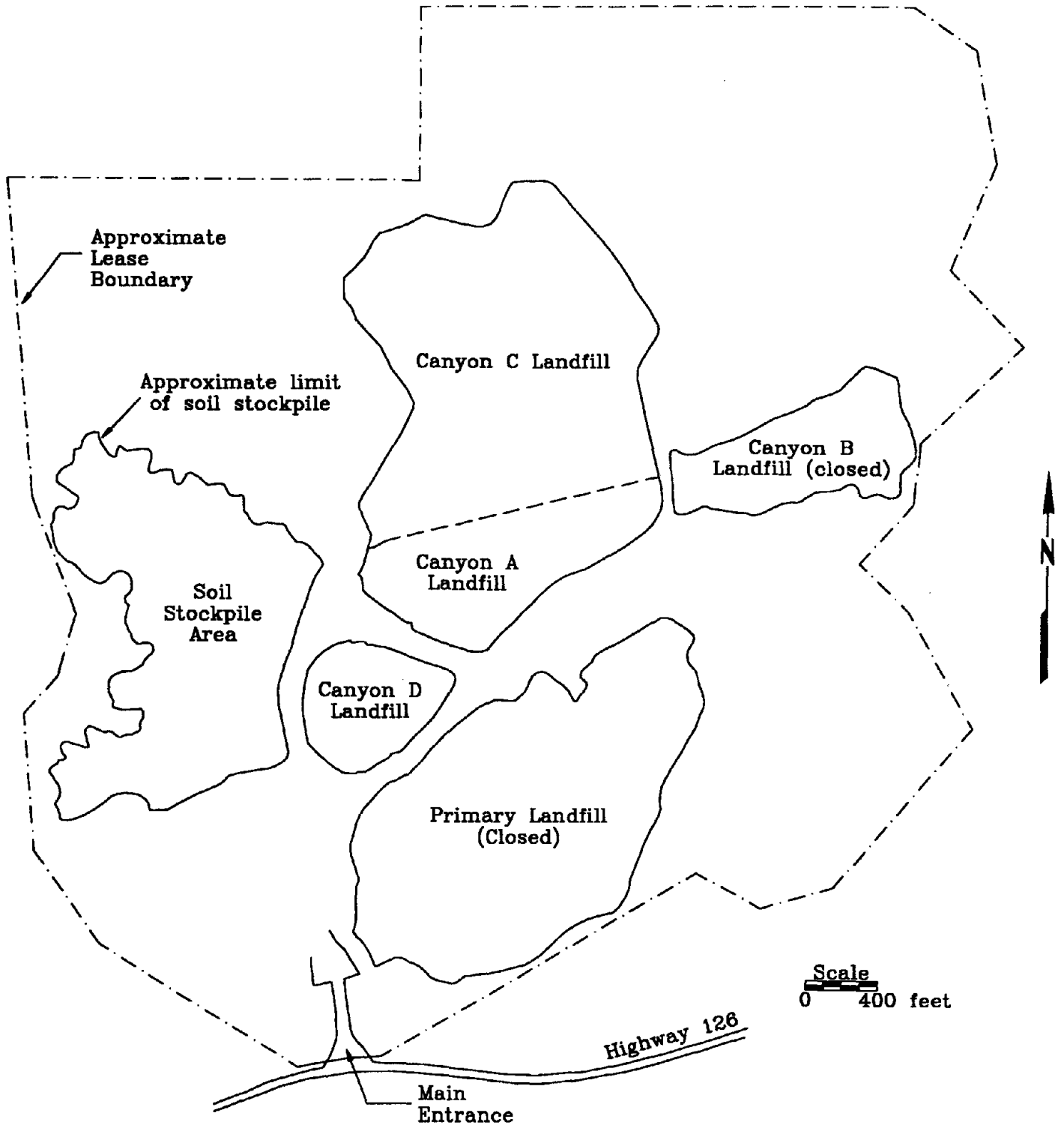


Fig. 6.75: Plan view of the Chiquita Canyon Landfill (adapted from EMCON Associates, 1994)



Fig. 6.76: Photo looking south towards the entrance of the Chiquita Canyon Landfill



Fig. 6.77: Waste placement operations in Cell C, four days after the Northridge Earthquake

Note:
Elevations shown are in feet.

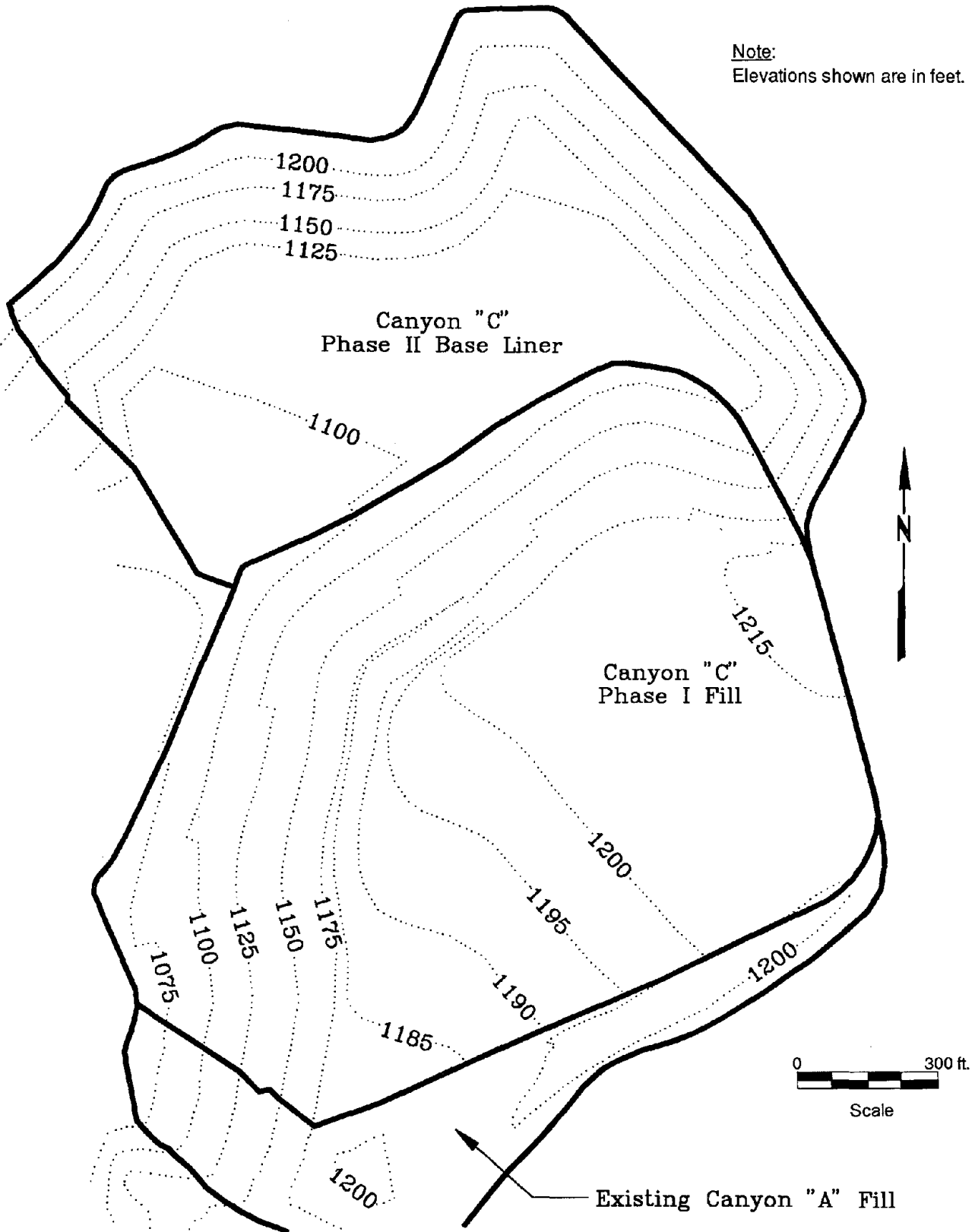


Fig. 6.78: Plan view of Cell C, Chiquita Canyon, showing contours of waste fill (adapted from Emcon Associates, 1994)



Fig. 6.79: Tear in HDPE geomembrane liner system, Cell C, Chiquita Canyon Landfill (photo courtesy of Calif. EPA, Integrated Waste Management Board)

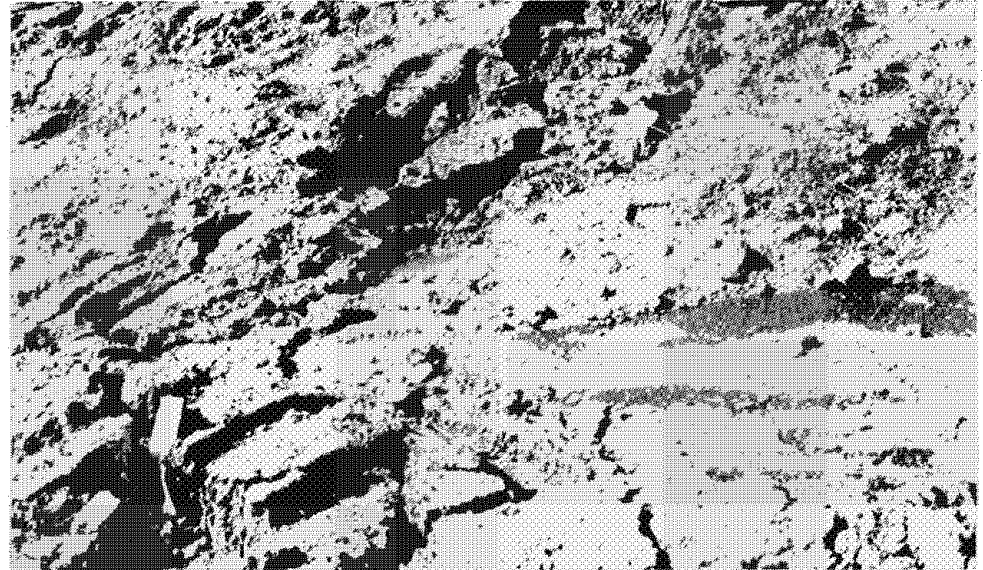


Fig. 6.80: Cracking along the top of the slope where the geomembrane liner was exposed, Cell D, Chiquita Canyon Landfill (photo courtesy of Calif. EPA, Integrated Waste Management Board)

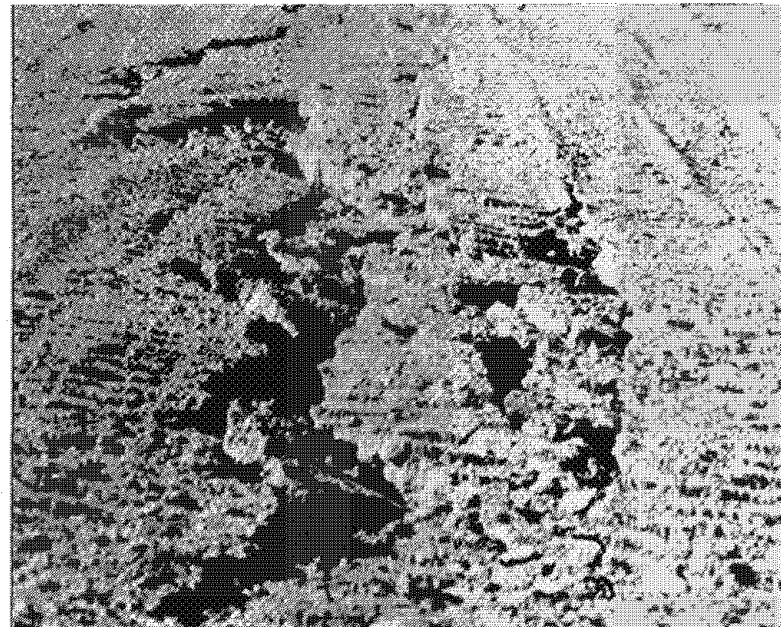


Fig. 6.81: Cracking along the top of the slope, Cell A, Chiquita Canyon Landfill (photo courtesy of Calif. EPA, Integrated Waste Management Board)

HDPE liner had been found in Cell D. The tear was approximately 23 m long and 30 cm wide. This tear was located by a gas technician monitoring for gas emissions (California Integrated Waste Management Board, 1994), and has not yet been studied as part of this investigation.

6.6.4 Sunshine Canyon Landfill

The Sunshine Canyon MSW landfill is located in the city of Sylmar just southwest of the Interstate Highway 5 / Highway 14 interchange approximately 11 km northeast of the epicenter. Figure 6.64 shows that this landfill is located close to the surface projection of the estimated fault rupture plane. The landfill is approximately 10 km from the zone of energy release. This landfill began operations in 1958 and has not been accepting waste since September 1991 and is awaiting final closure. The interim soil cover system is approximately 2.5 to 3.75 m thick. The landfill has no geosynthetic liner system. The landfill is constructed such that the south face of the landfill is the canyon wall. Figure 6.82 is a plan view of the Sunshine Canyon MSW landfill showing the contours of waste fill. The slope of the north face is graded at approximately 1.75H:1V. This slope has approximately a 2.5 m thick soil cover.

Strong motion stations in the area recorded peak ground accelerations on the order of 0.9g, but this may have been influenced by site effects and/or topographic effects. The Idriss (1991) rock attenuation relationship would predict a mean peak bedrock acceleration on the order of 0.4 g at this site for a Magnitude 6.7 event.

At the Sunshine Canyon site, longitudinal cracks were observed along the top of the waste fill along the interface with the natural canyon walls. The cracks varied from less than 2 cm to as much 30 cm wide, showing in some areas 15 to 30 cm of differential vertical offset. Figures 6.83, 6.84 and 6.85 show the cracking observed in the soil cover of the top deck at the western end of the Sunshine Canyon landfill after the earthquake. Figure 6.86 shows the crack in the soil cover in the center of the landfill near the water tank which was built on natural ground. This cracking did not appear to represent any threat of overall instability. It appeared instead to have been caused by settlement of the waste fill which occurred as a result of the earthquake shaking. However, it is difficult to differentiate cracking associated with ground shaking induced settlements from cracking at the back of the waste fill potentially resulting from limited downslope movement of waste along a failure plane. The landfill gas extraction system was temporarily shutdown due to a loss of power, and was restarted several days later.

6.6.5 Lopez Canyon Landfill

The Lopez Canyon MSW landfill is located in the San Gabriel mountains approximately 16 km east of the epicentral region (see Figure 6.64) The landfill is approximately 11 km from the zone of energy release. CSMIP recording stations in the area recorded peak ground accelerations on the order of 0.5g.

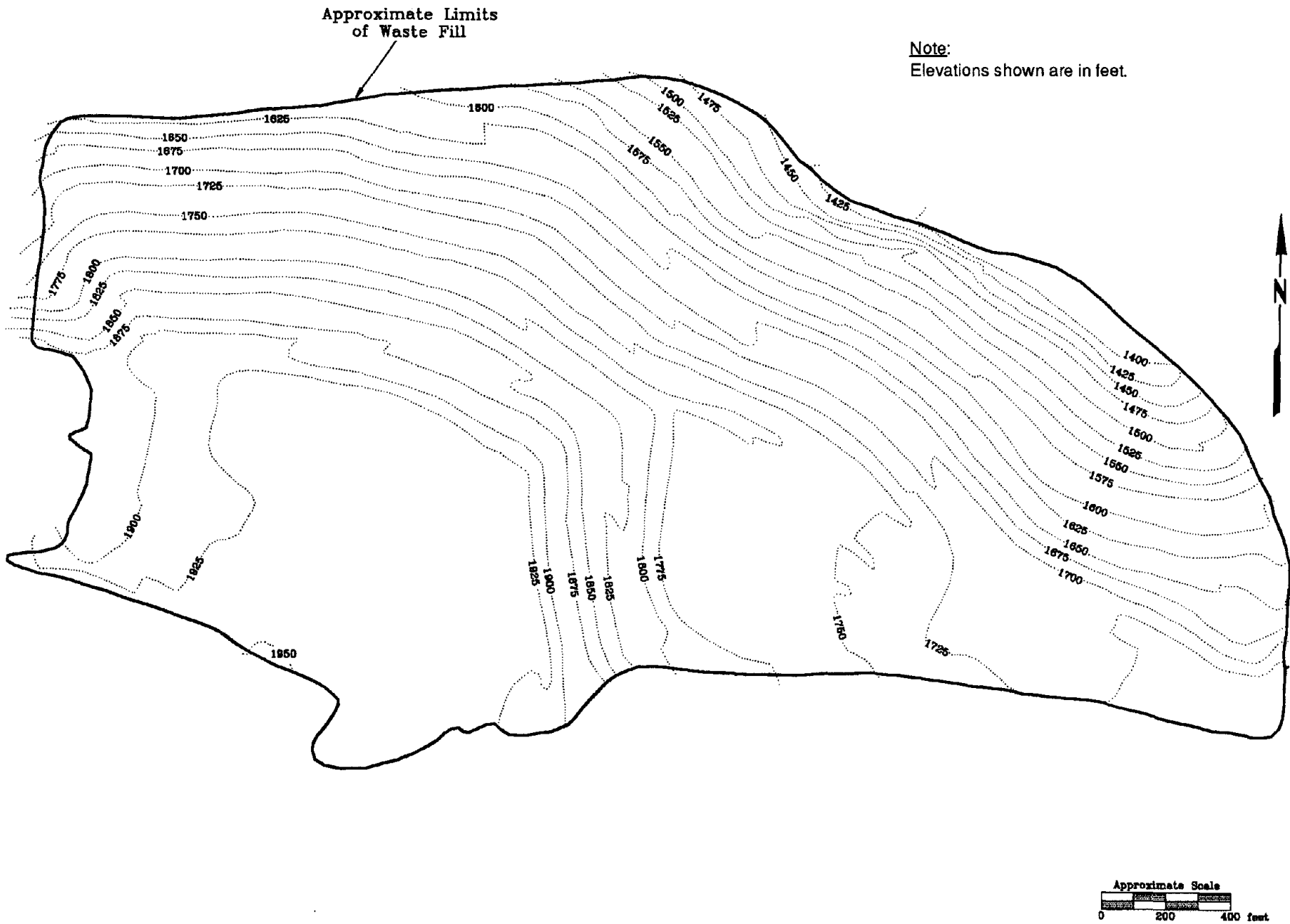


Fig. 6.82: Plan view of the Sunshine Canyon Landfill (adapted from PRA Group, 1992)

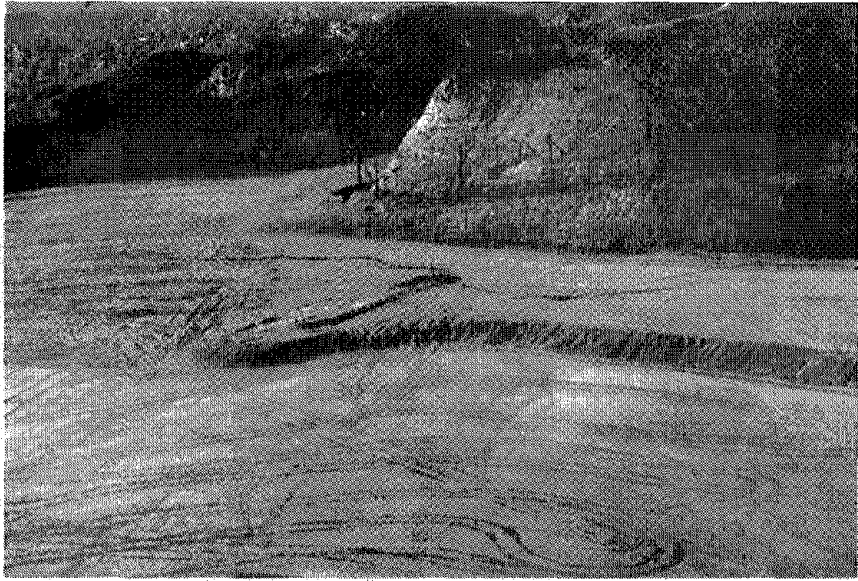


Fig. 6.83: Air photo of crack along the top deck at the western end of the Sunshine Canyon Landfill



Fig. 6.84: Crack along the top deck at the western end of the Sunshine Canyon Landfill (photo courtesy of Calif. EPA, Integrated Waste Management Board)

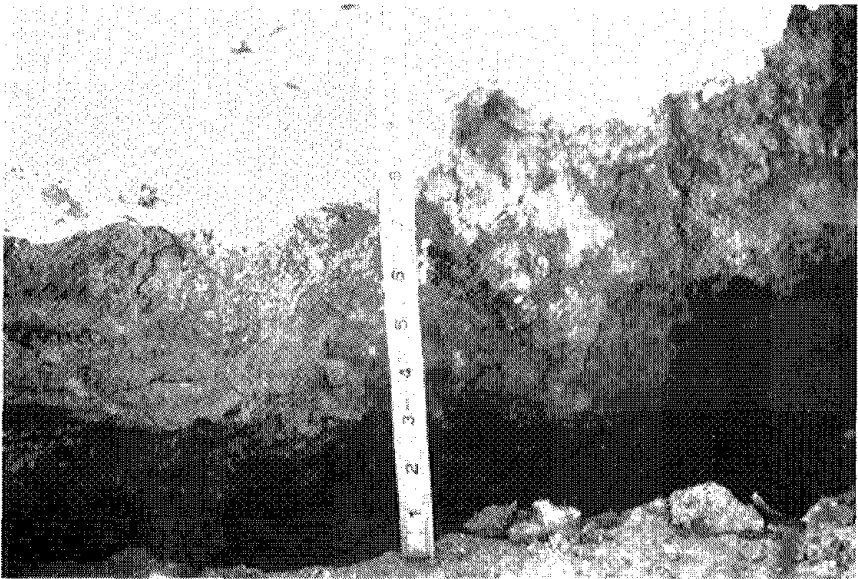


Fig. 6.85: Close-up of crack along the top deck at the western end of the Sunshine Canyon Landfill (photo courtesy of Calif. EPA, Integrated Waste Management Board)

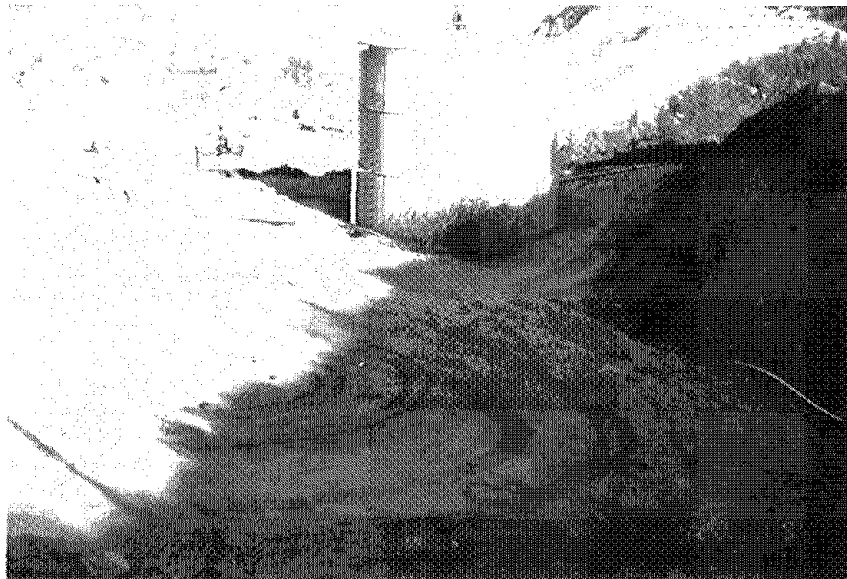


Fig. 6.86: Crack in the soil cover along the interface between the natural soil and the waste fill at the center of the Sunshine Canyon Landfill near the water tank

The Lopez Canyon landfill currently receives all of the municipal waste of the city of Los Angeles. The landfill is separated into four areas designated Disposal Area A, Disposal Area B, Disposal Area AB+ and Disposal Area C. Disposal Areas A,B, and AB+ are no longer accepting waste and are awaiting final closure. At the time of the earthquake, the western and northern sections of Area C were being filled. Figure 6.87 is a plan view of the layout of the Lopez Canyon Landfill. Figure 6.88 is a plan view of Disposal Area AB showing the contours of the waste fill. Figure 6.89 looks northeast towards the water tank from the southwestern end of Area C showing Area AB+ on the left hand side of the photograph.

At Lopez Canyon, minor cracking was observed in the interim soil cover at the interface between the older unlined waste fills and the natural canyon slopes. Landfill slopes in the unlined landfill cells are approximately 90 m high with an average slope angle of 2H:1V and locally as steep as 1.75H:1V. Figure 6.90 shows the interface between the southeastern end of Area AB and the natural canyon wall where cracks were observed. The cracks in this area were minor, typically being on the order of 2-3 cm wide (Figure 6.91). The cracking in the interim cover soils appeared to be brittle cracking caused by the difference in the relative stiffnesses of the older waste fill areas and the canyon walls. There was no sign of permanent relative displacement between the waste fill and the subgrade in the newer geosynthetically lined areas. The 1 million gallon water tank visible in Figure 6.89 ruptured during the earthquake. However, the water, which probably drained slowly since the rupture could not be located, was removed by the surface water runoff collection system shown in Figures 6.89 and 6.90 without erosion of the interim cover system. The landfill also suffered minor damage to the surface gas extraction system which was quickly repaired.

6.6.6 Other MSW Landfills

The Simi Valley, Calabasas, Scholl Canyon and Mission Canyon landfills experienced minor levels of cracking while the Puente Hills landfill suffered no apparent damage as a result of the earthquake. The Simi Valley landfill is located in Ventura County approximately 26 km west of the epicenter and 22 km west of the zone of energy release. The landfill was accepting waste at the time of the earthquake. The Calabasas landfill, which was also accepting waste, is located approximately 21 km from the epicenter and 23 km from the zone of energy release in the city of Agoura. Most of the landfill is unlined, however the eastern section of the site was constructed using a compacted clay liner and the northern section has a composite liner system. The Scholl Canyon landfill is located in the city of Glendale approximately 22 km east of the epicenter and 17 km east of the zone of energy release. This landfill has no liner system. The Mission Canyon landfill, which is closed, is located on Sepulveda Boulevard in the Santa Monica Mountains 14 km south of the epicenter and 21 km south of the zone of energy release. This landfill also has no liner system. The Puente Hills landfill is located in the city of Whittier approximately 54 km southeast of the epicenter and 56 km southeast of the zone of energy release. The majority of the landfill is unlined, however the northeast section has been constructed with a composite liner system.

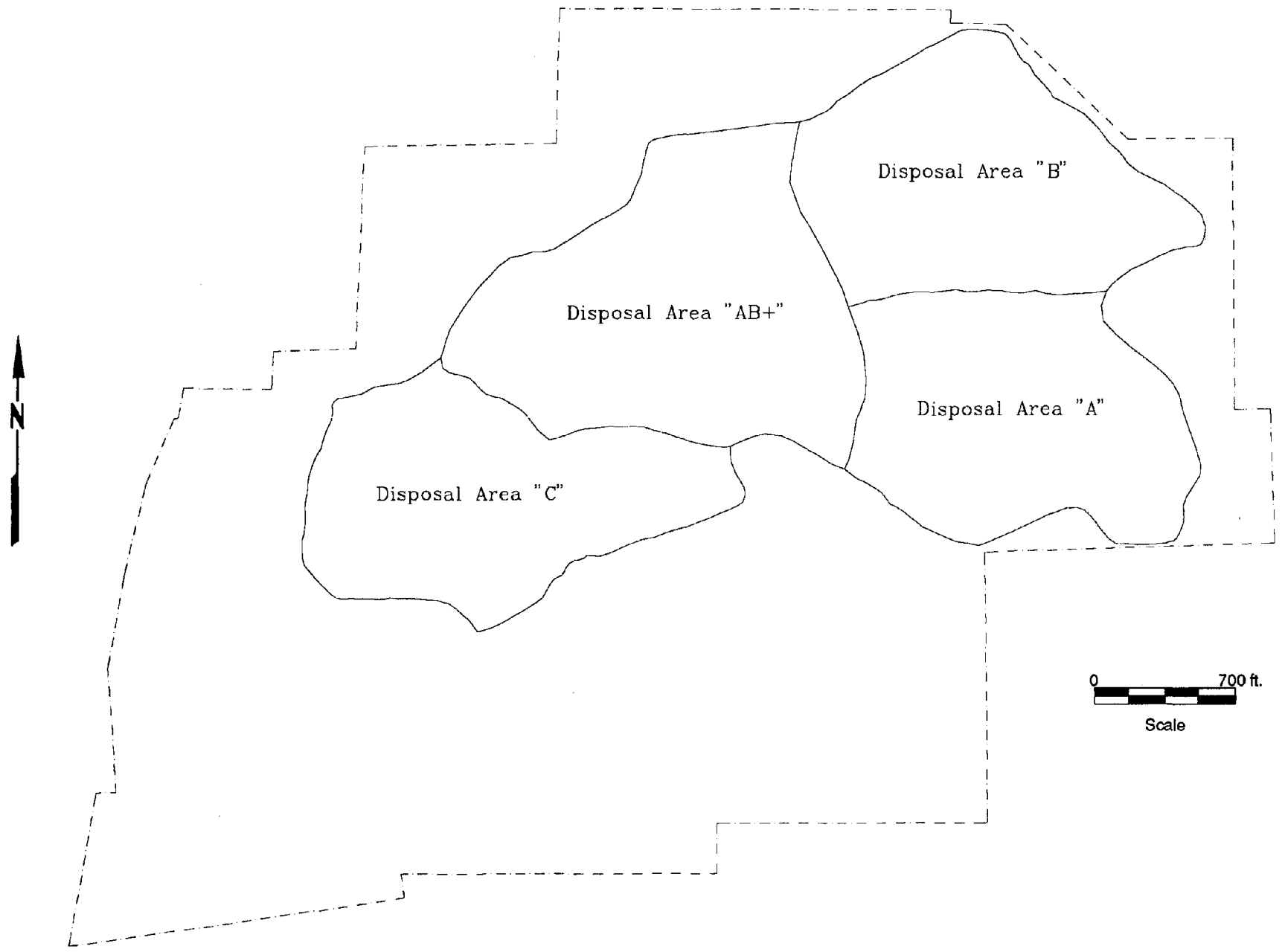


Fig. 6.87: General layout of the Lopez Canyon Landfill (adapted from Geosyntec, 1993)

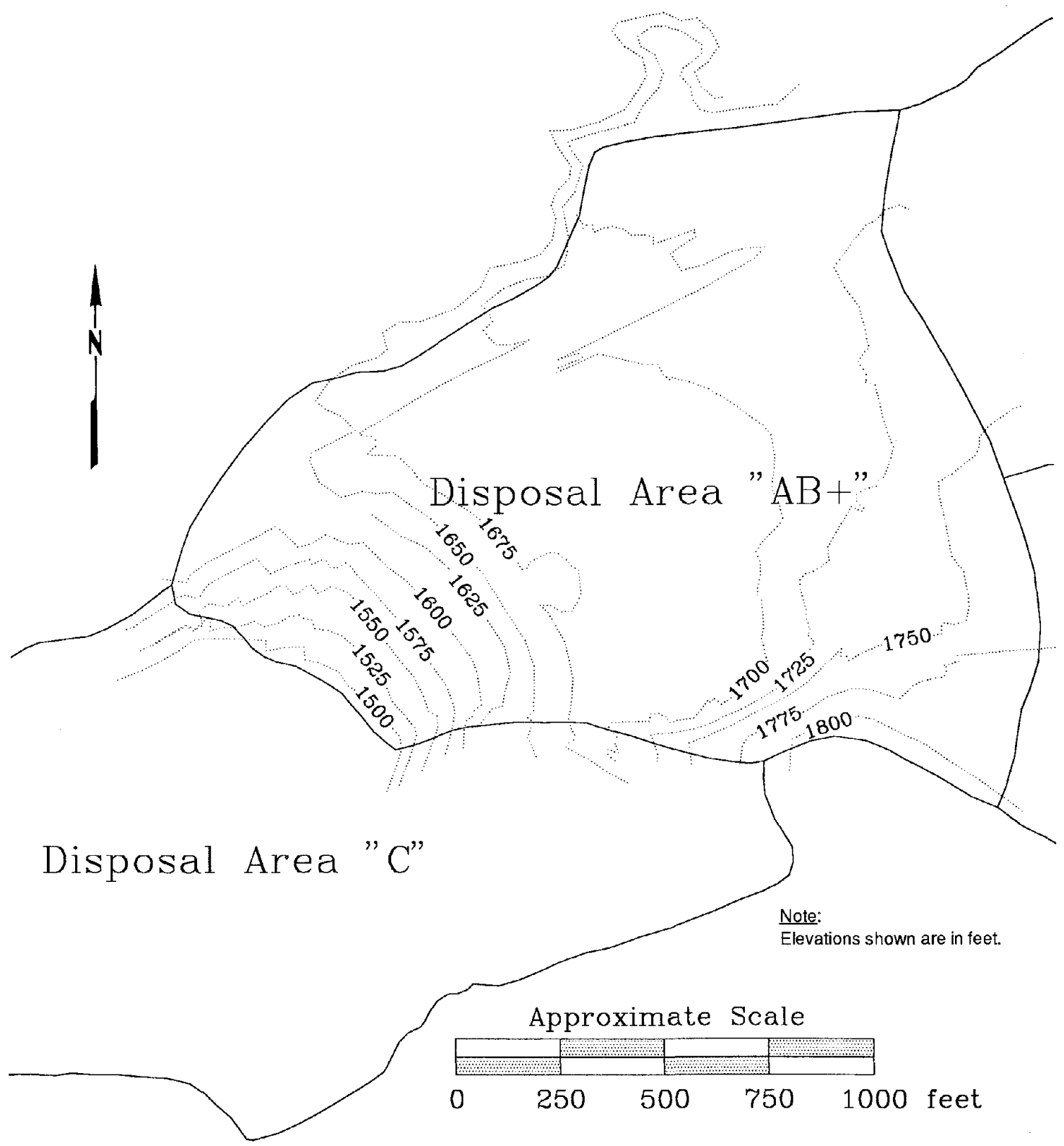


Fig. 6.88: Plan view of Disposal Area AB+ showing contours of waste fill (adapted from Geosyntec, 1993)

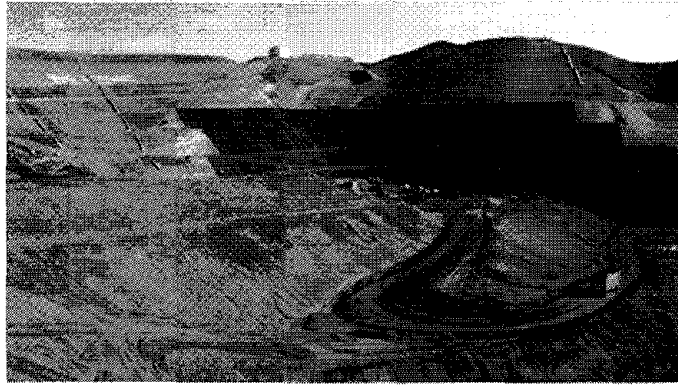


Fig. 6.89: Photo looking northeast towards the water tank taken from the southwestern end of Disposal Area C, Disposal Area AB+ is visible on the left hand side



Fig. 6.90: Photo of the interface between the waste fill of Disposal Area AB+ and the natural canyon walls where cracking was typically observed



Fig. 6.91: Close-up of crack observed at the interface between the waste fill and the natural canyon walls

6.6.7 Summary

Overall, the performance of landfills during the Northridge Earthquake was encouraging. None of the inspected landfills showed any signs of major instability. However, many of the inspected landfills experienced some form of cracking in the soil covers. This cracking may have resulted from one or more of the following: (a) brittle cracking of the stiffer soil veneer overlying the ductile waste fill; (b) settlement (dynamic compaction) of the waste fill; (c) limited downslope movement; or (d) cracking caused by the build up of landfill gas underneath the soil cover due to rapid release of gas produced by the shaking and/or the temporary loss of the gas extraction system. The temporary loss of a waste landfill's gas extraction system, which occurred at a number of landfills, is also an important consideration because of the potential for fire or explosion.

Ongoing studies are utilizing these observations, as well as collecting additional data, to investigate the seismic response of municipal solid waste landfills. These studies include collecting remote sensing data (aerial photography and infra-red imagery) that will be useful in assessing damage to landfill cover systems. Because of the major difficulties associated with laboratory evaluation of the dynamic properties of waste materials, field observations appear to present a more reliable means for obtaining these properties. However, at the present time the OII landfill is the only major landfill in the United States instrumented with strong motion accelerographs at which significant recordings have been obtained. As a result of the Northridge Earthquake, at least one other landfill is being instrumented with accelerographs. Increasing the number of instrumented landfills will provide valuable data regarding the seismic performance of landfills.

Chapter Seven: Summary and Conclusions

7.1 General

Although overall damage evaluations are not yet complete, the Northridge Earthquake of January 17, 1994 appears to have been the most costly natural disaster in U.S. history. Sixty-one fatalities and 18,500 injuries have been attributed to this earthquake, and more than 414,000 families were at least temporarily displaced from their homes. In addition to the well-publicized collapses of a number of highway structures, more than 14,000 buildings were damaged by the earthquake, and approximately 2,900 of these were sufficiently damaged as to be unsafe for entry. Current estimates of damage directly attributable to this earthquake are on the order of \$13 to \$15 billion.

These numbers reflect enormous losses, but these losses must be viewed in perspective. The Northridge event was a significant earthquake ($M_w = 6.7$) centered beneath one of the largest metropolitan areas of the United States. Although damage was widespread, loss of life was relatively low given the large population of the region. This was due in no small part to the fortuitous timing of the event in the early morning hours (4:30 a.m., PST), when many of the heavily damaged structures, including shopping malls and highway bridges, were largely deserted. However, the relatively low loss of life also serves as a testament to the significant advances made in earthquake engineering practice over the past 25 years. Nonetheless, the Northridge event has also demonstrated that much more remains to be done in this regard. The very high economic losses demonstrate a need to extend the current practice in seismic design of general structures, which is based primarily on protection of life safety, to further consideration of preservation of structural serviceability and minimization of losses so as to insure repairability.

The greater Los Angeles area continues to have a high seismic hazard; current estimates suggest a 70% cumulative probability of occurrence of one or more events of magnitude $M_w = 7.0$ or greater over the next 30 years in this seismically active region. Given this high level of seismic exposure, it is vitally important that further steps be taken to improve overall seismic safety in this populous region.

7.2 Ground Motions

The ground motions recorded at instrument stations situated on rock were, for the most part, not unusual for a West Coast event of this magnitude, and were generally well represented by existing attenuation relationships for motions on rock. Isolated exceptions were sites where unusual localized topographic conditions and/or shattering of the rock appear to have affected the motions recorded.

Geotechnical factors, including "local site effects" and "basin effects," appear to have significantly affected the severity of motions throughout the region, and appear to have contributed to significant concentrations of structural damage. Considerable damage occurred in the highly developed epicentral area, and additional concentrations of structural damage occurred in a number of other geographically well-defined areas including: (a) Sherman Oaks,

near Highway 101 just east of Highway 405, (b) Hollywood, north of Santa Monica Boulevard between Interstate Highway 5 and La Brea Avenue, (c) an arc in central Los Angeles just to the northeast of Culver City, (d) the Newhall area east of Interstate Highway 5 in Santa Clarita, and (e) Santa Monica, north of Colorado Avenue. With the exception of the damage concentrated in the Santa Monica area, a majority of the damage appears to have occurred within regions underlain by Holocene sediments. The damage in the Santa Monica area may represent an example of ground motion amplification due to deep, older, stiffer soils.

The severity of motions in the near-field region significantly exceeded those employed in the most widely used U.S. seismic building code provisions (UBC, 1991). This was due in large part to the fact that the UBC design spectra are "capped," or limited, to levels constrained by a maximum peak ground acceleration of 0.4g. Given the actual severity of motions recorded in the near-field epicentral region, and the widespread resultant damage, it appears that this limit on maximum levels of motion for code-based design merits reconsideration.

It is also important to note that the improvements in codes and in practice likely to occur as a result of the Northridge event will generally be applied initially to new construction, and so will do little to improve the levels of safety of existing facilities. Proper structural evaluation, with appropriate consideration of the influence of local ground conditions on the nature and severity of potential shaking in future events, can identify the structures and facilities at greatest risk. As a society, however, we have a poor history with respect to implementing the often difficult measures necessary to reduce this risk to existing structures.

7.3 Ground Failure

A significant geotechnical feature of the Northridge Earthquake was the occurrence of ground failure in portions of the epicentral area and several surrounding regions. The most heavily impacted regions were basin, valley, and coastal areas within approximately 35 miles of the epicenter. Damage resulting from soil liquefaction included thousands of pipe breaks, widespread disruption of pavements, and occasional structural distress.

Much of the ground failure resulted from liquefaction of near-surface soils, a mechanism well-recognized as representing a significant hazard to the engineered infrastructure. An important feature of the Northridge Earthquake, however, was the apparent occurrence of ground failure by other mechanisms such as deep soil liquefaction (producing "block-like" displacements and shifting of overlying intact soils) and dynamic ground compaction. These mechanisms appear to provide plausible explanations for the occurrences of ground failure in several areas which are believed to have deep groundwater (greater than 50 feet). Localized differential ground deformations associated with these mechanisms have often been thought to be relatively small, and hence not to represent a significant hazard to structures or other components of the infrastructure. This reasoning was tested to some degree during the Northridge Earthquake. While surface deformations believed to have resulted from these mechanisms were typically only of moderate consequence to structures, damage to critical "lifeline" systems such as buried pipelines was often relatively severe. Hence, these mechanisms would appear to represent a potential hazard to developed areas on a regional scale, although the local hazard (i.e. to a particular residence) may be relatively modest in many cases.

In general, available data suggests that the regional liquefaction microzonation techniques employed for Los Angeles County provided reasonably good insight regarding seismic ground failure hazards. However, a notable exception to this finding was the significant ground failure believed to have resulted from deep soil liquefaction and/or dynamic ground compaction. As these mechanisms do not pose the same level of high risk to structures typically associated with liquefaction of shallow soils, and as the mapping of such hazards might be relatively difficult, it may be impractical for many regional ground failure studies to incorporate such mechanisms. Nonetheless, it should be recognized by engineers that, in light of the data gathered following the Northridge Earthquake, ground failure can occur by several mechanisms in a variety of geologic conditions.

7.4 Landslides

The Northridge Earthquake caused hundreds of slope failures throughout the region. The most significant impact of these failures was the disruption of traffic along roads in the Santa Monica, San Gabriel, and Santa Susana Mountains. Fortuitously, in only one case, in Pacific Palisades, did sliding directly impinge upon and damage houses. Most of the failures occurred on natural slopes, and most of the slides were relatively shallow. Deep-seated landslides were rare, although the failures in the Ramona field and its vicinity were of substantial size and could have caused more significant damage had the area been more densely developed.

Overall, the pattern of landsliding caused by the Northridge Earthquake was quite consistent with that observed in previous earthquakes in this region, and in the 1989 Loma Prieta Earthquake. It should be noted that the Northridge Earthquake, like the Loma Prieta Earthquake, occurred during an unusually dry period for the time of the year, and therefore the amount of landslide damage may have been misleadingly light. Given the general propensity to continuously expand new development into more rugged and remote terrain, earthquake-induced landslide hazard must be given serious consideration.

7.5 Geotechnical Structures

Several dams of various sizes were subjected to moderate to strong ground motion from the 1994 Northridge Earthquake. With the possible exception of Pacoima Dam, all dams performed reasonably well, and no significant damage was sustained by any earth dams. However, the movements sustained at the partly saturated Upper and Lower San Fernando Dams (which were severely damaged in the 1971 San Fernando Earthquake but do not currently impound reservoirs) serve as a reminder of the potential instability of unimproved hydraulic fills during strong shaking. The only failure of a significant "dam" structure involved a flow slide of a tailings dam and its impounded tailings in Tapo Canyon, located north of Simi Valley. Fortunately, the area downstream of the flow slide is sparsely populated, and no injuries or deaths resulted from the failure.

Numerous hillside structural fills, largely constructed to establish road sections or building pads for structures, were damaged by the Northridge Earthquake. The mechanisms to which this distress has most commonly been attributed include: (a) ground failure or landsliding in underlying foundation soils or rock, (b) differential dynamic response between cut and fill

portions of building pads, and (c) settlement and lateral "bulging" of the fill due to deviatoric (shear) deformations and/or dynamic ground compaction. Earth retaining structures, including reinforced soil structures, soil nailed walls and crib walls, generally performed well during the Northridge Earthquake, although several cases of relatively poor performance were observed, including: (1) the failure of an approximately 5 meter-high conventional concrete retaining wall in Sherman Oaks, and (2) minor distress (such as wall movement, damage to structural elements, and settlement of the backfill) to several concrete crib retaining walls in Universal City and Woodland Hills.

The overall performance of solid waste landfills during the Northridge Earthquake was encouraging, as none of the inspected landfills showed any signs of major instability. However, many of the inspected landfills experienced some form of cracking in the soil covers, which may have resulted from one or more of the following: (a) brittle cracking of the stiffer soil veneer overlying the ductile waste fill; (b) settlement (dynamic compaction) of the waste fill; (c) limited downslope movement; or (d) cracking caused by the build up of landfill gas beneath the soil cover due to rapid release of gas produced by the shaking and/or the temporary shutdown of the gas extraction system. In addition, HDPE liner systems were slightly torn at one landfill as a result of earthquake shaking.

The ability to investigate the seismic response of municipal solid waste landfills had been hampered, until the 1994 Northridge Earthquake, by a lack of data from instrumented landfills. A significant case history is provided by the OII landfill, located in the City of Monterey Park. The landfill is well-instrumented with survey monuments, inclinometers and a pair of strong motion recording stations (one on top of the waste fill, and one adjacent to the toe of the fill). The strong motion recordings and other instrumentation data obtained present a unique opportunity to study the deformations resulting from seismic loading and to back-calculate the dynamic properties of the waste fill, as several earthquake events with different levels of excitation have now been recorded at this site.

7.6 Conclusions

The Northridge Earthquake of January 17, 1994 serves as a reminder of the unacceptably high level of seismic risk associated with the likely occurrence of larger and considerably more damaging future earthquakes both in the greater Los Angeles Area and around the world. There is an urgent need to pursue the research opportunities provided by the Northridge Earthquake, and to rapidly transfer the benefits of such research into the mainstream of professional practice. In addition, there is also an urgent need to educate policy makers, the insurance industry, and the general public, and to motivate them to undertake the often difficult actions necessary to begin to remediate the levels of seismic hazard exposure associated with existing conditions.

References

- Abrahamson, N.A. and Silva, W.J. (1993). "Attenuation of Long Period Strong Ground Motions," Proceedings, American Society of Mechanical Engineers, PZP, Denver, Colorado, July.
- Anderson, D.G., Hushmand, B. and Martin, G.R. (1992). "Seismic Response of Landfill Slopes", Stability and Performance of Slopes and Embankments, ASCE Geotechnical Special Publication No. 31, Berkeley, CA.
- Bausch, D., Gath, E.M., Gonzalez, T., Dolan, J., and Sieh, K. (1992). "Application of New Developments in Seismic Hazard Assessment, Revised Safety Element of the General Plan, City of Santa Monica, California," Proceedings of the 35th Annual Meeting, Association of Engineering Geologists, October
- California America Water Company (1994). Personal communication with Bernie Quiroga regarding locations of water pipe breaks.
- California Division of Mines and Geology (1965). "Geologic Map of California, Bakersfield Sheet," Scale 1:250,000.
- California Division of Mines and Geology (1962). "Geologic Map of California, Long Beach Sheet," Scale 1:250,000.
- California Division of Mines and Geology (1969). "Geologic Map of California, Los Angeles Sheet," Scale 1:250,000.
- California Division of Mines and Geology (1969). "Geologic Map of California, San Bernardino Sheet," Scale 1:250,000.
- California Division of Mines and Geology (1962). "Geologic Map of California, San Diego-El Centro Sheet," Scale 1:250,000.
- California Division of Mines and Geology (1966). "Geologic Map of California, Santa Ana Sheet," Scale 1:250,000.
- California Division of Mines and Geology (1963). "Geologic Map of California, Trona Sheet," Scale 1:250,000
- California Integrated Waste Management Board (1994). "Observations of Landfill Performance, Northridge Earthquake of January 17, 1994", Internal Report to Director of Permitting and Enforcement Division.
- California State Fire Marshall (1994). Personal communication (fax) with Charles Samo of the Pipeline Safety Division regarding locations of oil pipeline breaks.
- Campbell, K.W., Chieruzzi, R., Duke, C.M., and Lew, M. (1970). "Correlations of Seismic Velocity with Depth in Southern California," UCLA-ENG-7965, October.
- City of Beverly Hills (1994). Personal communication (fax) with Howard Fischkes regarding water pipe break locations.
- City of Culver City (1994). Personal communication with Kyle Snay regarding locations of water pipe break locations.

- City of Los Angeles (March 1994). Map of "Earthquake Damage Sites, January 17, 1994, in the City of Los Angeles", prepared by the Land Development and Mapping Division, damage assessment provided by the Department of Building and Safety.
- City of Los Angeles, Department of Water and Power (1994). Maps showing locations of water pipe breaks and leaks reported by customers in the West Valley, East Valley, and Western Service Areas following the Northridge Earthquake, Graphics, Maps and Records Group.
- City of Los Angeles, Department of Water and Power (1994). Miscellaneous data regarding dams.
- City of Redondo Beach (1994). Personal communication with Desi Alvarez regarding damages at Mole B and Seaside Lagoon.
- City of San Fernando (1994). Personal communication with Jerry Wedding regarding damages within city limits.
- City of Santa Clarita (1991). "Safety Element of the City of Santa Clarita General Plan", June.
- City of Santa Monica (1994). Map of "Damage Assessment in Santa Monica," prepared by ISD-GIS, March.
- City of Santa Monica (1994). Personal communication with William Buol regarding water pipe break locations.
- Collin, J.G., Chouery-Curtis, V.E. and Berg, R.R., (1992). "Field Observation of Reinforced Soil Structures under Seismic Loading", Earth Reinforcement Practice, Proceedings of a symposium held in Fukuoka, Vol. 1, Japan, pp. 223-228.
- Conrey, B.L. (1967). "Early Pliocene History of the Los Angeles Basin, California," California Division of Mines and Geology, Special Report 93.
- Cooke, R.U. (1984). "Geomorphological Hazards in Los Angeles; A study of slope and sediment problems in a metropolitan county," The London Research Series in Geography, George Allen and Unwin, London.
- Dames and Moore (undated). "Report of Foundation Investigation, Proposed Office Building, Main Street and Seaside Terrace, Santa Monica, California, for The Rand Corporation," provided by the City of Santa Monica.
- Dames and Moore (1994). "The Northridge Earthquake of January 17, 1994", special report.
- Darragh, R. et al. (1994). "Processed CSMIP Strong-Motion Records from the Northridge, California Earthquake of January 17, 1994: Releases 1 through 4 (complete) and Releases 5 and 6 (incomplete), Reports No. OSMS 94-06B, 94-08, 94-09, 94-10, 94-11A, 94-11C, 94-11D, and 94-12A, various dates February through June 1994.
- Davis, T.L. and Namson, J.S. (1994). "A Balanced Cross-Section Analysis of the 1994 Northridge Earthquake and Thrust Fault Seismic Hazards in Southern California", Northridge Abstracts Program for the 89th Annual Meeting of SSA, nr 37.
- Dibblee, T.W. (1991). "Geologic Map of the Beverly Hills and Van Nuys (South ½) Quadrangles, Los Angeles County, California", Dibblee Geological Foundation Map #DF-31.
- Dibblee, T.W. (1991). "Geologic Map of the Hollywood and Burbank (South ½) Quadrangles, Los Angeles County, California", Dibblee Geological Foundation Map #DF-30.

- Dibblee, T.W. (1991). "Geologic Map of the San Fernando and Van Nuys (North ½) Quadrangles, Los Angeles County, California", Dibblee Geological Foundation Map #DF-33.
- Dibblee, T.W. (1992). "Geologic Map of the Oat Mountain and Canoga Park (North ½) Quadrangles, Los Angeles County, California", Dibblee Geological Foundation Map #DF-36.
- Donnellan, A. (1994). Personal communication.
- Donnellan, A., Lyzenga, G.A., Hager, B.H., and King R.W. (1994). "Relation Between Geodetic Observations in the Ventura Basin and the Northridge Earthquake and Post-Seismic Motions Associated with the Earthquake", Northridge Abstracts Program for the 89th Annual Meeting of SSA, n 41.
- Dreger, D.S. (1994). "Empirical Green's Function Study of the January 17, 1994 Northridge Mainshock (Mw=6.7)," Geophysical Research Letters (in press).
- Dreger, D., Pasyanos, M., Loper, S., McKenzie, R., Gregor, N., and Romanowicz, B. (1994). "The January 17, 1994 Northridge Earthquake: A Regional Perspective", Northridge Abstracts Program for the 89th Annual Meeting of SSA, nr 11.
- Dreger, D.S. and Helmberger, D.V. (1993). "Determination of Source Parameters at Regional Distances with Three-Component Sparse Network Data", J. Geophys. Res., 98, 8107-8125.
- Duke, C.M., Johnson, J.A., Kharraz, Y., Campbell, K.W., and Malpiede, N.A. (1971). "Subsurface Site Conditions and Geology in the San Fernando Earthquake Area," UCLA-ENG-7206, December.
- Duke, C.M. and Johnson, J.A. (1973). "Subsurface Geology of Portions of San Fernando Valley and Los Angeles Basin," San Fernando, California, Earthquake of February 9, 1971, U.S. Department of Commerce, National Oceanic and Atmospheric Administration, Volume III, pp. 155-164.
- Eguchi, R.T., Campbell, K.W., Duke, C.M., Chow, A.W., and Paternina, J. (1976). "Shear Velocities and Near-Surface Geologies at Accelerograph Sites that Recorded the San Fernando Earthquake," UCLA-ENG-7653, June.
- Federal Emergency Management Agency (1994). "Building and Safety Structure Damage Assessment", Northridge Earthquake Disaster DR-1008, map.
- Fumal, T.E., Gibbs, J.F., and Roth, E.F. (1981). "In-situ Measurements of Seismic Velocity at 19 Locations in the Los Angeles, California Region," USGS Open-File Report 81-399.
- Fumal, T.E., Gibbs, J.F., and Roth, E.F. (1984). "In-situ Measurements of Seismic Velocity at 16 Locations in the Los Angeles, California Region," USGS Open-File Report 84-681.
- Gath, Eldon (1992). "Geologic Hazards and Hazard Mitigation in the Los Angeles Region", in Engineering Geology Practice in Southern California, Bernard W. Pipkin and Richard J. Proctor, Eds., Special Publication No. 4 of the Association of Engineering Geologists, Southern California Section, Star Publishing Company.
- Geomatrix Consultants, (1994). Personal communication (fax) with F.I. Makdisi regarding geologic site classification of selected USGS strong-motion stations, May.
- Gillibrand, Phil (1994). Personal communication related to Tapo Canyon Tailings Dam.

- Hall, J.F. editor (1994). "Preliminary Reconnaissance Report, Northridge Earthquake, January 17, 1994," Earthquake Engineering Research Institute, March.
- Hanks, T.C. (1975). "Strong Ground Motion of the San Fernando California Earthquake", *Bull. Seism. Soc. Am.*, 65, 193-225.
- Harding-Lawson Associates (1980). "Geotechnical Engineering Investigation, Santa Monica City Hall Addition, Santa Monica, California," HLA Job No. 9851,001.11, February.
- Hauksson, E. and Jones, L. (1989). "The 1987 Whittier Narrows Earthquake Sequence in Los Angeles, Southern California: Seismological and Tectonic Analysis", *Journal Geophys. Res.*, 94, 9569-9589.
- Hauksson, E., Hutton, K., Kanamori, H., Jones, L., and Mori, J. (1994). "The M_w 6.7 Northridge, California, Earthquake of January 17, 1994 and its Aftershocks", Northridge Abstracts Program for the 89th Annual Meeting of SSA, nr 4.
- Hayden, R. (1994). Chapter on Port Facilities in "Special Publication on Northridge Earthquake", published by ASCE Technical Committee on Lifelines and Earthquake Engineering. (in press).
- Heaton, T.H. (1982). "The 1971 San Fernando Earthquake: A Double Event?," *Bulletin of the Seismological Society of America*, Vol. 72, No. 6, pp. 2037-2062, December.
- Heaton, T.H. and Helmberger, D. (1979). "Generalized Ray Models of the San Fernando Earthquake, *Bull. Seism. Soc. Am.*, 69, 1311-1341.
- Hudnut, K.W., Murray, M.H., Donnellan, A. et al. (1994). "Co-Seismic Displacements of the 1994 Northridge, California, Earthquake", Northridge Abstracts Program for the 89th Annual Meeting of SSA, nr 14.
- Hushmand, B., Anderson, D.G., Crouse, C.B. and Robertson, R.J. (1990). "Seismic monitoring and Evaluation of a Solid Waste Landfill", *Proceedings 4th U.S. National Conference on Earthquake Engineering*, Palm Springs, CA.
- Hushmand Associates (1994). "Landfill Response to Seismic Events", Technical Report to CDM Federal Programs, Hushmand Associates, Laguna Niguel, CA.
- Idriss, I.M. (1991). "Earthquake Ground Motions at Soft Soil Sites," *Proceedings: Second International Conference on Recent Advances in Geotechnical Earthquake Engineering and Soil Dynamics*, March.
- Idriss, I.M. and Sun, J.I. (1992). "User's Manual for SHAKE91, A Computer Program for Conducting Equivalent Linear Seismic Response Analyses of Horizontally Layered Soil Deposits, Program Modified based on the Original SHAKE program published in December 1972 by Schnabel, Lysmer & Seed," August.
- Idriss, I.M. (1993). "Procedures for Selecting Earthquake Ground Motions at Rock Sites, A Report to the National Institute of Standards and Technology," University of California at Davis, March.
- James E. Slosson & Associates (1972). "Geologic-Seismic Investigation, Proposed Veterans Administration Hospital Site, Santa Monica, California," October.
- Jensen Design Group (1994). "Tapo Canyon Dike Restoration", maps.
- Joyner, W.B., and Boore, D.M. (1988). "Measurement, Characterization, and Prediction of Strong Ground Motion," *Earthquake Engineering and Soil Dynamics II-Recent Advances in Ground-Motion Evaluation*, ASCE Geotechnical Special Publication No. 20, June.

- Langston, C.A. (1978). "The February 9, 1971, San Fernando Earthquake: a Study of Source Finiteness in Teleseismic Body Waves", *Bull. Seism. Soc. Am.*, 68, 1-29.
- Leighton and Associates (1972). "Groundwater Study of East and West Basin Areas, Simi Valley, California", November.
- Leighton and Associates (1985). "Simi Valley West End Groundwater Study", September.
- Leighton and Associates (1993). "Additional Inclinometer Readings for the Month of January, 1994, Tensar Slope A, Tract 4227, Spanish Hills, Camarillo, California", dated February 16, 1994.
- Leighton and Associates (1994). Personal communication with Mr. Gan Mukhopadhyay.
- Los Angeles County (1990). "Technical Appendix to the Safety Element of the Los Angeles County General Plan, Hazard Reduction in Los Angeles County", Department of Regional Planning, December.
- Los Angeles County, Department of Harbors and Beaches (1994). Personal communication.
- Los Angeles County Water Works (1994). Personal communication with Ken Westphal regarding locations of water pipe breaks.
- Los Angeles Metropolitan Water District (1994). Personal communication with William Pecsí regarding conditions at Joseph Jensen Filtration Plant.
- Maley, R.P. and Cloud, W.K. (1973). "Strong-Motion Accelerograph Records," San Fernando, California, Earthquake of February 9, 1971, U.S. Department of Commerce, National Oceanic and Atmospheric Administration, Volume III, pp. 325-348.
- Marshall, G. (1994). Personal communication.
- M & T Agra, Inc. (1994). "Final Geotechnical Report, Earthquake Damage Reconstruction, Mole B, King Harbor, Redondo Beach, California", prepared for City of Redondo Beach, April.
- Mitchell, J.K. and Christopher, B.R. (1990). "North American Practice in Reinforced Soil Systems", *Design and Performance of Earth Retaining Structures*, Geotechnical Special Publication No.25, ASCE, pp. 322-346.
- Moehle, J. et al. (1994). "Preliminary Report on the Seismological and Engineering Aspects of the January 17, 1994, Northridge Earthquake", Report No. UCB/EERC- 94/01, Earthquake Engineering Research Center, University of California, Berkeley, January.
- National Geodetic Data Center, May 1994, Personal communication (fax) with P. Dunbar regarding the latitudes and longitudes of strong-motion stations that recorded that 1971 San Fernando Earthquake
- Newhall County Water District (1994). "Summary of Earthquake Damage on January 17, 1994", April.
- OES-FEMA, "Building Damage Assessment Database," April 1994
- Porcella, R.L., Etheredge, E.C., Maley, R.P., and Acosta, A.V. (1994). "Accelerograms Recorded at USGS National Strong-Motion Network Stations During the Ms=6.6 Northridge, California Earthquake of January 17, 1994," USGS Open-File Report 94-141, February.

- Port of Los Angeles (1994). Personal communication with Doug Thiessen regarding damages to port facilities from earthquake.
- "Rebuilding Decision is Complex for Property Owners," Los Angeles Times, 22 January 1994, p. A2, figure of "Widespread Damage."
- Romanowicz, B., Dreger, D., Pasyanos, M., Uhrhammer, R. (1994). "Monitoring of Strain Release in Central and Northern California Using Broadband Data", *Geophys. Res. Letters*, 20, 1643-1646.
- Sadigh, K.A., Chang, C.Y., Makdisi, F.I., and Egan, J.A. (1993). "Attenuation Relationship for Horizontal Peak Ground Acceleration and Response Spectra for Rock Sites," *Applied Technology Council ATC-17*.
- Saikia, C.K., Dreger, D.S., and Helmberger, D.V., (1994). "Modeling of Energy Amplification Recorded within Greater Los Angeles Using Irregular Structure," *Bulletin of the Seismological Society of America*, Vol. 84, No. 1, pp. 47-61, February.
- Santa Clarita Water Company (1994). Personal communication with William Manetta regarding water pipe break locations.
- Satalich, R. (1994). Personal communication.
- Scott, R.F. (1971). "San Fernando Earthquake, 9 February 1971, Preliminary Soil Engineering Report", in *Engineering Features of the San Fernando Earthquake, February 9, 1971*, P. Jennings, ed., California Institute of Technology, Earthquake Engineering Research Laboratory.
- Schwartz, D. (1994). Personal communication.
- Seed, H.B. and Whitman, R.V. (1970), "Design of Earth Retaining Structures for Dynamic Loads", Specialty Conference on Lateral Stresses and Design of Earth-Retaining Structures, ASCE, Cornell University, pp. 103-147.
- Seed, H. B., Lee, K. L., Idriss, I. M., Makdisi, F. (1973). "Analysis of the Slides in the San Fernando Dams During the Earthquake of Feb. 9, 1971," Report UCB/EERC- 73/02, Earthquake Engineering Research Center, University of California, Berkeley.
- Seed, H.B., Murarka, R., Lysmer, J., and Idriss, I.M. (1976). "Relationships of Maximum Acceleration, Maximum Velocity, Distance from Source, and Local Site Conditions for Moderately Strong Earthquakes," *Bulletin of the Seismological Society of America*, 66, 1323-1342
- Seed, H.B., Tokimatsu, K., Harder, L.F. and Chung, R. (1985). "Influence of SPT Procedures in Soil Liquefaction Resistance Evaluations", *ASCE Journal of Geotechnical Engineering*, 111 (12).
- Seed, R.B., Dickenson, S.E., Riemer, M.F., Bray, J.D., Sitar, N., Mitchell, J.K., Idriss, I.M., Kayen, R.E., Kropp, A., Harder, L.F., and Power, M.S. (1990). "Preliminary Report on the Principal Geotechnical Aspects of the October 17, 1989 Loma Prieta Earthquake", Report No. UCB/EERC- 90/05, Earthquake Engineering Research Center, University of California, Berkeley, April.
- Shakal, A., Huang, M., Darragh, R., Cao, T., Sherburne, R., Malhotra, P., Cramer, C., Sydnor, R., Graizer, V., Maldonado, G., Petersen, C., and Wampole, J. (1994). "CSMIP Strong-Motion Records from the Northridge, California Earthquake of 17 January 1994," Report No. OSMS 94-07, California Strong Motion Instrumentation Program, Division of Mines and Geology, February.

- Siegel, R.A., Robertson, R.J. and Anderson, D.G. (1990), "Slope Stability Investigations at a Landfill in Southern California", *Geotechnics of Waste Fill - Theory and Practice*, ASTM STP 1070, American Society of Testing and Materials, Philadelphia, PA.
- Southern California Water Company (1994). Personal communication (fax) with Chet Anderson regarding locations of water pipe breaks.
- State of California, Department of Transportation (1994). Personal communication with Thomas Schantz and Dr. Clifford Roblee regarding data from boring logs drilled near highway overcrossing structures along Highway 118 and Interstate Highway 10.
- State Water Rights Board (1962). "Report of Referee, The City of Los Angeles, a Municipal Corporation, Plaintiff, vs. City of San Fernando, a Municipal Corporation, et al., Defendants, No. 650079," Volume 1, July.
- Steidl, J., Martin, A., Tumarkin, A., Lindley, G., Nicholson, C., Archuleta, R., Vernon, F., Edelman, A., Tolstoy, M., Chin, J., Li, Y., Robertson, M., Teng, L., Scott, J., Johnson, D., Magistrale, H., USGS Staff (1994). "SCEC Portable Deployment Following the 1994 Northridge Earthquake". Northridge Abstracts Program for the 89th Annual Meeting of SSA, nr14.
- Switzer, J., Johnson, D., Maley, R., and Matthiesen, R. (1981). "Western Hemisphere Strong-Motion Accelerograph Station List-1980," USGS Open-File Report 81-644, October.
- The Reinforced Earth Company, (1990). "Seismic Design of Reinforced Earth Retaining Walls and Bridge Abutments", 12 p.
- Tinsley, J.C. and Fumal, T.E. (1985). "Mapping Quaternary Sedimentary Deposits for Areal Variations in Shaking Response," *Evaluating Earthquake Hazards in the Los Angeles Region--An Earth Science Perspective*, U.S. Geological Survey Professional Paper 1360, pp. 101-126.
- Tinsley, J. (1994). Personal communication.
- Topozada, T.R., Bennett, J.H., Borchardt, G., Saul, R., and Davis, J.F. (1988). "Planning Scenario for a Major Earthquake on the Newport-Inglewood Fault Zone," California Division of Mines and Geology Special Publication 99.
- Trifunac, M.D., Todorovska, M.I., and Ivanovic, S.S. (1994) "A Note on Distribution of Uncorrected Peak Ground Accelerations During the Northridge, California, Earthquake of 17 January 1994," University of Southern California, Civil Engineering Department, (in press).
- United States Geological Survey (1951). Topographic Map of the Simi Valley East Quadrangle, photorevised 1969.
- United States Geological Survey (1951). Topographic Map of the Simi Valley West Quadrangle, photorevised 1969.
- United States Geological Survey, May 1994, Personal communication (fax) with R. Porcella regarding identification of free-field strong-motion stations.
- Valencia Water Company (1994). "Valencia Water Company, January 17, 1994 Earthquake System Damage and Repair Log", prepared by Penfield and Smith.

- Wentworth, C.M. and Yerkes, R.F. (1971). "Geologic Setting and Activity of Faults in the San Fernando Area, California", in The San Fernando Earthquake of February 9, 1971, U.S. Geological Survey and National Oceanic and Atmospheric Administration, Geologic Survey Professional Paper 733.
- Williams, P.L., Foxall, W., Romanowicz, B. and Moehle, J. (1994). "Rupture Geometry and Stress Redistribution in the Northridge Earthquake", Northridge Abstracts Program for the 89th Annual Meeting of SSA, nr 38.
- Yeats, R. S. (1994). "Oak Ridge Fault System and the 1994 Northridge, California, Earthquake, submitted to Nature.
- Yerkes, R.F., McCulloh, T.H., Schoellhamer, J.E., and Vedder, J.G. (1965). "Geology of the Los Angeles Basin California-an Introduction," U.S. Geological Survey Professional Paper 420-A.
- Youd, T.L. (1971). "Landsliding in the Vicinity of the Van Norman Lakes", in The San Fernando Earthquake of February 9, 1971, U.S. Geological Survey and National Oceanic and Atmospheric Administration, Geologic Survey Professional Paper 733.
- Youd, T.L., Tinsley, J., Perkins, D., King, E., and Preston, R. (1978). "Liquefaction potential map of the San Fernando Valley, California", Proc. 2nd Int. Conf. on Microzonation, San Francisco, California, Vol. 1, 267-278.
- Youd, T.L. and Perkins D.M. (1978). "Mapping liquefaction-induced ground failure potential", ASCE J. Geotech. Engrg. Div., 104 (4) 433-446.

EARTHQUAKE ENGINEERING RESEARCH CENTER REPORT SERIES

EERC reports are available from the National Information Service for Earthquake Engineering (NISEE) and from the National Technical Information Service (NTIS). Numbers in parentheses are Accession Numbers assigned by the National Technical Information Service; these are followed by a price code. Contact NTIS, 5285 Port Royal Road, Springfield Virginia, 22161 for more information. Reports without Accession Numbers were not available from NTIS at the time of printing. For a current complete list of EERC reports (from EERC 67-1) and availability information, please contact University of California, EERC, NISEE, 1301 South 46th Street, Richmond, California 94804.

- UCB/EERC-84/01 "Pseudodynamic Test Method for Seismic Performance Evaluation: Theory and Implementation," by Shing, P.-S.B. and Mahin, S.A., January 1984, (PB84 190 644)A08.
- UCB/EERC-84/02 "Dynamic Response Behavior of Kiang Hong Dian Dam," by Clough, R.W., Chang, K.-T., Chen, H.-Q. and Stephen, R.M., April 1984, (PB84 209 402)A08.
- UCB/EERC-84/03 "Refined Modelling of Reinforced Concrete Columns for Seismic Analysis," by Kaba, S.A. and Mahin, S.A., April 1984, (PB84 234 384)A06.
- UCB/EERC-84/04 "A New Floor Response Spectrum Method for Seismic Analysis of Multiply Supported Secondary Systems," by Asfura, A. and Der Kiureghian, A., June 1984, (PB84 239 417)A06.
- UCB/EERC-84/05 "Earthquake Simulation Tests and Associated Studies of a 1/5th-scale Model of a 7-Story R/C Frame-Wall Test Structure," by Bertero, V.V., Aktan, A.E., Charney, F.A. and Sause, R., June 1984, (PB84 239 409)A09.
- UCB/EERC-84/06 "Unassigned," by Unassigned, 1984.
- UCB/EERC-84/07 "Behavior of Interior and Exterior Flat-Plate Connections Subjected to Inelastic Load Reversals," by Zee, H.L. and Moehle, J.P., August 1984, (PB86 117 629/AS)A07.
- UCB/EERC-84/08 "Experimental Study of the Seismic Behavior of a Two-Story Flat-Plate Structure," by Moehle, J.P. and Diebold, J.W., August 1984, (PB86 122 553/AS)A12.
- UCB/EERC-84/09 "Phenomenological Modeling of Steel Braces under Cyclic Loading," by Ikeda, K., Mahin, S.A. and Dermitzakis, S.N., May 1984, (PB86 132 198/AS)A08.
- UCB/EERC-84/10 "Earthquake Analysis and Response of Concrete Gravity Dams," by Fenves, G.L. and Chopra, A.K., August 1984, (PB85 193 902/AS)A11.
- UCB/EERC-84/11 "EAGD-84: A Computer Program for Earthquake Analysis of Concrete Gravity Dams," by Fenves, G.L. and Chopra, A.K., August 1984, (PB85 193 613/AS)A05.
- UCB/EERC-84/12 "A Refined Physical Theory Model for Predicting the Seismic Behavior of Braced Steel Frames," by Ikeda, K. and Mahin, S.A., July 1984, (PB85 191 450/AS)A09.
- UCB/EERC-84/13 "Earthquake Engineering Research at Berkeley - 1984," by EERC, August 1984, (PB85 197 341/AS)A10.
- UCB/EERC-84/14 "Moduli and Damping Factors for Dynamic Analyses of Cohesionless Soils," by Seed, H.B., Wong, R.T., Idriss, I.M. and Tokimatsu, K., September 1984, (PB85 191 468/AS)A04.
- UCB/EERC-84/15 "The Influence of SPT Procedures in Soil Liquefaction Resistance Evaluations," by Seed, H.B., Tokimatsu, K., Harder, L.F. and Chung, R.M., October 1984, (PB85 191 732/AS)A04.
- UCB/EERC-84/16 "Simplified Procedures for the Evaluation of Settlements in Sands Due to Earthquake Shaking," by Tokimatsu, K. and Seed, H.B., October 1984, (PB85 197 887/AS)A03.
- UCB/EERC-84/17 "Evaluation of Energy Absorption Characteristics of Highway Bridges Under Seismic Conditions - Volume I (PB90 262 627)A16 and Volume II (Appendices) (PB90 262 635)A13," by Imbsen, R.A. and Penzien, J., September 1986.
- UCB/EERC-84/18 "Structure-Foundation Interactions under Dynamic Loads," by Liu, W.D. and Penzien, J., November 1984, (PB87 124 889/AS)A11.
- UCB/EERC-84/19 "Seismic Modelling of Deep Foundations," by Chen, C.-H. and Penzien, J., November 1984, (PB87 124 798/AS)A07.
- UCB/EERC-84/20 "Dynamic Response Behavior of Quan Shui Dam," by Clough, R.W., Chang, K.-T., Chen, H.-Q., Stephen, R.M., Ghanaat, Y. and Qi, J.-H., November 1984, (PB86 115177/AS)A07.
- UCB/EERC-85/01 "Simplified Methods of Analysis for Earthquake Resistant Design of Buildings," by Cruz, E.F. and Chopra, A.K., February 1985, (PB86 112299/AS)A12.
- UCB/EERC-85/02 "Estimation of Seismic Wave Coherency and Rupture Velocity using the SMART 1 Strong-Motion Array Recordings," by Abrahamson, N.A., March 1985, (PB86 214 343)A07.
- UCB/EERC-85/03 "Dynamic Properties of a Thirty Story Condominium Tower Building," by Stephen, R.M., Wilson, E.L. and Stander, N., April 1985, (PB86 118965/AS)A06.
- UCB/EERC-85/04 "Development of Substructuring Techniques for On-Line Computer Controlled Seismic Performance Testing," by Dermitzakis, S. and Mahin, S., February 1985, (PB86 132941/AS)A08.
- UCB/EERC-85/05 "A Simple Model for Reinforcing Bar Anchorages under Cyclic Excitations," by Filippou, F.C., March 1985, (PB86 112 919/AS)A05.
- UCB/EERC-85/06 "Racking Behavior of Wood-framed Gypsum Panels under Dynamic Load," by Oliva, M.G., June 1985, (PB90 262 643)A04.

- UCB/EERC-85/07 "Earthquake Analysis and Response of Concrete Arch Dams," by Fok, K.-L. and Chopra, A.K., June 1985, (PB86 139672/AS)A10.
- UCB/EERC-85/08 "Effect of Inelastic Behavior on the Analysis and Design of Earthquake Resistant Structures," by Lin, J.P. and Mahin, S.A., June 1985, (PB86 135340/AS)A08.
- UCB/EERC-85/09 "Earthquake Simulator Testing of a Base-Isolated Bridge Deck," by Kelly, J.M., Buckle, I.G. and Tsai, H.-C., January 1986, (PB87 124 152/AS)A06.
- UCB/EERC-85/10 "Simplified Analysis for Earthquake Resistant Design of Concrete Gravity Dams," by Fenves, G.L. and Chopra, A.K., June 1986, (PB87 124 160/AS)A08.
- UCB/EERC-85/11 "Dynamic Interaction Effects in Arch Dams," by Clough, R.W., Chang, K.-T., Chen, H.-Q. and Ghanaat, Y., October 1985, (PB86 135027/AS)A05.
- UCB/EERC-85/12 "Dynamic Response of Long Valley Dam in the Mammoth Lake Earthquake Series of May 25-27, 1980," by Lai, S. and Seed, H.B., November 1985, (PB86 142304/AS)A05.
- UCB/EERC-85/13 "A Methodology for Computer-Aided Design of Earthquake-Resistant Steel Structures," by Austin, M.A., Pister, K.S. and Mahin, S.A., December 1985, (PB86 159480/AS)A10 .
- UCB/EERC-85/14 "Response of Tension-Leg Platforms to Vertical Seismic Excitations," by Liou, G.-S., Penzien, J. and Yeung, R.W., December 1985, (PB87 124 871/AS)A08.
- UCB/EERC-85/15 "Cyclic Loading Tests of Masonry Single Piers: Volume 4 - Additional Tests with Height to Width Ratio of 1," by Sveinsson, B., McNiven, H.D. and Sucuoglu, H., December 1985, (PB87 165031/AS)A08.
- UCB/EERC-85/16 "An Experimental Program for Studying the Dynamic Response of a Steel Frame with a Variety of Infill Partitions," by Yanev, B. and McNiven, H.D., December 1985, (PB90 262 676)A05.
- UCB/EERC-86/01 "A Study of Seismically Resistant Eccentrically Braced Steel Frame Systems," by Kasai, K. and Popov, E.P., January 1986, (PB87 124 178/AS)A14.
- UCB/EERC-86/02 "Design Problems in Soil Liquefaction," by Seed, H.B., February 1986, (PB87 124 186/AS)A03.
- UCB/EERC-86/03 "Implications of Recent Earthquakes and Research on Earthquake-Resistant Design and Construction of Buildings," by Bertero, V.V., March 1986, (PB87 124 194/AS)A05.
- UCB/EERC-86/04 "The Use of Load Dependent Vectors for Dynamic and Earthquake Analyses," by Leger, P., Wilson, E.L. and Clough, R.W., March 1986, (PB87 124 202/AS)A12.
- UCB/EERC-86/05 "Two Beam-To-Column Web Connections," by Tsai, K.-C. and Popov, E.P., April 1986, (PB87 124 301/AS)A04.
- UCB/EERC-86/06 "Determination of Penetration Resistance for Coarse-Grained Soils using the Becker Hammer Drill," by Harder, L.F. and Seed, H.B., May 1986, (PB87 124 210/AS)A07.
- UCB/EERC-86/07 "A Mathematical Model for Predicting the Nonlinear Response of Unreinforced Masonry Walls to In-Plane Earthquake Excitations," by Mengi, Y. and McNiven, H.D., May 1986, (PB87 124 780/AS)A06.
- UCB/EERC-86/08 "The 19 September 1985 Mexico Earthquake: Building Behavior," by Bertero, V.V., July 1986.
- UCB/EERC-86/09 "EACD-3D: A Computer Program for Three-Dimensional Earthquake Analysis of Concrete Dams," by Fok, K.-L., Hall, J.F. and Chopra, A.K., July 1986, (PB87 124 228/AS)A08.
- UCB/EERC-86/10 "Earthquake Simulation Tests and Associated Studies of a 0.3-Scale Model of a Six-Story Concentrically Braced Steel Structure," by Uang, C.-M. and Bertero, V.V., December 1986, (PB87 163 564/AS)A17.
- UCB/EERC-86/11 "Mechanical Characteristics of Base Isolation Bearings for a Bridge Deck Model Test," by Kelly, J.M., Buckle, I.G. and Koh, C.-G., November 1987, (PB90 262 668)A04.
- UCB/EERC-86/12 "Effects of Axial Load on Elastomeric Isolation Bearings," by Koh, C.-G. and Kelly, J.M., November 1987.
- UCB/EERC-87/01 "The FPS Earthquake Resisting System: Experimental Report," by Zayas, V.A., Low, S.S. and Mahin, S.A., June 1987, (PB88 170 287)A06.
- UCB/EERC-87/02 "Earthquake Simulator Tests and Associated Studies of a 0.3-Scale Model of a Six-Story Eccentrically Braced Steel Structure," by Whittaker, A., Uang, C.-M. and Bertero, V.V., July 1987, (PB88 166 707/AS)A18.
- UCB/EERC-87/03 "A Displacement Control and Uplift Restraint Device for Base-Isolated Structures," by Kelly, J.M., Griffith, M.C. and Aiken, I.D., April 1987, (PB88 169 933)A04.
- UCB/EERC-87/04 "Earthquake Simulator Testing of a Combined Sliding Bearing and Rubber Bearing Isolation System," by Kelly, J.M. and Chalhoub, M.S., December 1990.
- UCB/EERC-87/05 "Three-Dimensional Inelastic Analysis of Reinforced Concrete Frame-Wall Structures," by Moazzami, S. and Bertero, V.V., May 1987, (PB88 169 586/AS)A08.
- UCB/EERC-87/06 "Experiments on Eccentrically Braced Frames with Composite Floors," by Ricles, J. and Popov, E., June 1987, (PB88 173 067/AS)A14.
- UCB/EERC-87/07 "Dynamic Analysis of Seismically Resistant Eccentrically Braced Frames," by Ricles, J. and Popov, E., June 1987, (PB88 173 075/AS)A16.
- UCB/EERC-87/08 "Undrained Cyclic Triaxial Testing of Gravels-The Effect of Membrane Compliance," by Evans, M.D. and Seed, H.B., July 1987, (PB88 173 257)A19.

- UCB/EERC-87/09 "Hybrid Solution Techniques for Generalized Pseudo-Dynamic Testing," by Thewalt, C. and Mahin, S.A., July 1987, (PB 88 179 007)A07.
- UCB/EERC-87/10 "Ultimate Behavior of Butt Welded Splices in Heavy Rolled Steel Sections," by Bruneau, M., Mahin, S.A. and Popov, E.P., September 1987, (PB90 254 285)A07.
- UCB/EERC-87/11 "Residual Strength of Sand from Dam Failures in the Chilean Earthquake of March 3, 1985," by De Alba, P., Seed, H.B., Retamal, E. and Seed, R.B., September 1987, (PB88 174 321/AS)A03.
- UCB/EERC-87/12 "Inelastic Seismic Response of Structures with Mass or Stiffness Eccentricities in Plan," by Bruneau, M. and Mahin, S.A., September 1987, (PB90 262 650/AS)A14.
- UCB/EERC-87/13 "CSTRUCT: An Interactive Computer Environment for the Design and Analysis of Earthquake Resistant Steel Structures," by Austin, M.A., Mahin, S.A. and Pister, K.S., September 1987, (PB88 173 339/AS)A06.
- UCB/EERC-87/14 "Experimental Study of Reinforced Concrete Columns Subjected to Multi-Axial Loading," by Low, S.S. and Moehle, J.P., September 1987, (PB88 174 347/AS)A07.
- UCB/EERC-87/15 "Relationships between Soil Conditions and Earthquake Ground Motions in Mexico City in the Earthquake of Sept. 19, 1985," by Seed, H.B., Romo, M.P., Sun, J., Jaime, A. and Lysmer, J., October 1987, (PB88 178 991)A06.
- UCB/EERC-87/16 "Experimental Study of Seismic Response of R. C. Setback Buildings," by Shahrooz, B.M. and Moehle, J.P., October 1987, (PB88 176 359)A16.
- UCB/EERC-87/17 "The Effect of Slabs on the Flexural Behavior of Beams," by Pantazopoulou, S.J. and Moehle, J.P., October 1987, (PB90 262 700)A07.
- UCB/EERC-87/18 "Design Procedure for R-FBI Bearings," by Mostaghel, N. and Kelly, J.M., November 1987, (PB90 262 718)A04.
- UCB/EERC-87/19 "Analytical Models for Predicting the Lateral Response of R C Shear Walls: Evaluation of their Reliability," by Vulcanano, A. and Bertero, V.V., November 1987, (PB88 178 983)A05.
- UCB/EERC-87/20 "Earthquake Response of Torsionally-Coupled Buildings," by Hejal, R. and Chopra, A.K., December 1987.
- UCB/EERC-87/21 "Dynamic Reservoir Interaction with Monticello Dam," by Clough, R.W., Ghanaat, Y. and Qiu, X-F., December 1987, (PB88 179 023)A07.
- UCB/EERC-87/22 "Strength Evaluation of Coarse-Grained Soils," by Siddiqi, F.H., Seed, R.B., Chan, C.K., Seed, H.B. and Pyke, R.M., December 1987, (PB88 179 031)A04.
- UCB/EERC-88/01 "Seismic Behavior of Centrally Braced Steel Frames," by Khatib, I., Mahin, S.A. and Pister, K.S., January 1988, (PB91 210 898/AS)A11.
- UCB/EERC-88/02 "Experimental Evaluation of Seismic Isolation of Medium-Rise Structures Subject to Uplift," by Griffith, M.C., Kelly, J.M., Coveney, V.A. and Koh, C.G., January 1988, (PB91 217 950/AS)A09.
- UCB/EERC-88/03 "Cyclic Behavior of Steel Double Angle Connections," by Astaneh-Asl, A. and Nader, M.N., January 1988, (PB91 210 872)A05.
- UCB/EERC-88/04 "Re-evaluation of the Slide in the Lower San Fernando Dam in the Earthquake of Feb. 9, 1971," by Seed, H.B., Seed, R.B., Harder, L.F. and Jong, H.-L., April 1988, (PB91 212 456/AS)A07.
- UCB/EERC-88/05 "Experimental Evaluation of Seismic Isolation of a Nine-Story Braced Steel Frame Subject to Uplift," by Griffith, M.C., Kelly, J.M. and Aiken, I.D., May 1988, (PB91 217 968/AS)A07.
- UCB/EERC-88/06 "DRAIN-2DX User Guide.," by Allahabadi, R. and Powell, G.H., March 1988, (PB91 212 530)A12.
- UCB/EERC-88/07 "Theoretical and Experimental Studies of Cylindrical Water Tanks in Base-Isolated Structures," by Chalhoub, M.S. and Kelly, J.M., April 1988, (PB91 217 976/AS)A05.
- UCB/EERC-88/08 "Analysis of Near-Source Waves: Separation of Wave Types Using Strong Motion Array Recording," by Darragh, R.B., June 1988, (PB91 212 621)A08.
- UCB/EERC-88/09 "Alternatives to Standard Mode Superposition for Analysis of Non-Classically Damped Systems," by Kusainov, A.A. and Clough, R.W., June 1988, (PB91 217 992/AS)A04.
- UCB/EERC-88/10 "The Landslide at the Port of Nice on October 16, 1979," by Seed, H.B., Seed, R.B., Schlosser, F., Blondeau, F. and Juran, I., June 1988, (PB91 210 914)A05.
- UCB/EERC-88/11 "Liquefaction Potential of Sand Deposits Under Low Levels of Excitation," by Carter, D.P. and Seed, H.B., August 1988, (PB91 210 880)A15.
- UCB/EERC-88/12 "Nonlinear Analysis of Reinforced Concrete Frames Under Cyclic Load Reversals," by Filippou, F.C. and Issa, A., September 1988, (PB91 212 589)A07.
- UCB/EERC-88/13 "Implications of Recorded Earthquake Ground Motions on Seismic Design of Building Structures," by Uang, C.-M. and Bertero, V.V., November 1988, (PB91 212 548)A06.
- UCB/EERC-88/14 "An Experimental Study of the Behavior of Dual Steel Systems," by Whittaker, A.S., Uang, C.-M. and Bertero, V.V., September 1988, (PB91 212 712)A16.
- UCB/EERC-88/15 "Dynamic Moduli and Damping Ratios for Cohesive Soils," by Sun, J.I., Golesorkhi, R. and Seed, H.B., August 1988, (PB91 210 922)A04.
- UCB/EERC-88/16 "Reinforced Concrete Flat Plates Under Lateral Load: An Experimental Study Including Biaxial Effects," by Pan, A. and Moehle, J.P., October 1988, (PB91 210 856)A13.

- UCB/EERC-88/17 "Earthquake Engineering Research at Berkeley - 1988," by EERC, November 1988, (PB91 210 864)A10.
- UCB/EERC-88/18 "Use of Energy as a Design Criterion in Earthquake-Resistant Design," by Uang, C.-M. and Bertero, V.V., November 1988, (PB91 210 906/AS)A04.
- UCB/EERC-88/19 "Steel Beam-Column Joints in Seismic Moment Resisting Frames," by Tsai, K.-C. and Popov, E.P., November 1988, (PB91 217 984/AS)A20.
- UCB/EERC-88/20 "Base Isolation in Japan, 1988," by Kelly, J.M., December 1988, (PB91 212 449)A05.
- UCB/EERC-89/01 "Behavior of Long Links in Eccentrically Braced Frames," by Engelhardt, M.D. and Popov, E.P., January 1989, (PB92 143 056)A18.
- UCB/EERC-89/02 "Earthquake Simulator Testing of Steel Plate Added Damping and Stiffness Elements," by Whittaker, A., Bertero, V.V., Alonso, J. and Thompson, C., January 1989, (PB91 229 252/AS)A10.
- UCB/EERC-89/03 "Implications of Site Effects in the Mexico City Earthquake of Sept. 19, 1985 for Earthquake-Resistant Design Criteria in the San Francisco Bay Area of California," by Seed, H.B. and Sun, J.I., March 1989, (PB91 229 369/AS)A07.
- UCB/EERC-89/04 "Earthquake Analysis and Response of Intake-Outlet Towers," by Goyal, A. and Chopra, A.K., July 1989, (PB91 229 286/AS)A19.
- UCB/EERC-89/05 "The 1985 Chile Earthquake: An Evaluation of Structural Requirements for Bearing Wall Buildings," by Wallace, J.W. and Moehle, J.P., July 1989, (PB91 218 008/AS)A13.
- UCB/EERC-89/06 "Effects of Spatial Variation of Ground Motions on Large Multiply-Supported Structures," by Hao, H., July 1989, (PB91 229 161/AS)A08.
- UCB/EERC-89/07 "EADAP - Enhanced Arch Dam Analysis Program: Users's Manual," by Ghanaat, Y. and Clough, R.W., August 1989, (PB91 212 522)A06.
- UCB/EERC-89/08 "Seismic Performance of Steel Moment Frames Plastically Designed by Least Squares Stress Fields," by Ohi, K. and Mahin, S.A., August 1989, (PB91 212 597)A05.
- UCB/EERC-89/09 "Feasibility and Performance Studies on Improving the Earthquake Resistance of New and Existing Buildings Using the Friction Pendulum System," by Zayas, V., Low, S., Mahin, S.A. and Bozzo, L., July 1989, (PB92 143 064)A14.
- UCB/EERC-89/10 "Measurement and Elimination of Membrane Compliance Effects in Undrained Triaxial Testing," by Nicholson, P.G., Seed, R.B. and Anwar, H., September 1989, (PB92 139 641/AS)A13.
- UCB/EERC-89/11 "Static Tilt Behavior of Unanchored Cylindrical Tanks," by Lau, D.T. and Clough, R.W., September 1989, (PB92 143 049)A10.
- UCB/EERC-89/12 "ADAP-88: A Computer Program for Nonlinear Earthquake Analysis of Concrete Arch Dams," by Fenves, G.L., Mojtahedi, S. and Reimer, R.B., September 1989, (PB92 139 674/AS)A07.
- UCB/EERC-89/13 "Mechanics of Low Shape Factor Elastomeric Seismic Isolation Bearings," by Aiken, I.D., Kelly, J.M. and Tajirian, F.F., November 1989, (PB92 139 732/AS)A09.
- UCB/EERC-89/14 "Preliminary Report on the Seismological and Engineering Aspects of the October 17, 1989 Santa Cruz (Loma Prieta) Earthquake," by EERC, October 1989, (PB92 139 682/AS)A04.
- UCB/EERC-89/15 "Experimental Studies of a Single Story Steel Structure Tested with Fixed, Semi-Rigid and Flexible Connections," by Nader, M.N. and Astaneh-Asl, A., August 1989, (PB91 229 211/AS)A10.
- UCB/EERC-89/16 "Collapse of the Cypress Street Viaduct as a Result of the Loma Prieta Earthquake," by Nims, D.K., Miranda, E., Aiken, I.D., Whittaker, A.S. and Bertero, V.V., November 1989, (PB91 217 935/AS)A05.
- UCB/EERC-90/01 "Mechanics of High-Shape Factor Elastomeric Seismic Isolation Bearings," by Kelly, J.M., Aiken, I.D. and Tajirian, F.F., March 1990.
- UCB/EERC-90/02 "Javid's Paradox: The Influence of Preform on the Modes of Vibrating Beams," by Kelly, J.M., Sackman, J.I. and Javid, A., May 1990, (PB91 217 943/AS)A03.
- UCB/EERC-90/03 "Earthquake Simulator Testing and Analytical Studies of Two Energy-Absorbing Systems for Multistory Structures," by Aiken, I.D. and Kelly, J.M., October 1990, (PB92 192 988)A13.
- UCB/EERC-90/04 "Damage to the San Francisco-Oakland Bay Bridge During the October 17, 1989 Earthquake," by Astaneh-Asl, A., June 1990.
- UCB/EERC-90/05 "Preliminary Report on the Principal Geotechnical Aspects of the October 17, 1989 Loma Prieta Earthquake," by Seed, R.B., Dickenson, S.E., Riemer, M.F., Bray, J.D., Sitar, N., Mitchell, J.K., Idriss, I.M., Kayen, R.E., Kropp, A., Harder, L.F., Jr. and Power, M.S., April 1990, (PB 192 970)A08.
- UCB/EERC-90/06 "Models of Critical Regions in Reinforced Concrete Frames Under Seismic Excitations," by Zulfikar, N. and Filippou, F.C., May 1990.
- UCB/EERC-90/07 "A Unified Earthquake-Resistant Design Method for Steel Frames Using ARMA Models," by Takewaki, I., Conte, J.P., Mahin, S.A. and Pister, K.S., June 1990.
- UCB/EERC-90/08 "Soil Conditions and Earthquake Hazard Mitigation in the Marina District of San Francisco," by Mitchell, J.K., Masood, T., Kayen, R.E. and Seed, R.B., May 1990, (PB 193 267/AS)A04.
- UCB/EERC-90/09 "Influence of the Earthquake Ground Motion Process and Structural Properties on Response Characteristics of Simple Structures," by Conte, J.P., Pister, K.S. and Mahin, S.A., July 1990, (PB92 143 064)A15.

- UCB/EERC-90/10 "Experimental Testing of the Resilient-Friction Base Isolation System," by Clark, P.W. and Kelly, J.M., July 1990, (PB92 143 072)A08.
- UCB/EERC-90/11 "Seismic Hazard Analysis: Improved Models, Uncertainties and Sensitivities," by Araya, R. and Der Kiureghian, A., March 1988.
- UCB/EERC-90/12 "Effects of Torsion on the Linear and Nonlinear Seismic Response of Structures," by Sedarat, H. and Bertero, V.V., September 1989, (PB92 193 002/AS)A15.
- UCB/EERC-90/13 "The Effects of Tectonic Movements on Stresses and Deformations in Earth Embankments," by Bray, J. D., Seed, R. B. and Seed, H. B., September 1989.
- UCB/EERC-90/14 "Inelastic Seismic Response of One-Story, Asymmetric-Plan Systems," by Goel, R.K. and Chopra, A.K., October 1990, (PB93 114 767)A11.
- UCB/EERC-90/15 "Dynamic Crack Propagation: A Model for Near-Field Ground Motion.," by Seyyedien, H. and Kelly, J.M., 1990.
- UCB/EERC-90/16 "Sensitivity of Long-Period Response Spectra to System Initial Conditions," by Blasquez, R., Ventura, C. and Kelly, J.M., 1990.
- UCB/EERC-90/17 "Behavior of Peak Values and Spectral Ordinates of Near-Source Strong Ground-Motion over a Dense Array," by Niazi, M., June 1990, (PB93 114 833)A07.
- UCB/EERC-90/18 "Material Characterization of Elastomers used in Earthquake Base Isolation," by Papoulia, K.D. and Kelly, J.M., 1990.
- UCB/EERC-90/19 "Cyclic Behavior of Steel Top-and-Bottom Plate Moment Connections," by Harriott, J.D. and Astaneh-Asl, A., August 1990, (PB91 229 260/AS)A05.
- UCB/EERC-90/20 "Seismic Response Evaluation of an Instrumented Six Story Steel Building," by Shen, J.-H. and Astaneh-Asl, A., December 1990, (PB91 229 294/AS)A04.
- UCB/EERC-90/21 "Observations and Implications of Tests on the Cypress Street Viaduct Test Structure," by Bollo, M., Mahin, S.A., Moehle, J.P., Stephen, R.M. and Qi, X., December 1990, (PB93 114 775)A13.
- UCB/EERC-91/01 "Experimental Evaluation of Nitinol for Energy Dissipation in Structures," by Nims, D.K., Sasaki, K.K. and Kelly, J.M., 1991.
- UCB/EERC-91/02 "Displacement Design Approach for Reinforced Concrete Structures Subjected to Earthquakes," by Qi, X. and Moehle, J.P., January 1991, (PB93 114 569/AS)A09.
- UCB/EERC-91/03 "A Long-Period Isolation System Using Low-Modulus High-Damping Isolators for Nuclear Facilities at Soft-Soil Sites," by Kelly, J.M., March 1991, (PB93 114 577/AS)A10.
- UCB/EERC-91/04 "Dynamic and Failure Characteristics of Bridgestone Isolation Bearings," by Kelly, J.M., April 1991, (PB93 114 528)A05.
- UCB/EERC-91/05 "Base Sliding Response of Concrete Gravity Dams to Earthquakes," by Chopra, A.K. and Zhang, L., May 1991, (PB93 114 544/AS)A05.
- UCB/EERC-91/06 "Computation of Spatially Varying Ground Motion and Foundation-Rock Impedance Matrices for Seismic Analysis of Arch Dams," by Zhang, L. and Chopra, A.K., May 1991, (PB93 114 825)A07.
- UCB/EERC-91/07 "Estimation of Seismic Source Processes Using Strong Motion Array Data," by Chiou, S.-J., July 1991, (PB93 114 551/AS)A08.
- UCB/EERC-91/08 "A Response Spectrum Method for Multiple-Support Seismic Excitations," by Der Kiureghian, A. and Neuenhofer, A., August 1991, (PB93 114 536)A04.
- UCB/EERC-91/09 "A Preliminary Study on Energy Dissipating Cladding-to-Frame Connection," by Cohen, J.M. and Powell, G.H., September 1991, (PB93 114 510)A05.
- UCB/EERC-91/10 "Evaluation of Seismic Performance of a Ten-Story RC Building During the Whittier Narrows Earthquake," by Miranda, E. and Bertero, V.V., October 1991, (PB93 114 783)A06.
- UCB/EERC-91/11 "Seismic Performance of an Instrumented Six-Story Steel Building," by Anderson, J.C. and Bertero, V.V., November 1991, (PB93 114 809)A07.
- UCB/EERC-91/12 "Performance of Improved Ground During the Loma Prieta Earthquake," by Mitchell, J.K. and Wentz, Jr., F.J., October 1991, (PB93 114 791)A06.
- UCB/EERC-91/13 "Shaking Table - Structure Interaction," by Rinawi, A.M. and Clough, R.W., October 1991, (PB93 114 917)A13.
- UCB/EERC-91/14 "Cyclic Response of RC Beam-Column Knee Joints: Test and Retrofit," by Mazzoni, S., Moehle, J.P. and Thewalt, C.R., October 1991, (PB93 120 277)A03.
- UCB/EERC-91/15 "Design Guidelines for Ductility and Drift Limits: Review of State-of-the-Practice and State-of-the-Art in Ductility and Drift-Based Earthquake-Resistant Design of Buildings," by Bertero, V.V., Anderson, J.C., Krawinkler, H., Miranda, E. and The CUREe and The Kajima Research Teams, July 1991, (PB93 120 269)A08.
- UCB/EERC-91/16 "Evaluation of the Seismic Performance of a Thirty-Story RC Building," by Anderson, J.C., Miranda, E., Bertero, V.V. and The Kajima Project Research Team, July 1991, (PB93 114 841)A12.
- UCB/EERC-91/17 "A Fiber Beam-Column Element for Seismic Response Analysis of Reinforced Concrete Structures," by Taucer, F., Spacone, E. and Filippou, F.C., December 1991, (PB94 117 629AS)A07.

- UCB/EERC-91/18 "Investigation of the Seismic Response of a Lightly-Damped Torsionally-Coupled Building," by Boroschek, R. and Mahin, S.A., December 1991, (PB93 120 335)A13.
- UCB/EERC-92/01 "Studies of a 49-Story Instrumented Steel Structure Shaken During the Loma Prieta Earthquake," by Chen, C.-C., Bonowitz, D. and Astaneh-Asl, A., February 1992, (PB93 221 778)A08.
- UCB/EERC-92/02 "Response of the Dumbarton Bridge in the Loma Prieta Earthquake," by Fenves, G.L., Filippou, F.C. and Sze, D.T., January 1992, (PB93 120 319)A09.
- UCB/EERC-92/03 "Models for Nonlinear Earthquake Analysis of Brick Masonry Buildings," by Mengi, Y., McNiven, H.D. and Tanrikulu, A.K., March 1992, (PB93 120 293)A08.
- UCB/EERC-92/04 "Shear Strength and Deformability of RC Bridge Columns Subjected to Inelastic Cyclic Displacements," by Aschheim, M. and Moehele, J.P., March 1992, (PB93 120 327)A06.
- UCB/EERC-92/05 "Parameter Study of Joint Opening Effects on Earthquake Response of Arch Dams," by Fenves, G.L., Mojtahedi, S. and Reimer, R.B., April 1992, (PB93 120 301)A04.
- UCB/EERC-92/06 "Seismic Behavior and Design of Semi-Rigid Steel Frames," by Nader, M.N. and Astaneh-Asl, A., May 1992.
- UCB/EERC-92/07 "A Beam Element for Seismic Damage Analysis," by Spacone, E., Ciampi, V. and Filippou, F.C., August 1992.
- UCB/EERC-92/08 "Nonlinear Static and Dynamic Analysis of Reinforced Concrete Subassemblages," by Filippou, F.C., D'Ambrisi, A. and Issa, A., August 1992.
- UCB/EERC-92/09 "Evaluation of Code Accidental-Torsion Provisions Using Earthquake Records from Three Nominally Symmetric-Plan Buildings," by De la Llera, J.C. and Chopra, A.K., September 1992, (PB94 117 611)A08.
- UCB/EERC-92/10 "Slotted Bolted Connection Energy Dissipators," by Grigorian, C.E., Yang, T.-S. and Popov, E.P., July 1992, (PB92 120 285)A03.
- UCB/EERC-92/11 "Mechanical Characteristics of Neoprene Isolation Bearings," by Kelly, J.M. and Quiroz, E., August 1992, (PB93 221 729)A07.
- UCB/EERC-92/12 "Application of a Mass Damping System to Bridge Structures," by Hasegawa, K. and Kelly, J.M., August 1992, (PB93 221 786)A06.
- UCB/EERC-92/13 "Earthquake Engineering Research at Berkeley - 1992," by EERC, October 1992.
- UCB/EERC-92/14 "Earthquake Risk and Insurance," by Brillinger, D.R., October 1992, (PB93 223 352)A03.
- UCB/EERC-92/15 "A Friction Mass Damper for Vibration Control," by Inaudi, J.A. and Kelly, J.M., October 1992, (PB93 221 745)A04.
- UCB/EERC-92/16 "Tall Reinforced Concrete Buildings: Conceptual Earthquake-Resistant Design Methodology," by Bertero, R.D. and Bertero, V.V., December 1992, (PB93 221 695)A12.
- UCB/EERC-92/17 "Performance of Tall Buildings During the 1985 Mexico Earthquakes," by Terán-Gilmore, A. and Bertero, V.V., December 1992, (PB93 221 737)A11.
- UCB/EERC-92/18 "Dynamic Analysis of Nonlinear Structures using State-Space Formulation and Partitioned Integration Schemes," by Inaudi, J.A. and De la Llera, J.C., December 1992, (PB94 117 702/AS/A05).
- UCB/EERC-93/01 "Seismic Performance of an Instrumented Six-Story Reinforced-Concrete Building," by Anderson, J.C. and Bertero, V.V., 1993.
- UCB/EERC-93/02 "Evaluation of an Active Variable-Damping-Structure," by Polak, E., Mecker, G., Yamada, K. and Kurata, N., 1993, (PB93 221 711)A05.
- UCB/EERC-93/03 "An Experimental Study of Flat-Plate Structures under Vertical and Lateral Loads," by Hwang, S.-H. and Moehle, J.P., February 1993, (PB94 157 690/AS)A13.
- UCB/EERC-93/04 "Seismic Performance of a 30-Story Building Located on Soft Soil and Designed According to UBC 1991," by Terán-Gilmore, A. and Bertero, V.V., 1993, (PB93 221 703)A17.
- UCB/EERC-93/05 "Multiple-Support Response Spectrum Analysis of the Golden Gate Bridge," by Nakamura, Y., Der Kiureghian, A. and Liu, D., May 1993, (PB93 221 752)A05.
- UCB/EERC-93/06 "On the Analysis of Structures with Viscoelastic Dampers," by Inaudi, J.A., Zambrano, A. and Kelly, J.M., August 1993, PB94-165867.
- UCB/EERC-93/07 "Earthquake Analysis and Response of Concrete Gravity Dams Including Base Sliding," by Chávez, J.W. and Fenves, G.L., December 1993, (PB94 157 658/AS)A10.
- UCB/EERC-93/08 "Model for Anchored Reinforcing Bars under Seismic Excitations," by Monti, G., Spacone, E. and Filippou, F.C., December 1993.
- UCB/EERC-93/09 "A Methodology for Design of Viscoelastic Dampers in Earthquake-Resistant Structures," by Abbas, H. and Kelly, J.M., November 1993.
- UCB/EERC-93/10 "Tuned Mass Dampers Using Viscoelastic Dampers," by Inaudi, J.A., Lopez-Almansa, F. and Kelly, J.M., December 1993.
- UCB/EERC-93/11 "Nonlinear Homogeneous Dynamical Systems," by Inaudi, J.A. and Kelly, J.M., December 1993.
- UCB/EERC-93/12 "Synthesized Strong Ground Motions for the Seismic Condition Assessment of the Eastern Portion of the San Francisco Bay Bridge," by Bolt, B.A. and Gregor, N.J., December 1993, PB94-165842.

- UCB/EERC-93/13 "On the Analysis of Structures with Energy Dissipating Restraints," by Inaudi, J.A., Nims, D.K. and Kelly, J.M., December 1993.
- UCB/EERC-94/01 "Preliminary Report on the Seismological and Engineering Aspects of the January 17, 1994 Northridge Earthquake," by EERC, January 1994, (PB94 157 666/AS)A05.
- UCB/EERC-94/02 "Energy Dissipation with Slotted Bolted Connections," by Grigorian, C.E. and Popov, E.P., February 1994, PB94-164605.
- UCB/EERC-94/03 "The Influence of Plate Flexibility on the Buckling Load of Elastomeric Isolators," by Kelly, J.M., March 1994.
- UCB/EERC-94/04 "Insitu Test Results from Four Loma Prieta Earthquake Liquefaction Sites: SPT, CPT, DMT and Shear Wave Velocity," by Mitchell, J.K., Lodge, A.L., Coutinho, R.Q., Kayen, R.E., Seed, R.B., Nishio, S. and Stokoe II, K.H., April 1994.
- UCB/EERC-94/05 "Seismic Response of Steep Natural Slopes," by Sitar, N. and Ashford, S.A., May 1994.
- UCB/EERC-94/06 "Small-Scale Testing of a Self-Centering Friction Energy Dissipator for Structures," by Nims, D.K. and Kelly, J.M., August 1994.
- UCB/EERC-94/07 "Accidental and Natural Torsion in Earthquake Response and Design of Buildings," by De la Llera, J.C. and Chopra, A.K., June 1994.
- UCB/EERC-94/08 "Preliminary Report on the Principal Geotechnical Aspects of the January 17, 1994 Northridge Earthquake," by Stewart, J.P., Bray, J.D., Seed, R.B. and Sitar, N., June 1994.

